Mechanistic studies of Ras nanoclusters and Ras effectors interacting with the lipid membrane

Dissertation

zur Erlangung des akademischen Grades eines

Doktors der Naturwissenschaften

(Dr. rer. nat.)

eingereicht an

der Fakultät Chemie und Chemische Biologie der

Technischen Universität Dortmund

vorgelegt von

Lei Li

Aus Hubei, China

Dortmund, August 2019

Mechanistic studies of Ras nanoclusters and Ras effectors interacting with the lipid membrane

Dissertation

For the achievement of the academic degree of the

Doctors in Natural Sciences

(Dr. rer. nat.)

Submitted to

The Faulty of Chemistry and Chemical Biology

TU Dortmund University

By

Lei Li

From Hubei, China

Dortmund, August 2019

Erklärung/Declaration

The work described in this Dissertation was performed from September 2016 to August 2019 at the Faculty of Chemistry and Chemical Biology, TU Dortmund University under the guidance of Prof. Dr. Roland Winter.

I hereby declare that I performed the work presented independently and did not use any other but the indicated aids.

Die in dieser Dissertation beschriebene Arbeit wurde von September 2016 bis August 2019 am der Fakultät für Chemie und Chemische Biologie der Technischen Universität Dortmund unter der Leitung von Prof. Dr. Roland Winter durchgeführt.

Hiermit versichere ich an Eides statt, dass ich die vorliegende Arbeit selbstständing und nur mit den angegebenen Hilfsmitteln angefertigh habe.

Dortmund, August 2019

Lei Li

1. Examiner

Prof. Dr. Roland Winter

2. Examiner

Prof. Dr. Claus Czeslik

Dedicated to my lovely parents.

Contents

Abbreviations

°C	Degree Celsius
Å	Angstrom (1 Å = 10^{-10} m)
AA	Amino acid
A	Absorption
Ala	Alanine
APS	Ammonium persulfate
AFM	Atomic force microscopy
Asn	Asparagine
Asp	Aspartic acid
BODIPY	Boron-dipyrromethene
c	Concentration
CaM	Calmodulin
CBD	Chitin-binding domain
CD	Circular dichroism
Chol	Cholesterol
C-terminal	Carboxyl-terminal
Cys	Cysteine
D	Diffusion coefficiency
Da	Dalton
DMEM	Dulbecco's modified eagle medium
DNA	Deoxyribonucleic acid
DMSO	Dimethyl sulfoxide
DOL	Degree of labeling
DOPC	1,2-dioleoyl-sn-glycero-3-phosphocholine
DOPG	1,2-dioleoyl-sn-glycero-3-phospho-(1'-rac-glycerol)
DOPS	1,2-dioleoyl-sn-glycero-3-phospho-L-serine
DPPC	1,2-dipalmitoyl-sn-glycero-3-phosphocholine
DPPG	1,2-dipalmitoyl-sn-glycero-3-phosphoglycerol
DPPS	1,2-Dipalmitoyl-sn-glycero-3-phosphoserine
DTE	1,4-Dithioerythritol
DTT	1,4-dithiothreitol
EDTA	Ethylenediaminetetraacetic acid
EGF	Epidermal growth factor
EGFP	Enhanced green fluorescent protein
EPL	Expressed protein ligation
ER	Endoplasmic Reticulum
ESI-MS	Electrospray ionization mass spectrometry
FBS	Fetal bovine serum
FCS	Fluorescence correlation spectroscopy
FCCS	Fluorescence cross-correlation spectroscopy
FRET	Förster resonance energy transfer
FTase	Farnesyltransferase
GAP	GTPase activating protein
GDP	Guanosine diphosphate
GEF	Guanine exchange factor

GGTase	Geranylgeranyltransferase
Gly	Glycine
GTP	Guanosine triphosphate
GUV	Giant unilamellar vesicle
HEPES	4-(2-hydroxyethyl)-1-piperazineethanesulfonic acid
HVR	Hypervariable Region
IPTG	Isopropyl-D-thiogalactopyranoside
ITC	Isothermal titration calorimetry
ITO	Indium tin oxide
LUV	Large unilamellar vesicle
Lys	Lysine
MAPK	Mitogen-activated protein kinases
MDCK	Madin-darby canine kidney cells
Mesna	2-Mercaptoethanesulfonic acid
MW	Molecular weight
N-Rh-DHPE	N-(LissamineTM Rhodamine B sulfonyl)-1,2-dihexadecanoyl- sn-glycero-3-phosphoethanolamin
NCL	Native chemical ligation
NHS	N-hydroxysuccinimide
NMR	Nuclear magnetic resonance
PBS	Phosphate-buffered saline
PC	Phosphatidylcholine
PE	Phosphatidylethanolamine
PG	Phosphatidylglycerol
PI	Phosphatidylinositol
PI3K	Phosphoinositide 3-kinase
PMSF	Phenylmethanesulfonyl fluoride
PS	Phosphatidylserine
Ras	Rat adeno sarcoma
RE	Recycling endosome
SDS	Sodium dodecyl sulfate
SM	Sphingomyelin
T	Temperature
TCEP	Tris(2-carboxyethyl)phosphine hydrochloride
TEMED	Tetramethylethylenediamine
TFA	Trifluoroacetic acid
TRIS	Tris(hydroxymethyl)aminomethane
Trp	Tryptophan
Tyr	Tyrosine
UV	Ultraviolet
V	Volume

Zusammenfassung

Ras-Proteine sind Onkoproteine und spielen eine wichtige Rolle bei Krebserkrankungen beim Menschen, bei denen sie das Signal für das Zellwachstum nicht abschalten. Mehr als 30 % der Krebserkrankungen beim Menschen sind auf Mutationen von Ras-Proteinen zurückzuführen, wobei K-Ras4B die am häufigsten vorkommende mutierte Isoform ist. Sie sind plasmamembranlokalisierte molekulare Schalter, die zwischen inaktiven GDP-gebundenen und aktiven GTP-gebundenen Formen wechseln. Die Signalgebung von K-Ras4B hängt stark von seiner korrekten Lokalisierung in der Plasmamembran ab.

Es wurde gezeigt, dass C6-Ceramid die Wachstumsaktivität von K-Ras4B-Mutanten hemmt. Der Mechanismus, der dieser Hemmung zugrunde liegt, ist jedoch noch nicht bekannt. In der vorliegenden Arbeit wurde eine heterogene Modellbiomembran mit C6-Ceramid etabliert, um zu demonstrieren, dass die Zugabe von K-Ras4B zu drastischen Veränderungen in der lateralen Membranorganisation führt. Im Gegensatz zum Verteilungsverhalten in anderen Membranen bildet K-Ras4B kleine, monodisperse Nanocluster, die in flüssigen Domänen der Membran verteilt sind, was aller Wahrscheinlichkeit nach durch einen Lipidsortierungsmechanismus verursacht wird. Fluoreszenzkreuzkorrelationsmessungen zeigten keine direkte Wechselwirkung zwischen C6-Ceramid und K-Ras4B an, was darauf hindeutet, dass K-Ras4B im Wesentlichen andere Lipide anzieht. Darüber hinaus zeigte ein FRET-basierter Bindungsassay, dass die Stabilität von K-Ras4B innerhalb einer C6-Ceramid enthaltenden Membran signifikant verringert ist. Aus den Ergebnissen dieser Studie wird ein molekularer Mechanismus für die Hemmung der Aktivität von K-Ras4B-mutierten Zellen durch C6-Ceramid postuliert.

In-vivo-Studien legen nahe, dass intermolekulare Wechselwirkungen die Selbstassoziation von N-Ras und K-Ras4B sowie die Bildung von Nanoclustern in der Zellmembran fördern. Es wird angenommen, dass die Bildung von Nanoclustern als Bindungsstelle für Effektorproteine dient, was für eine effektive Signalübertragung sowohl von N-Ras als auch von K-Ras4B wesentlich ist. Es kann auch zur

Überlappung von Nanoclustern der verschiedenen Isoformen der Ras-Protein kommen.

Um den zugrundeliegenden Mechanismus besser zu verstehen, untersuchten wir die simultane Lokalisierung von N-Ras und K-Ras4B und deren Auswirkung auf die laterale Organisation einer heterogenen Modellbiomembran mithilfe von AFM und FRET-Methoden. Es konnte gezeigt werden, dass N-Ras und K-Ras4B aufgrund der unterschiedlichen Eigenschaften ihres Membranankersystems nicht nur die Assemblierung in Pufferlösungen vermeiden, sondern auch nicht in der Membran kolokalisieren. Sie bilden einzelne Nanocluster, die unabhängig voneinander in den flüssigen Membranbereichen lateral diffundieren.

Die Entwicklung wirksamer K-Ras4B-Inhibitoren für Pharmazeutika erzielte bisher keine Erfolge, weshalb dringend neue Strategien zur Hemmung dieses onkogenen Proteins entwickelt werden müssen. Der Lysin-reiche Abschnitt der polybasischen Domäne von K-Ras4B ist für das Targeting von Wirkstoffen und die Lokalisierung innerhalb der Plasmamembran von wesentlicher Bedeutung. Mittels CD- und Fluoreszenzspektroskopie, konfokaler Fluoreszenz- und Rasterkraftmikroskopie wurde gezeigt, dass die molekulare Pinzette CLR01 in der Lage ist, effizient an den Lysin-Abschnitt in der polybasischen Domäne von K-Ras4B zu binden. Infolgedessen kommt es zur Dissoziation des K-Ras4B-Proteins von der Lipidmembran und zum Zerfall von K-Ras4B-Nanoclustern in der Lipiddoppelschicht. Diese Ergebnisse legen nahe, dass das Targeting der polybasischen Domäne von K-Ras4B durch molekulare Pinzetten eine wirksame Strategie zur Inaktivierung der K-Ras4B-Signalübertragung darstellen könnte.

Die Interaktion des Raf-Proteins mit K-Ras4B ist von großer Bedeutung, da diese ein Schlüsselschritt des MAP-Kinase-Signalwegs ist. Da die Isoformen B- und C-Raf im Cytosol durch Bindung an die inhibitorischen Domänen des Proteins 14-3-3 in einer geschlossenen Konformation vorliegen, müssen sie durch GTP-gebundenes, aktives K-Ras4B-Protein dephosphoryliert werden, um in die offene Konformation überzugehen. Durch AFM-Messungen konnte gezeigt werden, dass die Ras-bindende Domäne (RBD) von A-, B- und C-Raf K-Ras4B in der Lipidmembran erkennen können. Dabei binden B- und C-Raf-RBD auch an die Lipidmembran, was aufgrund des bisherigen Verständnisses über die Ras-Bindungsdomäne nicht zu erwarten war. A-

Raf-RBD hat einen zusätzlichen Effekt auf die Lipidmembran. Aus der gemessenen Höhe der A-Raf-RBD in der Lipidmembran, kann auf eine räumliche Ausdehnung im Vergleich zu A-Raf-RBD außerhalb von Membranen geschlossen werden. Das deutet darauf hin, dass A-Raf-RBD bevorzugt Nanocluster in der Lipidmembran bildet. Die RBDs von A-, B- und C-Raf bestimmen nachweislich die Population der Raf/K-Ras4B-Komplexbildung in der Lipidmembran. Da die Bildung von Raf/K-Ras4B für die Ras-Raf-Aktivierung von entscheidender Bedeutung ist, spielt die RBD von Raf möglicherweise eine Rolle bei der Regulierung der Raf-Aktivierung.

Abstract

Ras proteins are oncoproteins and play a major role in human cancers where they fail to switch off the signal for cell growth. More than 30% of human cancers are related to mutations of Ras proteins with K-Ras4B being the most frequently mutated isoform. They are plasma membrane localized molecular switches that function by shuttling between inactive GDP-bound and active GTP-bound forms. Signaling of K-Ras4B strongly depends on its correct localization in the plasma membrane.

C6-ceramide has been shown to inhibit the growth activity of K-Ras4B mutated cells. However, the mechanism underlying this inhibition remains elusive. We established a heterogeneous model biomembrane containing C6-cermaide and used this membrane to demonstrate that the addition of K-Ras4B leads to drastic changes in the lateral membrane organization. In contrast to the partitioning behavior in other membranes, K-Ras4B forms small, monodisperse nanoclusters dispersed in a fluid-like environment, in all likelihood induced by some kind of lipid sorting mechanism. Fluorescence cross-correlation data indicate no direct interaction among C6-ceramide and K-Ras4B, suggesting that K-Ras4B essentially recruits other lipids. Moreover, a FRET-based binding assay reveals that the stability of K-Ras4B inserted in the membranes containing C6-ceramide is significantly reduced. A molecular mechanism for the inhibition of K-Ras4B mutated cells' activity through C6-ceramide is postulated from the results of this study.

In vivo studies suggest that intermolecular interactions foster the self-association of both N-Ras and K-Ras4B and the formation of nanoclusters in the cell membrane. As sites for effector binding, nanocluster formation is thought to be essential for effective signal transmission of both N-Ras and K-Ras4B. To shed more light on the spatial arrangement and mechanism underlying the proposed crosstalk between spatially segregated Ras proteins, we studied the simultaneous localization of N-Ras and K-Ras4B and their effect on the lateral organization of a heterogeneous model biomembrane using AFM and FRET methodology. We show that, owing to the different nature of their membrane anchor system, N-Ras and K-Ras4B not only avoid

assembly in bulk solution, they also do not colocalize, but rather form individual nanoclusters which diffuse independently in the fluid membrane plane.

Development of effective K-Ras4B inhibitors has been challenging, hence new approaches to inhibit this oncogenic protein are urgently required. The polybasic domain of K-Ras4B with its stretch of lysine residues is essential for its plasma membrane targeting and localization. Employing CD and fluorescence spectroscopy, confocal fluorescence and atomic force microscopy we show that the molecular tweezer CLR01 is able to efficiently bind to the lysine stretch in the polybasic domain of K-Ras4B, resulting in dissociation of the K-Ras4B protein from the lipid membrane and disintegration of K-Ras4B nanoclusters in the lipid bilayer. It was shown that targeting of the polybasic domain of K-Ras4B by properly designed tweezers might represent an effective strategy for inactivation of K-Ras4B signaling.

Raf interaction with K-Ras4B is of great significance, which is the key step of MAPK signaling. Since B- and C-Raf proteins are autoinhibited in the cytosol with a closed conformation by binding of 14-3-3 and its inhibitory domains, they have to be recruited by GTP-bound, active K-Ras4B protein and dephosphorylated in order to be an open conformation. We found that A-, B- and C-Raf-RBD are all able to recognize the K-Ras4B in the lipid membrane. Interestingly, B and C-Raf-RBD directly bind to the lipid membrane, which was unexpected through the current understanding of Ras binding domain. A-Raf-RBD has a different effect on the lipid membrane. It was shown that the height of A-Raf-RBD in the lipid membrane is far beyond the size of A-Raf-RBD proteins, which indicates that A-Raf-RBD preferentially forms nanoclusters in the lipid membrane. Importantly, RBDs of A-, B- and C-Raf are proved to determine the population of Raf/K-Ras4B complex formation in the lipid membrane. Considering the formation of Raf/K-Ras4B is crucial for Ras-Raf activation, the RBD of Raf may plays a role in regulating Raf activation.

2. Introduction

2.1 Lipid and lipid model biomembranes

Throughout the living world, the cell membrane typically separates the interior of all cells from the outside environment that serves as the margin between life and death for individual cells. Biochemical and biophysical findings have provided a detailed model of the composition and structure of membranes (1, 2). It plays a crucial role in regulating cell signaling and controlling the transportation of substances in and out of cells. Through lateral segregation of lipids, proteins and cholesterol, liquid-liquid phase segregated lipid domains are formed in the cell membrane, which is known as the concept of lipid rafts (3). The lipid raft hypothesis has originally come from the properties that sphingolipid and cholesterol in vitro could facilitate lateral segregation in the membrane plane. This lipid-based sorting mechanism has been widely accepted in cell biology, such as the sorting of proteins to enter into specific exocytic and endocytic pathways and transient signalling platforms (4). Though the highly importance of this basic hypothesis in explaining many cell biological processes, proving their existence is problematic. The small size of lipid rafts and no defined ultrastructure limits the exploration by fluorescent microscopy. The limitations of the biochemical approaches make the biophysical study of model membranes more valuable (5). Lipid rafts in model membranes (10-100 nm) are clearly visible using atomic force microscopy (AFM). Since the morphology and composition of lipid model membranes can be tailored with great precision and resolution, it has been attracted more and more attention in exploring the protein-lipid and protein-protein interaction in lipid model membranes.

2.1.1 Discovery of the lipid membrane

The first try to discover the cell membrane by Robert Hooke in 1665 (6) led to a theory that cells contained a hard cell wall since only plant cells could be observed at that time. The finding of the plant cells could be separated in the early 19th century updated the cell theory that include animal cells, the ‘cell wall’ protected the cell from outside environment. In the end of the 19th century, the study of microscopists leads to a finding that a cell membrane existed instead of cell wall. Ernest Overton proposed that cell membranes were made of lipids at first time (7). In light of crystallographic studies and soap bubble observations, Gorter and Grendel proposed the lipid bilayer

hypothesis in 1925 (8). Since then, the theory of lipid membrane evolved into ‘lipid rafts’ which is now widely accepted by the researchers.

2.1.2 Lipid and lipid membrane structures

Lipids are broadly defined as a complex molecular class with enormous structural diversity, originating from various combinations of a hydrophilic polar head group and fatty acid chains. The presence of ethylene-interrupted or methylene-spaced double bonds on fatty acid moieties and various types of fatty acid linkages such as phosphodiester, ether and vinyl ether bonds to the glycerol backbone provide further diversity in lipids (9, 10).

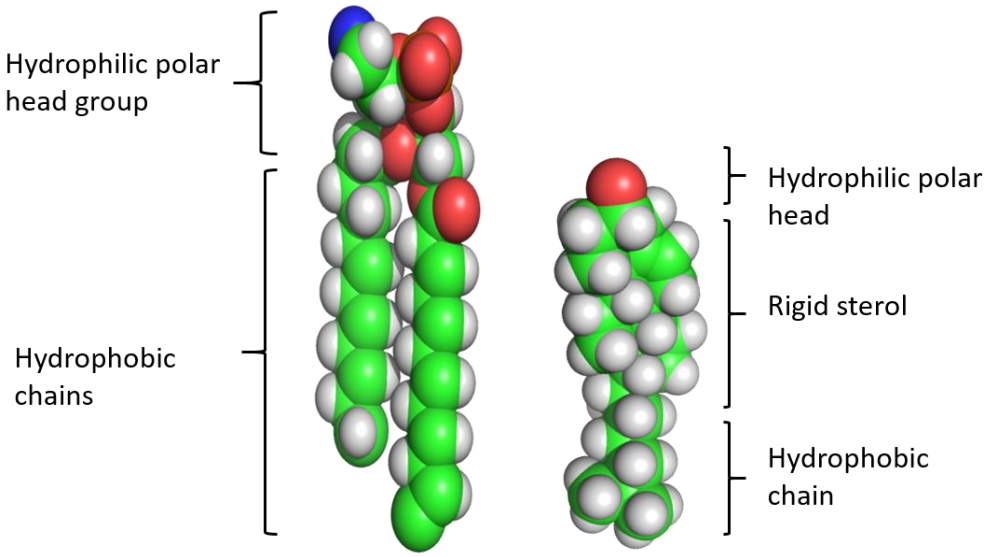

Figure 2-1 Sphere models of two major components of lipid rafts, DPPC (left) and cholesterol (right). Note, these models were generated using PyMOL.

Lipids play important roles in energy storage, cellular membrane formation and signaling processes in biological systems. Because of their relatively reduced state, lipids in the cells can be reused for energy storage, like triacylglycerol and steryl esters in lipid droplets. Due to the polar lipid structure including a hydrophobic and a hydrophilic portion, the lipid membrane can be formed with polar lipids. The self-association of hydrophobic moieties driven by water entropically and interaction of hydrophilic moieties with aqueous environments are the physical driving forces to form lipid membranes. Lipids can participate in signaling process via acting as first or second messengers in signal transduction and molecular recognition processes (11).

According to the structure of membrane lipids, the majority lipids consist of fatty acids, glycerophospholipids, sphingolipids, sterol lipids, prenol lipids, saccharolipids, and polyketides.

Table 2-1. Theoretical number of molecular lipids (11).

Type of lipid	# of molecular lipids in class
40 common fatty acids	40
40 fatty acid acyl-CoA	40
Monoacylglycerols	120
Diacylglycerols	4800
Triacylglycerols	64000
Phospholipids (6 classes)	9600
Ceramide and Sphingomyelin	>400
Glycosphingolipids	>100000
Cholesterol/Cholesterol ester	41
Total #	**180000**

2.1.3 Construction and application of lipid model biomembranes

Accumulating evidence suggests that the cellular membranes are laterally heterogeneous and distinct membrane compartments are present in the cell membrane (12). The lipid membrane raft hypothesis explains the lateral membrane inhomogeneity. It originally comes from the specific interactions between different lipids which induce the formation of ordered membrane regions that recruit other lipids and proteins (1). This hypothesis was supported by the observations of lipid model biomembranes, which clearly show that certain lipids have a preference to interact with other lipids and form large lateral domains (13). The physical state of these domain is considered to be a liquid-ordered (l_o) and liquid-disordered (l_d) phase. Comparing with the liquid-disordered domains, liquid-ordered domains have extremely ordered and tight packing. However, the presence and relevance of lipid raft in cell membrane are unclear. Even though several biochemical and biophysical studies have provided evidence of these domain in cell membranes and suggest that they play a key role in various cellular functions, the lack of direct observation of these domain renders this hypothesis of lipid raft still controversial.

2.1.3 Construction and application of lipid model biomembranes

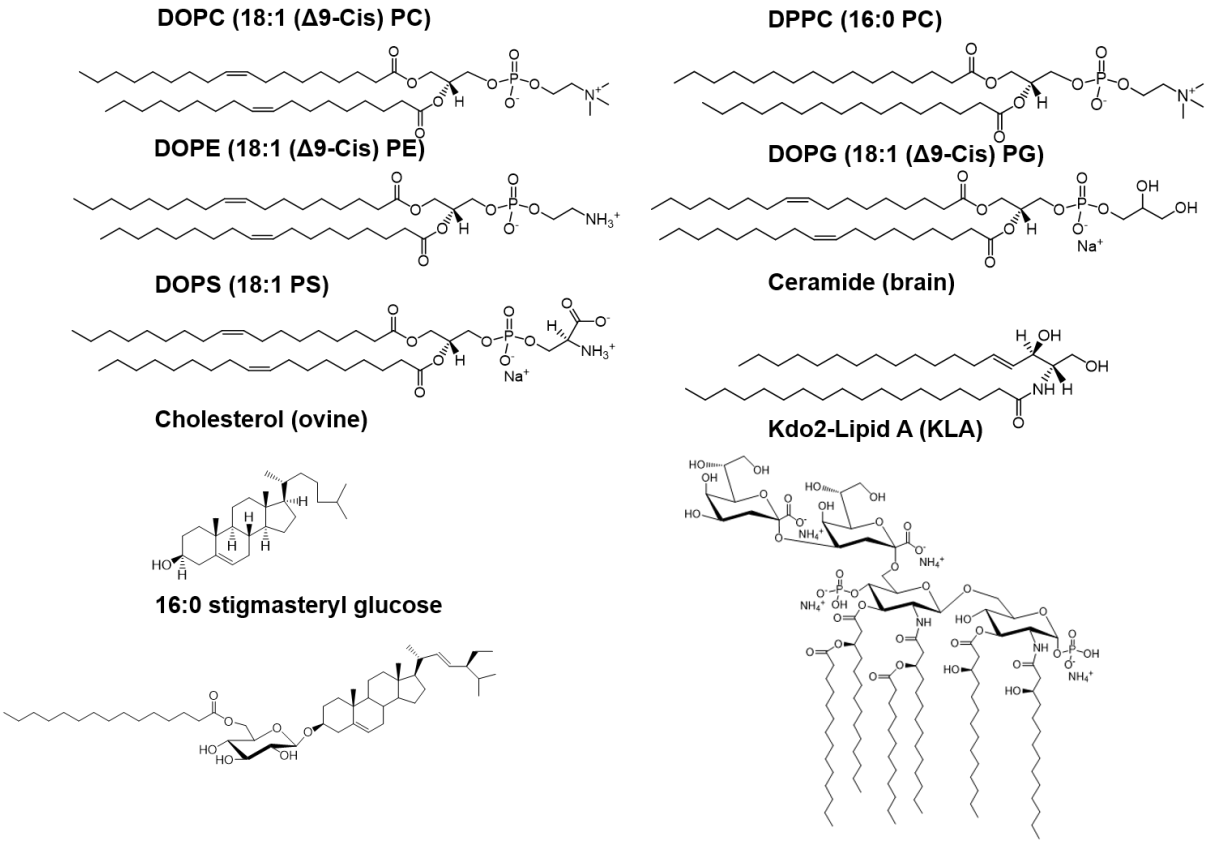

Figure 2-2 Several common lipids structures. The structures were adapted from the structure files attached in the Avanti Polar Lipids (Alabaster, Alabama, USA) company website using software ChemDraw 18.0.

As the formation of ordered domains and disordered domains is driven by lipid-lipid and lipid-protein interactions, these model membranes can be created by incorporation of certain concentrations of lipids. Since the morphology and composition of model membrane systems can be tailored with great precision and resolution, it allows us to reveal the interaction of lipidated proteins with lipid membranes. Different composition of lipids are likely to exhibit different phase behaviours (14). Phase diagrams are a valuable tool to establish lipid model membranes with variable lipid composition. The Gibbs triangle describes all possible combinations of the three different lipids. Any point inside the triangle represents one defined lipid composition. The techniques to study the phase behavior of such lipid mixtures are *X*-ray diffraction, fluorescence microscopy.

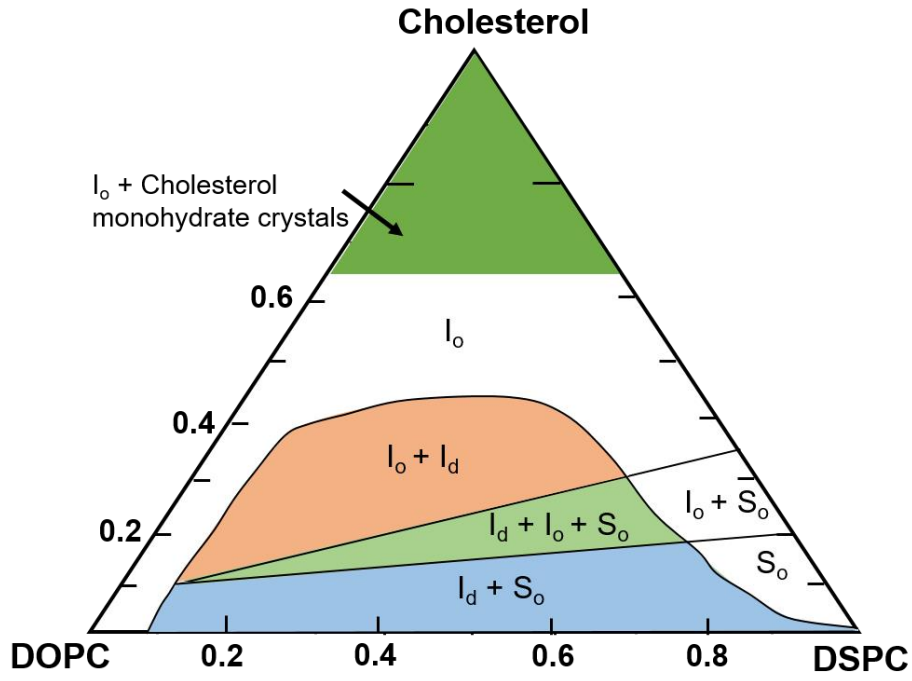

Figure 2-4 Schematic phase diagrams of DOPC, DSPC, and Cholesterol. l_o: liquid-ordered phase, l_d: liquid-disordered phase, s_o: solid gel phase.

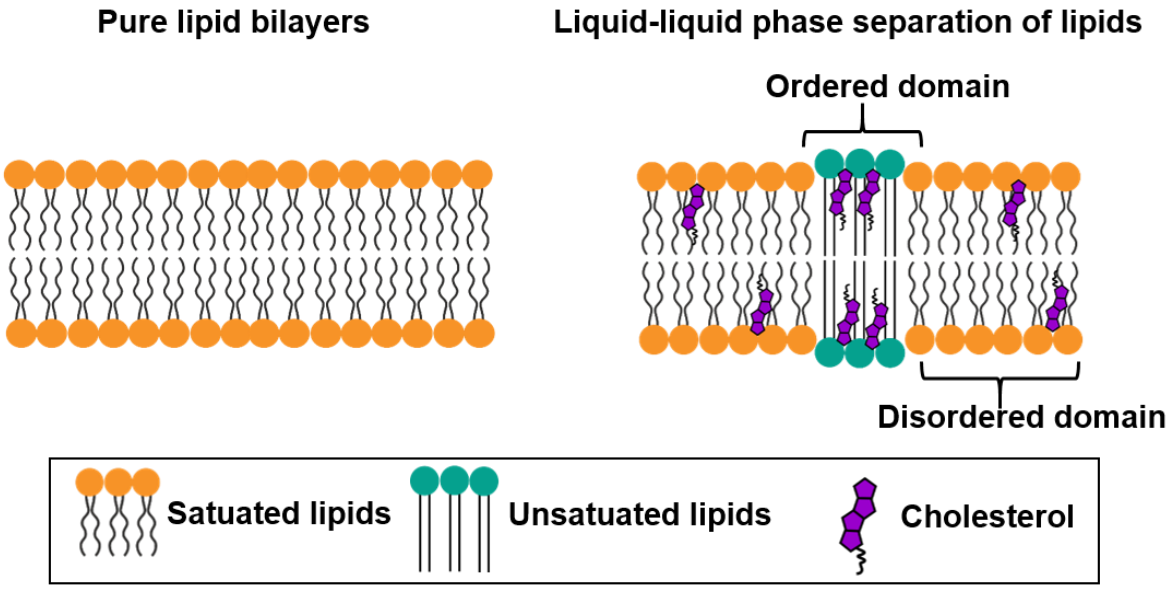

Figure 2-3 Lipid-associated membrane domains.

Biology and biophysics have always been intimately connected. Biological membranes fulfil a variety of cellular activities, such as acting as permeable barriers and platform for signaling activation and inactivation. Although light microscopy has been widely used to detect lipid domain structures and cell activities, the resolution is

limited to the wavelength of the light source (~200 nm) (4). It is believed that lipid rafts with small membrane domains (10-100 nm) play important biologic roles (15). The membrane proteins, including glycosylphosphatidyl inositol (GPI)-anchored proteins and lipidated proteins, and some Ras family proteins partition into lipid rafts. Ras proteins are known to form nanoclusters in the inner plasma membrane. The size of Ras protein nanoclusters is close to 4-6 nm (16, 17, and 18). Atomic force microscopy (AFM) offers nanoscale resolution for exploring the nanoscale properties of membranes. Supported lipid bilayers (SLBs) are valuable model membranes to study the interaction between

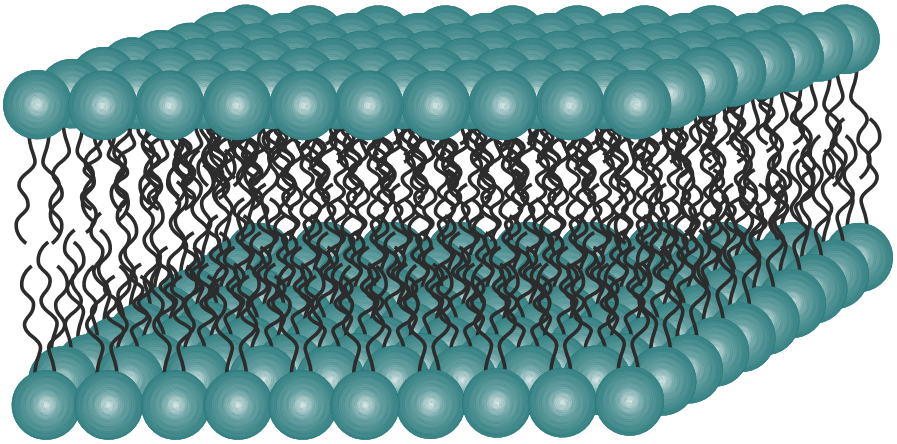

Figure 2-5 Structure of supported lipid bilayers.

lipidated proteins with the lipid membrane. The fusion of lipid vesicles on solid supports, usually mica, is the most popular method. Small unilamellar vesicles (SUVs) are first generated using standard procedures, e.g. 5 freeze-thaw-vortex cycles and extrusion. A small volume of SUVs with optimized concentration is deposed to freshly cleaved mica surface together with several microliters of buffer. To fuse SUVs on the mica surface, heating the systems at a temperature above the transition temperature (T_m) of the lipid composition is required. Finally, the SLBs are made by 2 hours fusion (Figure 2-5) (19). Although the exact mechanism of SLBs formation from SUVs is not fully understood, the process basically involves absorption of the SUVs on the mica surface, deformation and flattening (Figure 2-6).

2.1.3 Construction and application of lipid model biomembranes

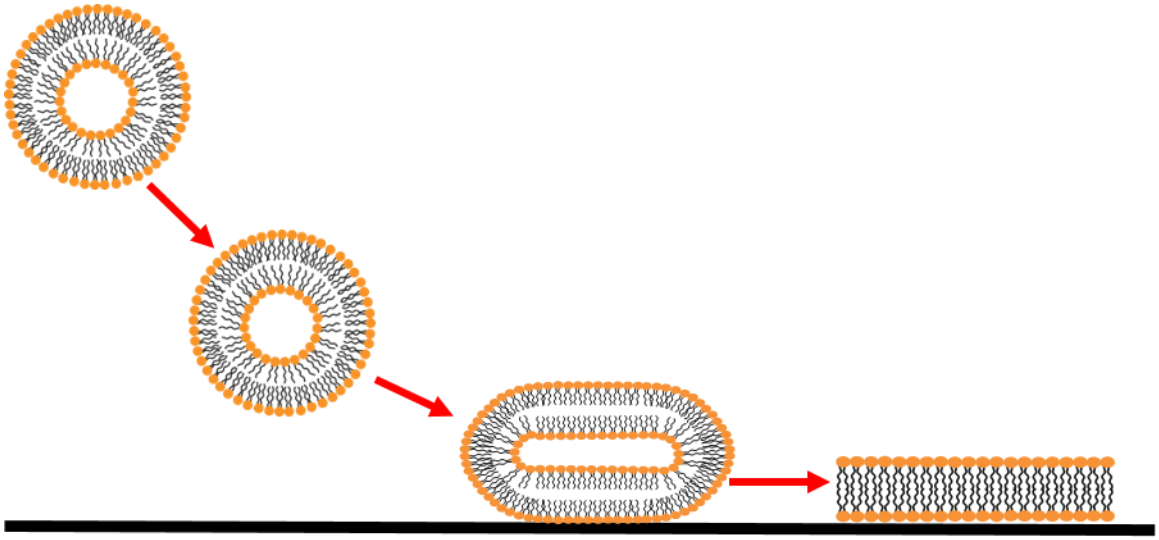

Figure 2-6 Fusion of lipid vesicles to prepare SLBs for atomic force microscopy analysis. Adapted from reference19.

Other widely used model membrane are giant plasma membrane vesicles (GUVs). They have been frequently used to explore domain dynamics and morphologies. Comparing the planar bilayers formed on mica of supported lipid bilayers, GUVs offer a micrometre-scale liquid-liquid phase separation model membrane with curvature (20). Combining a variety of florescence phase marker, fluorescence microscopy has proven useful to investigate different phases. However, cell membranes are present in a very complicated physical mixture with many different lipids and proteins. The proteins in biological membranes are estimated up to 25% of the area of the membrane. Also the ordered domain of GUVs has extremely high molecular order and tight packing, which is not the case in the cell membrane. Due to this limitation of GUVs, the giant plasma membrane vesicles (GPMVs) model membrane system was developed. Since the GPMVs are cell-derived, they contain most of the lipids and proteins in of cell plasma membrane. This makes the use of GPMVs more attractive than GUVs (21).

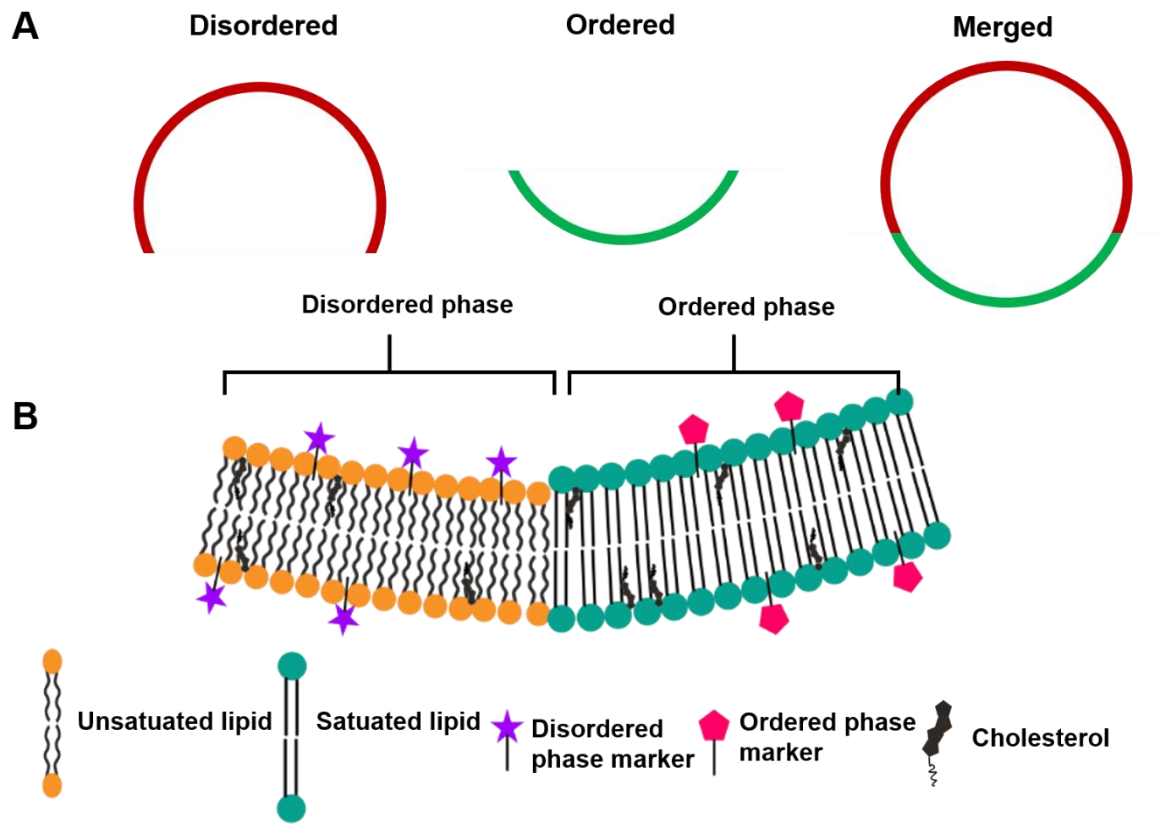

Figure 2-7 Giant plasma membrane vesicles (GUVs) as membrane system. (A) Fluorescent probes can be used to study raft phase-separated domains. For example, *N*-Rh-DHPE is used to label the disordered phase and DSPE-PEG-KK114 is used to label the ordered phase. (B) Representative scheme of the disordered and ordered domain with fluorescent probes inserted into the lipid membrane.

2.2 Function of Ras and Raf proteins

2.2.1 Function of Ras proteins

Ras is a small GTPase with a molecular weight of 21 kDa. It functions as a molecular switch, which regulates many cellular processes including proliferation, apoptosis and cell growth [22, 23]. Ras proteins are switching between an active GTP bound and an inactive GDP bound state in a tightly regulated cycle, which is controlled by guanine nucleotide exchange factors (GEFs) and GTPase-activating proteins (GAPS). The nucleotide-exchange leads to conformational changes between the switch-I and switch-II regions in the Ras proteins effector binding area [24].

There are four Ras protein isoforms, H-Ras, N-Ras, K-Ras4A, and K-Ras4B. They share a strongly conserved G domain (residues 1-164) in their N-terminal and differ significantly in their C-terminal with a hypervariable region (HVR) [25].

2.2.1.1 Ras function as a binary switch

Ras proteins act as a binary switch between a GTP- (active state) and GDP- (inactive state) bound state. In its active state, GTP-Ras binds to downstream effectors, leading to Ras-relative signaling pathway 'on'. Once inactivation of the signaling pathway is needed, Ras-GAPs bind to the Ras to increase the intrinsic hydrolysis rate of Ras proteins, resulting in exchange of GTP-Ras to GDP-Ras [26]. While Ras-GEFs catalyse the release of nucleotide allowing GDP-Ras to bind GTP. This GDP-GTP cycle functions as a binary switch, regulating Ras-related pathways. However, mutations of Ras proteins in cancer cells can impair the Ras-GAPs activity, leading to aberrant activation of downstream effectors [27, 28]. This makes Ras proteins constitutively active. Residues G12, G13 and Q61 are the three common mutation sites for Ras proteins. They account for more than 95% of identified mutations. During all the Ras isoforms, K-Ras4B is the most frequently mutated isoform [29].

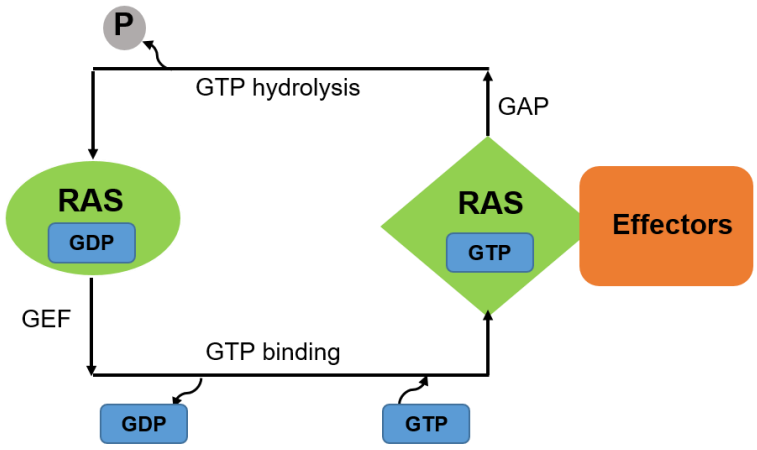

Figure 2-8 Ras GDP-GTP cycle. Ras proteins function as a binary switch. Ras-GAPs can increase the intrinsic hydrolysis rate of Ras proteins, which makes GTP-Ras exchange to GDP-Ras (inactive state). While Ras-GEFs catalyse the release of nucleotide GDP-Ras exchanges to GTP-Ras (active state).

2.2.1.2 Posttranslational modifications of Ras proteins

The Ras proteins share a highly conserved G domain, which is unique for the Ras superfamily. The G domain consists of six strands β-sheets and five α-helices. Ras

proteins are most frequently found in complex with GTP or GDP in cell or even after purification in vitro. Large conformational changes are observed in Ras proteins after exchanging of GDP to GTP. The mostly influenced regions are named ‘switch’ as they function as a switch to regulate the G-domain interaction with their effectors [30]. The five conserved fingerprint motif in the loops that cluster around the GDP and GTP binding site are often called G1-G5. G1 or also called P-loop is the glycine-rich phosphate-binding loop. It can directly interacts with the β- and γ-phosphate oxygen, which is crucial for nucleotide binding. The switch I (residues 32-38 in H-Ras) and switch II (residues 59-67 in H-Ras) localize to G2 and G3, respectively. Upon exchange of GDP to GTP, switch I is one of the regions involved with effector protein binding. The switch II region also involved in effector interaction and plays an important role in nucleotide exchange [27, 28].

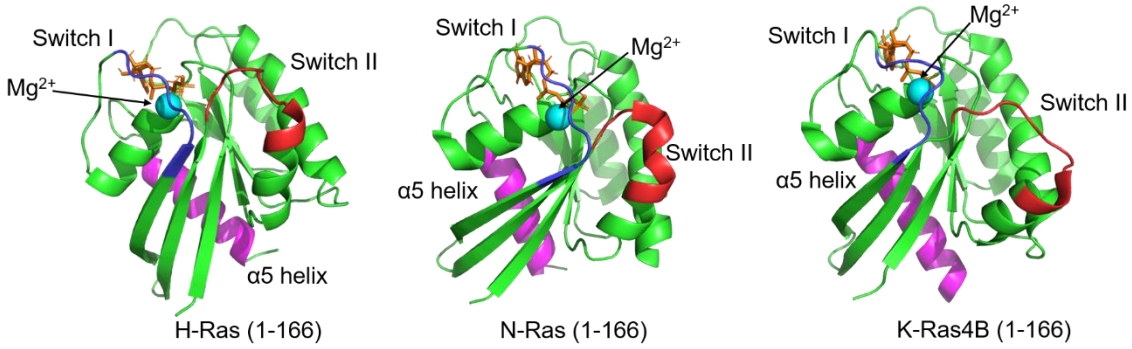

Figure 2-9 Ras protein structures. The switch I regions are colored in blue and the switch II are in red. The α5 helix is colored in pink. The pictures of H-Ras, N-Ras and K-Ras4B were generated using PyMOL with PDB 121P, 5UHV and 5V9O, respectively.

The three Ras protein isoforms differ significantly in the Ras C-terminal with the HVR domain. Ras proteins function strongly depends on its association with the plasma membrane [31, 32]. For this, Ras proteins need to undergo post-translational modification in their HVR domain. Association with the plasma membrane constrains Ras proteins in two dimensions, and thereby facilitates its interaction with Ras effectors and other Ras-related proteins. The CAAX motif localizes in the Ras HVR domain and three enzymes work sequentially on it [33, 34]. The first step is the prenylation of cysteine in the CAAX motif by one of two cytosolic prenyltransferases. If the ‘X’ is Leu, the cysteine in the CAAX motif will be added with a 20-carbon geranylgeranyl lipid tail by geranylgeranyltransferase I (GGTase I). If the ‘X’ is not Leu, which is the case of all Ras isoforms, then the cysteine in the CAAX motif will be added

with a 15-carbon farnesyl lipid tail by farnesyltransferase (FTase). In the most cases, Ras proteins are farnesylated since the 'X' is not Leu. However, Ras proteins can be geranylgeranylated by GGTase I when the activity of FTase is inhibited by farnesyltransferase inhibitors [35, 36, 37, and 38]. Farnesylation is not enough for Ras protein targeting the plasma membrane. Farnesylated Ras proteins are then transported to the cytoplasmic face of the endoplasmic reticulum (ER) membrane, where the next step modification occurs by Ras-converting enzyme 1 (RCE1) [39]. RCE1 is an endoprotease that can remove AAX amino acids in the CAAX motif. This modification renders the Ras protein a substrate of isoprenylcysteine carboxylmethyltransferase (ICMT), resulting in catalysing the methyl esterification of the α-carboxyl group of the farnesylcysteine [40, 41]. These modifications allow the Ras proteins' C-terminal to insert into the cellular membrane, leading by exchange of the Ras proteins C-terminal of a hydrophilic region to a hydrophobic region.

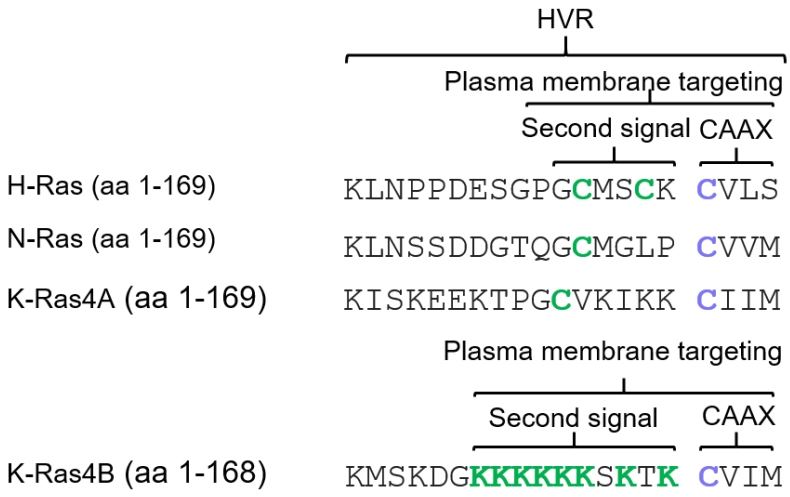

Figure 2-10 Post-translational modification (PTM) of the C-terminal membrane targeting region of Ras proteins. The cysteine of all Ras isoforms in the CAAX motif are farnesylated. The 'C' in green representing the cysteine in the HVR that is palmitoylated. In the case of H-Ras, N-Ras and K-Ras4A, the palmitoylation functions as a second signal, which is necessary for the plasma membrane targeting. While K-Ras4B cannot be palmitoylated, the polybasic domain (8 lysines, shown in green color) functions as the second signal instead.

Although the three modifications in the CAAX motif are necessary for the association and localization of Ras proteins with plasma membrane, this is still not sufficient. They require a second signal for plasma membrane targeting [32]. For H-Ras, N-Ras and K-Ras4A, palmitoylation functions as second signal, whereas the polybasic domain of K-Ras4B functions as the second signal since there is no other

cysteine in the HVR domain available for palmitoylation. H-Ras proteins have two more cysteine residues in the HVR domain, thereby two 16-carbon palmitoyl chains can be added as the second signal. For N-Ras and K-Ras4A, they only have one more cysteine residue in HVR domain, only one 16-carbon palmitoyl chain can be added as a second signal [42]. K-Ras4B is a unique Ras isoform since it cannot be palmitoylated. The polybasic domain of K-Ras4B functions as the second signal instead [32].

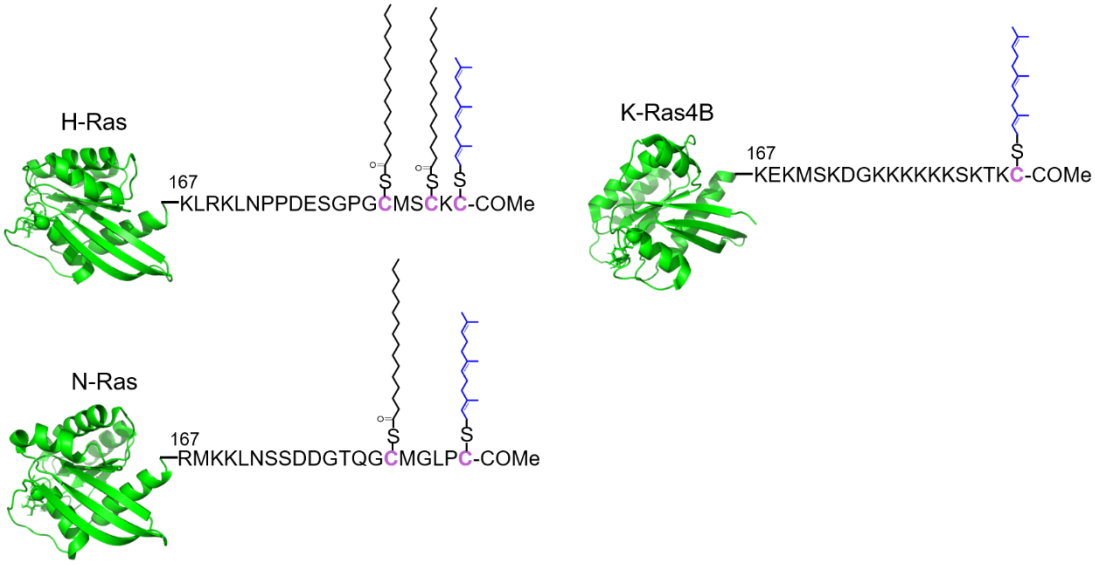

Figure 2-11 Schematic of the three human Ras proteins: H-Ras, N-Ras and K-Ras4B. The G domains are shown in cartoon representation using PyMOL with the PDB, 121P, 5UHV and 5V9O, respectively. The farnesyl and palmitoyl lipid chains are shown in black and blue color, respectively.

K-Ras4B was first reported to be phosphorylated by protein kinase C (PKC) at its C-terminal [43]. Recently, it has been reported that K-Ras4B phosphorylation reduces the electrical net charge of polybasic domain, leading to weak binding with the plasma membrane and accumulating on endomembranes. The phosphorylation site at K-Ras4B was mapped to be Ser181. While it seems that the PKC phosphorylation plays a crucial role in regulating K-Ras4B-membrane association, more studies are needed to understand how the physiological stimulus induces K-Ras4B phosphorylation and dephosphorylation [44, 45 and 46]. Besides the PTMs in the HVR domain, there are other modifications that also occur in Ras proteins. All three Ras isoforms were reported to have an ubiquitination and deubiquitination. Based on mutagenesis studies, many ubiquitination sites for H-Ras and K-Ras4B have been found. Such as on Lys117, Lys147 and Lys170, H-Ras proteins were found to be ubiquitylated as

monoubiquitylation and diubiquitylation. K-Ras4B proteins were found to be monoubiquitylated on Lys104 and Lys147. This modification was proved to enhance GTP loading and increase the K-Ras4B binding affinity with its effectors [47, 48].

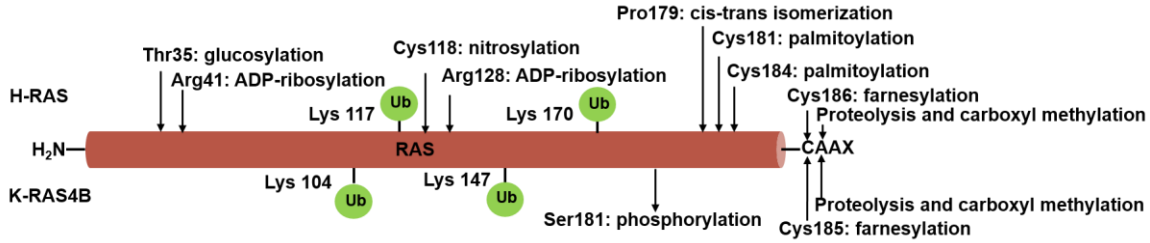

Figure 2-12 PTMs of H-Ras and K-Ras4B proteins. All reported PTMs of H-Ras and K-Ras4B are shown along the amino acid sequence of the Ras proteins. The ubiquitylation sites on H-Ras and K-Ras4B are shown with green spheres. All of these PTMs are related to Ras trafficking and signalling. Ub: ubiquitylation.

2.2.1.3 Ras proteins' cellular trafficking

Ras proteins trafficking starts with the nascent Ras proteins that were synthesized in the cytosol. FTase in the cytosol works on Ras proteins first [49]. Once farnesylated, the Ras proteins gain modest affinity binding with membranes, particularly with the ER membrane. The mechanism of how the farnesylated Ras proteins are delivered to ER membrane remains unknown. Since the RCE1 and ICMT also need to work on Ras proteins on the ER, the delivery of farnesylated Ras to ER is necessary. After the PTMs CAAX motifs are complete, Ras isoforms diverge in their subsequent trafficking. H-Ras, N-Ras and K-Ras4A are transported to the cytoplasmic face of the Golgi, where they are palmitoylated and then trapped in Golgi membranes. The way of delivering these proteins to plasma membrane is entering the secretory pathway. K-Ras4B proceeds with no palmitoylation, it cannot be trapped on the Golgi membrane. Recent study revealed that the chaperone protein PDE6δ is required for K-Ras4B trafficking to the plasma membrane [50]. Upon binding with PDE6δ, it favours passive diffusion of K-Ras4B and this makes K-Ras4B arrive at the plasma membrane.

2.2.1.4 Ras activation pathway and Ras effectors

Ras activity is regulated by Ras-GEFs and Ras-GAPs. Ras-GEFs can accelerate the slow intrinsic guanine nucleotide exchange rate of Ras proteins. Since the typical concentrations of GTP and GDP in cells and tissues are 0.3-0.5 mM and 0.03-0.06 mM, respectively, this favors formation for the active Ras-GTP complex [51, 52]. Once GTP-bound, Ras is considered to be nanoclustered. Ras effectors are recruited to the nanocluster and bind with Ras proteins [53]. In order to terminate the Ras signalling, Ras-GAPs bind to Ras and significantly accelerate its weak intrinsic GTP hydrolysis activity. However, Ras proteins are kept in a GTP-bound state when Ras proteins are mutated to impair GAPs intrinsic GTP hydrolysis activity. In normal cells, Ras proteins are predominantly GDP-bound (95%). Upon stimulation by growth factor, Ras-GEFs are activated, leading to exchange of GDP-bound Ras to GTP-bound Ras. When the Ras-GAPs are active, the intrinsic GTPase activity and GTP hydrolysis accelerate, resulting in restoring the inactive GDP-bound Ras protein state. [27, 28]

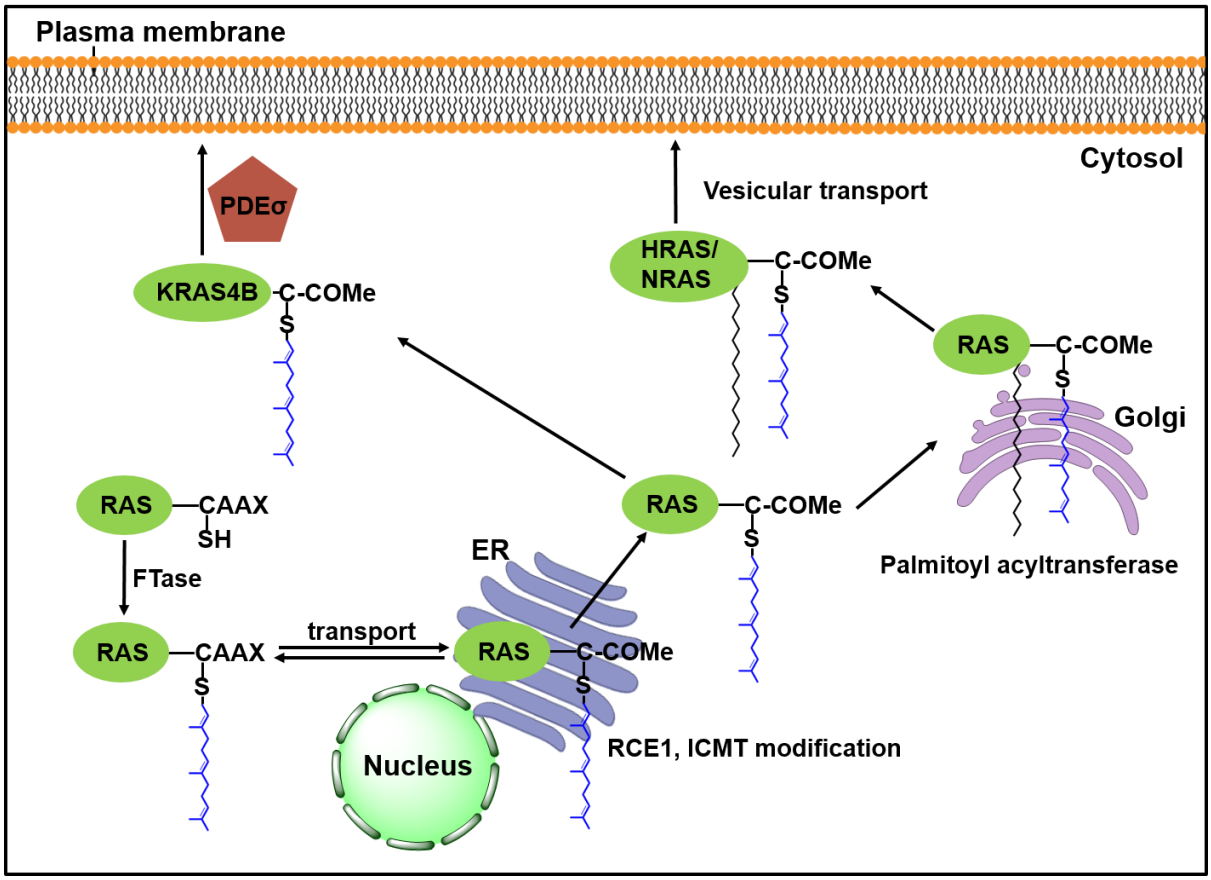

Figure 2-13 Ras proteins' trafficking. Endoplasmic reticulum: ER. Ras-converting enzyme 1: RCE1. Isoprenylcysteine carboxylmethyltransferase (ICMT). Farnesyltransferase: FTase.

There are more than 11 catalytic Ras effectors. The best characterized Ras effectors are Raf serine/threonine kinases, class I phosphatidylinositol-4,5-bisphosphate 3-kinases (PI3K) and Raf. Because of their frequent mutations in human cancer cells, their downstream proteins are also well characterized [53]. It was shown that Raf and PI3K signaling cascades can be used as drug targets [54].

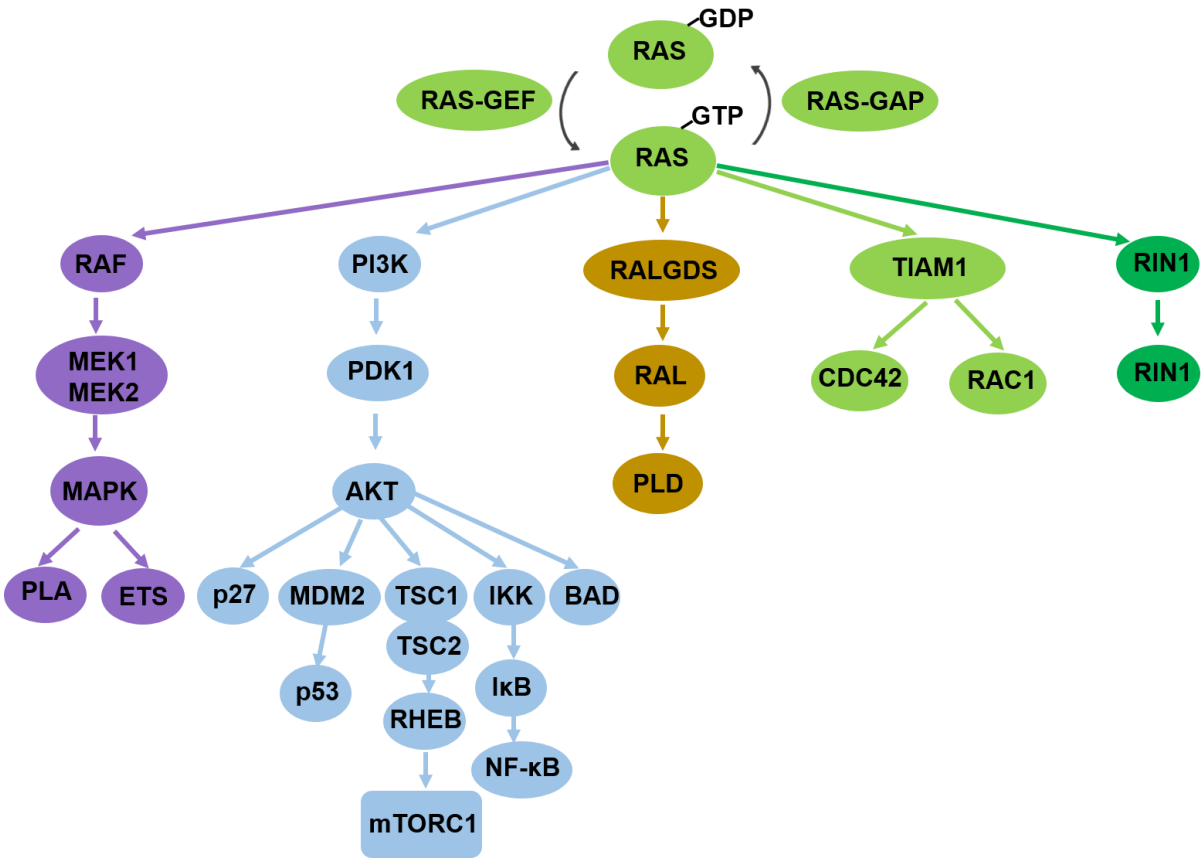

Figure 2-14 Ras effector signaling. GTP-bound Ras proteins bind to characteristic Ras effectors. MEK, MAPK/ERK kinase. PI3K, phosphoinositide 3-kinase. RALGDS, RAL guanine nucleotide dissociation stimulator. TIAM1, T lymphoma invasion and metastasis-inducing 1. RIN1, RAS and RAB interactor 1.

2.2.1.5 Ras nanoclusters

The three Ras isoforms are all lipidated proteins. Ras signaling strongly depends on their right localization in the lipid membrane. Recent studies suggest that a complex nanoscale spatial organization is also required for the biological activity of Ras proteins [55, 56]. The nanoscale spatial organization is normally called a nanocluster. This has been proved by both biological and biophysical studies [57].

2.2.1.5.1 Ras nanoclusters formation in the lipid membrane

The first observation of Ras nanoclusters in the cell was reported by the Hancock group [56]. They reported that Ras proteins are spatially segregates into domains with a radius of 8-9 nm, named nanoclusters. The technique they used is electron microscopy (EM) combined with fluorescence imaging [58]. Basically, GFP-tagged Ras proteins that are expressed in the inner plasma membrane are attached to EM grids, where gold nanoparticles are conjugated to an anti-GFP antibody. EM imaging was carried out and data analysis was carried out using Ripley's K-function. It was shown that only about 44% of Ras proteins were segregated into nanoclusters, while the other Ras proteins remained as monomers [58, 59, 60]. They also suggest that each nanoclusters contains 6-7 Ras protein molecules. The life times of these nanoclusters are reported to be very short, GDP-H-Ras has a lifetime shorter than 0.1 s, while GTP-H-Ras and GTP-K-Ras4B nanoclusters have a longer time of 0.5-1 s [61]. Although these experiments turned out to be crucial for understanding Ras signal transmission, further studies and other techniques are needed to yield additional mechanistic information on nanocluster formation.

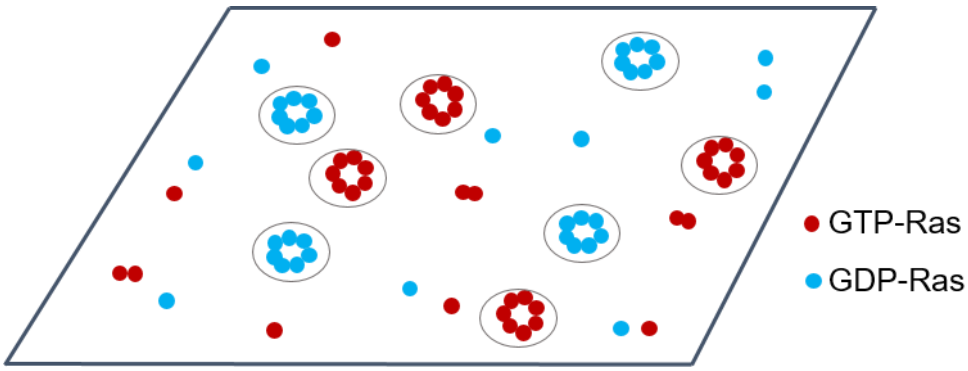

Figure 2-15 Ras proteins are segregated into nanoclusters and function a platforms for Ras effectors recruiting. Ras proteins form isoform- and guanine nucleotide-specific nanoclusters (56).

Later on, full-length and complete active semisynthetic K-Ras proteins were synthesized [62, 63]. Biophysical study of these semisynthetic proteins using atomic force microscopy (AFM) in tapping mode suggested that GDP- and GTP-bound K-Ras4B protein both can form nanoclusters in artificial lipid membranes. The size of the nanoclusters is about 1-1.5 µm. Height quantification analysis reveals a mean height of about 2 nm for GDP-bound K-Ras4B nanoclusters and a similar value of about 2.5

nm for GTP-bound K-Ras4B nanoclusters [16, 17]. This also suggests that the active-state of GTP-bound K-Ras4B proteins have a more pronounced clustering effect than inactive-state GDP-bound K-Ras4B nanoclusters. The observation of K-Ras4B nanoclusters by AFM is a direct observation and was explored in a controllable and in pure lipid systems.

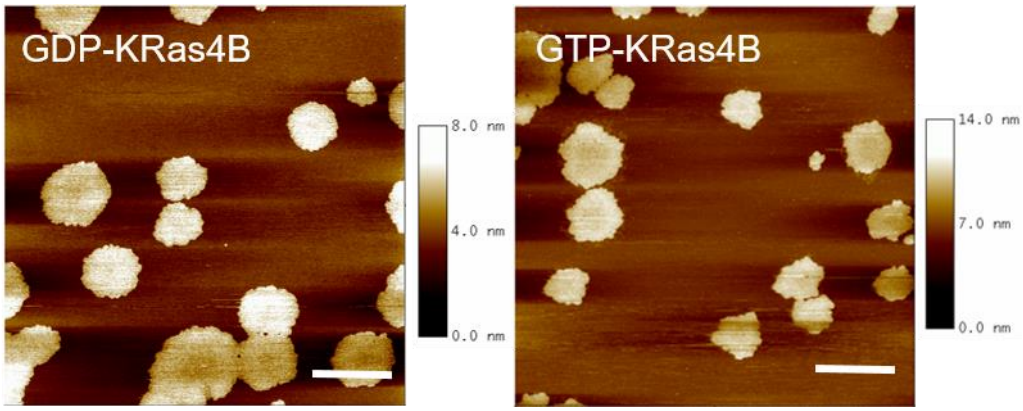

Figure 2-16 GDP- and GTP-K-Ras4B nanoclusters in the lipid membrane. Lipid membrane: DOPC. The concentration of both GDP-K-Ras4B and GTP-K-Ras4B is 2 µM. The scale bar is 1 µm. The measurements were performed on a tapping-mode AFM with a fluid cell. After incubation of GDP- and GTP K-Ras4B proteins in the lipid membranes, Tris buffer (20 mM Tris, 5 mM $MgCl_2$, pH=7.4) was used to wash the system in order to remove unbound K-Ras4B protein. AFM images were recorded with the resolution of 512 × 512 pixels.

2.2.1.5.2 The mechanism of Ras nanoclusters formation

Since studies showed that different Ras isoforms form different and distinct clusters, this suggests that different lipidated Ras isoforms favor different lipid environments. Additionally, the differences of G-domain orientation between lipid membrane and Ras proteins allows for different lipid sorting. Recent studies have shown that the lipid composition of the membrane has a significantly effect on Ras nanocluster formation [58, 64]. PS is suggested to be a structural component of K-Ras4B nanoclusters and cholesterol modulates the lateral separation of K-Ras4B nanoclusters [58, 65]. These findings were found by the combination of EM with the FLIM-FRET technique.

2.2.1.6 Ras and cancer

Ras proteins act as a binary switch and play a crucial role in cellular proliferation, survival and differentiation [66, 67, and 68]. The three Ras isoforms share 90% sequence identity in the G domain (1-164), where Ras effectors bind and nucleotide exchange occurs. In contrast, the Ras C-terminal exhibits significantly differences. This divergent domain is therefore referred to as hypervariable region (HVR) [69]. Ras-GEFs and Ras-GAPs modulate the Ras proteins' activity. Once activation of Ras signaling by the stimulation of growth factor occurs, Ras-GEFs can bind to GDP-Ras and catalyse the release of nucleotide allowing GDP-Ras to bind GTP. Since the intracellular concentration of GTP is 10-fold higher than GDP, this catalytic process is favoured [51-52]. Once bound to GTP, Ras is activated and forms nanoclusters to serve as a platform for recruiting Ras effectors. In order to stop Ras signaling, RAS-GAPs are recruited to bind to GTP-Ras and facilitate intrinsic GTP hydrolysis activity, resulting in rending the Ras state to GDP-bound and inactive state. In normal cells, Ras is predominately inactive state (~95%), while Ras can be continuously active in cancer cells where the Ras-GAPs activity is impaired [70, 71].

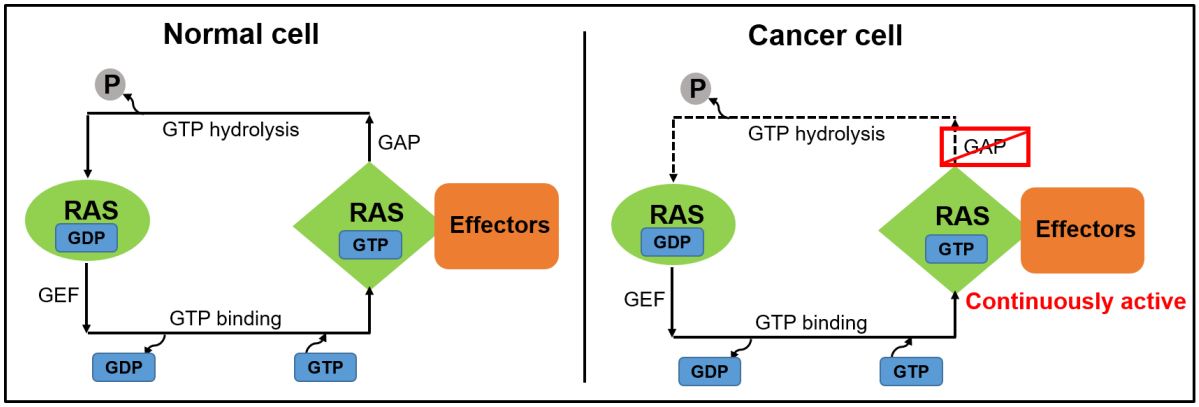

Figure 2-17 Regulation of the Ras GDP-GTP cycle in normal cells and in cancer cells. In the normal cells, the activation signal of growth factor stimulates Ras-GEFs to bind to GDP-Ras. As consequence of this binding, Ras-GEFs catalyse the release of nucleotide, allowing GDP-Ras to bind GTP. Once bound to GTP, Ras is activated and recruit its effectors to active Ras signaling pathway. When the signalings needed to terminate, Ras-GAPs bind to GTP-Ras and facilitate GTP hydrolysis, resulting in them forming GTP-Ras to GDP-Ras. However, in the cancer cells, the Ras mutations impair the Ras-GAPs' intrinsic GTP hydrolysis activity, which leads to a continuously active state.

Many Ras gene mutations were found after the first Ras gene was identified in human cancers in 1982 [72]. The most frequently mutated Ras isoform is K-Ras. The

available mutation data in human cancers show that K-Ras mutations contains 21.2 % of all mutations of human cancers [73]. This highly mutated portion makes the K-Ras most attractive as a drug target.

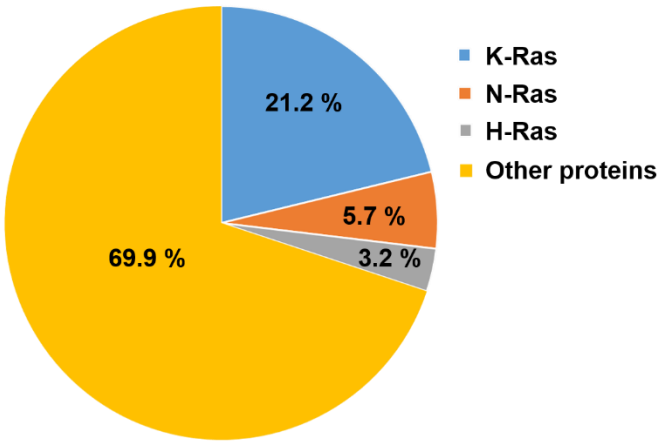

Figure 2-18 The Ras protein mutations occur in three Ras isoforms. This figure was adapted from the reference 73. K-Ras mutations contain 21.2 % of all the mutations of human cancers, followed by N-Ras with 5.7 % and H-Ras with 3.2 %. In total, Ras mutations contain 30.1 % in all the mutations of human cancers (74).

There is a preferential mutation of the three Ras isoforms in different human cancers. For the most frequent mutated Ras mutations in 15 common human cancers, K-Ras mutations play a predominantly role in pancreatic ductal adenocarcinoma, colorectal adenocarcinoma, multiple myeloma and lung adenocarcinoma cancers. N-Ras mutations play a predominantly role in skin cutaneous melanoma, thyroid carcinoma and acute myeloid leukaemia cancers. H-Ras mutations only play an important role in head and neck squamous cell carcinoma cancers [74, 75].

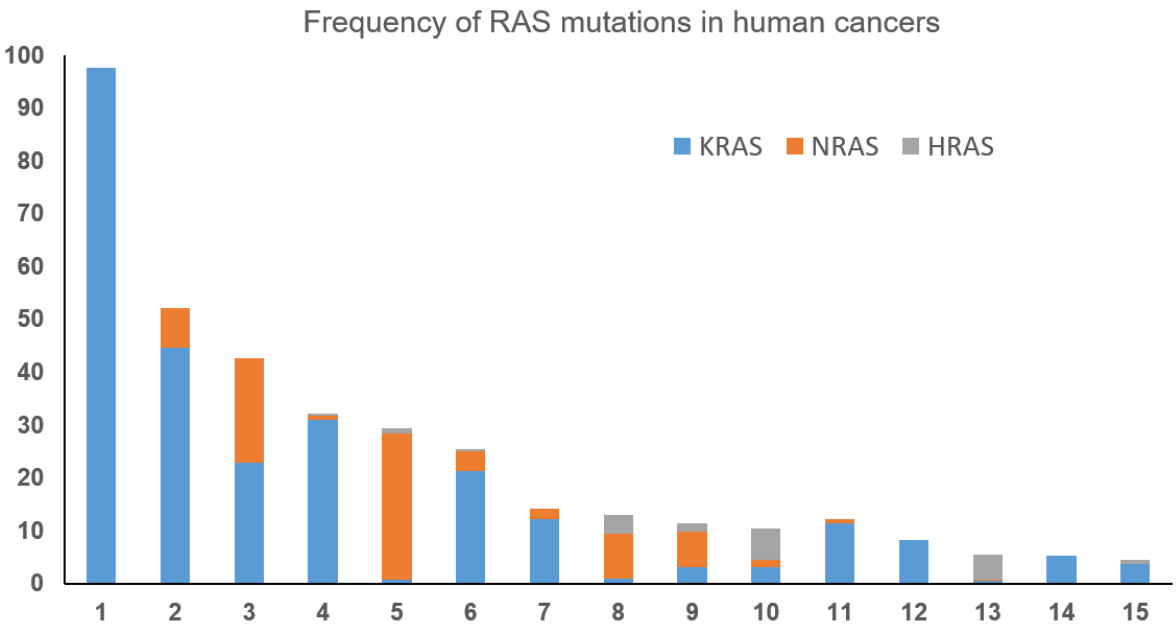

1: Pancreatic ductal adenocarcinoma 2: Colorectal adenocarcinoma 3: Multiple myeloma 4: Lung adenocarcinoma 5: Skin cutaneous melanoma 6: Uterine corpus endometriosis carcinoma 7: Uterine carcinosarcoma 8: Thyroid carcinoma 9: Acute myeloid leukaemia 10: Bladder urothelial carcinoma 11: Gastric adenocarcinoma 12: Cervical adenocarcinoma 13: Head and neck squamous cell carcinoma 14: Diffuse large B cell lymphoma 15: Oesophageal adenocarcinoma

Figure 2-19 Frequency of RAS mutations in human cancers. K-Ras mutations predominate in the cancers of pancreatic ductal adenocarcinoma, colorectal adenocarcinoma, multiple myeloma, uterine corpus endometriosis carcinoma, uterine carcinosarcoma, gastric adenocarcinoma. N-Ras mutations predominate in the cancers of multiple myeloma, skin cutaneous melanoma and thyroid carcinoma. H-Ras mutations predominate in the cancers of bladder urothelial carcinoma, head and neck squamous cell carcinoma. Adapted from reference 75.

2.2.2 Function of Raf proteins

Raf proteins mainly function as Ras effectors as far as we know. There are three known Raf isoforms: A-Raf, B-Raf and C-Raf. They share a similar sequence and conserved domain like Ras isoforms. Although these three Raf isoforms have many similarities, they still differ in cellular activities [76].

2.2.2.1 Raf function as Ras effector

Three Raf isoforms participate in the Raf-MEK-ERK pathway. Each of the Raf isoforms shares three conserved regions: CR1, CR2 and CR3 [77, 78]. The CR1 region contains a Ras-binding domain (RBD) and a cysteine-rich domain, where two zinc ions bind. It was shown that the RBD plays a critical role in Raf association with the switch I (amino acids 32-40) region of Ras proteins [79, 80]. RBD binding with switch I of Ras proteins is favoured by the multiple polar and hydrophobic interactions with the alignment of β-sheets between RBD and switch I of Ras proteins. The CRD was suggested to facilitate Raf protein binding to the plasma membrane and it can interact with distinct kinds of lipids in the plasma membrane [81]. GTP-bound Ras proteins recruit Raf proteins to the plasma membrane, leading to the activation of Raf proteins. The three Ras isoforms display different activities in Raf proteins. Generally, B-Raf and C-Raf can be activated in a similar way, whereas A-Raf is slightly activated by Ras proteins only [82]. Recent studies suggest that A-Raf might play aslo crucial roles in other signaling path ways [83].

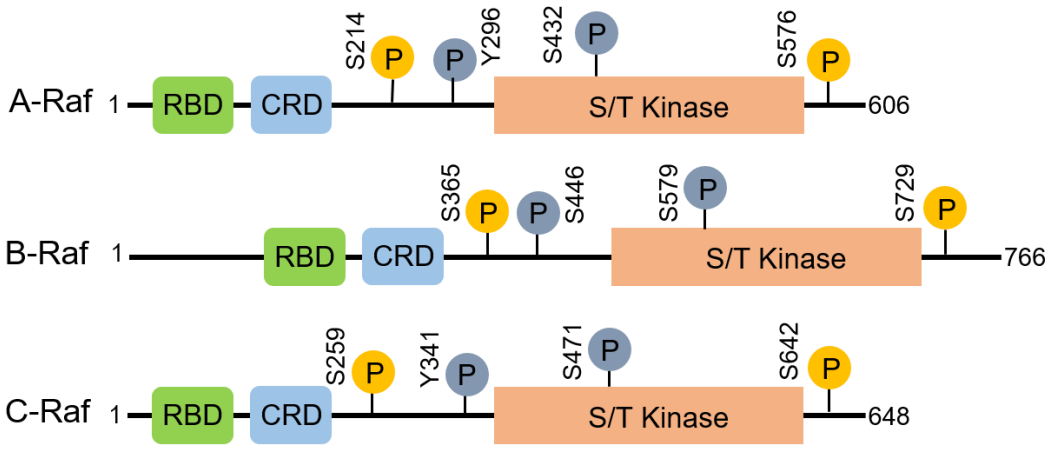

Figure 2-20 Scheme representation of the three components of Raf isoforms. RBD: Ras-binding domain. CRD: cysteine-rich domain. S/T: seine/threonine. P: phosphorylation.

There is still no reported structure of full-length Raf proteins. However, the structure of several RBD, CRD and kinase domains of Raf proteins alone was reported. RBD interacts with switch I of Ras proteins and CRD associates with the membrane and several distinct phospholipids [81, 84]. The kinase domain has a typical N-terminal lobe and large C-terminal lobe. The N-terminal lobe has an antiparallel β-sheet structure, where ATP can bind and orient. It has a glycine-rich ATP-phosphate-binding loop. The large lobe binds its substrates MEK1/2. These two lobes of the kinase

domain can open or close depending on the activation state [85]. The two conformation states regulate the Raf-MEK-ERK signaling process in concert with several other related proteins.

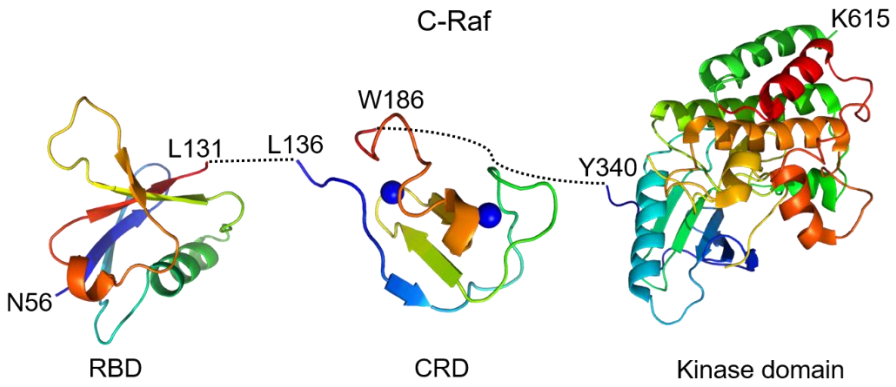

Figure 2-21 Crystal structures of the C-Raf-RBD (PDB: 4G0N), C-Raf-CRD (PDB: 1FAR) and C-Raf-kinase domain (PDB: 3OMV). Different domain structures are connected using dotted lines. The structural figures were generated using PyMOL.

2.2.2.2 The mechanism of the Raf proteins' pathway activation

The mechanism of Raf proteins activation is complex and still not fully understood. Different Raf isoforms are activated in a different way in the cell.

2.2.2.2.1 C-Raf activation

The inactive state of C-Raf proteins stays in a closed stable conformation by 14-3-3 proteins [86]. The S259 phosphorylation is dephosphorylated by PP1 phosphatase, leading to GTP-Ras efficient binding to C-Raf-RBD [87]. The further phosphorylated modification on the C-terminal region actives the C-Raf protein by Src, PAK and other kinases [88]. The next step is the dimerization. C-Raf can homo- or heterodimerize favoured by some scaffold proteins, like 14-3-3, KSR-1. When the dimerization is accomplished, C-Raf is highly active and phosphorylates its substrates MEK1/2 [89, 90]. As a consequence, ERK is also phosphorylated and being active. Ras-Raf signaling is then activated.

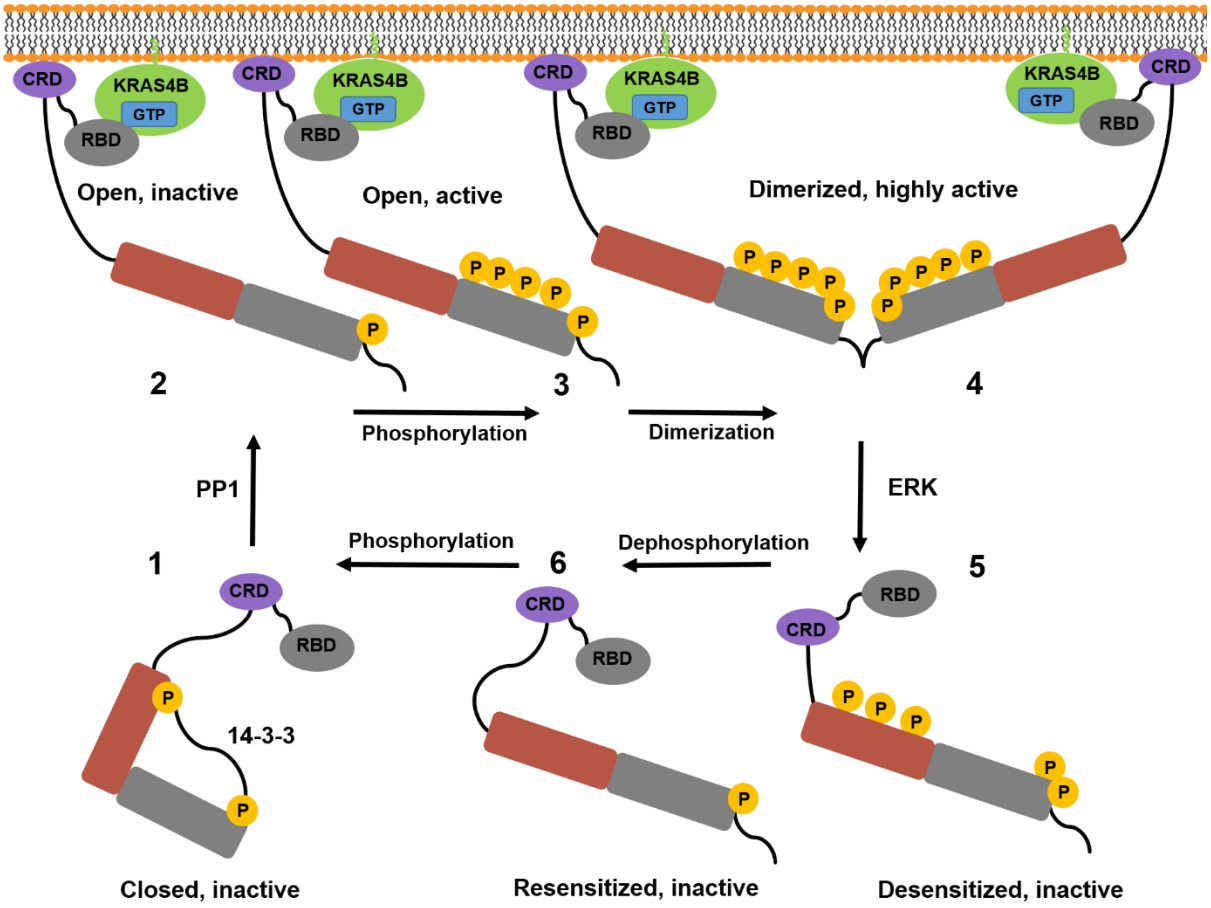

Figure 2-22 The Raf-proteins' activation pathway. As a consequence of stimulation, GDP-Ras proteins are exchanged to GTP-Ras proteins. PP1 dephosphorylates Raf in its closed, inactivated state, allowing GTP-Ras proteins recruit Raf to the plasma membrane. Once phosphorylation is accomplished, the Raf proteins form dimers and therefore are highly active. MEK1/2 bind to Raf proteins and phosphorylation occurs. ERK1/2 can be phosphorylated by MEK1/2 subsequently. Adapted from the references 87, 88, 89, and 90.

2.2.2.2.2 B-Raf activation

B-Raf proteins contain a highly negative charged N-terminal domain. Except for this difference, the mechanism of B-Raf activation is quite similar to C-Raf. It also requires Ras and 14-3-3 proteins to form a complex for activation. Subsequently, MEK1/2 and ERK1/2 are phosphorylated [91, 92].

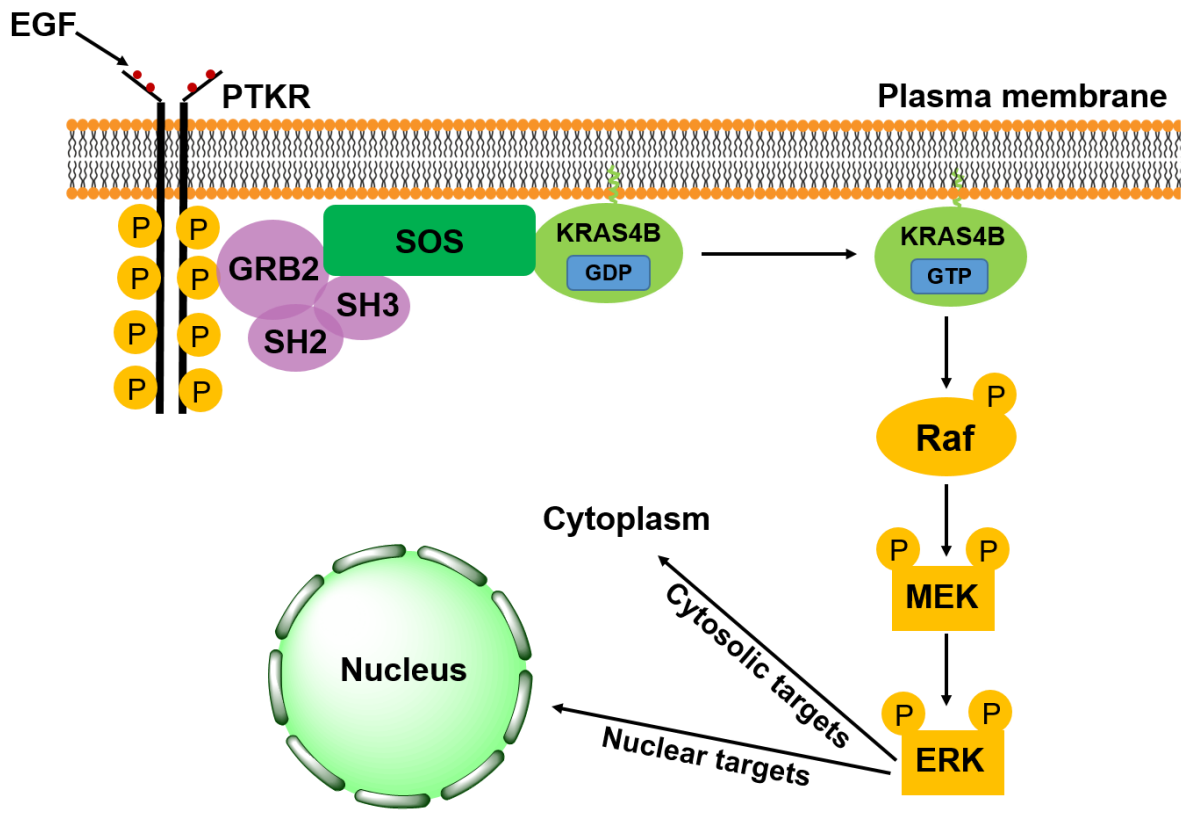

Figure 2-23 The Ras-Raf-MEK-ERK pathway. EGF: Epidermal growth factor. PTKR: Protein tyrosine kinase receptor. GRB2: Growth factor receptor-bound protein 2. SH2: Src homology 2 domain. SH3: Src homology 3 domain. SOS: Son of Sevenless. Raf: Rapidly accelerated fibrosarcoma kinases. MEK: Mitogen-activated protein kinase kinase. ERK: Extracellular signal-regulated kinases. Briefly, in the consequence of EGF stimulation, GRB2 binds to the phosphorylated PTKR. SOS, a Ras-GEF, binds to the SH3 domain of GRB2, resulting in the activation of Ras in the GTP-bound form. The Ras signaling cascade Ras/Raf/MEK/ERK will be subsequently activated.

2.2.2.2.3 A-Raf activation

Among the three Raf isoforms, A-Raf is the most poorly understood isoform. Observations suggested that A-Raf can only be activated weakly by GTP-Ras proteins. However, A-Raf signaling has been found in many other pathways, suggesting that A-Raf might play important roles in other cellular activities [93, 94].

2.2.2.3 Raf and cancer

Raf proteins have been found to play a role in cell cycle regulation, cell proliferation, differentiation and cell survival [94]. Insights from biochemical studies of Raf isoforms in mammalian systems and knockout studies in mice suggest that all Raf isoforms are

required for the normal cells. However, different Raf isoforms have distinct effects on various cancer type cells or genetically knockout mice models. Much of our understanding of the Raf proteins' function in cancer comes from the cell culture studies. Recent data from transgenic mice models improve our understanding of Raf proteins and cancer. C-Raf was reported to restrain apoptosis during embryogenesis and plays a crucial role in the development of the placenta, liver and haematopoietic organs by knockout studies [95]. B-Raf knockout mice die from vascular and neuronal defects [96]. Although A-Raf knockout mice are born alive, they die after one to three weeks [97]. In summary, it was shown that the three Raf isoforms are all required for sustaining life.

The Raf-MEK-ERK signaling cascade is necessary and sufficient for Ras signaling transformation. Considering Rafs' important function in Ras signaling, Raf has been validated extensively as a potential target for cancer therapies [94].

2.2.3 Function of SOS proteins

SOS (Son of Sevenless) is a widely distributed Ras-GEF protein. It plays a crucial role in regulating Ras signaling [98]. SOS has two human homologues, hSOS1 and hSOS2. The activation of Ras by SOS is crucial for many important signaling processes, such as cell growth, cell differentiation and the development of T-cells [99].

2.2.3.1 SOS proteins as GEF proteins

Ras proteins are membrane-anchored proteins which regulate many crucial signaling processes, such as cell proliferation, survival, apoptosis, morphology and metastasis. Ras proteins have two nucleotide binding state, the GDP-bound state as an inactive state and the GTP-bound state as an active state. They function as a binary molecular switch. The conversion from the inactive GDP-bound state to GTP-bound active state is favoured by guanine nucleotide exchange-factors (GEFs). The GTPase-activating proteins (GAPs) mediate GTP-bound active forms to become GDP-bound inactive forms [24]. The Ras-GEFs and Ras-GAPs regulate the level of active and inactive Ras proteins, which control the Ras signaling pathway [25].

The human SOS form (hSOS1) is a Ras-GEF protein, which controls the activation of Ras signaling. The activation of SOS contains many processes involving membrane recruitment, release of autoinhibition and allosteric modulation by Ras proteins. The

PxxP motif of the C-terminal proline-rich (PR) domain is thought to initially associate with the lipid membrane. SOS contains a series of N-terminal domains. They are a Db1 homology (DH), pleckstrin homology (PH) and a histone-fold (HF) domain, which inactive SOS proteins in solution. Upon association with lipid membranes, the autoinhibition is released. The allosteric pocket located at the REM and CDC25 domain (named as catalytic domain) binds to Ras proteins, resulting in full activation of SOS proteins [100, 101, 102]. Human SOS2 has a very similar domain architecture as human SOS1. Most studies has focused on human SOS1 [103].

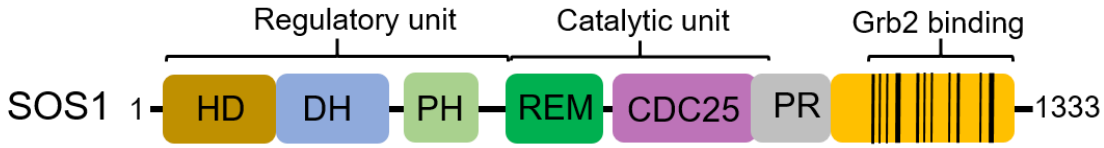

Figure 2-24 The domain architecture of full-length hSOS1 proteins (109).

2.2.3.2 SOS proteins' cellular pathway

The role of SOS1 as Ras-GEF has been explored extensively. Since Ras proteins play a crucial role in regulating the cell growth, survival, differentiation and many cellular fundamental processes, the activation of SOS1 is important for these cellular processes [104]. The Ras signaling pathway starts with the stimulation of the transmembrane tyrosine kinase receptor (EGFR) by EGF, resulting in activation by auto-phosphorylation of the receptor. The SH2 (Src homology 2) domain of Grb2 (growth factor receptor-bound protein 2) binds to the phosphotyrosine. Grb2 that can interact directly with RTK (EGFR or hepatocyte growth factor receptor). The cytosolic SOS1 can be recruited to the cell membrane as consequence of Grb2 binding to RTK. The N-terminal PH domain and the C-terminal proline-rich domain of SOS1 interact with the phosphatidic acid in the cell membrane. After localization of SOS1 in the cell membrane, the REM domain of the catalytic domain will undergo a rotation of a helical hairpin at the SOS1 catalytic site, allowing Ras binding and nucleotide exchange [105].

The structure of Ras-SOS1 complex reveals that SOS1 interacts tightly with Ras in a nucleotide-free state with a displacing mechanism [105]. The regions of Ras interacting most closely with SOS1 are the P-loop (residues 10-17), switch I (25-40)

and switch II (57-75). Helix α3 (57-75) is also found to interact with SOS1. The interface between Ras and SOS1 is very hydrophilic and extensive, which opens the nucleotide binding site as a consequence of the displacement of switch I of Ras [105, 106].

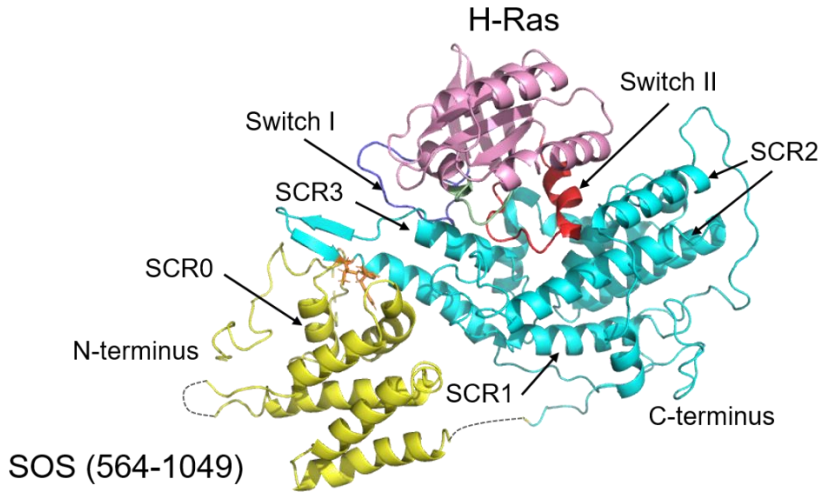

Figure 2-25 The complex of H-Ras (1-166) with human SOS1 (564-1049). The switch I and switch II regions of H-Ras are shown as blue and red, respectively. The region of Ras next to the switch I and switch II regions is shown in pink. The N-terminal domain of SOS (568-741) is shown in orange and the catalytic domain (752-1044) in cyan. Adapted from reference 105.

Since SOS1 is activated, GDP-bound Ras proteins can undergo nucleotide exchange to the GTP-bound active state. The Ras-ERK-MEK pathway will be subsequently activated, resulting in regulating a series of cellular activities [107].

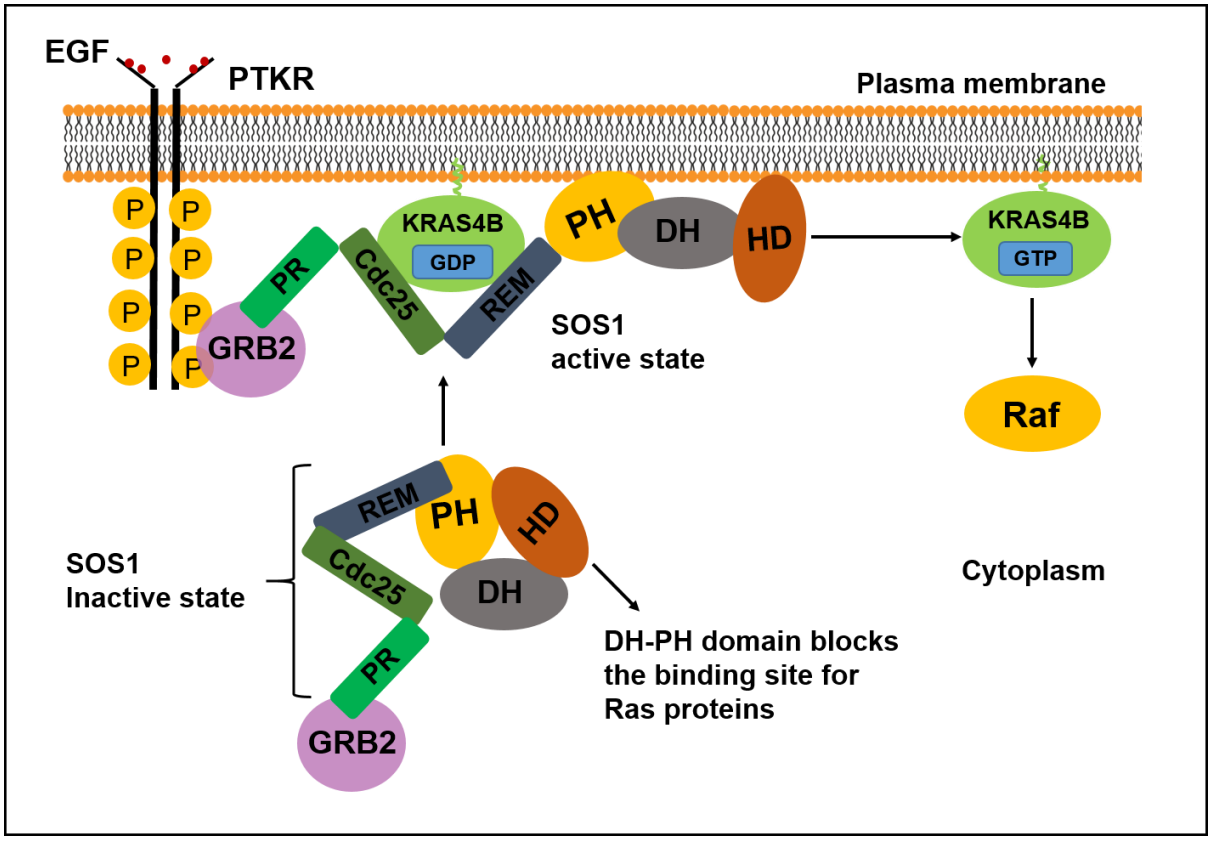

Figure 2-26 The activation of SOS proteins' cellular pathway. EGF: Epidermal growth factor. PTKR: Protein tyrosine kinase receptor. GRB2: Growth factor receptor-bound protein 2. SOS: Son of Sevenless. Raf: Rapidly accelerated fibrosarcoma kinases. MEK: Mitogen-activated protein kinase kinase. ERK: Extracellular signal-regulated kinases. Briefly, in the consequence of EGF stimulation, GRB2 binds to the phosphorylated PTKR. SOS, a Ras-GEF, which binds to the SH3 domain of GRB2, resulting in the activation of Ras in its GTP-bound form. The cellular pathway of SOS proteins will be subsequently activated.

2.2.3.3 SOS and cancer

Considering the activation of SOS proteins in the Ras signaling pathway, there are two main avenues for the design of inhibitors to block the activation of Ras by SOS. A nucleotide analogue of the SOS-Ras complex interface mimic could be designed to stabilize the complex, resulting in blocking the activation of Ras. Alternatively, displacement of the Ras binding site by some hydrophobic compound might effectively inhibit SOS activation. These are all indirect inhibition strategies of Ras activity through SOS proteins in cancer cells. Until now, there is still no cancer-related mutation in SOS reported [108, 109].

2.3 Ras protein inhibitors

The three Ras genes (H-Ras, N-Ras, and K-Ras) are the most frequently mutated genes in human cancers. K-Ras comprises two variable genes, K-Ras4A and K-Ras4B. Ras genes encode small GTPases (H-Ras, N-Ras and K-Ras), which have crucial roles in regulating cytoplasmic networks, including the Raf-MEK-ERK and PI3K-PDK1-AKT signaling cascades. Ras proteins can be an inactive state, GDP-bound Ras and an active state, GTP-bound state. They function as a binary molecular switch in regulating cellular signaling [25].

2.3.1 Ras proteins mutations

Ras mutations occur in cancer cells, which impair or greatly reduce the hydrolysis activity of GAPs which favours the formation of constituently active, GTP-bound Ras proteins. It was the important biochemical defect that prompted researchers and companies to develop inhibitors targeting mutant Ras proteins in cancer cells. At an early stage, there was an expectation that Ras-mutant driven cancers are a homogeneous subset of all cancers and one inhibitor can target a series of cancers. It turned out that each cancer type has its own preferably mutated site and specific mutations [110]. The development of inhibitors targeting Ras-driven cancers may need to be tailored to both the mutated site and the specific mutation.

Ras-driven cancer gene mutations comprise more than 30% of all cancer gene mutations [111]. Numerous genetic studies in mouse models suggest that expression of mutant Ras proteins is necessary for maintenance [112]. This makes Ras extremely attractive as a drug target for the treatment of Ras-driven cancers. Among all mutation isoforms, K-Ras is the predominantly mutated isoform (86%), followed by N-Ras (11%) and H-Ras (3%) [113]. It was found that 98% of Ras-related cancer mutations occur at residues G12, G13 and Q61. G12 mutations are predominant in H-Ras (35%) and K-Ras (83%), while Q61 mutations are found predominant in N-Ras (62%) [114]. The mutation sites are tremendously different among all the Ras-driven human cancers. In PDAC and CRC, K-Ras predominant mutations are G12D, while the major mutations are G12C in non-small-cell lung cancer (NSCLC) [115].

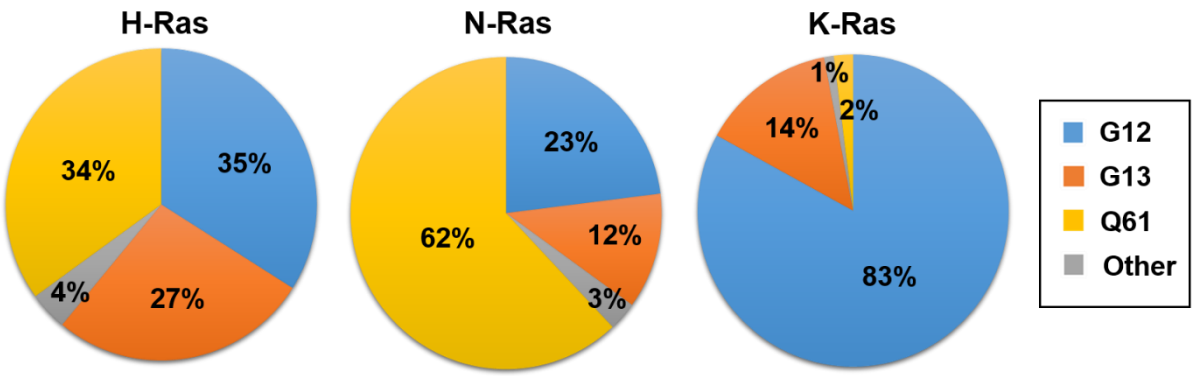

Figure 2-27 The frequency and distribution of Ras mutations in human cancers. In the mutations of H-Ras and K-Ras proteins, the G12 site predominates. In the case of N-Ras, the Q61 site predominates most mutations. The mutation frequency of the Ras proteins at the same sites differ significantly (114).

2.3.2 Strategy of developing inhibitors targeting Ras proteins

Since the mutated Ras genes are found in many human cancers and disruption of Ras function will impair the cancer cells growth, intensive efforts are made to develop inhibitors targeting Ras proteins in human cancers. However, despite more than 30 years of effort by pharmaceutical industry and academia, no effective drugs are found to be capable of fighting against the Ras-driven cancers [116]. Currently, many strategies of developing inhibitors targeting Ras proteins are on the agenda. Basically, any method that disrupts the Ras cellular function can be considered as a strategy of developing Ras inhibitors.

Ras proteins' signaling strongly depends on its correct localization in the lipid membrane [33]. Ras proteins require posttranslational modifications in their C-terminal CAAX motif. All Ras proteins can be farnesylated in the cytosol by farnesyltransferase. H-Ras, N-Ras and K-Ras variant split K-Ras4A can be palmitoylated as a second signal for membrane targeting, while K-Ras4B can't be palmitoylated because there is only one cysteine in the HVR domain of K-Ras4B. Instead, the polybasic domain (contains 8 lysine residues) in the HVR domain of K-Ras4B functions as a second signal [31, 32]. Many potent and selective farnesyltransferase inhibitors (FTIs) are developed. Despite the positive inhibition results of cell culture and mouse models with FTIs, FTIs failed to show any benefit in pancreatic cancer patients. Further studies showed that K-Ras and N-Ras can be geranylgeranylated for membrane targeting

when the activity of the farnesyltransferase was blocked [36, 37]. The high toxicity of FTIs with geranylgeranyltransferase-I enzyme (GGTase-I) limits the duration of FTIs with geranylgeranyltransferase-I enzyme inhibitors (GGTIs) in human cancers [38].

K-Ras4B is considered as a major target in fighting Ras-driven cancers. PDE- δ is reported to regulate the localization and signaling of K-Ras4B by facilitating its diffusion in the cytosol. Impairment of the binding between K-Ras4B and PDEδ suppress oncogenic Ras signaling by altering its localization to endomembrane. This finding might inspire drug companies and researches to develop inhibitors targeting K-Ras4B-PDEδ [117]. Inhibitors targeting the binding of K-Ras4B to PDEδ are still under the evaluation in clinic trials.

Oncogenic Ras signaling is highly involved in two classical and well-characterized pathways, Ras-Raf-MEK-ERK and Ras-PI3K-PDK1-AKT [118, 119]. Although Ras proteins are combined with multiple effectors, inhibition of one of these effectors is not enough to stop oncogenic Ras signaling in cancer cells [120]. Many inhibitors targeting the effectors of these two signaling pathways have been developed [120, 121]. However, the clinic evaluation of these inhibitors shows that inhibition of oncogenic Ras signaling using these inhibitors is limited.

Other strategies considered for fighting the Ras-driven cancers include targeting the GEFs (SOS1) [122], effector binding (B, C-Raf-RBD binding with Ras proteins) [123], metabolic changes in glucose and glutamine metabolism [124], autophagy [125, 126]. Since there is still no effective drugs for fighting Ras-driven cancers, new and effective strategies for developing Ras inhibitors are needed.

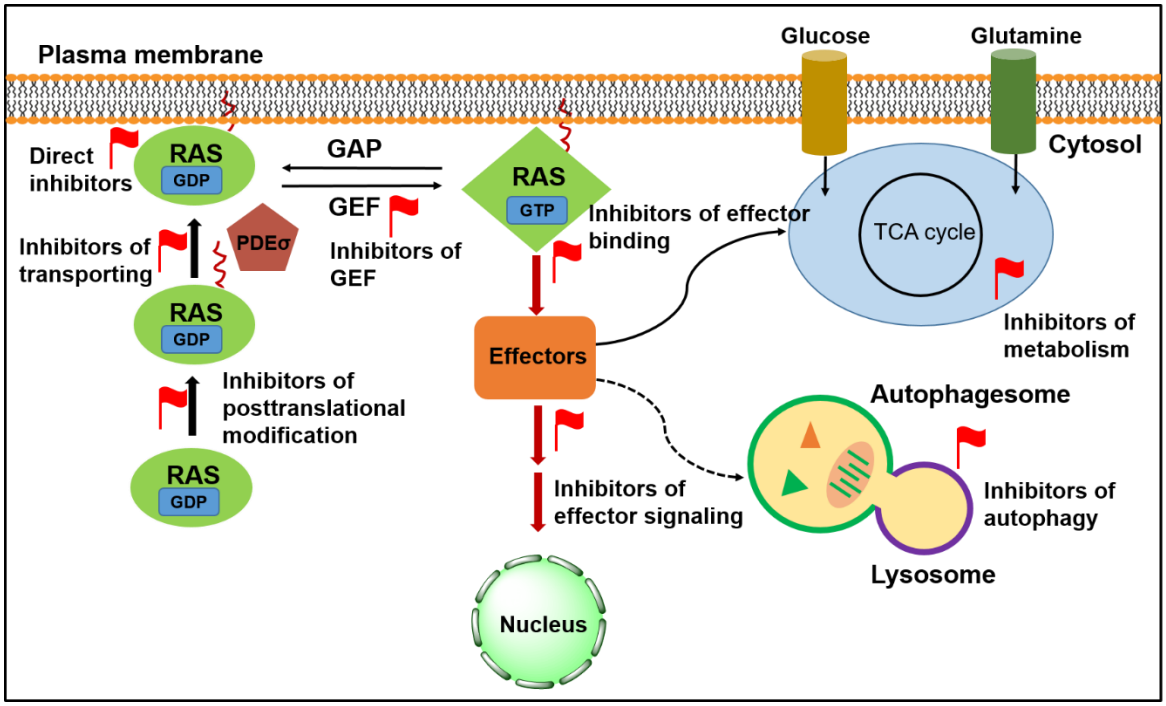

Figure 2-28 Schematic representation of the strategies for developing inhibitors targeting Ras proteins (160).

2.4 Chemical protein ligation

2.4.1 Native chemical ligation

Chemical synthesis is an attractive approach to generate polypeptides or proteins when applying the biological expression method is difficult. Synthesis of peptides or proteins provide fully modulation of the peptides or proteins in order to understand their function. Many signaling proteins regulate cellular signaling activities through the protein posttranslational modification [127]. However, total chemical synthesis or semi-synthesis of peptide or proteins is a great challenge.

In the early 1990s, the Kent lab developed a breakthrough approach for the chemical ligation using a chemoselective reaction to couple unprotected peptide segments in chemical protein synthesis [128]. In 1994, the approach of native chemical ligation (NCL) was introduced to synthesize a peptide, where two unprotected, synthetic peptide segments are coupled in mild aqueous conditions to form a native peptide bond at the ligation site [129].

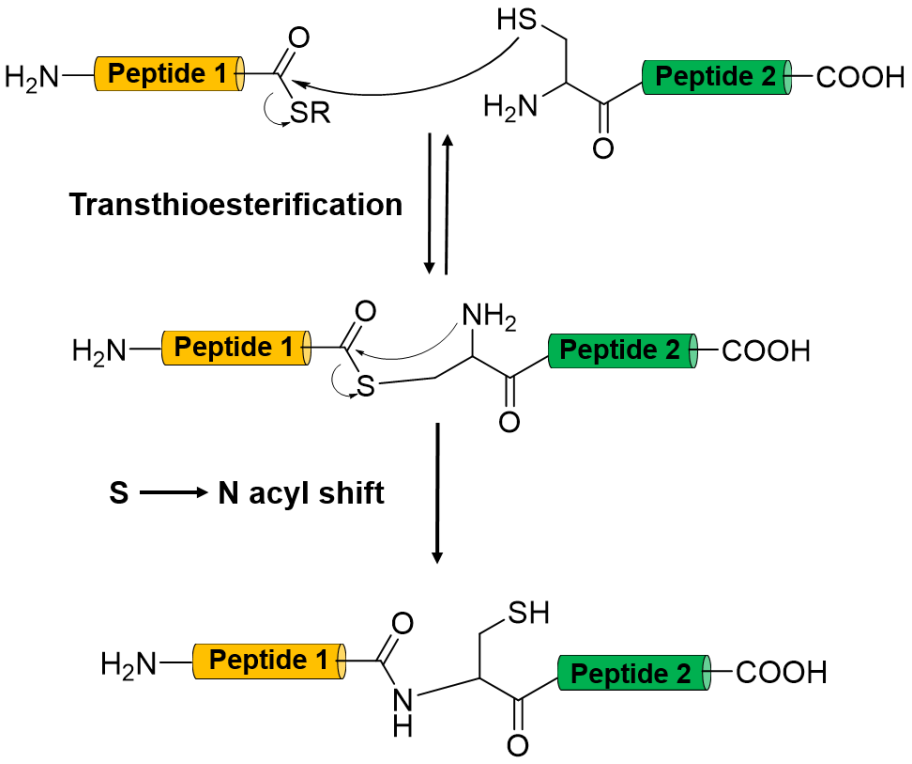

Figure 2-29 Principle mechanism of native chemical ligation. Peptide1 and peptide 2 are unprotected and coupled at aqueous and mild, neutral conditions. For native chemical ligation, one peptide should contain a C-terminal α-thioester and the other an N-terminal cysteine. A native peptide bond can be formed at the ligation site (129).

The mechanism of NCL is depicted in Figure 2-29. Briefly, this approach is based on the chemoselective reaction between one peptide containing an N-terminal cysteine and a C-terminal α-thioester. The initial step is the chemoselective transthioesterification with a reversible reaction, whereas the next step, the S → N acyl shift is irreversible and spontaneous. A native, amine bond is formed specifically at the ligation site even in the presence of an unprotected cysteine in the reaction system [130].

NCL can react at very mild, neural aqueous conditions and subsequently generate a native amine bond at the ligation site. These advantages makes NCL extremely attractive for the total synthesis of difficult peptide, small molecules and protein domains. NCL was also applied to synthesize full-length proteins with modification using the C-terminal thioester and N-terminal cysteine [131].

2.4.2 Expressed protein ligation

An N-terminal containing cysteine peptide is ligated to a second peptide containing a C-terminal α-thioester, resulting in formation of a native amine bond at the ligation site. Chemical synthesis of peptide or small molecule α-thioesters has enabled the total synthesis of peptides, small molecules and protein domains by using native chemical ligation. However, native chemical ligation has not been extended to synthesis of large proteins (beyond 15 KDa). Combined with cleavable tag recombinant protein expression technology, N-terminal cysteine residues can be produced. The difficulty of producing recombinant protein α-thioesters limits the extension to the protein synthesis field [132].

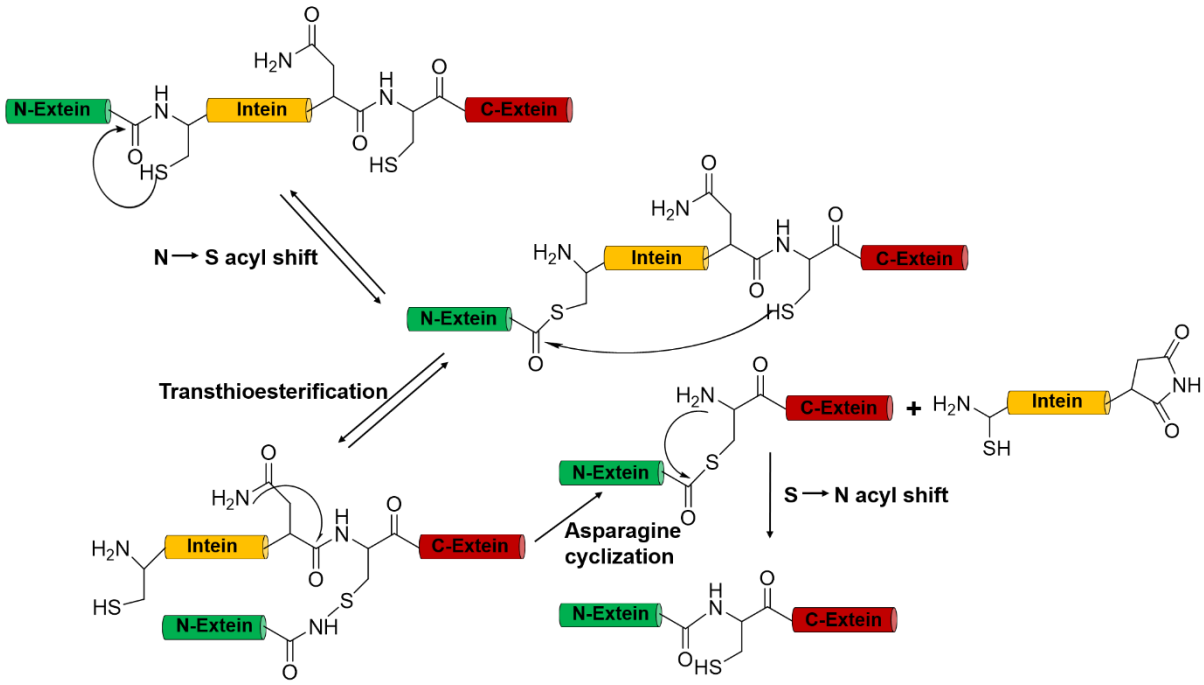

Figure 2-30 Schematic representation of the protein splicing mechanism (130).

Expressed protein ligation (EPL) has proven very useful for the synthesis of large proteins since the protein splicing was introduced to generate protein α-thioesters [132]. As shown in the figure 2-30, protein splicing is a process, where a protein undergoes intramolecular rearrangement, resulting in the formation of a α-thioester. The first step in protein splicing involves an N → S acyl rearrangement, where the N-extein moves to the side chain of an N-terminal cysteine. This process might be catalyzed by the intein domain itself. The side chain of a conversed cysteine residue

located at the N-terminus of C-extein attacks the thioester at N-extein. Transthioesterification occurs, followed by a cyclization reaction. In the end, the amine bond forms at the site between N- and C-extein.

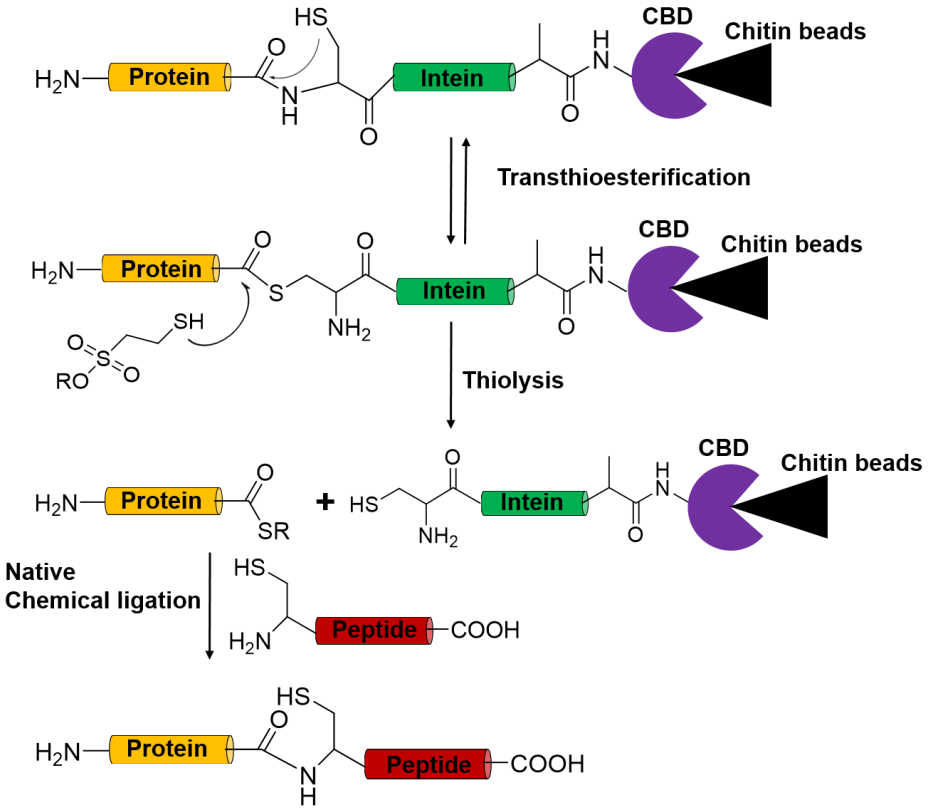

Figure 2-31 Principle of expressed protein ligation (EPL). Protein α-thioester can be produced using the intein technology, where a protein of interest is expressed in the frame fused with an intein-chitin binding domain (CBD) sequence. The second protein or peptide containing an N-terminal cysteine can be either chemically synthesized or expressed using a proteolytic cleavage method. Adapted from the reference 133.

The intein with a mutation of Asp to Ala has been applied to generate protein α-thioesters [133]. The C-terminal mutation of intein disturbs the completion of the intein splicing reaction but still keeps the N → S acyl shift to form a thioester intermediate. Thus, the protein of interest fuses to the N-terminal of the engineered intein that can be cleaved from the recombinant protein by thiol reagents. As shown in Figure 2-31, the final protein α-thioester can be produced using chitin beads for purification. Facilitated by NCL, site-specific modification of peptides or proteins can be

synthesized by EPL. Therefore, EPL provides a powerful tool to synthesize site-specific modified proteins and difficult to synthesize peptides [134].

3. Aims of this work

This work used a combination of chemical, biological and biophysical approaches to reveal Ras-related biological processes and to solve specific biological problems.

Ras proteins are o oncoproteins, which regulate a series of signaling processes that include cellular proliferation, survival and differentiation [135]. They are switching between an active GTP-bound, and an inactive GDP-bound state in a tightly regulated cycle, which is controlled by guanine nucleotide exchange factors (GEFs) and GTPase-activating proteins (GAPs). Once bound to GTP, Ras is considered activated. In normal cells, the Ras-GAPs can restore GTP-bound Ras to GDP-bound Ras using the intrinsic GTPase activity for GTP hydrolysis [136]. However, in cancer cells, mutations of Ras impair or greatly decrease the activity of Ras-GAPs, resulting in a persistently active, GTP-bound form. The signaling of Ras proteins strongly depends on its correct localization in the plasma membrane. All Ras proteins can be farnesylated by the farnesyl transferase (FTase) [31]. Beside this 15-carbon farnesyl lipid tail in the C-terminal CAAX cysteine, H-Ras, N-Ras have to be palmitoylated for membrane targeting. However, no additional cysteine residue can be used for K-Ras4B palmitoylation. Instead, a polybasic domain containing 8 lysine residues functions as a second signal for K-Ras4B membrane targeting [32]. Biological and biophysical studies have proven that Ras proteins form nanoclusters in the lipid membrane, which offers a platform for Ras effectors interacting with Ras proteins.

Since Ras protein are found in approximately 30% of human cancers, inhibition of the Ras proteins' activity in cancer cells emerged as a very promising approach [29]. Although enormous efforts are being made in developing inhibitors targeting Ras proteins, no effective drug capable of fighting Ras-driven cancers has been developed so far. The polybasic domain of K-Ras4B is essential for plasma membrane targeting and localization. We planned to rationally design a molecular tweezer by supramolecular chemistry targeting polybasic domain. A new strategy for inactivation of K-Ras4B signaling by targeting the polybasic domain of K-Ras4B using a properly designed molecular tweezer might be expected to be developed.

It has been reported that C6-ceramide can directly inhibit the growth activity of K-Ras4B mutated cells, and further analysis indicated that C6-ceramide induces cancer cell death synergistically with chemotherapy [137]. Another purpose of this work is to understand this inhibition mechanism and to provide a biophysical understanding of the interaction between K-Ras4B and C6-ceramide in the membranous context.

In vivo studies suggest that intermolecular interactions foster the self-association of both N-Ras and K-Ras4B and the formation of nanoclusters with in the cell membrane. As the only site for effector binding, nanocluster formation is thought to be essential for effective signal transmission. Further, it has been reported that a lipid-mediated effect can induce a cross-talk between spatially segregated H-Ras and K-Ras4B. In this study, we wanted to probe the colocalization of N-Ras and K-Ras4B lipoproteins in model biomembranes.

Raf proteins mainly function as Ras effectors and participate in the Ras-Raf-MEK-ERK pathway [76]. Raf has three isoforms, A-Raf, B-Raf and C-Raf. They share the membrane targeting conserved region, CR1. The CR1 region contains a Ras-binding domain (RBD) and a cysteine-rich domain (CRD). Crystal structure of Ras-Raf-RBD complex proves that RBD binds to the switch I (amino acid residues 32-40) region of Ras proteins, which is favoured by multi-polar and hydrophobic interactions [80]. Biophysical and simulation studies suggest that the CRD can interact with distinct lipids in the lipid membrane and further supports Raf proteins with lipid membrane [81]. The kinase domain of Raf proteins is connected to the CRD with a very long and flexible linker, which supposes that the kinase domain stays in the cytosol and interacts with the ERK and other Raf-related proteins. Biological studies indicate that B- and C-Raf can be activated in a similar way, whereas A-Raf is only slight activated by Ras proteins [76]. This suggests that besides the function of membrane targeting for Raf proteins, Raf membrane targeting region might play an important role in regulating the interaction of Ras and Raf. Another purpose of this study was to identify and characterize the interaction of Raf and Ras proteins in the lipid membrane.

SOS1 is a Ras-GEF protein, which regulates the nucleotide exchange of GDP-Ras to GTP-Ras[98]. The activation of Ras by SOS1 is crucial for a series of cellular processes, which is autoinhibited by several N-terminal domains in solution. SOS1 associates with the lipid membrane via the PxxP motif in the C-terminal PR domain

with Grb2 [100]. Located in the lipid membrane, the autoinhibition is released through the interaction with membrane lipids [102]. In this work, we wanted to explore the SOS1 interaction with K-Ras4B and the lipid membranes in order to gain fully understanding of the mechanism of Ras activation by SOS1.

4. Results and Discussion

Part of the work (chapter 4.1, 4.2 and 4.3) herein has been published in the following peer-reviewed research articles and subsequently reprinted in parts with the permission of the journals. The contributions of co-authors are either distinctly marked or not shown as they are a result of this thesis.

1. L. Li, N. Erwin, S. Möbitz, F. Niemeyer, and T. Schrader, R. Winter. "Dissociation of the Signaling Protein K-Ras4B from Lipid Membranes Induced by a Molecular Tweezer." *Chem. Eur. J.*, 25 (**2019**), 9827 – 9833.

Copyright: was published online on 29 September, 2019 and DOI is 10.1002/chem.201901861. In this publication is partially reproduced in section 4.3 with the permission by John Wiley & Sons, Inc. Copyright ©2015Wiley-VCH Verlag GmbH & Co. KGaA, Weinheim.The used text paragraphs and figures were reformatted to the format of thesis (e.g. text font, reference and figure numbering). In addition, the figures of Supporting Information were moved to the main text and the Methods and Materials section were moved to the part of Chapter 5, Materials and Methods.

Author contribution: R. W. and T. S. designed the research, L. L., N. E., S. M., and F. N. performed the research, L. L. and F. N. analyzed data, L. L., T. S. and R. W. interpreted the data and wrote the paper with refinement by all co-authors.

2. L. Li, M. Dwivedi, S. Patra, N. Erwin, S. Möbitz, and R. Winter. "Probing Colocalization of N-Ras and K-Ras4B Lipoproteins in Model Biomembranes." *ChemBioChem*, 20 (**2019**), 1190-1195.

Copyright: was published online on 02 January, 2019 and DOI is 10.1002/cbic.201800776. In this publication is partially reproduced in section 4.2 with the permission by John Wiley & Sons, Inc. Copyright ©2015Wiley-VCH Verlag GmbH & Co. KGaA, Weinheim.The used text paragraphs and figures were reformatted to the format of the thesis (e.g. text font, reference and figure numbering). In addition, the figures of the Supporting Information were moved to the main text and the Methods and Materials section were moved to the part of Chapter 5, Materials and Methods.

Author contribution: R. W and L. L designed the research, L. L., M. D., S. P., N. E., S. M., performed research, L. L. analyzed data, L. L. and R. W. interpreted the data and wrote the paper with refinement by all co-authors.

3. L. Li, M. Dwivedi, N. Erwin, S. Möbitz, P. Nussbaumer, and R. Winter. "Interaction of K-Ras4B Protein with C6-ceramide Containing Lipid Model Membranes", *Biochim. Biophys. Acta, Biomembr.,* 1860 (**2018**) 1008-1014.

Author contribution: R. W. and L. L. designed the research, L. L., N. E., S. M., performed the research, L. L. analyzed data, L. L. and R. W. interpreted the data and wrote the paper with refinement by all co-authors.

4. Results and Discussion

4.1 Interaction of K-Ras4B protein with C6-ceramide containing lipid model membranes

4.1.1 The function of C6-ceramide in cells and targeting K-Ras4B-driven cancers

Ras proteins are involved in cellular signaling pathways regulating cell growth, differentiation and survival. Oscillation between their active GTP-bound and inactive GDP-bound state is controlled in a tightly regulated cycle by guanine nucleotide exchange factors and GTPase-activating proteins [139]. Mutations in RAS genes, which render Ras proteins to be constitutively active, are found in approximately 30% of human cancers. Signaling of Ras proteins strongly depends on their correct localization in the cell membrane. The Ras isoform K-Ras4B (Figure 1A) appears to be particularly prone to mutations (86%) [140]. Farnesylation of K-Ras4B, i.e. covalent addition of a 15-carbon farnesyl lipid tail to the C-terminal CAAX cysteine by the enzyme farnesyltransferase, leads to association of K-Ras4B with the lipid bilayer and is essential for its correct cellular localization. A polybasic domain containing six consecutive lysine residues acts as an additional element for K-Ras4B plasma membrane localization [32, 50]. After insertion into the plasma membrane, K-Ras4B has been shown to form nanoclusters, which appears to be essential for the activation of mitogen-activated protein kinase (MAPK) signaling. Such K-Ras4B nanoclusters offer an efficient platform for the binding of effector proteins [141-143]. As a result of the frequent occurrence of cancer-related K-Ras4B mutations, enormous efforts are being made both in the pharmaceutical industry and in academia to develop inhibitors for K-Ras4B [29, 144]. However, no effective drug capable of fighting K-Ras4B-related cancers has been developed so far.

Recently, it has been reported that the C6-ceramide (Figure 1B) directly inhibits the growth activity of K-Ras4B mutated cells, and further analysis indicated that C6-ceramide can induce cancer cell death synergistically with chemotherapy [145, 146 and 147]. Natural ceramides are important cellular lipids, which function as secondary messengers and play an important role in the regulation of programmed cell-death [148, 149]. Unlike the C16-, C18-, C20-long fatty-acid chain ceramides, the shorter

C6-ceramide is known to be a cell membrane permeable lipid. It has also been reported that incubation of permeable C6-ceramide with human colon carcinoma cells and ovarian carcinoma cells induces apoptosis [146]. Recruitment for a Phase I study of C6- ceramide nanoliposomes in patients with advanced solid tumors is registered on ClinicalTrials.gov (https://clinicaltrials.gov/ct2/show/NCT02834611). Based on the findings mentioned above, C6-ceramide constitutes a promising inhibitor with the potential to target also K-Ras4B-related cancers. However, the mechanism underlying the inhibition of cell activity remains unknown. To shed light on this mechanism and to promote drug discovery targeting K-Ras4B, a biophysical understanding of the interaction between K-Ras4B and C6-ceramide in the membranous context is urgently required.

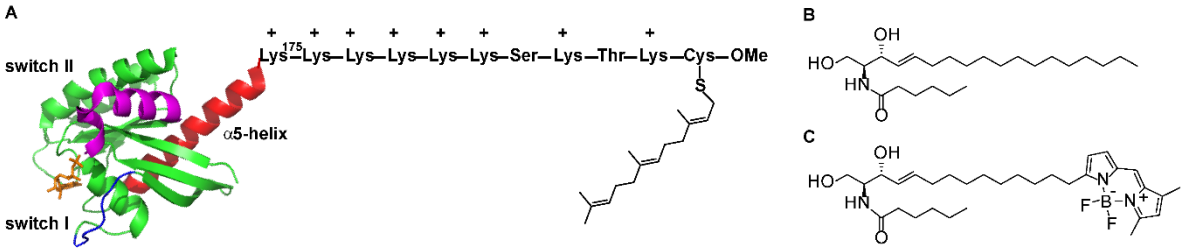

Figure 4-1-1. (A) Schematic of the semisynthetic K-Ras4B protein. The structure of the K-Ras4B G-domain was adapted from the crystal structure (PDB: 5TAR). Chemical structure of C6-ceramide (B) and backbone-labeled BODIPY-C6-ceramide (C).

4.1.2 Preparation of C6-ceramide included in lipid model membranes

In this study, we set out to investigate the effect of C6-ceramide incorporation into model biomembrane systems and to uncover the details of its interaction with K-Ras4B. To this end, a heterogeneous ("raft-like") lipid bilayer consisting of DOPC/DPPC/Cholesterol/C6-ceramide at a molar ratio of 25:50:20:5 was used (DOPC = 1,2-dioleoyl-sn-glycero-3-phosphocholine, DPPC = 1,2-dipalmitoyl-sn-glycero-3-phosphocholine). Atomic force microscopy (AFM) data revealed that incorporation of 5 mol% of C6-ceramide still leads to segregation of the lipid mixture into liquid-ordered (l_o) and liquid-disordered (l_d) domains at room temperature (Figure 4-1-2), and the appearance of the lateral organization is similar to that of the three-component mixture lacking the C6-ceramide. Isolated islands of fluid l_d domains (dark

brown) are clearly visible in a coherent pool of raft-like (I_o) protruding phase (light brown). The height difference between the I_o and I_d phases (Figure 4-1-2B as example) is 1.45 ± 0.1 nm (mean value ± s.d., n = 141), which is analogous to previously reported values for such heterogeneous membrane systems. Time-lapse AFM image recordings reveal a stable lipid bilayer with I_o-I_d domain coexistence for at least 15 h (Figure 4-1-3). This contradicts some reports suggesting that C6-ceramide could disrupt lipid membranes.

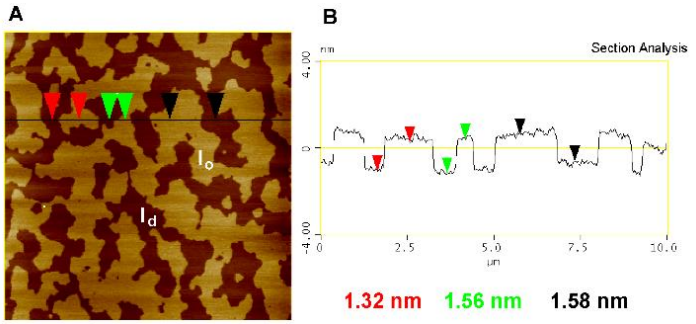

Figure 4-1-2. AFM image of a DOPC/DPPC/Cholesterol/C6-ceramide (molar ratio = 25:50:20:5) lipid membrane on mica before injection of protein solution. In A, the whole scan area is shown with a vertical color scale from dark to white, corresponding to 6 nm. The AFM image shows a homogeneously spread lipid bilayer with coexisting domains of I_o and I_d phase. B shows the concomitant section profile of the AFM image. The horizontal black line in the AFM image on the left is the location of the section analysis shown on the right side, and also indicates the vertical distances between pairs of arrows (red, green, black).

As previously reported, C18-ceramide can form C18-ceramide-rich gel-like domains in lipid model membranes already at very low concentrations, which can be readily distinguished [17]. In our case, no C6-ceramide-rich domains are observed in the heterogeneous membrane containing 5 mol% C6-ceramide (Figures 4-1-2 and 4-1-3). This is likely to be due to its shorter second chain length which favors partitioning in disordered lipid phases [18].

By directly injecting a solution containing K-Ras4B protein into the AFM fluid cell, the same region of the lipid bilayer can be observed both before and after incorporation of the protein. Moreover, owing to the absence of convection, the diffusion process to the lipid interface is rather slow, allowing kinetic AFM measurements to be carried out.

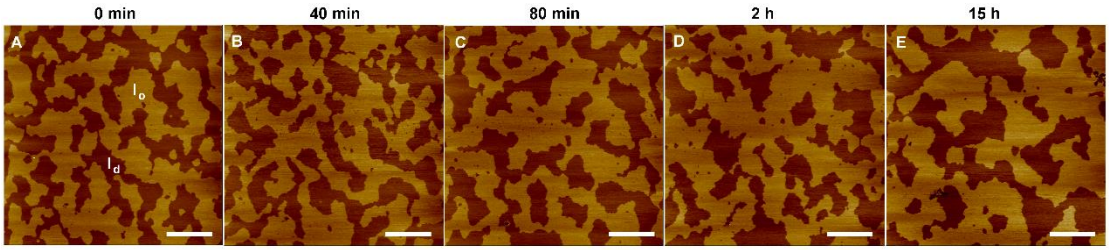

Figure 4-1-3. Time-lapse AFM images of lipid bilayers consisting of DOPC/DPPC/Cholesterol/C6-ceramide (molar ratio = 25:50:20:5). Tris buffer (20 mM Tris, 5 mM $MgCl_2$, pH 7.4) was used to prepare LUVs, which were used to form a bilayer on mica surface (fresh cleaved) by liposome fusion. The AFM images taken at different time points indicate long-term stability of the lateral membrane organization, i.e. coexistence of l_o and l_d domains, and their slow lateral diffusion in the membrane plane.

4.1.3 C6-ceramide intervenes K-Ras4B forming nanoclusters in the lipid membrane

Before injecting the K-Ras4B solution into the fluid cell, we verified deposition of a homogeneous lipid bilayer film and the coexistence of the l_o and l_d domains of the lipid bilayer (Figure 4-1-4A). After addition of K-Ras4B, tapping-mode AFM measurements were carried out at several time points. As GDP-bound and GTP-bound K-Ras4B proteins share a similar partitioning behavior in lipid membranes [17], we used the GDP-bound variant here.

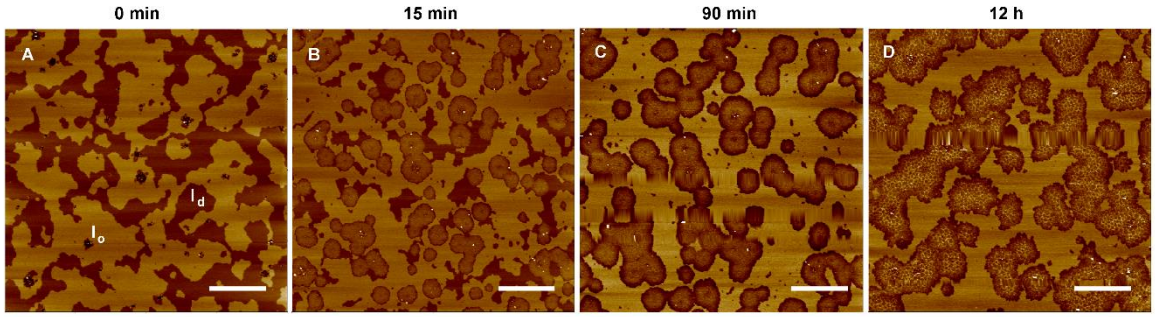

Figure 4-1-4. AFM images of the time-dependent partitioning and lateral organization of K-Ras4B in the lipid bilayer consisting of DOPC/DPPC/Cholesterol/C6-ceramide (molar ratio = 25:50:20:5). The AFM images are shown before (A) and at selected time points (B: 15 min, C: 90 min, D: 12 h) after injection of 200 µL of K-Ras4B (cK-Ras4B = 2 µM) in Tris buffer (20 mM Tris, 5 mM $MgCl_2$, pH 7.4) into the AFM fluid cell. The overall height of the vertical color scale from dark brown to white corresponds to 6 nm. The scale bar in all images represents 2 µm. Please note that all the images were taken in the same region of the lipid bilayer.

Figure 4-1-4B clearly shows that K-Ras4B nanoclusters are readily formed in the l_d phase. This scenario is reminiscent of our previous reports on K-Ras4B nanocluster formation in heterogeneous lipid membranes lacking the C6-ceramide.[62, 150] The addition of K-Ras4B leads to a significant decrease in the amount of neat l_d phase, whereas the K-Ras4B nanoclusters enriched fluid domain areas increase concomitantly. As shown in Figures 4-1-4B and D, the K-Ras4B proteins over time change the initial lateral organization of the membrane drastically, which in turn influences the K-Ras4B nanocluster distribution in the C6-ceramide containing membrane. Interestingly, under equilibrium conditions (after 12 h of incubation), large K-Ras4B protein containing areas are formed and no extended l_d phase remains (Figure 4-1-4D).

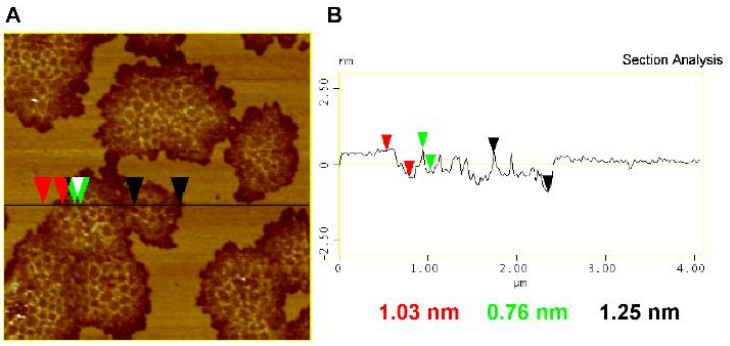

Figure 4-1-5. Analysis of the zoomed-in AFM picture shown in Figure 4-1-4D. The section profile (B) of the AFM images (A) is shown with a vertical color scale from dark brown to white corresponding to an overall height of 6 nm. The horizontal black line presents the location of the section analysis given at the right side, and indicates the vertical distances between pairs of arrows (red, l_o/l_d phase difference; black, thickness difference of K-Ras4B protein compared to fluid l_d phase; green, thickness difference of K-Ras4B protein compared to mixed lipid phase surrounding the protein nanoclusters dispersed in the fluid-like phase of the bilayer).

The zoomed-in image of the lower part of Figure 4-1-4-D reveals further details. K-Ras4B forms small and rather monodisperse nanoclusters, dispersed in a fluid-like lipid environment (Figure 4-1-5). A quantitative AFM analysis yields a mean height difference of 1.09 ± 0.3 nm (mean value ± s.d., n = 146) between the K-Ras4B nanoclusters and the C6-ceramide containing lipid bilayer, which is significantly lower than the mean height of K-Ras4B protein nanoclusters (2.0 ± 0.7 nm, mean value ± s.d., n = 304) forming in lipid bilayer membranes lacking the C6-ceramide [17, 18]. This decreased thickness of the K-Ras4B nanoclusters may be explained by the smaller size of K-Ras4B protein clusters, and a different orientation and deeper

membrane insertion of the proteins, potentially induced by the fluidizing C6-ceramide [151].

4.1.4 C6-ceramide and K-Ras4B both localize in the liquid-disordered phase of the lipid membrane

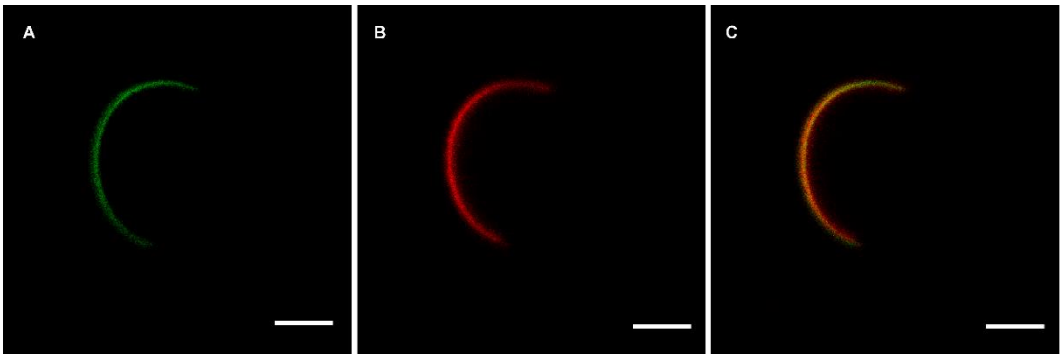

Figure 4-1-6. Confocal laser scanning microscopy images (cross section) of the localizat$_{lo}$n of C6-ceramide in GUVs. GUVs were composed of DOPC/DPPC/Cholesterol/C6-ceramide (molar ratio = 25:50:20:5), which segregate into I_o and I_d domains at room temperature. *N*-Rh-DHPE (0.2 mol %) was used as I_d phase marker (red channel, B), and the C6-ceramide (0.2 mol %) was BODIPY-labeled (green channel, A). The overlay of the red and green channel (C) shows that C6-ceramide inserts preferentially into the I_d lipid phase. The scale bar represents 4 µm.

Complementary confocal laser scanning microscopy was used to monitor the C6-ceramide partitioning behavior in the lipid membrane on a larger length scale. The same lipid mixture DOPC/DPPC/Cholesterol/C6-ceramide (molar ratio = 25:50:20:5) was used to prepare giant unilamellar vesicles (GUVs). To distinguish between the I_o and I_d phases and the localization of C6-ceramide, *N*-Rh-DHPE was used as an I_d phase marker [152], and the C6-ceramide was labeled with BODIPY in the backbone (Figure 4-1-1C). In Figure 4-1-1B, the red channel with *N*-Rh-DHPE corresponds to the I_d phase, whereas the dark region of the GUV's cross-section consists of I_o phase. Superposition of the green channel (BODIPY-labeled C6-ceramide) and the red channel clearly shows that BODIPY-C6-ceramide (green) is essentially localized in the Id phase of the lipid bilayer (Figure 4-1-6C).

4.1.5 C6-ceramide does not colocalize with K-Ras4B in the lipid membrane

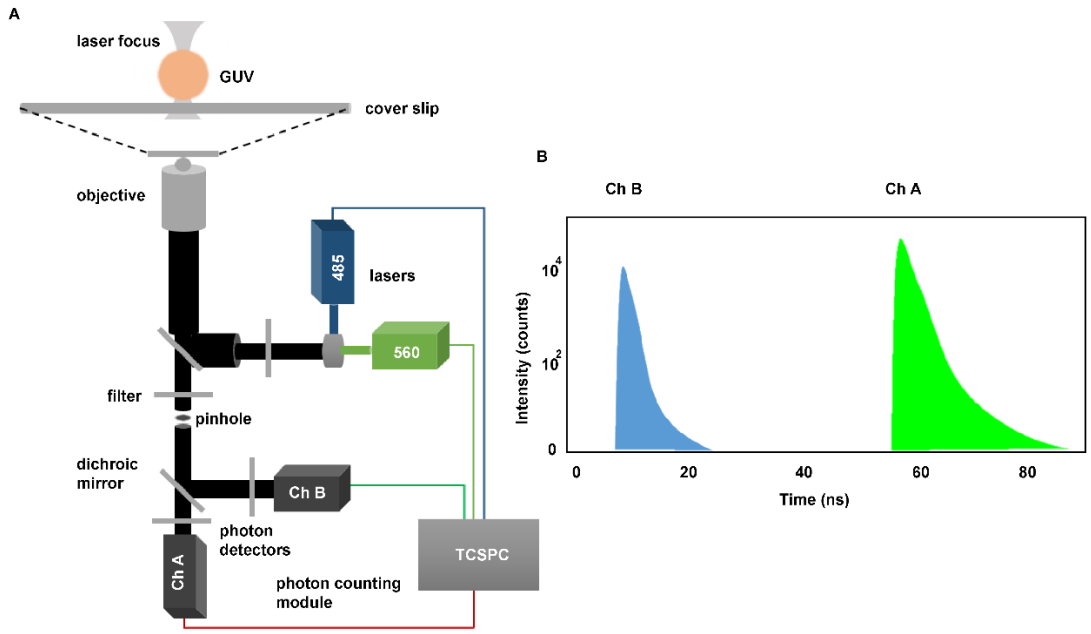

Figure 4-1-7 (A, B) Schematic of the two-color PIE-FCCS and time-correlated single photon counting (TCSPC) method for generating histograms of donor and acceptor fluorescence obtained due to excitation by a pulsed blue laser and green laser, respectively (Ch A: channel A; Ch B: channel B). Rhodamine-labeled K-Ras4B protein and BODIPY-labeled C6-ceramide were excited by the blue laser (485 nm) and green laser (560 nm), respectively. Since the laser pulses are separated by a lag time (B), it is possible to assign the photons arriving to their respective channels, which also reduces spectral cross talk.

Next, fluorescence correlation spectroscopy (FCS) and pulsed interleaved excitation fluorescence cross correlation spectroscopy (PIE-FCCS) were applied to study the clustering propensity of K-Ras4B in the C6-ceramide containing membrane in more detail and to reveal whether the C6-ceramide is able to directly interact with the K-Ras4B protein. FCS was used to determine the lateral mobility (diffusion constant, D) of BODIPY-C6-ceramide and Rhodamine-labeled K-Ras4B in C6-ceramide containing membrane. PIE-FCCS has the ability to detect the differently labeled co-diffusing particles, which can be used to determine whether K-Ras4B proteins colocalize with C6-ceramide. FCS measurements were carried out on GUVs composing DOPC/BODIPY-C6-ceramide (0.005 mol%) with 10 nM of Rhodamine-labeled K-Ras4B inserted into the lipid membrane. As can be inferred from the

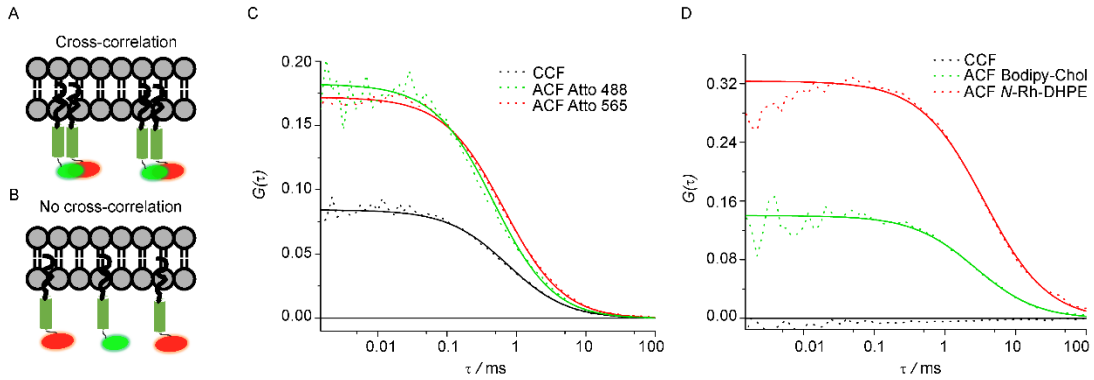

Figure 4-1-8. (A, B) Schematic of dually labeled species in the lipid membrane. (A) Two dually labeled species bind together, indicating high cross-correlation. (B) Two dually labeled species localize independently in the lipid membrane, leading to no cross-correlation. (C) Autocorrelation (ACF) and cross-correlation (CCF) fluorescence curves of a dually (Atto-488 and Atto-565) labeled oligonucleotide, which was used as a positive control. (D) Autocorrelation (ACF) and cross-correlation (CCF) curves of BODIPY-Cholesterol and N-Rh-DHPE inserted into pure DOPC membrane, which represent non-co-diffusion species, hence serving as a negative control.

diffusion data (Figure 4-1-9), the lateral mobility of BODIPY-labeled C6-ceramide (lateral diffusion coefficient, D = 10.2 ± 2.3 μm^{2}s^{-1}) is not significantly different from the lateral diffusion of a lipid in a pure fluid DOPC membrane [153]. The lateral mobility of Rhodamine-labeled K-Ras4B is also similar to BODIPY-labeled C6-ceramide and the surrounding lipid matrix, indicating the absence of formation of gel-like ordered clusters (Figure 4-1-9), in agreement with the AFM and fluorescence microscopy data.

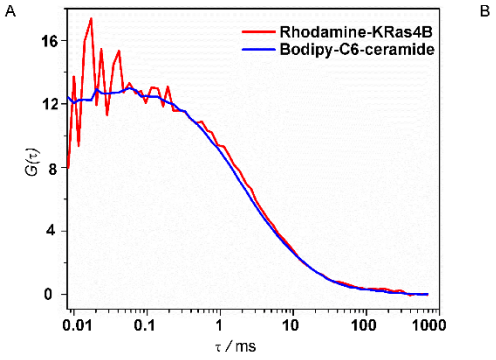

	Diffusion coefficient (μm^{2}s^{-1})
Bodipy-C6-ceramide	10.2 ± 2.3
Rhodamine-KRas4B	8.5 ± 1.6

Figure 4-1-9. FCS measurements of BODIPY-C6-ceramide and Rhodamine-K-Ras4B in a pure DOPC membrane. GUVs composed of DOPC + 0.005 mol% BODIPY-C6-ceramide were prepared. 10 nM of Rhodamine-K-Ras4B protein was added to this system. The autocorrelation curves (A) of BODIPY-C6-ceramide and Rhodamine-K-Ras4B were then fitted with a 2D diffusion model, and the diffusion coefficients were determined (B).

For the PIE-FCCS measurements, different concentrations of Rhodamine-labeled K-Ras4B were added to the GUVs (DOPC/DPPC/Cholesterol/C6-ceramide, molar ratio = 25:50:20:5, 0.005 mol% BODIPY-labeled C6-ceramide).

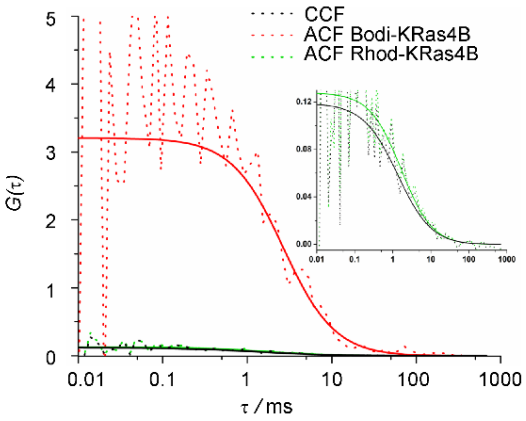

Figure 4-1-10 Autocorrelation (ACF) and cross-correlation (CCF) fluorescence curves of Bodipy-labeled and Rhodamine-labeled K-Ras4B protein in pure DOPC GUVs, which proves that the K-Ras4B protein is forming nanoclusters in lipid bilayers, and further act as a positive control for PIE-FCCS measurements in lipid membranes. The PIE-FCCS measurements were performed on pure DOPC GUV membranes. 10 nM Bodipy-labeled and 10 nM Rhodamine-labeled K-Ras4B protein were injected into the homemade chamber which was used to prepare the GUVs. More than 20 measurements were recorded to determine the cross-correlation value between two different fluorophore labeled K-Ras4B proteins in the membrane.

The relative cross-correlation amplitude between BODIPY-labeled C6-ceramide and Rhodamine-labeled K-Ras4B is close to zero (Figure 4-1-11), contrasting with the positive control (Figure 4-1-10 and 4-1-11). This clearly shows that K-Ras4B does not co-localize with the C6-ceramide in the bilayer plane, indicating that the influence of C6-ceramide on K-Ras4B nanocluster formation does not take place through a direct interaction between C6-ceramide and K-Ras4B, but is rather mediated through its effect on the lateral lipid phase organization.

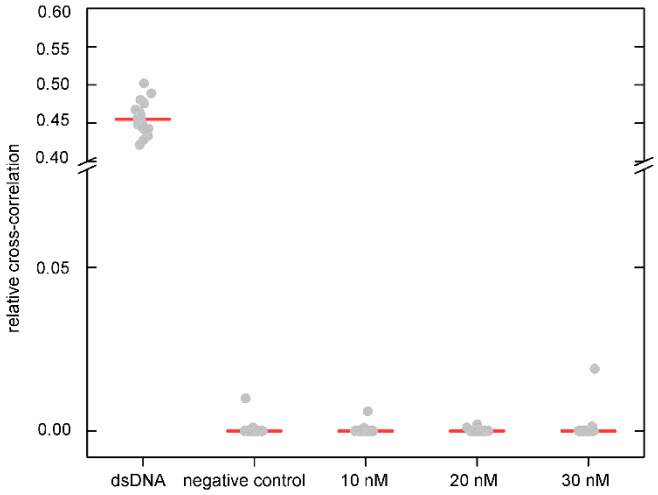

Figure 4-1-11. Relative cross-correlation values for a dually labelled oligonucleotide acting as a positive control, *N*-Rh-DHPE and BODIPY-cholesterol inserted into pure DOPC membrane acting as a negative control, and different concentrations of Rhodamine-K-Ras4B (10 nM, 20 nM and 30 nM) with 0.005 mol% BODIPY-C6-ceramide in the DOPC/DPPC/Cholesterol/C6-ceramide membrane. Data are represented as a scatterplot with the red line representing the median value.

4.1.6 Binding affinity analysis using a Förster resonance energy transfer (FRET) based assay

The binding affinity of K-Ras4B with the heterogeneous raft membrane was determined by the Förster resonance energy transfer (FRET) technique. LUVs composed of DOPC/DPPC/Cholesterol (molar ratio = 1:2:1) + 0.1 mol% *N*-Rh-DHPE + 5 mol% unlabeled C6-ceramide and without C6-ceramide. Atto488-labeled K-Ras4B, which forms the donor (d), was titrated with the indicated LUVs as acceptor (a). The sample was excited at 490 nm and the fluorescence spectra were collected at different concentrations of the acceptor. The decrease of the donor intensity was used to obtain a binding curve by calculating $1-(I_{da}/I_d)$, where I_{da} is the fluorescence intensity at the emission maximum in the presence of acceptor and I_d is the intensity in the absence of acceptor. All spectra obtained were corrected for dilution during titration. The binding curves were then fitted using a two-site binding model according to the equation

$$E = Bmax_1\left(\frac{[L]}{K_{d1}+[L]}\right) + Bmax_2\left(\frac{[L]}{K_{d2}+[L]}\right) \quad \text{(S4-1-1)}$$

where K_{d1} is the dissociation constant of the high affinity binding step and K_{d2} is the dissociation constant of low affinity binding step. $Bmax_1$ and $Bmax_2$ are the maximum values of the specific binding events of the two sites. *E* is the measured FRET efficiency as a function of lipid concentration, [L]. Different binding models were considered to obtain the best representation of the observed kinetic data, including the simple Langmuir adsorption model and models containing cooperative parameters, such as introducing a stoichiometric factor, *n*, operating on the concentration of the lipid. Best fits were obtained by a two-site binding model and the corresponding two dissociation constant values, K_{d1} and K_{d2}, were obtained.

The fluorescence spectroscopic measurements were carried out using a K2 multifrequency phase and modulation fluorometer (ISS, Champaign, IL). The measuring temperature was maintained at 25 ± 0.1 °C using a circulating water bath. The Atto-488 labeled K-Ras4B protein was excited at 488 nm using a xenon lamp through a monochromator. Emission spectra were collected between 502-700 nm at 90° through a second monochromator.

Finally, the influence of C6-ceramide on the binding affinity of K-Ras4B with heterogeneous raft membranes was studied using a Förster resonance energy transfer (FRET) based binding assay. Atto488-labeled K-Ras4B (FRET-donor) was titrated with *N*-Rh-DHPE-labelled (0.1 mol%, FRET-acceptor) large unilamellar vesicles (LUVs) (DOPC/DPPC/Cholesterol, molar ratio = 25:50:25 or DOPC/DPPC/Cholesterol/C6-ceramide, molar ratio = 25:50:20:5). Upon addition of the LUVs, the decrease of the donor fluorescence was measured and the FRET efficiency calculated, which was plotted as a function of concentration of the LUVs to obtain the binding curves (Figure 4-1-12).

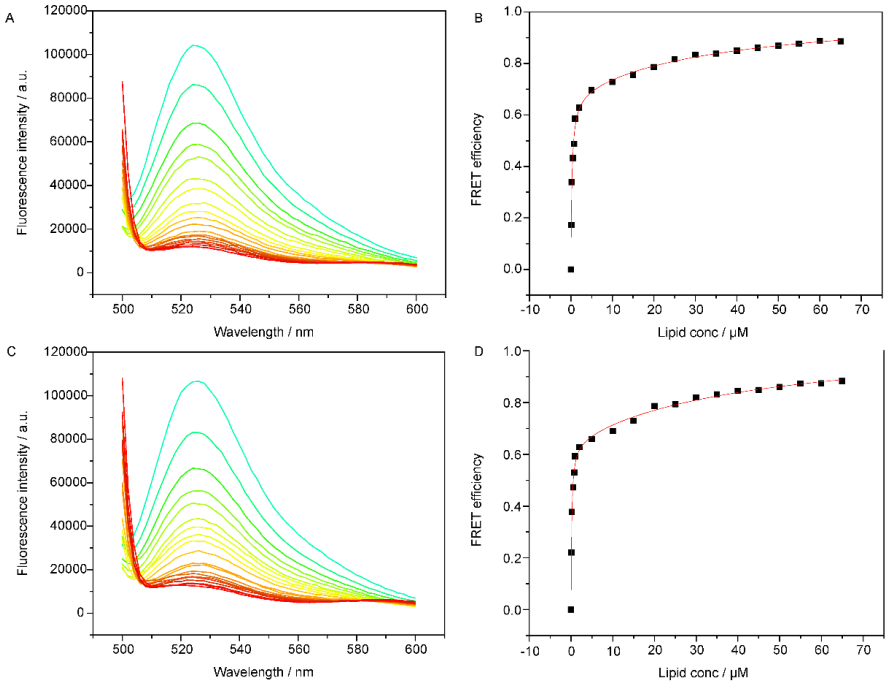

Figure 4-1-12. Binding affinity measurements of K-Ras4B in the absence and presence of 5 mol % C6-ceramide containing heterogeneous lipid membranes using a FRET based assay. LUVs were composed of DOPC/DPPC/Cholesterol (1:2:1) + 0.1 mol % *N*-Rh-DHPE + 5 mol% unlabeled C6-ceramide and without the ceramide. Atto488-labeled K-Ras4B protein as donor was titrated with acceptor-labeled LUVs. Figure 4-1-12A (with 5 mol% C6-ceramide) and Figure 4-1-12C (without C6-ceramide) both show that the donor fluorescence decreases upon addition of the acceptor (LUVs). The FRET efficiency of the two different membrane systems can be calculated, which is then plotted as a function of lipid concentration to obtain the binding curve (C, with C6-ceramide; D, without C6-ceramide). Best fits were obtained by a two-site binding model and the corresponding two dissociation constants, $K_{d1,2}$, were obtained.

Different binding models were considered, including the simple Langmuir adsorption model and models containing cooperative parameters. Best fits were obtained for a two-site binding model and the two dissociation constant values, $K_{d1,2}$, were obtained (Figure 4-1-13). The process of K-Ras4B farnesyl lipid anchor inserting into the lipid membrane can be considered as the first, high affinity binding step. Nonspecific binding of K-Ras4B and/or rearrangement in the lipid plane can be allocated to the second, low affinity binding step. The K_{d1} value for the high affinity binding step increases from 0.15 ± 0.017 µM for the three-component raft membrane to 0.25 ± 0.005 µM for the C6-ceramide containing membrane. The observed increase in K_{d1}, i.e. the decrease of the K-Ras4B binding affinity of the C6-ceramide-containing

membrane, may contribute to the retardation of K-Ras4B mutated cells' activity. However, the binding does not seem to depend drastically on the composition of the

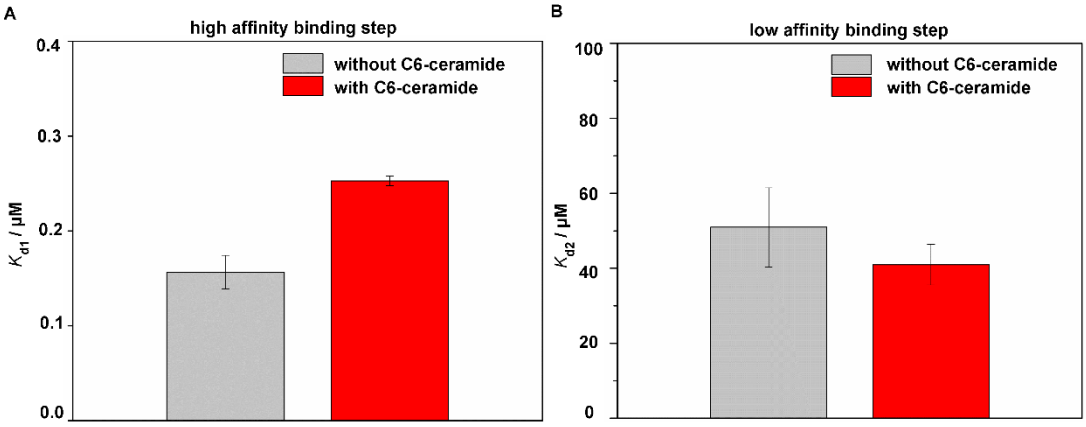

Figure 4-1-13. K-Ras4B binding affinity data, obtained from the FRET based assay, as determined in the absence and presence of 5 mol% ceramide containing heterogeneous lipid membranes (LUVs, prepared from DOPC/DPPC/Cholesterol/C6-ceramide, molar ratio = 25:50:20:5, or DOPC/DPPC/Cholesterol, molar ratio = 25:50:25, respectively). The values of the high affinity binding step (A) and the low affinity binding step (B) for the three-component raft membrane and the C6-ceramide containing membrane are plotted as column bar diagrams.

lipid membrane, indicating that the anti-cancerous activity of C6-ceramide is probably not due to a pronounced decrease of the binding affinity. C6-ceramide changes the lateral organization of K-Ras4B significantly, and may thereby affect the propensity to transmit signals and impact on downstream signaling. In fact, it was reported that C6-ceramide induces apoptosis through the caspase cascade and the mitochondrial pathway [154,155].

4.1.7 Conclusion and discussion

In summary, we have established a new heterogeneous model biomembrane system containing C6-ceramide. In contrast to the long-chain ceramides, the C6-ceramide does not lead to ordered gel-like segregated clusters in the membrane plane owing to the unfavourable packing properties of C6-ceramide in bulk long chain lipid phases. Instead, it sustains l_o-l_d phase coexistence and does not disrupt lipid membranes even at concentrations as high as 5 mol%. Using this four-component

heterogeneous model membrane, we demonstrated that addition of the signaling protein K-Ras4B leads to drastic changes in the lateral membrane organization of the membrane, contrasting with the partitioning behavior in other heterogeneous membrane types [17]. This difference may be due to the ability of the C6-ceramide to fill void volumes and enable H-bonding interactions to neighbouring phospholipid moieties. Unlike the membrane without C6-ceramide, K-Ras4B forms rather small, monodisperse nanoclusters, dispersed in a fluid-like environment of the membrane, potentially induced by some kind of lipid sorting mechanism. As revealed by the FCCS data, there is no direct interaction between the C6-ceramide and K-Ras4B, indicating that K-Ras4B essentially recruits other lipids. Collectively, our results demonstrate that different compositions of heterogeneous lipid membranes are able to markedly influence the size and distribution of the K-Ras4B nanoclusters forming in lipid membranes, in all likelihood leading to signaling platforms of different levels of efficiency. Such protein nanoclustering is in turn accompanied by drastic changes in the lateral membrane organization, which is likely to encompass deleterious effects on other membrane-related biochemical processes. Moreover, the stability of K-Ras4B in C6-ceramide containing membranes is reduced, which is a likely consequence of the fluidizing nature of the short-chain C6-ceramide. These findings are consistent with recent reports indicating that the lipid composition of cell membrane is able to shape K-Ras4B protein's signaling output and hence biological function through formation or deletion of protein nanoclusters [58, 156].

4.2 Probing Colocalization of N-Ras and K-Ras4B Lipoproteins in Model Biomembranes

4.2.1 N-Ras and K-Ras4B form nanoclusters in the same domain of the lipid membrane

N-Ras and K-Ras4B proteins are oncoproteins and play a major role in human cancers [144, 157]. They are switching between an active GTP bound, and an inactive GDP bound state in a tightly regulated cycle, which is controlled by guanine nucleotide exchange factors (GEFs) and GTPase-activating proteins (GAPs). The nucleotide-exchange leads to conformational changes between the switch-1 (SW1) and switch-2 (SW2) regions in the Ras effector binding area [158, 159]. Once activated, Ras proteins' signaling can be terminated by GAPs. However, mutations of Ras proteins in cancer cells impair the GAPs' activity. More than 30% of human tumors are related to Ras mutations. The mutated proteins are constitutively active in N-Ras or K-Ras4B which are the most frequently mutated isoforms. For example, 95% of pancreatic cancers are driven by K-Ras4B mutants and 27% of skin cutaneous melanoma cancers are driven by mutant N-Ras [160, 161 and 162].

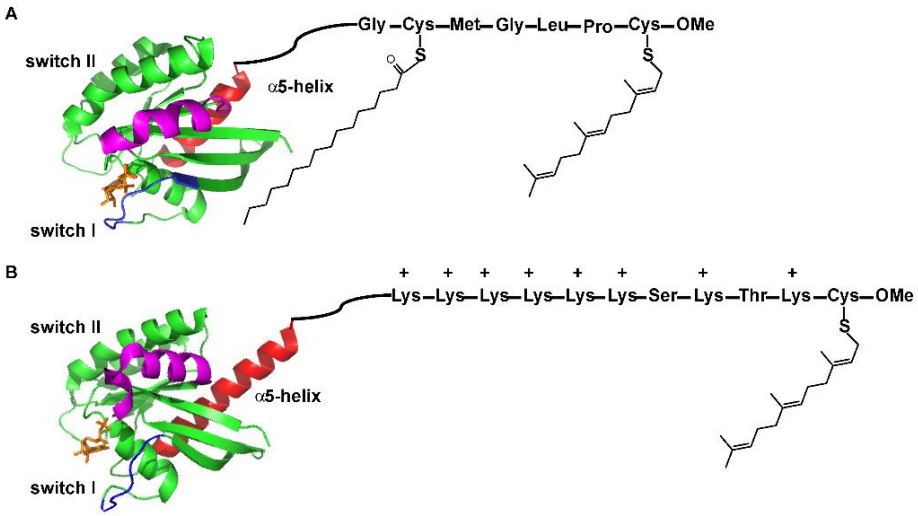

Figure 4-2-1. Schematic of the structure of the N-Ras (A) and KRas-4B (B) protein. The structure of the G-domain of N-Ras and K-Ras4B were adapted from the crystal structure, PDB 5UHV and 5TAR, respectively.

Signaling of N-Ras and K-Ras4B strongly depends on their correct localization in the cell membrane. All Ras proteins have to be farnesylated by the farnesyl transferase (FTase). Besides this 15-carbon farnesyl lipid tail in the C-terminal CAAX cysteine, N-Ras proteins are palmitoylated. As K-Ras4B proteins do not have a cysteine residue immediately upstream of Cys186, they are not palmitoylated. Instead, a polybasic domain containing six lysine residues in one row functions as the second anchor motif allows for stable K-Ras4B membrane insertion (Figure 4-2-1) [17, 32]. Given the importance of N-Ras and K-Ras4B in driving tumorigenesis, enormous efforts have been undertaken both in the pharmaceutical industry and in academia to develop pharmacological inhibitors for N-Ras and K-Ras4B in recent years. Although farnesyl transferase inhibitors showed inhibition of Ras proteins *in vivo*, these inhibitors have revealed to be ineffective against mutant N-Ras and K-Ras4B owing to alternative geranylgeranylation, rendering membrane partitioning by these proteins still possible. Recent efforts have also turned to develop inhibitors targeting Ras effectors, such as Raf. Unfortunately, till now still no effective drug has been found to be capable of fighting N-Ras and K-Ras4B related cancers [36, 140].

In vivo studies suggest that intermolecular interactions foster the membrane-induced self-association of N-Ras and K-Ras4B and the formation of nanoclusters in cellular membranes [156]. As sole sites for effector binding, nanocluster formation seems to be essential for both N-Ras and K-Ras4B effective signal transmission. Furthermore, it has been reported that a lipid-mediated effect can induce a cross talk between spatially segregated H-Ras and K-Ras4B [55, 163]. The mechanism of the cross talk between spatially segregated Ras proteins in cell membranes remains elusive, however. Previous *in vitro* studies reported that N-Ras and K-Ras4B localize in the disordered phase of heterogeneous model membranes, and both of them form nanoclusters in heterogeneous membranes, of different appearance, however. K-Ras4B proteins preferentially localize and cluster the liquid-disordered (I_d) lipid phase, N-Ras proteins partition into the I_d phase and migrate to the I_d/I_o phase boundary of heterogeneous membranes with time [16]. We might presume that N-Ras and K-Ras4B reveal a membrane-induced spatial correlation or even interaction if present at the same time. In this study, we set out to explore the colocalization scenario in model biomembranes. Their morphology and composition can be tailored with great precision

and resolution, allowing us to reveal the spatial relation of the two lipoproteins within the lipid matrix and to explore details of their interaction.

4.2.2 Preparation of the lipid membrane

GUVs were prepared in a temperature-controlled chamber on optically transparent and electrically conductive indium tin oxide (ITO) coated glass slides (SPI supplies, West Chester USA). Lipid mixtures were prepared in a glass vial. 20 µL of 1.5 mg/mL lipid mixture was added to the ITO surface and a very thin lipid film was prepared using a spin coater. For the preparation of LUVs, the indicated lipid mixture was prepared and dried under a stream of nitrogen gas. The dried lipid mixture was put into a freeze dryer for complete drying. The dried lipid film was then rehydrated with Tris buffer (20 mM Tris, 5 mM $MgCl_2$, pH 7.4). After five freeze-thaw-vortex cycles, homogeneously sized LUVs were generated using an extruder (Avanti Polar Lipids, USA) with 100 nm polycarbonate membranes at 65 ˚C.

Heterogeneous (raft-like) lipid bilayers consisting of the lipid mixture DOPC/DPPC/cholesterol at a molar ratio of 1:2:1, presenting coexistence of liquid-ordered (l_o) and liquid-disordered (l_d) domains, have been widely used in studying the interaction of lipidated proteins with membranes. Atomic force microscopy (AFM) was used to reveal the localization of N-Ras and K-Ras4B within the lipid matrix, i.e., if they localize in the same or a different lipid environment and if they change the lateral organization of the lipid bilayer.

4.2.3 N-Ras and K-Ras4B both form nanoclusters in the disordered phase of the lipid membrane

Before injecting the protein solutions containing N-Ras and K-Ras4B into the AFM fluid cell, we verified deposition of a homogeneously spread lipid bilayer film with coexistence of l_o and l_d domains (Figure 4-2-2 A). Figure 4-2-2 B shows that the height difference between the two phases is about 1.34 nm, which is in agreement with the reported height difference of l_o and l_d domains (variance 1.2 ± 02 nm). Thereafter, 200 µL of N-Ras ($c_{N\text{-}Ras}$ = 8 µM) and K-Ras4B ($c_{K\text{-}Ras4B}$ = 2 µM) in Tris buffer (20 mM Tris, 5 mM $MgCl_2$, pH 7.4) were injected into the AFM fluid cell and equilibrated for 1 h. Before imaging, 500 µL Tris buffer were injected into the AFM fluid cell to remove unbound N-Ras and K-Ras4B protein. Figures 4-2-2 C-D show that K-Ras4B and N-

Ras both localize in the I_d phase. The partitioning behavior is similar to that obtained for independent insertion of N-Ras and K-Ras4B into the heterogeneous membrane (Figures 4-2-2G and J) and similar to published data [16]. Figure 4-2-2D is the zoomed-in image of the top left part of Figure 4-2-2C. The height analysis of this image shows that the height of K-Ras4B nanoclusters is about 1.02 nm and the height of N-Ras nanoclusters amounts to 3.55 nm (Figure 4-2-2E). The heights of the nanoclusters we attributed to N-Ras and K-Ras4B simultaneously administered to the model membrane are close to those of N-Ras and K-Ras4B when added individually. Hence, we may assume that both lipoproteins simultaneously partition into the I_d phase of the raft-like membrane, localize in spatially separated areas however. Furthermore, the addition of N-Ras and K-Ras4B proteins leads to drastic changes in the lateral membrane organization of the membrane as seen in Figures 4-2-2A-J.

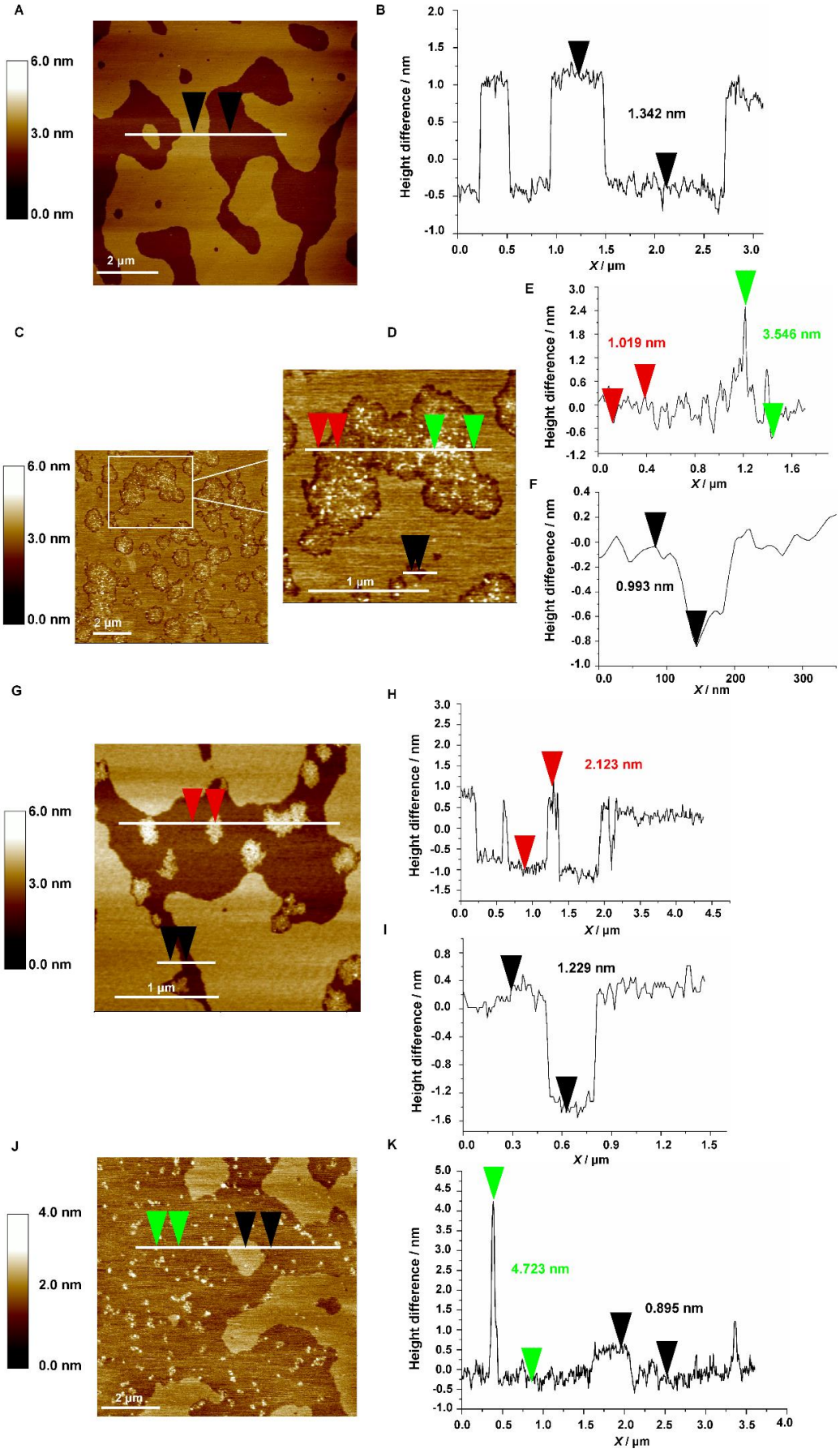
A
6.0 nm
3.0 nm
0.0 nm
2 µm
B
Height difference / nm
1.342 nm
X / µm
C
6.0 nm
3.0 nm
0.0 nm
2 µm
D
1 µm
E
Height difference / nm
1.019 nm
3.546 nm
X / µm
F
Height difference / nm
0.993 nm
X / nm
G
6.0 nm
3.0 nm
0.0 nm
1 µm
H
Height difference / nm
2.123 nm
X / µm
I
Height difference / nm
1.229 nm
X / µm
J
4.0 nm
2.0 nm
0.0 nm
2 µm
K
Height difference / nm
4.723 nm
0.895 nm
X / µm

Figure 4-2-2. AFM images of the partitioning and lateral organization of N-Ras and K-Ras4B in the lipid bilayer consisting of DOPC/DPPC/cholesterol (molar ratio = 1:2:1) and of N-Ras and K-Ras4B independently. (A) AFM image of the lipid bilayer consisting of DOPC/DPPC/cholesterol (molar ratio = 1:2:1). (B) Cross-sectional profile of the lipid bilayer shown in A. The two black arrows represent the height difference of the two points indicated in the Fig. 4-2-2 A. (C) After adding 200 µL of N-Ras ($c_{N\text{-}Ras}$ = 8 µM) and K-Ras4B ($c_{K\text{-}Ras4B}$ = 2 µM) in Tris buffer (20 mM Tris, 5 mM $MgCl_2$, pH 7.4) into the AFM fluid cell for 3 h. (D) The zoomed-in AFM image shown on the top left of Fig. 4-2-2 C. (E) Height profile of Fig. 4-2-2 C. The red arrows represent the height attributed to K-Ras4B nanoclusters and the green arrows represent the height ascribed to N-Ras nanoclusters in the lipid bilayer. (F) AFM height profile of Fig. 4-2-2 D. The black arrows represent the height difference of I_o/I_d domains. (G) AFM image of K-Ras4B localization in the lipid bilayer consisting of DOPC/DPPC/cholesterol (molar ratio = 1:2:1) after adding 200 µL K-Ras4B ($c_{K\text{-}Ras4B}$ = 2 µM) in Tris buffer (20 mM Tris, 5 mM $MgCl_2$, pH 7.4) into the AFM fluid cell for 3 h. (H, I) AFM height profile of Fig. 4-2-2 G. The red arrows represent the height of K-Ras4B nanoclusters and the black arrows represent the height difference of I I_o/I_d domains. (J) AFM image of N-Ras (200 µL of N-Ras ($c_{N\text{-}Ras}$ = 8 µM)) localization in the lipid bilayer consisting of DOPC/DPPC/cholesterol (molar ratio = 1:2:1). (K) AFM height profile of Figure 4-2-2J. The two green arrows represent the height of N-Ras nanoclusters in the lipid bilayer and the two black arrows represent the height difference of I_o/I_d domains.

4.2.4 Spatial correlation between N-Ras and K-Ras4B within the Förster radius in the lipid membrane

Next, the spatial correlation, i.e., average intermolecular distance between N-Ras and K-Ras4B proteins embedded in the membrane plane was studied using Förster resonance energy transfer (FRET) methodology. Bodipy-labeled N-Ras (FRET-donor) and rhodamine-labeled K-Ras4B (FRET-acceptor) were added to large unilamellar vesicles (LUVs) prepared from DOPC/DPPC/cholesterol (molar ratio = 1:2:1). After equilibration for 1 h, the system of Bodipy-labeled N-Ras and rhodamine- labelled K-Ras4B embedded in the lipid membrane was excited at 488 nm. To probe the existence of FRET between N-Ras and K-Ras4B in the lipid membrane, fluorescence spectra of a sample with both Bodipy-labeled N-Ras and rhodamine-labeled K-Ras4B in the membrane were recorded and compared to the fluorescence spectra of the single protein components in the lipid bilayer. Clearly, a decrease of the donor fluorescence and a concomitant increase of the acceptor fluorescence intensity is observed (Figure 4-2-3), indicating spatial correlations between N-Ras and K-Ras4B within the Förster radius, i.e. 10 nm, of the two fluorophores.

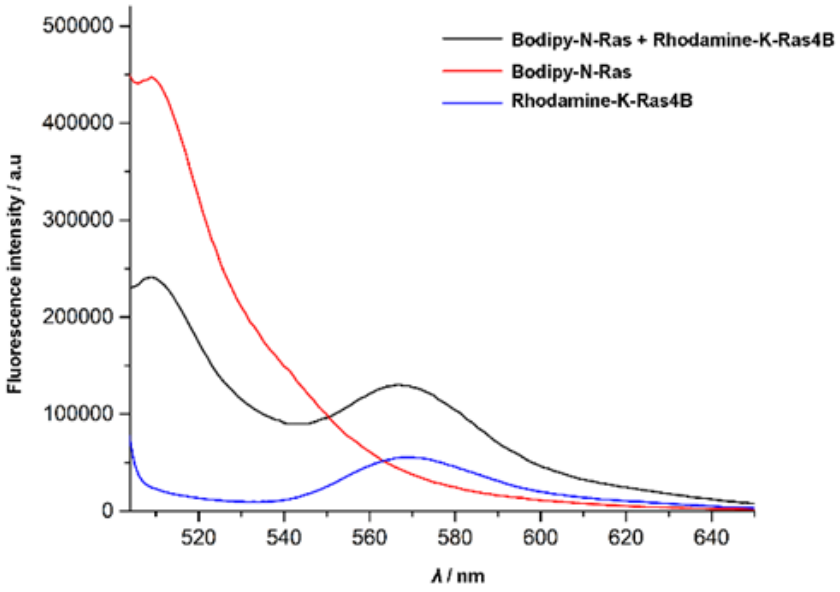

Figure 4-2-3. FRET between Bodipy-labeled N-Ras and rhodamine-labeled K-Ras4B in the lipid membrane. LUVs (DOPC:DPPC:cholesterl (1:2:1 molar ratio) were used as lipid membrane. Bodipy-labeled N-Ras functions as donor and rhodamine-labeled K-Ras4B serves as acceptor. All labeled proteins were excited at 488 nm and emission spectra were collected between 502 and 700 nm.

4.2.5 N-Ras and K-Ras4B proteins do not colocalize in the lipid membrane

Finally, to explore if a proximal co-localization between N-Ras and K-Ras4B occurs in the lipid membrane, or if they diffuse independently in the fluid lipid matrix, pulsed interleaved excitation fluorescence cross correlation spectroscopy (PIE-FCCS) was applied. PIE-FCCS measurements were carried out on GUVs (giant unilamellar vesicles) composed of DOPC/DPPC/cholesterol (molar ratio = 1:2:1) with Bodipy-labeled N-Ras and rhodamine-labeled K-Ras4B protein inserted into the lipid bilayer membrane. After the addition of N-Ras and K-Ras4B proteins into the GUVs for 1 h, unbound N-Ras and K-Ras4B was removed by washing with Tris buffer. As depicted in Figure 4-2-4, the relative cross-correlation amplitude of Bodipy-labeled N-Ras and rhodamine-labeled K-Ras4B in the lipid membrane is close to zero, contrasting with the positive controls (Figure. 4-2-5 B and 4-2-6). This clearly shows that N-Ras does not colocalize with K-Ras4B, i.e., there is no direct interaction between N-Ras and K-Ras4B molecules in the lipid membrane.

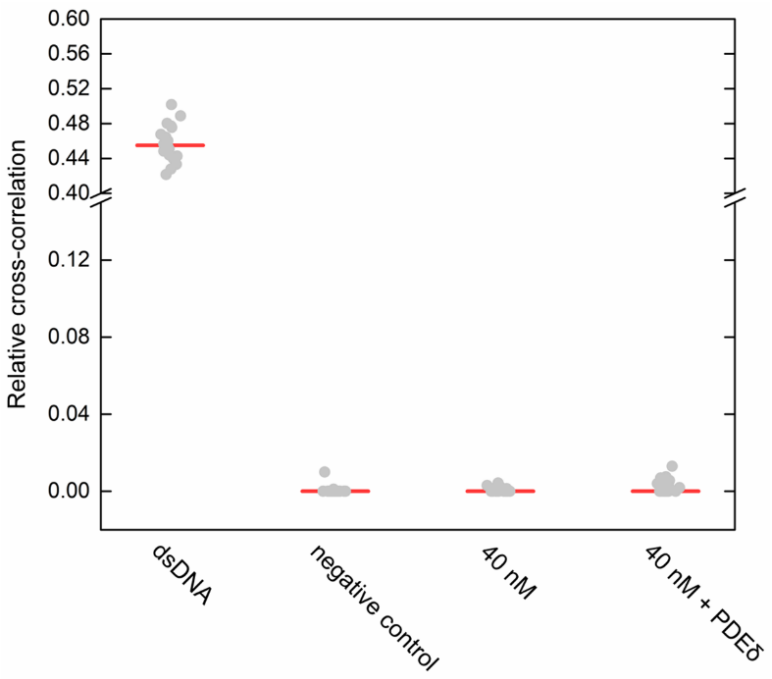

Figure 4-2-4. Relative cross-correlation values for a dually labelled oligonucleotide acting as a positive control, N-Rh-DHPE and Bodipy-cholesterol inserted into a pure DOPC membrane acting as negative control, and Bodipy-labeled N-Ras and rhodamine-labeled K-Ras4B (40 nM, 40 nM with 1 μM PDEδ) in the buffer (Tris 20 mM, $MgCl_2$ 5 mM, pH 7.4). Data are represented as a scatterplot with the red line representing the median value.

The protein PDEδ has been reported to bind K-Ras4B in the cytosol and play an important role in transporting it to the cellular membrane [164]. The protein forms a K-Ras4B-PDEδ complex in bulk solution and releases the K-Ras4B upon membrane contact [165]. This implies that, if colocalization between N-Ras and K-Ras4B would take place, the transporter protein PDEδ is expected to influence the partitioning behavior and localization of the two signaling proteins. The PDEδ protein was simultaneously injected together with N-Ras and K-Ras4B into the GUVs containing solution and PIE-FCCS measurements were carried out. The relative cross-correlation amplitude between Bodipy-labeled N-Ras and rhodamine-labeled K-Ras4B in the presence of PDEδ is found to be close to zero as well. This additional control indicates that the partitioning behavior of the two proteins is similar to the case where the transporter PDEδ is absent, and similar to the scenario observed for the individual lipoproteins.

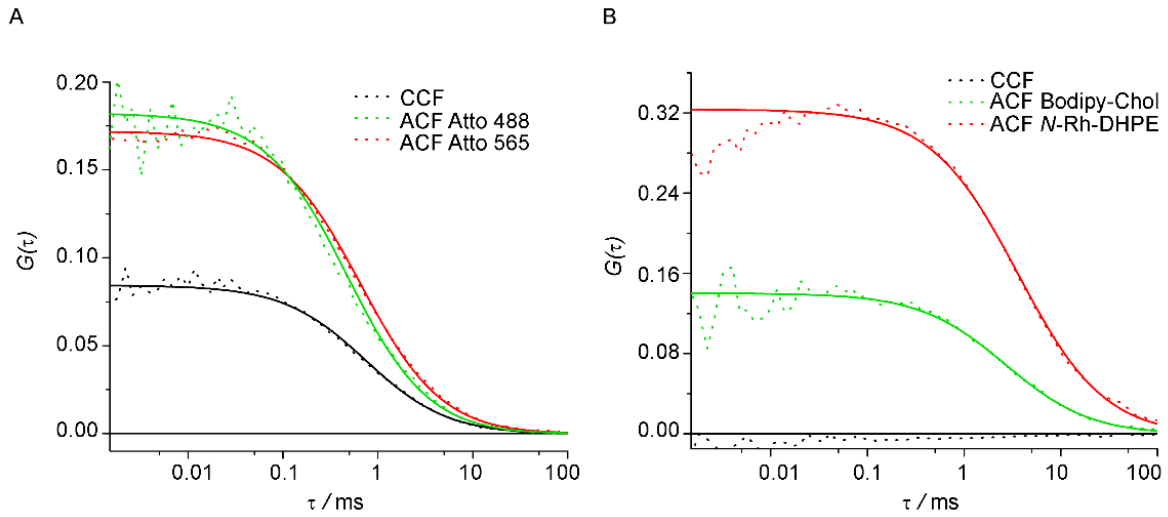

Figure 4-2-5. Autocorrelation fluorescence (ACF) and cross-correlation fluorescence (CCF) curves of a dually (Atto-488 and Atto-565) labeled oligonucleotide, which was used as a positive control. (D) Autocorrelation (ACF) and cross-correlation (CCF) fluorescence curves of Bodipy-cholesterol and N-Rh-DHPE inserted into a pure DOPC membrane, which represent non-co-diffusing species, hence serve as a negative control.

PIE-FCCS measurements on N-Ras and K-Ras4B proteins in neat buffer, mimicking cytosol solution conditions, were carried out as well. The results show that the relative cross-correlation amplitude between Bodipy-N-Ras and K-Ras4B in the buffer solution is also close to zero (Figure 4-2-4), which indicates that N-Ras proteins diffuse independently of K-Ras4B proteins, i.e., they do not interact in bulk solution.

4.2.6 Conclusion and discussion

Recent work by the Hancock and Gorfe groups suggested that K-Ras4B binds to selected anionic lipids with defined head groups and lipid side chains in the plasma membrane by electrostatic interactions and lipid sorting [58]. Further, in vivo studies suggested that intermolecular interactions foster the self-association of both N-Ras and K-Ras4B and the formation of nanoclusters in cell membranes. Interactions between K-Ras4B and lipids were proposed to shape the K-Ras4B signaling output through formation of nanoclusters. Here, we found that the two lipidated signaling proteins N-Ras and K-Ras4B do not colocalize in the lipid bilayer, they rather diffuse independently as individual clusters in the fluid membrane matrix. They also diffuse independently in bulk solution. As revealed by the AFM data, the simultaneous

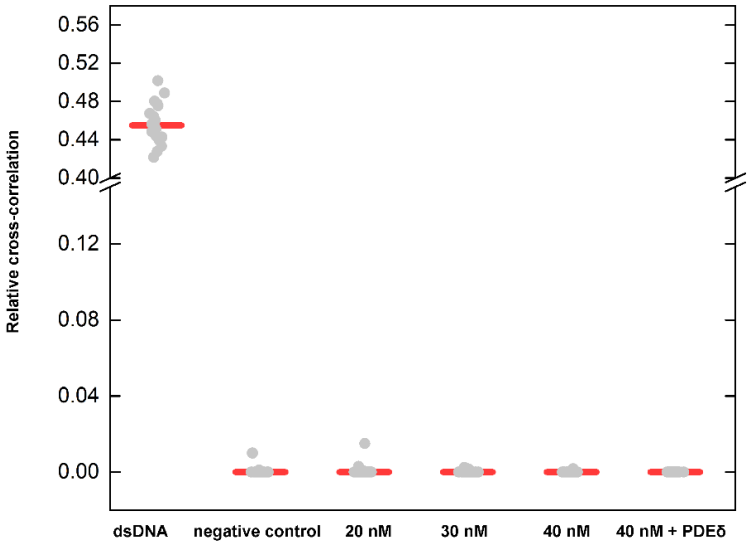

Figure 4-2-6. Relative cross-correlation values for a dually oligonucleotide acting as a positive control, *N*-Rh-DHPE and Bodipy-Chol inserted into a pure DOPC membrane acting as negative control, and different concentrations of Bodipy-labeled N-Ras and rhodamine-labeled K-Ras4B (20 nM, 30 nM, 40 nM) and of 40 nM K-Ras4B with PDEδ (1 µM) in the DOPC/DPPC/cholesterol (molar ratio = 1:2:1) model biomembrane. Data are represented as a scatterplot with the red line representing the median value.

localization of N-Ras and K-Ras4B in the lipid membrane caused changes in the lateral organization of the membrane. The changes observed are reminiscent of those the two proteins induce when added individually. The FRET experiments revealed that N-Ras and K-Ras4B localize adjacent (<10 nm) in the disordered phase of the heterogeneous membrane, but do not approach each other closely. Clustering of K-Ras has not only been observed in such zwitterionic lipid bilayers, but also, as expected, to a slightly larger extent in anionic lipid mixtures, where electrostatic interactions with the lysine stretch of K-Ras4B and recruitment of anionic lipids is taking place [17, 32]. The same scenario seems to hold true for N-Ras. With its longer

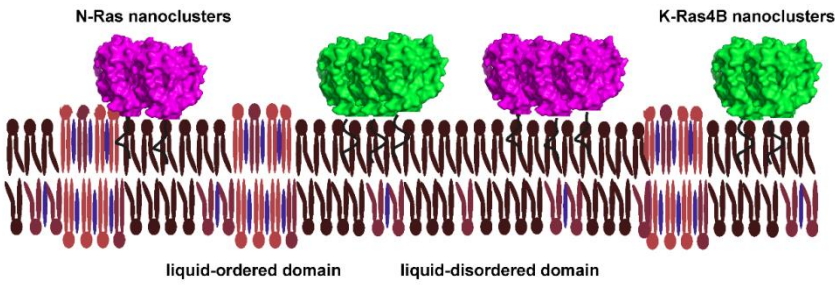

Figure 4-2-7. Scheme proposed for the N-Ras and K-Ras4B colocalization in heterogeneous model biomembrane systems.

palmitoyl chain as second anchor motif, next to the farnesyl anchor, the protein seems to prefer extensive self-association to avoid hydrophobic mismatch. Altogether, a picture emerges from our data which is schematically depicted in Figure 4-2-7. By using different anchor types with different interaction mechanisms, formation of individual signaling platforms is warranted. Such scenario resembles the situation proposed to prevail in cellular membranes. It has been suggested that a lipid-mediated effect may induce a crosstalk between spatially segregated H-Ras and K-Ras4B [55, 163]. Here, the crosstalk seems to be repulsive in nature, as the two cluster types are of different nature, allowing them to diffuse independently in the fluid lipid matrix. Such knowledge might be useful in developing inhibitors for N-Ras and K-Ras.

4.3 Dissociation of the Signaling Protein K-Ras4B from Lipid Membranes Induced by a Molecular Tweezer

4.3.1 Prevention of membrane targeting of K-Ras4B proteins in the lipid membrane by molecular tweezers

Ras proteins are oncoproteins and play a major role in human cancers where they fail to switch off the signal for cell growth. More than 30% of human cancers are related to mutations of Ras proteins with K-Ras4B being the most frequently mutated isoform. They are plasma membrane localized molecular switches that function by shuttling between inactive GDP-bound and active GTP-bound forms [29,144]. Signaling of K-Ras4B strongly depends on its correct localization in the plasma membrane. The polybasic domain (including 8 lysine residues altogether) of K-Ras4B acts in combination with a CAAX motif to target this protein to the membrane [32]. For stable insertion, K-Ras4B has to be farnesylated in the C-terminal CAAX cysteine by farnesyl transferase (FTase) [50]. Mutant K-Ras4B proteins in which two, three, or four lysines in the polybasic domain were mutated to glutamine showed a significant decrease of the amount of K-Ras4B partitioning in the plasma membrane [32, 167]. Further, mutations with five or six glutamine substitutions showed cytoplasmic diffusion of K-Ras4B only, with no K-Ras4B remaining localized in the plasma membrane. This suggests that targeting of the polybasic domain of K-Ras4B might constitute an effective strategy to inhibit the activity of K-Ras4B. The development of K-Ras4B inhibitors has been challenging and we still lack an effective drug being capable of fighting K-Ras4B-related cancers [140, 168]. Inhibitors reported so far generally target the interaction of K-Ras4B with PDEδ, c-Raf and other effectors [169, 117 and 123]. Here we are exploring an approach to modulate the activity of K-Ras4B using molecular tweezers.

The molecular tweezer CLR01 (Figure 4-3-1C) binds selectively to lysine and arginine [170]. Based on the ability of specifically binding to lysine residues, CLR01 has been explored to combat various diseases. Studies on amyloidosis showed that CLR01 inhibits the formation of infectivity-enhancing seminal amyloids and remodels preformed fibrils through the specific binding to lysines and arginines [171]. It has also been shown that CLR01 is able to inhibit pathologic protein aggregation in multiple

neurodegenerative diseases (AD, PD, Huntington etc.) [172] and CLR01 was also found to be able to steer protein-protein interactions [173].

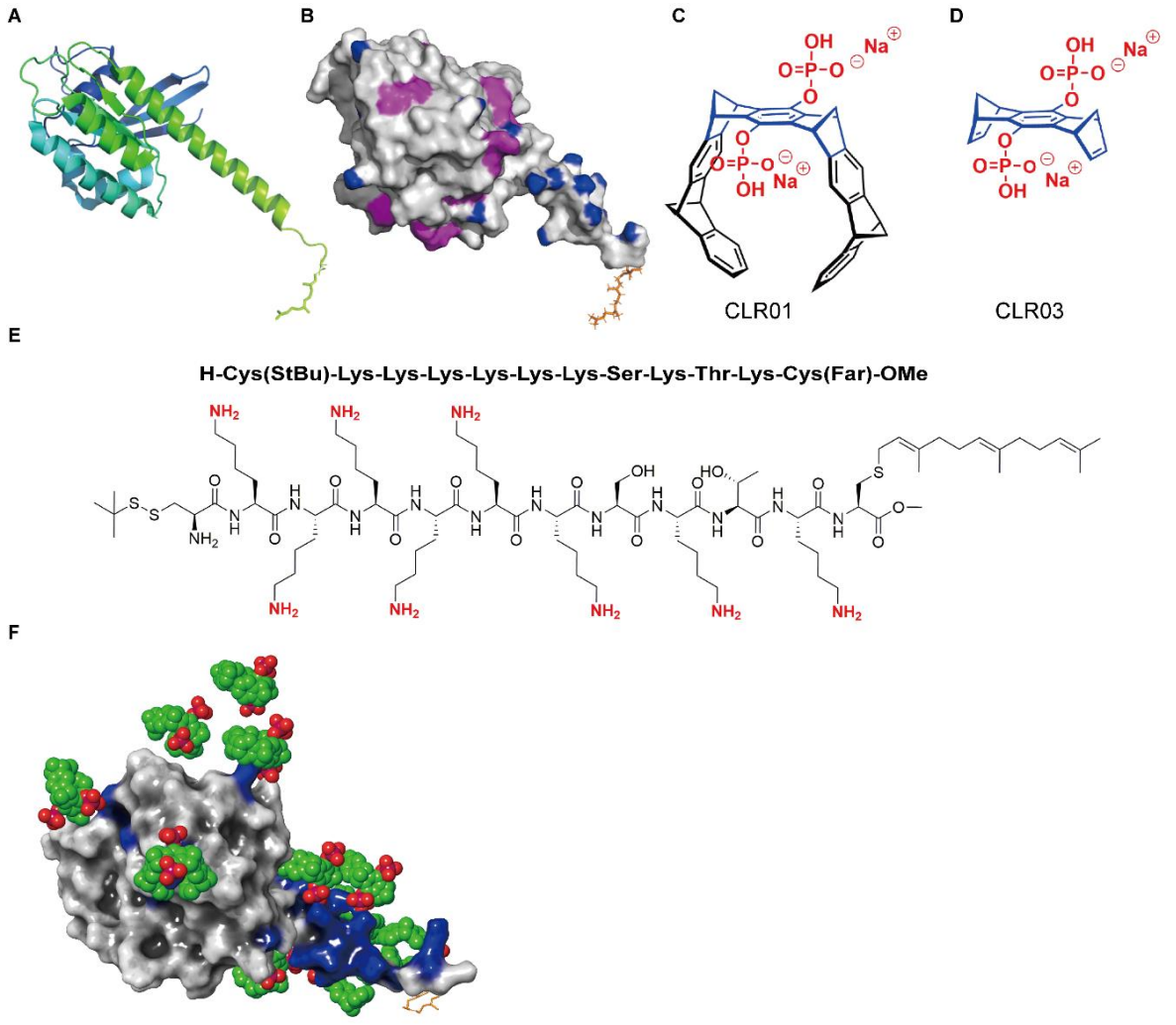

Figure 4-3-1. (A) Schematic representation of the structure of the K-Ras4B protein, adapted from the crystal structure (PDB: 5TAR). (B) Schematic of the K-Ras4B protein's surface generated using PyMOL (PDB: 5TAR). The arginines on the protein surface are shown in violet and the amine of lysines in blue. (C) Chemical structure of the tweezer CLR01. (D) Chemical structure of the tweezer CLR03 serving as control. (E) Structure of the K-Ras4B peptide (residues 175-185, an additional cysteine was added in the N-terminus for native chemical ligation). (F) Final structure from a 200 ns MD simulation in 150 mM aq. NaCl with explicit water. Note that from eleven docked tweezer molecules in the start configuration, three dissociated into the bulk solvent and eight remained bound to the protein. From these, four bound to lysines by side chain inclusion and the other four by formation of highly dynamic ammonium phosphate clusters.

Here we describe a new principle, i. e. prevention of membrane targeting of a regulatory protein by molecular tweezers. Specifically, we demonstrate, how the lysine binder CLR01 is capable of dissociating K-Ras4B from the lipid membrane by targeting the polybasic domain of K-Ras4B. Our results show that the tweezer CLR01 binds to K-Ras4B peptide (Figure 4-3-1E) containing the polybasic domain with a K_d of ~4.0 µM in bulk solution and with a K_d of ~11.6 µM even in the presence of lipid membranes. Further, we show that CLR01 can dissociate both the active GTP-bound and the inactive GDP-bound K-Ras4B protein from the lipid bilayer membrane and thereby disrupt the K-Ras4B nanoclusters formed in the lipid membrane. Figure 4-3-1B depicts the exposed lysine residues in the largely disordered polybasic domain of the hypervariable region of K-Ras4B (in blue) and the arginine residues (in violet) - further potential binding partners of the tweezer - on the surface of the K-Ras4B protein [50, 174]. When K-Ras4B binds to the lipid membrane, simulations and biophysical studies have shown that the lysines of the polybasic domain are located outside the lipid bilayer, whereas the farnesylated lipid anchor is inserted in the lipid membrane [175, 58 and 176], so that the polybasic domain should still be largely accessible for the tweezer CLR01.

4.3.2 Preparation of large unilamellar vesicles (LUVs) and giant unilamellar vesicles (GUVs)

For the preparation of LUVs, the DOPC lipid was dried by a stream of nitrogen gas and then placed into a freeze drier overnight for complete drying. After that, the lipid film was rehydrated with Tris buffer (20 mM Tris, 5 mM $MgCl_2$, pH = 7.4). LUVs were generated after five freeze-thaw-vortex cycles. Homogeneous LUVs were obtained using an extruder (Avanti Polar Lipids, USA) with polycarbonate membrane of 100 nm diameter at 65 ˚C. GUVs were prepared by electroformation [16,177] in a homemade chamber consisting of a closed bath imaging chamber RC-21B with a volume of 360 µL mounted on a P-2 platform (both Warner Instruments, Hamden, USA). The dried DOPC lipids were dissolved in chloroform, mixed with 0.2 mol% *N*-Rh-DHPE and then spread onto optically transparent and electrically conductive indium tin oxide (ITO) coated glass slides (SPI supplies, West Chester USA) (20-30 µL) and spin coated at 800-100 rpm for 1 min. In order to remove residual chloroform, the glass cover slips

were freeze-dried overnight. After that, Tris buffer was added into the chamber. A 5 V, 10 Hz sinusoidal excitation was applied for 2 h to induce repetitive stress on the hydrated lipid bilayer, leading to vesicle swelling and GUV formation.

4.3.3 Tweezer CLR01 is able to bind to the K-Ras4B peptide containing the polybasic domain of K-Ras4B

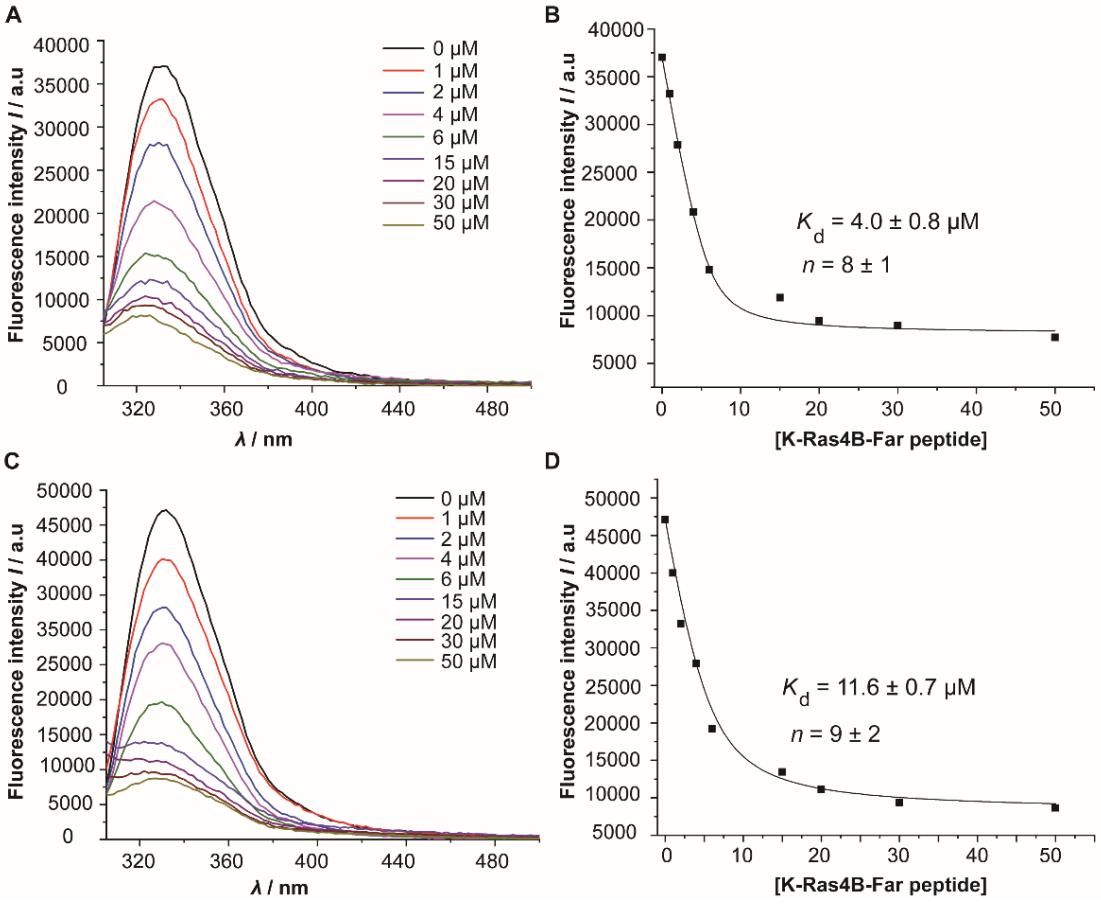

Figure 4-3-2. (A, C) Emission spectra of the tweezer CLR01 (Figure 4-3-1C) as a function of K-Ras4B peptide (Figure 1E) concentration in the absence (A, B) and presence (C, D) of a lipid bilayer membrane (LUVs of DOPC) in Tris buffer (20 mM Tris, 5 mM $MgCl_2$, pH = 7.4). (A, C) Emission spectra were monitored in the range of 305 to 500 nm with excitation at a wavelength of 285 nm. (B, D) Plots of the emission intensity of the tweezer CLR01 at λ_{em} = 336 nm as a function of K-Ras4B peptide concentration.

Previous studies have shown that the tweezer CLR01 has a strong emission band at ~330 nm upon UV/Vis excitation at ~285 nm, and complexation of lysine residues by the tweezer CLR01 results in partial quenching of this emission intensity. Hence, the dissociation constant, Kd, of the CLR01-guest complex can be determined by

fluorimetric titration experiments.[178] Using this approach, we measured the K_d values of the tweezer CLR01 binding to the K-Ras4B peptide in the absence and presence of a 1,2-dioleoyl-phosphatidylcholine (DOPC) lipid bilayer, which serves as model biomembrane (Figure 4-3-2). The dissociation constant for the tweezer CLR01 binding to the K-Ras4B peptide in Tris buffer (20 mM Tris, 5 mM $MgCl_2$, pH = 7.4) amounts to 4.0 ± 0.8 µM (Figures 4-3-2A, 2B, for fitting). The corresponding K_d-value for CLR01 binding to the K-Ras4B peptide in the presence of the lipid membrane amounts to 11.6 ± 0.7 µM (Figures 4-3-2C, 2D); it is about three times larger, but still

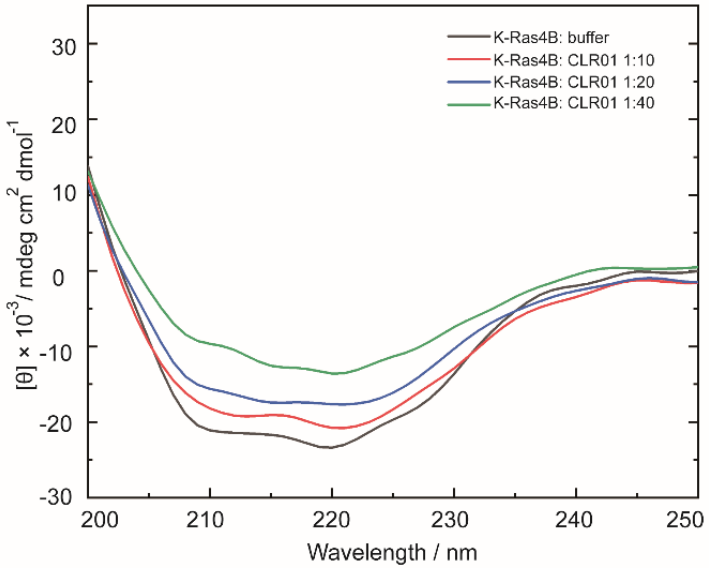

Figure 4-3-3. CD spectra of the K-Ras4B protein in buffer (10 mM Na_2HPO_4, 2 mM KH_2PO_4, pH = 7.4) at different concentrations of the tweezer CLR01.

of similar magnitude. The number of binding sites, *n*, for the tweezer CLR01 binding to the K-Ras4B peptide is obtained from the fit as well and amounts to 8 ± 1. This value indicates that essentially all lysine residues in the K-Ras4B peptide are accessible for the tweezer. A similar value of n = 9 ± 2 is even obtained for CLR01 binding to the K-Ras4B peptide when bound to the DOPC lipid bilayer, indicating that the presence of the competing bilayer does not compromise K-Ras4B complexation by the tweezers. This finding explains the high potential of CLR01 to destabilize K-Ras4B binding to the membrane and to extract the K-Ras4B peptide from the lipid bilayer as observed by microscopy (see below). Complementary CD spectra recorded of the K-Ras4B protein upon addition of CLR01 suggest that the tweezer CLR01-

lysine/arginine complexation is only accompanied by small conformational changes (conformational drift) within K-Ras4B (Figure 4-3-3) [179], lending further support that the tweezer CLR01 is able to bind to the lysines of K-Ras4B.

The fluorescence titration measurements were performed on a K2 multifrequency phase and modulation fluorometer (ISS, Champaign, IL, USA). In the titration experiment, 100 µL of the 50 µM tweezer CLR01 solution was placed in a quartz cuvette and the peptide was added stepwise. The fluorescent tweezer was excited at a wavelength of 285 nm and the emission spectra were recorded in the range of 300 to 600 nm. All measurements were performed at 25 °C using a circulating water bath. The dissociation constant, Kd, and number of binding sites, *n*, was determined by Equation (2) using a multiple binding sites fitting procedure:

$$I = \left[\frac{1}{2[T]_0}\left(([T]_0 + n[P] + K_\mathrm{d}) - \sqrt{(([T]_0 + n[P] + K_\mathrm{d})^2 - 4n[T]_0[P])}\right)\right] \times (I_\mathrm{min} - I_\mathrm{o}) + I_\mathrm{o}$$

(S4-2-1)

$[T]_0$ is the total concentration of the tweezer CLR01 and $[P]$ is the concentration of added K-Ras4B peptide; n is the number of binding sites and K_d is the dissociation constant. Imin is the lowest fluorescence intensity of the tweezer CLR01 that can be reached upon quenching with K-Ras4B peptide. Io is the fluorescence intensity of the tweezer CLR01 in the absence of K-Ras4B peptide, and I is the fluorescence intensity of the tweezer CLR01 in the presence of different concentrations of K-Ras4B peptide.

4.3.4 MD simulations of the tweezer CLR01 with K-Ras4B protein

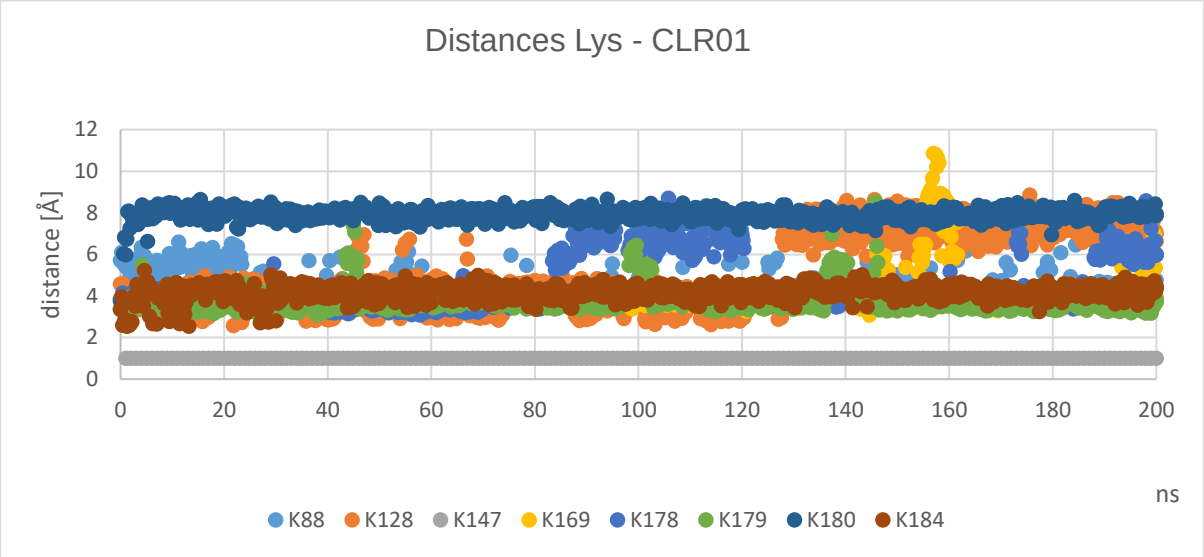

Figure 4-3-4. Distances between CLR01 and the lysines it was placed on, extracted from the MD simulation (Carried out by Dr. Felix Niemeyer). Atom pairs were defined consisting of the lysine side chain nitrogen and the outer phosphorus atom of the corresponding tweezer. Top view: Survey of all lysine/tweezer distances; bottom view: close-up of those tweezers whose overall distances from their lysine binding partners remained below 8 Å.

In-silico studies were performed by Dr. Felix Niemeyer (University of Duisburg-Essen, Germany) to support the thermodynamic affinity data and to better understand the microscopic observations (Fig. 4-3-1F). To this end, 11 lysine residues were chosen by accessibility – three of them on the surface of the K-Ras4B protein and eight in the hypervariable region (K88, K128, K147, K169, K175, K177, K178, K179, K180, K182 and K184). 11 tweezers were placed upon them; however, in the polybasic region not all lysines could accommodate a tweezer molecule. The following 200 ns molecular dynamics simulation with explicit water supports the observed overall stoichiometry from the titrations of about 8 to 9 tweezers per protein, for those on lysine 175 and 182 dissociated after 40 and 52 ns, respectively. A third tweezer dissociated after 150 ns from lysine 177. All the other tweezers remained within 8 Å of the original lysines.

All calculations were performed in Maestro 11.9. The protein structure was retrieved from the PDB as 5TAR. Subsequent preparation was done using the protein preparation wizard (bond order assignment with the help of the CCD database, addition of hydrogens, filling of missing sidechain atoms, deletion of all waters and the generation of het states at pH 7.0) followed by H-bond assignment using PROPKA at pH 7.0 and a restrained minimization to converge the heavy atoms to RMSD below 0.3 Å. Tweezers were imported into Maestro as SMILES and subsequently placed manually onto the lysines. The resulting protein structure with 11 tweezers was relaxed by means of a restrained minimization.

MD simulations were performed with Desmond from D. E. Shaw. The solvent model was SPC and the box shape orthorhombic with the box size at 10 Å buffer to the protein. Charges were neutralized by the addition of 41 sodium ions and sodium chloride was added to a total concentration of 150 mM. The following molecular dynamics simulation was set up to run for 200 ns with the trajectory saved every 200 ps resulting in 1000 trajectory frames (energy saved every 1.2 ps). The ensemble class was NPT with a temperature of 300 K and a pressure of 1013 mbar. The model system was relaxed before the productive run by the standard relaxation protocol provided. Calculations were performed on a Nvidia GTX 1070 graphics card.

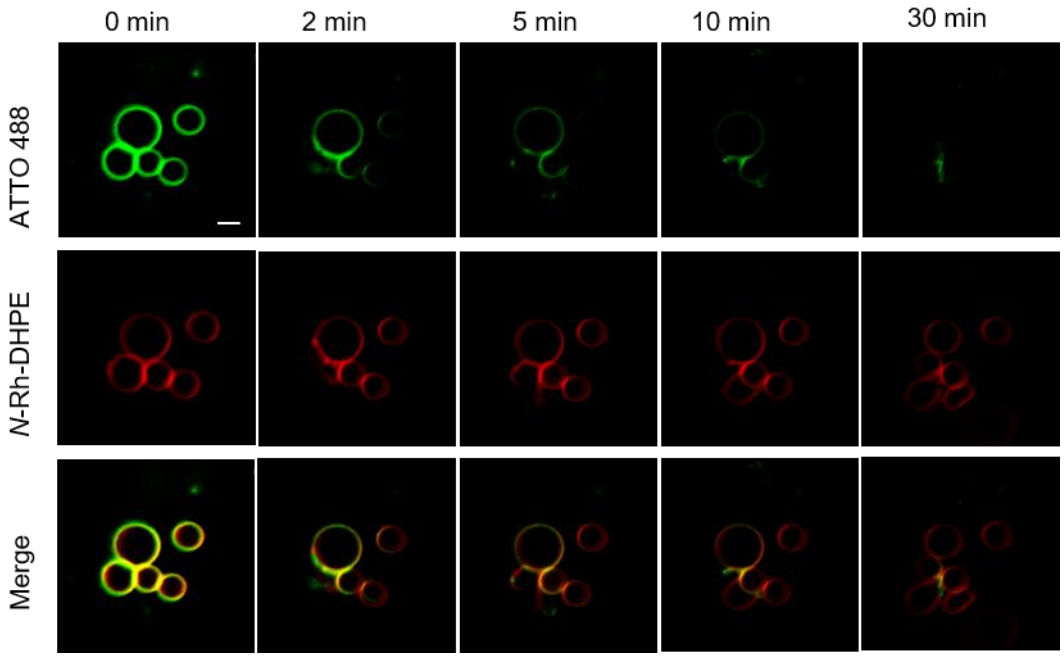

Figure 4-3-5. Confocal laser scanning images of the time-dependent ATTO 488-labeled GDP-K-Ras4B (2 µM in 360 µL Tris buffer) after addition of 100 µM CLR01 in GUVs composed of DOPC. N-Rh-DHPE (0.2 mol%) was used as membrane marker. Scale bar = 10 µm.

The resulting MD simulation was first analyzed by visual inspection, followed by extraction of the distances between CLR01 and the lysines it was placed on. For this, the simulation event analysis tool was used and atom pairs were defined consisting of the lysine side chain nitrogen and the outer phosphorus atom of the corresponding tweezer.

Interestingly, the only half of all tweezers display their typical binding mode towards lysine side chains that point into the cavity for lysines 88 and part of the time for lysines 128, 178 and 184. The other tweezers show a different behavior: here, the negatively charged phosphates interact with one or two ammonium ions of the neighbouring lysines via salt bridges. In this case the hydrophobic aromatic rings point away from the charged protein surface and may to a certain extent shield it. Binding is partially assisted by π-cation interactions between lysine ammonium ions and the aromatic rings of the tweezers. This unique clustering binding mode may indeed assist the detachment process from the membrane by inducing conformational changes in the hypervariable region of K-Ras4B.

4.3.4 Tweezer CLR01 dissociates the K-Ras4B protein from the lipid membrane

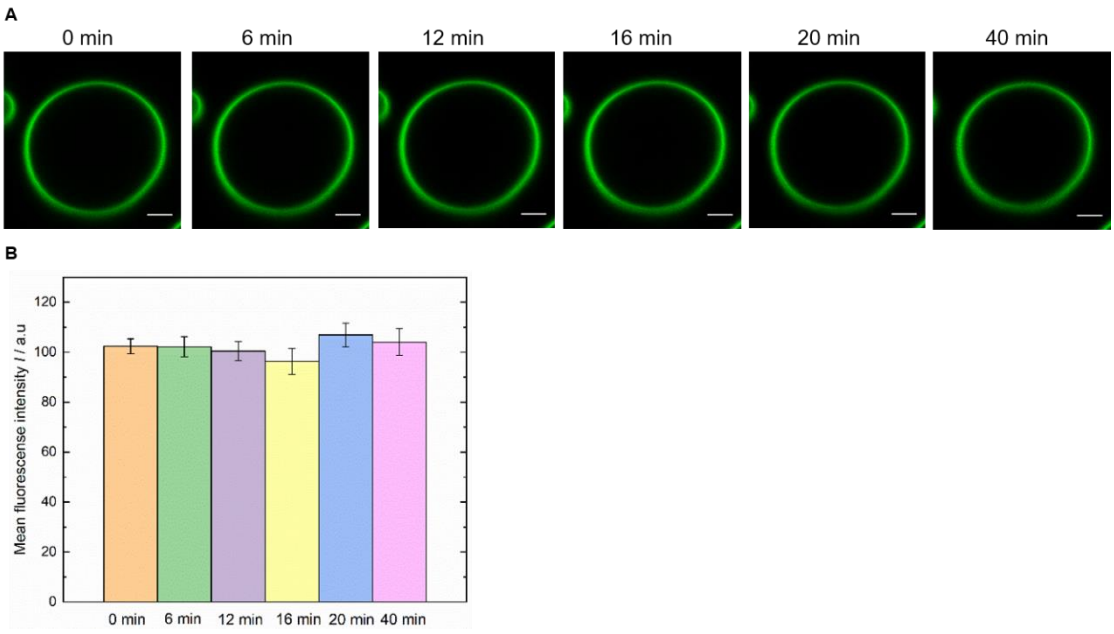

Figure 4-3-6. (A) Confocal laser scanning microscopy images of the time-dependent ATTO 488-labeled GTP-K-Ras4B (2 µM in 260 µL, Tris buffer) in GUVs composed of DOPC. Scale bar = 5 µm. (B) Quantification of fluorescence intensity of time-dependent ATTO 488-labeled GTP-K-Ras4B in GUVs of DOPC.

Confocal laser scanning microscopy experiments were carried out in order to directly visualize the complexation event of CLR01 tweezer molecules to K-Ras4B bound to the lipid membrane. Giant unilamellar vesicles (GUVs) of DOPC with diameters of about 30 µm were used as model membrane. The GUVs were prepared using the electroformation method (details are given in the SI). GTP-bound and ATTO 488-labeled K-Ras4B protein was injected into the optical chamber, allowing to bind to the lipid membrane for 30 min. Before injecting the tweezer CLR01 (150 µM) into the chamber, the system was washed with Tris buffer to remove potentially unbound K-Ras4B protein. As can be clearly seen in Figure 4-3-5, the fluorescence intensity of ATTO 488-labeled K-Ras4B bound to the lipid vesicle decreases significantly after injection of the tweezer. Fluorescence intensity quantification of the ATTO 488-labeled K-Ras4B at different time points after injecting CLR01 shows an about 90% decrease within 2 min (Figure 4-3-7B). In a control study, Figure 4-3-6 shows that in the absence of the tweezer, there is only a 0.1% fluorescence intensity decrease of ATTO 488-labeled GTP-K-Ras4B after 6 min. which might be due to minor photobleaching with time. These data provide experimental evidence for the tweezer's ability to extract active GTP-bound K-Ras4B protein from the lipid membrane. Figure 4-3-5 shows that the tweezer CLR01 is also able to dissociate K-Ras4B in its inactive GDP-bound form.

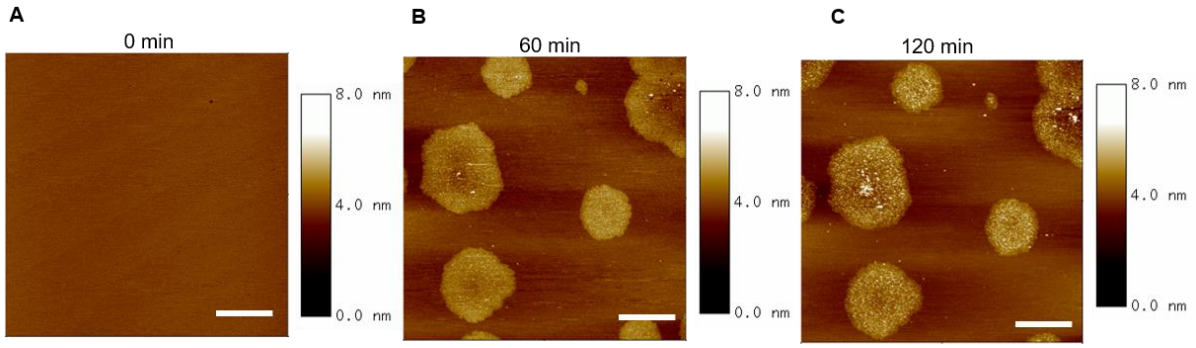

Figure 4-3-8. AFM images of the time-dependent partitioning and lateral organization of GDP-K-Ras4B in the lipid bilayer composed of DOPC. The AFM images are shown before (A) and after injection of 200 µL of GDP-K-Ras4B ($c_{K\text{-}Ras4B}$ = 2 µM) in Tris buffer (20 mM Tris, 5 mM $MgCl_2$, pH = 7.4) into the AFM fluid cell. After 60 min, the AFM fluid cell was washed using Tris buffer and the AFM image (B) was taken. Tweezer CLR03 at a concentration of 25 µM in Tris buffer was injected into the AFM fluid cell. After 120 min, the AFM fluid cell was washed and the AFM image (C) was recorded. Scale bar = 1 µm.

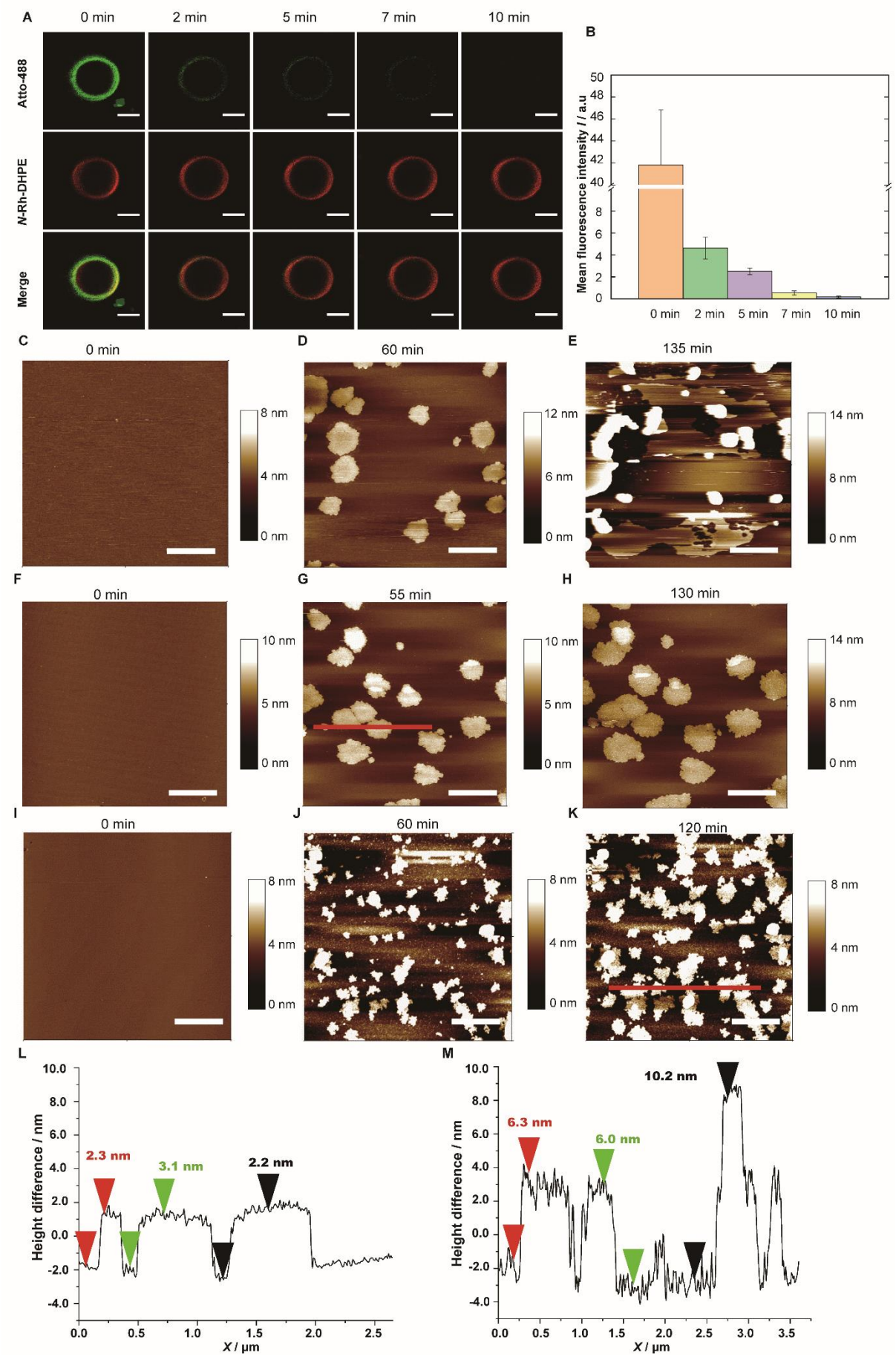
A
0 min
2 min
5 min
7 min
10 min
Atto-488
N-Rh-DHPE
Merge
B
Mean fluorescence intensity I / a.u
0 min
2 min
5 min
7 min
10 min
C
0 min
8 nm
4 nm
0 nm
D
60 min
12 nm
6 nm
0 nm
E
135 min
14 nm
8 nm
0 nm
F
0 min
10 nm
5 nm
0 nm
G
55 min
10 nm
5 nm
0 nm
H
130 min
14 nm
8 nm
0 nm
I
0 min
8 nm
4 nm
0 nm
J
60 min
8 nm
4 nm
0 nm
K
120 min
8 nm
4 nm
0 nm
L
Height difference / nm
2.3 nm
3.1 nm
2.2 nm
X / µm
M
Height difference / nm
6.3 nm
6.0 nm
10.2 nm
X / µm

Figure 4-3-7. (A) Confocal laser scanning microscopy images of the time-dependent ATTO 488-labeled GTP-K- Ras4B protein (2 µM of 360 µL Tris buffer) after addition of 150 µM CLR01 in GUVs prepared from DOPC. N-Rh-DHPE (0.2 mol%) was used as membrane marker. Scale bar = 20 µm. (B) Quantification of the fluorescence intensity of ATTO 488-labeled GTP-K-Ras4B protein in DOPC GUVs. (C, D, E) AFM images of the time-dependent partitioning and lateral organization of GTP-K-Ras4B in the DOPC lipid bilayer. The AFM images are shown before (C) and after injection of 200 µL of GTP-K-Ras4B ($c_{K\text{-}Ras4B}$ = 2 µM) in Tris buffer (20 mM Tris, 5 mM $MgCl_2$, pH = 7.4) into the AFM fluid cell. After 60 min, the sample was washed using Tris buffer and AFM images of GTP-K-Ras4B nanoclusters (D) were recorded. In the following, tweezer CLR01 (45 µM) in Tris buffer was injected into the AFM fluid cell. After 135 min, the AFM fluid cell was washed using Tris buffer and AFM image were taken (E). (F, G, H) AFM images of the time-dependant partitioning and lateral organization of GTP-K-Ras4B in the DOPC lipid bilayer. The AFM images are shown before (F) and after injection of 200 µL of GTP-K-Ras4B (cK-Ras4B = 2 µM), showing again formation of K-Ras4B nanoclusters (G). Upon injection of the tweezer CLR03 (45 µM), washing after 130 min using Tris buffer, AFM images were recorded (H), showing no significant changes in the lateral organisation (nanoclustering) of the K-Ras4B protein. (I, J, K) AFM images of the DOPC bilayer in the absence (I) and presence of pre-incubated CLR01-K-Ras4B complex in bulk solution after 60 and 120 min, showing adsorption of large K-Ras4B-tweezer aggregates attached to the lipid interface, only. Scale bar = 1 µm. (L, M) AFM height profiles of the areas marked with a red line (x-axis) in Figures 3G and 3K, respectively.

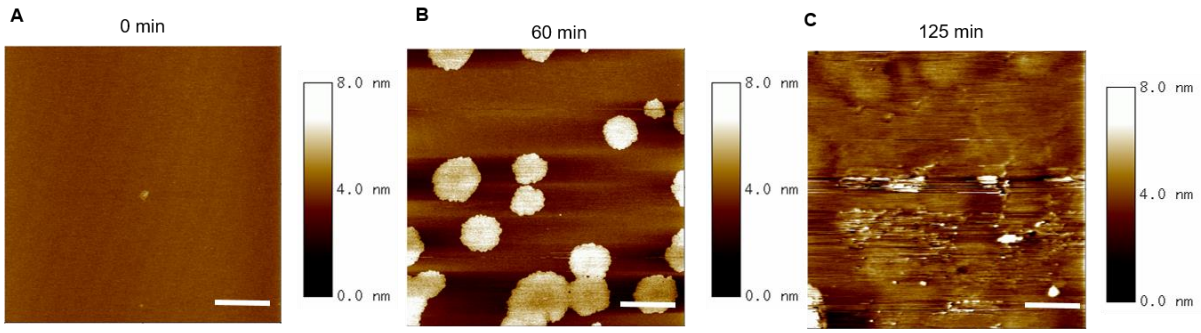

Figure 4-3-9. AFM images of the time-dependent partitioning and lateral organization of GDP-K-Ras4B in the lipid bilayer composed of DOPC. The AFM images are shown before (A) and after injection of 200 µL of GDP-K-Ras4B (cK-Ras4B = 2 µM) in Tris buffer (20 mM Tris, 5 mM $MgCl_2$, pH = 7.4) into the AFM fluid cell. After 60 min, the AFM fluid cell was washed using Tris buffer and the AFM image (B) was taken. Tweezer CLR01 at a concentration of 25 µM in Tris buffer was injected into the AFM fluid cell. After 125 min, the AFM fluid cell was washed and the AFM image (C) was taken. Scale bar = 1 µm.

K-Ras4B is known to form nanoclusters in the cell membrane, which is essential for high-fidelity activation of K-Ras4B signaling [55]. Spontaneous nanoclustering has also been observed in homogeneous and heterogeneous model membrane systems

[17, 62 and 180]. To reveal the influence of the tweezer CLR01 on the K-Ras4B nanoclusters at molecular resolution, we conducted time-lapse tapping-mode atomic force microscopy (AFM) experiments. Using the technique of *in situ* injection of a K-Ras4B protein solution into the AFM fluid cell, the same region of the lipid bilayer could be observed before and after incorporation of the protein (details of the preparation are described elsewhere [17, 62]. Before injecting K-Ras4B protein into the fluid cell, we verified deposition of a homogeneous DOPC lipid bilayer on the atomically flat hydrated mica surface (Figure 4-3-7C). After addition of GTP-bound K-Ras4B protein, tapping-mode AFM measurements were carried out at several time points. Figure 4-3-7D reveals that K-Ras4B nanoclusters are readily formed in the lipid bilayer, in agreement with literature data [17, 62 and 180]. Our own previous studies have shown that embedding K-Ras4B into membranes results in (lipid-mediated) attractive protein-protein interactions and formation of nanoclusters with heights of about 2.0 to 2.5 nm [17, 62 and 180].

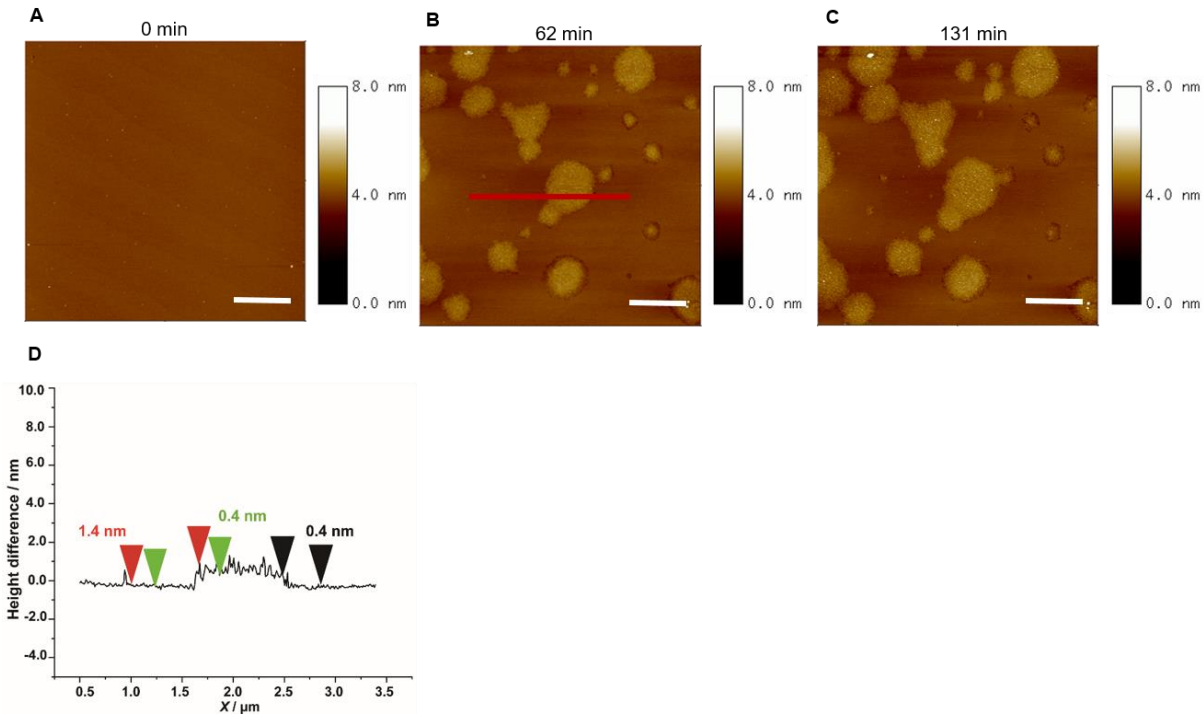

Figure 4-3-10. GDP-K-Ras4B pre-incubated for 1 h with the tweezer CLR01 (20 µM) in Tris buffer. AFM images are shown before (A) and after injecting the solution of pre-incubated K-Ras4B+CLR01 into the AFM fluid cell. After 60 min and 120 min, the AFM fluid cell was washed using Tris buffer and AFM images (B, C) were taken subsequently. All scale bars in the AFM images indicate 1 µm. (D) AFM height profile of the area marked by the red line in B.

Before injecting the tweezer CLR01 into the AFM fluid cell, the neat bilayer system was washed using Tris buffer to remove potentially unbound K-Ras4B protein. Comparison of the images 4-3-7D and 4-3-7E demonstrates that tweezer addition is able to disrupt these membrane-bound K-Ras4B nanoclusters and leaves behind some dissociated large CLR01-complexed protein aggregates on top of the lipid membrane next to dissociated K-Ras4B protein accumulated in the buffer solution. As a valuable control, an inactive structurally related compound without sidewalls, CLR03 (Figure 4-3-1D), which is not able to include lysine residues, was used for the AFM experiments. In contrast to CLR01, the control CLR03 had no effect on both GTP-bound and GDP-bound K-Ras4B nanoclusters in the lipid membrane (see Figures 4-3-7F-4-3-7H and Figures 4-3-6, 4-3-8).

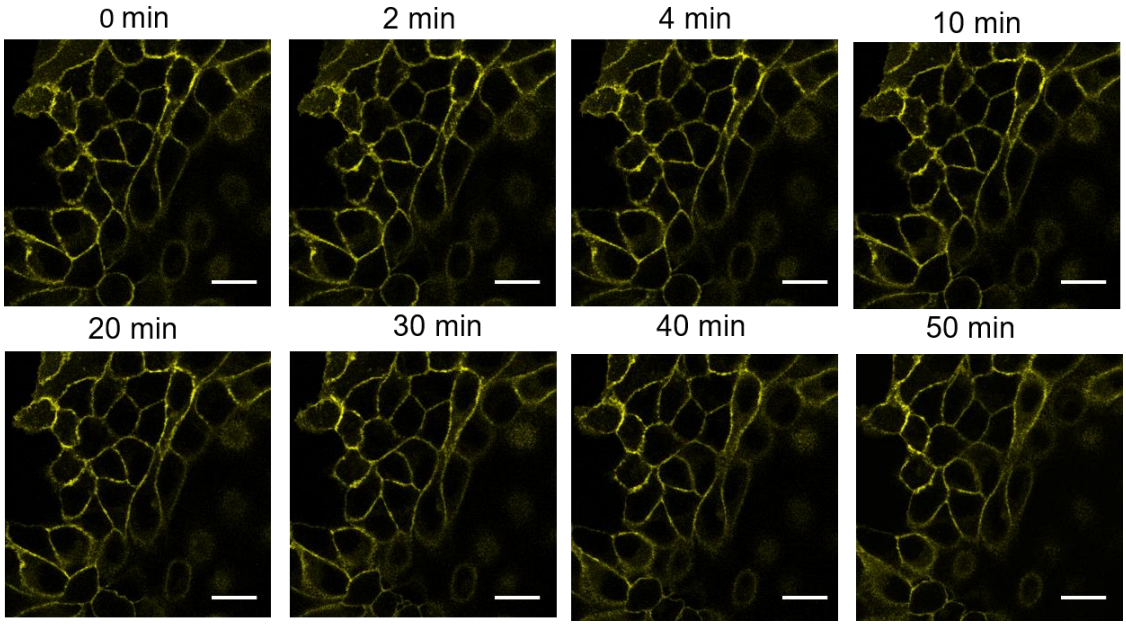

Figure 4-3-11 MDCK cells of Citrine-K-Ras4B were treated with 150 µM of tweezer CLR01. Images were recorded by laser-scanning confocal microscopy at different time points. Citrine was excited by a wavelength of 488 nm light and emission were collected from 510 nm to 670 nm. A long-pass filter of 500 nm was used for the emission collection. MDCK cells were placed in an incubator mounted on the confocal microscopy (Leica SP5), where can keep the temperature at 37 C° and 5% CO_2. The medium was in the absence of phenol red, which can intervene the fluorescence of the MDCK cells of Citrine-K-Ras4B. Scale bar = 50 µm.

Besides dissociation of K-Ras4B from the membrane, the prevention of de novo K-Ras4B nanoclustering inside the lipid membrane can also be expected to be an effective strategy for modulating K-Ras4B signaling. To explore, if the tweezer is

indeed able to suppress nanocluster formation in the DOPC lipid bilayer, different concentrations of CLR01 were incubated with K-Ras4B protein in bulk solution. After incubation for 1 h, this solution was injected into the AFM fluid cell containing the model membrane and tapping-mode AFM measurements were carried out. While in the absence of CLR01, K-Ras4B nanoclusters were smoothly formed in the lipid bilayer, no such nanoclusters were formed upon incubation with CLR01 (Figures 4-3-7-I-K). Rather, some large K-Ras4B -tweezer aggregates (with heights of about 6-8 nm) were found loosely attached to the lipid interface. Importantly, at low tweezer concentrations, K-Ras4B nanoclusters were again formed but with smaller sizes.

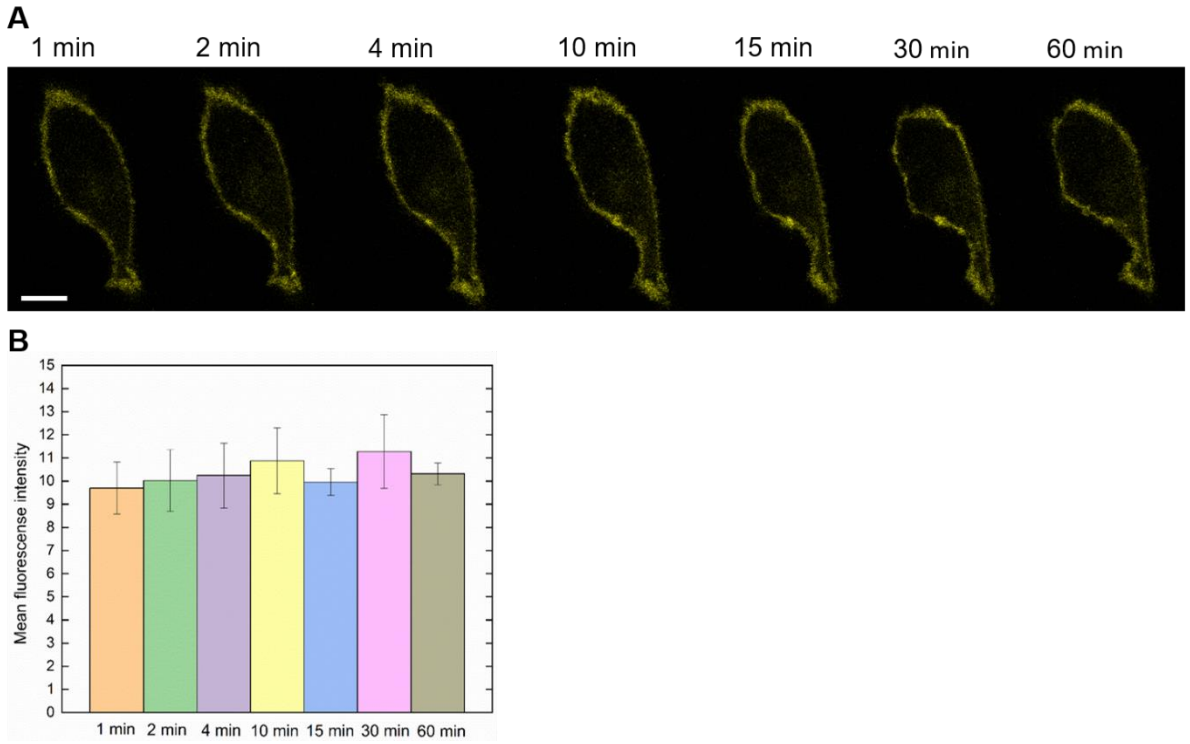

Figure 4-3-12 (A) MDCK cells of Citrine-K-Ras4B were treated with 500 µM of tweezer CLR01. Images were recorded by laser-scanning confocal microscopy at different time points. Citrine was excited by a wavelength of 488 nm light and emission were collected from 510 nm to 670 nm. A long-pass filter of 500 nm was used for the emission collection. MDCK cells were placed in an incubator mounted on the confocal microscopy (Leica SP5), where can keep the temperature at 37 C° and 5% CO_2. The medium was in the absence of phenol red, which can intervene the fluorescence of the MDCK cells of Citrine-K-Ras4B. Scale bar= 20 µm. (B) Quantification of fluorescence of Citrine-K-Ras4B of MDCK cells in the presence of tweezer CLR01 of 500 µM. The quantification analysis was performed using software ImageJ.

Since it has been proved that tweezer CLR01 is able to dissociate K-Ras4B from the lipid membrane, we presumed that the tweezer CLR01 may also be capable of dissociating K-Ras4B in the plasma membrane. To explore the effect of tweezer CLR01 on K-Ras4B in the plasma membrane, we constructed a stable MDCK cell lines of Citrine-K-Ras4B. The cells were seeded in the imaging wells and grew for the measurements for 12 h. Different concentrations of tweezer CLR01 were incubated with the MDCK cells of Citrine-K-Ras4B. The fluorescent images at each time points were recorded by laser-scanning confocal microscopy. The recorded images with quantification of fluorescence in the plasma membrane suggest that the tweezer CLR01 has no effect on the K-Ras4B in the plasma membrane. However, *in vivo* data (unpublished) of tweezer CLR01 by the group of Prof. Thomas Schrader (University of Duisburg-Essen) indicate that the tweezer CLR01 cannot cross the plasma membrane is a consequence, no effect of the tweezer CLR01 on K-Ras4B in the inner surface of the plasma membrane can be explained as seen here.

4.3.4 Conclusion and discussion

In summary, we have presented a new strategy to prevent K-Ras4B signaling by Supramolecular Chemistry. It is based on the ability of the molecular tweezer CLR01 to bind efficiently to the polybasic domain of the K-Ras4B protein. Due to the powerful shielding of the entire polybasic domain of the protein, its electrostatic attraction to the phospholipid head groups is cancelled. Thus CLR01 is able to markedly weaken the essential K-Ras4B/membrane interaction and dissociate bound K-Ras4B protein from the lipid interface. Moreover, the tapping-mode AFM measurements indicate that the tweezer is also able to disrupt the K-Ras4B nanoclusters formed in the lipid bilayers, thereby efficiently reducing the protein's signaling output. Finally, we could show that the tweezer CLR01 is able to already induce complex formation with K-Ras4B protein in bulk solution, thereby reducing its propensity to bind to the lipid membrane and form nanoclusters (Figure 4-3-7 I, J and K). Taken together, these data suggest that targeting of the polybasic domain of K-Ras4B using molecular tweezers might represent an effective strategy for inactivation of K-Ras4B signaling.

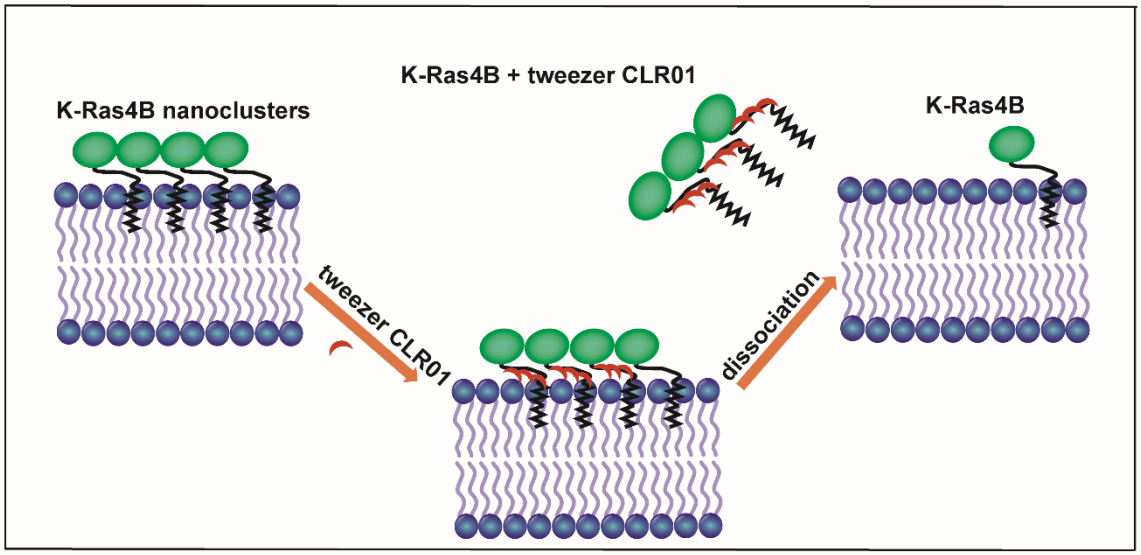

Figure 4-3-13. Schematic representation of the mechanism of dissociation of K-Ras4B from the lipid membrane by the molecular tweezer CLR01.

To conclude, direct and indirect approaches to targeting Ras cancers are underway in academia and in many pharmaceutical companies. Small molecules that bind tightly to RAS proteins have been difficult to find, mostly because RAS proteins lack a deep pocket to which small molecules could bind with high affinity. Several low-affinity compounds have been reported but do not appear to have been developed beyond their initial characterization [25, 144]. Other approaches have focused on compounds that prevent GEF-mediated GDP/GTP exchange.[181, 182] Further inhibitors being studied and discussed for inhibiting Ras signaling encompass K-Ras4B (G12C), the prenyl-binding protein PDEσ, Raf-RBD, and SOS1 [117,182, 183, 123, 122]. The inhibitor targeting the mutant K-Ras4B (G12C) can disrupt the binding with Raf and SOS, its application is limited to the K-Ras4B (G12C)-driven cancer, however. For drugs that do not need to discriminate between wild-type and mutant forms, other strategies are needed. Transferase inhibitors can potently inhibit the farnesyltransferase enzyme which adds a farnesyl lipid tail to the cysteine in the HVR domain of K-Ras4B [184]. However, it has been reported that K-Ras4B can escape the farnesyltransferase inhibitor because it can be geranylgeranylated instead. These compounds can truly inhibit K-Ras4B farnesylation, but K-Ras4B can still associate with membrane though the compensatory activity of geranylgeranyltransferase-I, and

the toxicity of the farnesyltransferase inhibitor with geranylgeranyltransferase-I inhibitor in vivo limits the duration of the treatment [140, 36 and 37].

In a different approach, the tweezer CLR01 disrupts the association of K-Ras4B with the membrane by targeting the polybasic domain. While the tweezer CLR01 has a weak binding affinity with K-Ras4B, it can recognize all mutations of K-Ras4B-related cancer through targeting the polybasic domain, i.e. it directly targets K-Ras4B. Similar polybasic domains, comprising lysine residues or a combination of lysine and arginine residues, are also found in other proteins of the Ras family, like RhoA, RhoC, Rap1A and Ral [185, 186], this strategy may therefore be also explored for the inactivation of other signaling proteins of that family. Selectivity for the specific Lys and Arg pattern and a stronger binding affinity may be achieved with multivalent tweezer constructs based on precision oligomers. To this end we have recently developed a synthetic strategy for the construction of tweezers with a single alkyne unit [187]. First dimeric and trimeric tweezers with well-defined distances have already been generated by “click chemistry” in our laboratory. Furthermore, cell culture experiments are on the agenda to explore the benefit of the approach in the context of the biological cell. Overall, considering the complexity of Ras isoforms, effector functions and downstream pathways as well as feedback loops and signaling redundancy, the challenge of shutting down Ras signaling remains an enormous task still to be achieved.

4.4 Identification and mechanistical characterization of Raf and SOS1 interacting with K-Ras4B in the lipid membrane

4.4.1 Raf and SOS1 proteins interact with K-Ras4B in cell membranes

K-Ras4B is a small GTPase and oncoprotein , which plays a major role in cellular signaling regulation, including proliferation, apoptosis and differentiation, by binding its effectors and regulators, such as Raf and SOS1 [188] . However, mutations in K-Ras4B and its isoforms, H-Ras, N-Ras and K-Ras4A are present in 20-30% of human tumors [116]. Some tumors, such as pancreatic ductal adenocarcinomas have K-Ras4B mutations (nearly 90%) and K-Ras4B is the most frequently mutated Ras isoform, which makes K-Ras4B an attractive target for Ras-driven cancers. Despite more than 30 years of intensive efforts to develop inhibitors of Ras, no effective inhibitors can fight Ras-driven cancers [185].

Ras proteins function as a molecular binary switch, oscillating between a GDP-bound, inactive form and a GTP-bound, active form. The nucleotide exchange from GDP-bound to GTP-bound is stimulated by guanine nucleotide exchange-effectors (GEFs) and the conversion back to the GDP-bound form by GTPase-activating proteins (GAPs) leading to fast GTP hydrolysis [52]. Mutations of Ras impair or greatly decrease intrinsic GTP hydrolysis rates of GAPs, resulting in formation and accumulation of GTP-bound Ras [72]. The binding affinity of Ras with GTP is picomolar and the cellular concentration of GTP is millimolar, which renders directly targeting GTP of Ras unsuccessful. Signaling of Ras strongly depends on the association with the inner face of the plasma membrane and the subsequent recruitment and interaction with Ras effectors. The cysteine of the C-terminal CAAX (C, cysteine; A, aliphatic amino acid; X, terminal amino acid) of Ras can be farnesylated by farnesyltransferase [189]. The modifications that occur in the cytosol by Ras converting enzyme 1 (RCE1) and isoprenylcysteine carboxyl methyl transferase (ICMT) make Ras C-terminal methylated in order to delete the negative charge and prevent plasma membrane repulsion [43]. The additional palmitoylation of H-Ras, N-Ras and K-Ras4A or the polybasic domain of K-Ras4B promote Ras association with the plasma membrane [31].

Three Raf isoforms, A-Raf, B-Raf, and C-Raf function as Ras effectors, which participate in Ras-Raf-MEK-ERK signaling cascades [190]. Sequence alignments shows that the Raf isoforms share conserved regions: CR1, CR2 and CR3. CR1 comprises the N-terminal Ras-binding domain (RBD), which followed by a cysteine-rich domain (CRD). CR2 is a serine/threonine-rich domain containing a 14-3-3 binding site. CR3 is the kinase domain with a long and flexible linker connected to CR2 [94]. Although K-Ras4B preferentially activates C-Raf, B-Raf can be activated by K-Ras4B similarly, whereas A-Raf is only weakly activated. B- and C-Raf stay in an inactive form, closed conformation in the cytosol, which is stabilized by 14-3-3 complex and other phosphatases [191]. RBD recognizes GTP-bound K-Ras4B and forms a tight and persistent complex through the effector binding site of Ras. Crystal structures of B-Raf-RBD with H-Ras reveal that RBD binds to the effector binding site of Ras with high affinity. The B-Raf-RBD/H-Ras complex formation alters amide exchange rates and induces allosteric changes in B-Raf-RBD. This suggests that Ras binding can induce the drastic domain rearrangements of RBDs in order to active Raf kinase [192]. All three Ras proteins share a conserved G domain with two flexible surface loops, named switch I (residues 30-40) and switch II (residues 60-76) involved in nucleotide, effectors and regulator binding. Further, the RBDs from B-Raf and C-Raf share 100% sequence identity in the function and Ras-interaction with two β strands: β1 and β2 strands (^{157}RVFLPNKQRTVV^{169}), and A-Raf with 83% (^{157}KVYLPNKQRTVV^{169}) [193], which suggests a highly similar binding model for the B-Raf-RBD and C-Raf-RBD, while there might be a different binding model for the A-Raf-RBD compared with B- and C-Raf-RBD.

The cysteine-rich domain (CRD) of Raf proteins is thought to play an important role for membrane contact and interaction. MD simulations show that the C-Raf-CRD reduces the fluctuations of C-Raf-RBD/K-Ras4B at the membrane and enhances the C-Raf-RBD/K-Ras4B binding affinity at the membrane, resulting in facilitating C-Raf kinase domain dimerization and activation [194], thus K-Ras4B dimerization and Raf-MEK-ERK signal transduction. H-Ras was shown to form an H-Ras/C-Raf-CRD complex and the farnesyl lipidated-membrane anchor is attracted by C-Raf-CRD. Moreover, C-Raf-CRD was reported to interact selectively with phosphatidylserine (PS) in the lipid membrane. Simulation studies indicate that the basic residues of C-Raf-CRD interact with the anionic lipids strongly to evolve into a lipid-anchored

conformation with electrostatic interaction being the driven force [194]. Lys-148 is the most important residue responsible for C-Raf-CRD binding, followed by Arg-143, Lys-144 and Lys-157, which is shown by simulation studies [194]. It was reported that these lysine residues defined the clusters and the interaction with PS induced by C-Raf-CRD in the lipid membrane, which is consistent with the hypervariable region (HVR) of K-Ras4B shaping the K-Ras4B nanoclusters. Since the linker connecting RBD to CRD only has six amino acid residues, C-Raf-CRD restrains the K-Ras4B/RBD fluctuations at the membrane. Sequence alignments show that at the relative position of Lys-148 of C-Raf-CRD, Ser-108 and Tyr-244 are located in the A-Raf-CRD and B-Raf-CRD, respectively [195]. This suggest that the A- and B-Raf-CRD interaction with membrane might be different from that with C-Raf-CRD.

Raf interaction with K-Ras4B is of great significance, which is the key step of MAPK signaling. Since B- and C-Raf proteins are autoinhibited in the cytosol with a closed conformation by binding of 14-3-3 and its inhibitory domains, they have to be recruited by GTP-bound, active K-Ras4B protein and dephosphorylated in order to be an open conformation [86]. Activation of B-Raf and C-Raf kinases is followed by phosphorylation of the activation sites with the kinase and conformation rearrangements lead to kinase domain dimerization as active state [196]. A-Raf activation is poorly understood and it seems to only be weakly activated by Ras [197]. Although the crystal structures of the complex of H-Ras with B-Raf-RBD and the solution structure of C-Raf-CRD by NMR provide their location, the relative position of RBD with respect to the CRD and the function of the CRD in the lipid membrane are unknown. To date, there are still no Raf-RBD-CRD or full-length Raf structures available. Simulation studies suggest that the RBDs recognize the GTP-K-Ras4B in the lipid membrane leading to an identical conformational change and CRDs are a membrane binding domain, which restrain the K-Ras4B/C-Raf-CRD complex fluctuations and enhance the binding affinity of K-Ras4B/C-Raf-RBD [195]. However, an integrated study of RBD and CRD with K-Ras4B in the lipid membrane is still missing. To activate Raf, Raf has to locate and contact with the lipid membrane through the binding of the RBD with K-Ras4B. Thus, a precise understanding of Raf interaction with membranes is essential to understand Raf activation. Furthermore, differential activation of Raf might be determined by the local lipid composition of the membrane. Understanding of the three Raf isoforms in the context of lipid membranes

is a fundamental aspect of Raf and Ras biology, and characterizing these interactions will be important for explaining the function of these three Raf isoforms different function in the MAPK pathway and interventions aimed at Ras-driven cancers.

The protein Son of Sevenless (SOS) has two human isoforms: SOS1 and SOS2 [198]. They are all Ras-GEF proteins, which catalyze the nucleotide exchange from the GDP-bound to the GTP-bound state. The GTPase-activating proteins (GAPs) mediate GTP-bound active forms to GDP-bound inactive forms. The Ras-GEFs and Ras-GAPs regulate the level of active and inactive Ras proteins, which control the Ras signaling pathway. In this study, we focused on SOS1.

The activation of SOS1 is a multistep process, which includes membrane recruitment, release of autoinhibition, and modulation by Ras [98, 99, 100]. The PxxP motif of the C-terminal proline-rich (PR) domain is thought to initially associate with the lipid membrane. SOS contains a series of N-terminal domains, namely the Db1 homology (DH), pleckstrin homology (PH) and a histone-fold (HF) domain, which inactivate SOS proteins in solution. Upon association with lipid membranes, the autoinhibition is released. The allosteric pocket located at the REM and CDC25 domain (named as catalytic domain) binds to Ras proteins, resulting in full activation of SOS proteins [108, 109]. Although the process of membrane recruitment and release of autoinhibition is fully understood, the interaction of the catalytic domain with the lipid membrane is poorly understood. Recent studies show that inhibitors targeting the K-Ras4B-SOS1 complex can block the GTP binding with K-Ras4B, leading to an antiproliferative activity. This suggests that targeting K-Ras4B/SOS1 might represent an effective strategy for Ras-driven cancer therapy. Therefore, a comprehensive understanding of the interaction between the catalytic domain of SOS1 and K-Ras4B in the lipid membrane is needed.

4.4.2.1 Raf-RBDs and SOS1 expression and purification

The B-Raf-RBD genes were inserted into vector pGEX-2T (MBP tagged with a thrombin cleavage site) using BamHI and EcoRI enzyme restriction sites from Gene script (USA). A, C-Raf-RBD plasmids with a pGEX-2T vector (GST-tagged with a thrombin cleavage site) and SOS1 (564-1059) plasmid with a pET28a vector (His6 tagged with a TEV cleavage site) were given from Christian Herrmann (MPI Dortmund) as a gift. SOS1 (564-1059) were transformed into *E.coli* (DE3) BL21. The cells were

grown at 37 °C with 5 liters of LB media. Protein expression was induced with 0.5 mM IPTG when the culture reached an OD_{600} of 0.5-0.6 for 16 hours. 5 liters of culture cells were resuspended to Tris buffer (20 mM Tris, 500 mM NaCl, 2 mM TCEP, pH=7.4) (Buffer A) using 10 ml. Appropriate units of protease inhibitor (SIGMA*FAST* Protease Inhibitor Tablets) were added to the unclarified lysate and centrifuged at 15,000 rpm for 30 min at 4 °C. All subsequent steps were performed at 4 °C. 20 mM imidazole was added into the clarified lysate and then loaded onto a His-Trap column (GE Healthcare, 5 ml). The equilibration buffer (20 mM imidazole in Buffer A) (Buffer B) was used to wash the His-Trap column. The column was washed to baseline using elution buffer (Buffer C, 500 mM imidazole in Buffer A) with a gradient from 20-500 mM imidazole. The fractions was collected and analyzed by SDS-PAGE and Coomassie-staining. The confirmed elution pool was transferred to a storage buffer (20 mM Tris, 5 mM $MgCl_2$, 2 mM TCEP, pH=7.4) using HiPrep 26/10 desalting column (GE Healthcare). His6-TEV protease (Sigma-Aldrich, USA) at 1:100 (w/w) was added into the elution pool and allowed to digest for 8 hours. The cutting was analyzed by SDS-PAGE and Coomassie-staining. The digested solution was loaded to His column to remove His6-TEV protease and some His6-tagged full-length proteins. The final proteins were concentrated to an appropriate volume and frozen as small aliquots.

A-, B-, C-Raf-RBD plasmids transformation and cell culture are the same with SOS1 (564-1059) purification. The clarified lysates were loaded onto a GST-trap FF (GE Healthcare) column and washed using Tris buffer (20 mM Tris, 500 mM NaCl, 2 mM TCEP, pH=7.4). The column was washed using elution buffer (20 mM Tris, 10 mM reduced glutathione, pH=8.0). The fractions were collected and analyzed by SDS-PAGE and Coomassie-staining. The confirmed elution pool was transferred to the storage buffer (20 mM Tris, 5 mM $MgCl_2$, 2 mM TCEP, pH=7.4) and thrombin protease (GE Healthcare) (8 unit per mg) was added into the elution pool and allowed to digest for 10 hours. The cutting was confirmed by SDS-PAGE and Coomassie-staining. The digested solution was reloaded onto GST column to remove GST and some GST-tagged full-length proteins. Next, the eluate was loaded onto a HiTrap Benzamidine FF (high sub) (GE Healthcare) column to remove the thrombin enzyme. The final proteins were concentrated to an appropriate volume and frozen as small aliquots.

4.4.2.2 K-Ras4B protein synthesis

Full-length K-Ras4B proteins were synthesized using expressed protein ligation (EPL) [62]. The plasmid of K-Ras4B-intein-CBD was given from the Prof. Herbert Waldmann group (MPI Dortmund). The plasmid was transformed into *E. coli* BL21 (DE3) and cells was grown at 37 °C. Protein expression was induced with 0.5 mM IPTG when the culture reached an OD_{600} of 0.5-0.6 for 16 hours. All the subsequent steps were performed at 4 °C. The cells were lysed by ultrasonification in lysis buffer (20 mM Tris, 500 mM NaCl, 2 mM $MgCl_2$, pH=7.4). The clarified lysate was loaded onto a chitin beads affinity column after equilibration with lysis buffer. The intein splicing was introduced by incubation of the column with intein splicing buffer (20 mM Tris, 500 mM NaCl, 2 mM $MgCl_2$, 50 mM MESNA, pH=8.5) overnight. The generated K-Ras4B (∆15)-MESNA thioester was transferred to lysis buffer using HiPrep 26/10 desalting column (GE Healthcare) and concentrated with size exclusion filtration (Amicon Ultra-15 MWCO 10 kD). The final protein was quick frozen and stored at -80 °C. The K-Ras4B peptide (H-Cys (StBu)-Lys_6-Ser-Lys-Thr-Lys-Cys (Far)-OMe) was synthesized using solid-phase peptide synthesis (SPPS) by Eurogentec Deutschland GmbH (Köln, Germany). The K-Ras4B peptide (0.1 µmol, 5 eq.) dissolved in the ligation buffer (20 mM Tris, 100 mM NaCl, 2 mM $MgCl_2$, pH=7.4). The K-Ras4B peptide was ligated to K-Ras4B (∆15)-MESNA thioester (1.32 mg) by native chemical ligation (NCL) in the ligation buffer at pH=7.2 (adjusted to the final pH using NaOH or HCL solution) for 5 h. The purification was performed on a Hi-Trap SP-XI (GE Healthcare, 1 ml) using cation exchange chromatography. The protein was characterized by SDS-PAGE, Coomassie-staining and ESI-MS. The final protein obtained was concentrated by size exclusion filtration (Amicon Ultra-15 MWCO 10 kD, Millipore) and frozen as small aliquots.

4.4.3 A-, B- and C-Raf-RBD are all recruited to the K-Ras4B protein in the lipid membrane

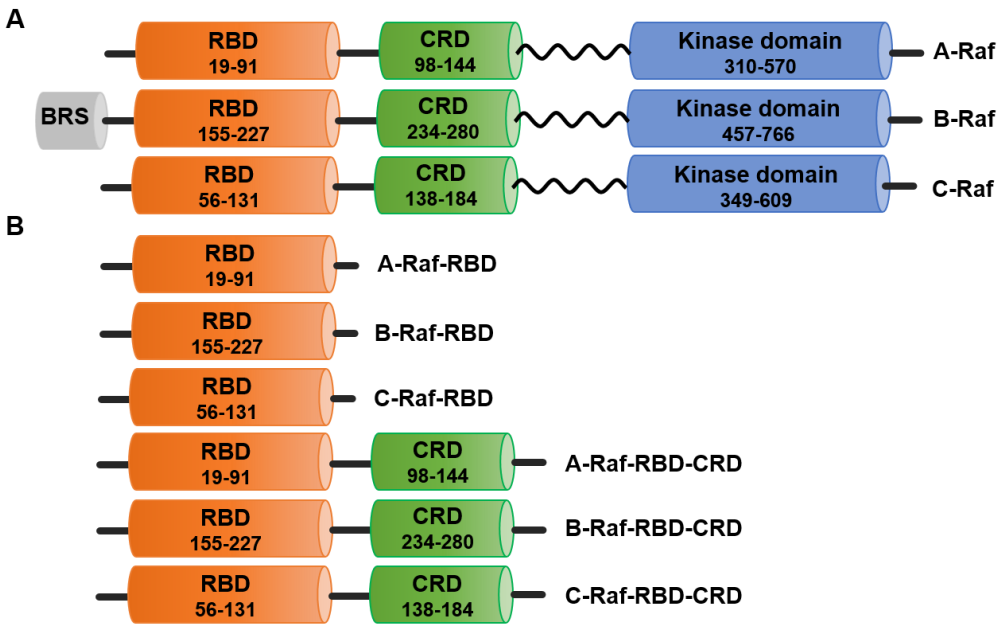

Figure 4-4-1 The Raf kinases and their truncation fragments. (A) Full-length A-, B- and C- Raf kinases. (B) The A-, B- and C-Raf truncation fragments were designed and used for this study. Detailed information can be found in the part of protein purification as described under ‘’Methods’’ in this chapter. The fragments of A-, B- and C-Raf-RBD-CRD are still in the process of expression and purification.

The RBD of the Rafs was initially proposed to interact with Ras proteins in the lipid membrane, resulting in recruitment of Raf proteins to the plasma membrane. However, recent data suggest that particular membrane lipids contribute to this process via interaction with the Raf proteins [199]. The crystal structure analysis of B-Raf-RBD/H-Ras indicates that the B-Raf-RBD/H-Ras complex formation alters amide exchange rates and induces allosteric changes in B-Raf-RBD [193]. These findings suggest that Raf RBDs might play unclarified roles in Raf kinase activation besides simply binding to Ras proteins. To investigate the potential mechanism of interaction between RBD and K-Ras4B proteins in the lipid membrane, we prepared three fragments containing RBD domains of A-, B- and C-Raf (Figure 4-4-1 B) and studied their interaction with the lipid membrane (Lipid composition: DOPC:DPPC:cholesterol=1:2:1) using tapping-mode atomic force microscopy (AFM) at molecular level. The kinetic tapping-AFM measurements were carried out in an AFM fluid cell with direct protein injection technology, and the same region of lipid bilayer can be observed both before and after incorporation of proteins. We found that the height of K-Ras4B nanoclusters increases dramatically upon A-, B- and C-Raf-RBD incorporation (Figure 4-4-3 A, C and E), which indicates that A-, B- and C-Raf-RBD are all recruited to the K-Ras4B protein residing in the lipid membrane. Further, these data indicates that A-, B- and C-Raf

RBD form a RBD/K-Ras4B complex with the RBD and located at the top of K-Ras4B proteins, resulting in a marked increase of height.

The RBD of Raf proteins recognize Ras proteins in the lipid membrane and bind to them with high affinities in the switch I region of the Ras proteins [192, 193]. As a consequence of this binding, the formation of asymmetric Raf homo- and heterodimers in the plasma membrane is promoted [192]. These Raf homo- or heterodimers recruit and phosphorylate MEK1 and MEK2, which are the downstream substrates of Raf [190]. Thus, the dimer formation is essential for Raf signaling activation. The RBD of all Raf isoforms are identical and enriched in the platform of K-Ras4B nanoclusters (Figure 4-4-3 A, C and E), which strongly facilitates Raf dimer formation in the lipid membrane. This further suggests that formation of K-Ras4B nanoclusters enhances Raf binding and signaling activation as it enriches the Raf proteins and facilitates formation of Raf dimers in the lipid membrane.

4.4.4 RBD of A-, B- and C-Raf determines the population of Raf-RBD/K-Ras4B complex formation in the lipid membrane

Although A-, B- and C-Raf share three conserved regions, they function different in cells [191, 200]. It has been reported that A-Raf is only weakly activated by Ras, whereas B-Raf is the strongest activated, followed by the moderately activated C-Raf [201]. A-Raf is poorly understood and the reason of weakly active A-Raf by Ras proteins is still unclear. Since we applied the kinetic AFM measurements on an AFM fluid cell with protein directly injection technology, it allows us to quantify the A-, B- and C-Raf-RBD binding to the K-Ras4B in the lipid membrane. The quantification shows that 73% of injected B-Raf-RBD binds to the K-Ras4B in the lipid membrane, followed by 68% of injected C-Raf-RBD that binds to either the K-Ras4B in the lipid membrane or to the disordered phase of the lipid membrane, while only 26% of injected A-Raf-RBD binds to the K-Ras4B in the lipid membrane (this calculation was performed using the concentration of K-Ras4B determined in the solution after 2 h incubation). This indicates that the RBD of A, B and C-Raf determines the degree of Raf-RBD/K-Ras4B complex formation in the membranous context. Further, this lower population of A-Raf-RBD/K-Ras4B complex might contribute to the weak activation of A-Raf by Ras in cells. The B-Raf-RBD induces a larger population of the Raf-RBD/K-

Ras4B complex than C-Raf-RBD as a large amount of C-Raf-RBD itself bind to the lipid membrane. Since Raf activation requires the B- and C-Raf to form either homodimers or heterodimers, the probability of forming Raf-RBD/K-Ras4B complex would be expected to determine the population of the Raf dimers formed and correlates with the Raf-MEK-ERK signaling output [190]. Sequence alignments of the RBD domain of A-, B- and C-Raf-RBD shows that a lysine at position 22 located within the A-Raf-RBD, whereas an arginine is located within the relevant position with respect to B- and C-Raf-RBD [202]. It was shown that the presence of the lysine at position 22 partly blocks the association of A-Raf with Ras [203]. Considering that A, B and C-Raf-RBD have a comparable strong binding affinity with K-Ras4B [204], the lysine at position 22 may interfere the A-Raf interaction with K-Ras4B indirectly. Based on the intimate engagement of Raf activation by K-Ras4B in the lipid membrane, we may postulate that the RBD of A, B and C-Raf might contribute to the Raf activation by controlling the population of Raf/K-Ras4B complex formation in the lipid bilayer plane.

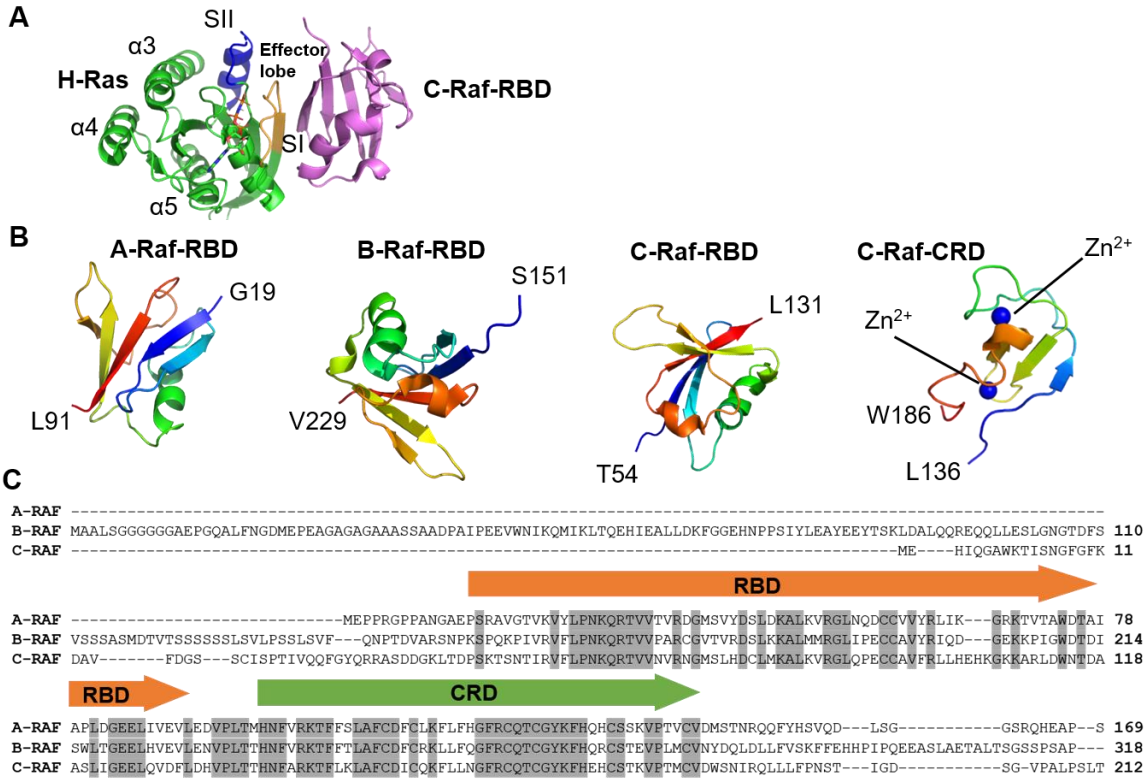

Figure 4-4-2 (A) The structure of H-Ras/C-Raf-RBD (PDB: 4G0N). C-Raf-RBD binds to the SI region of H-Ras. (B) The structure of A-, B-, C-Raf-RBD and C-Raf-CRD. (C) Sequence alignment of the A-, B- and C-Raf-RBD-CRD regions.

4.4.5 B- and C-Raf-RBD bind to the lipid membrane, whereas A-Raf-RBD forms nanoclusters in the lipid membrane

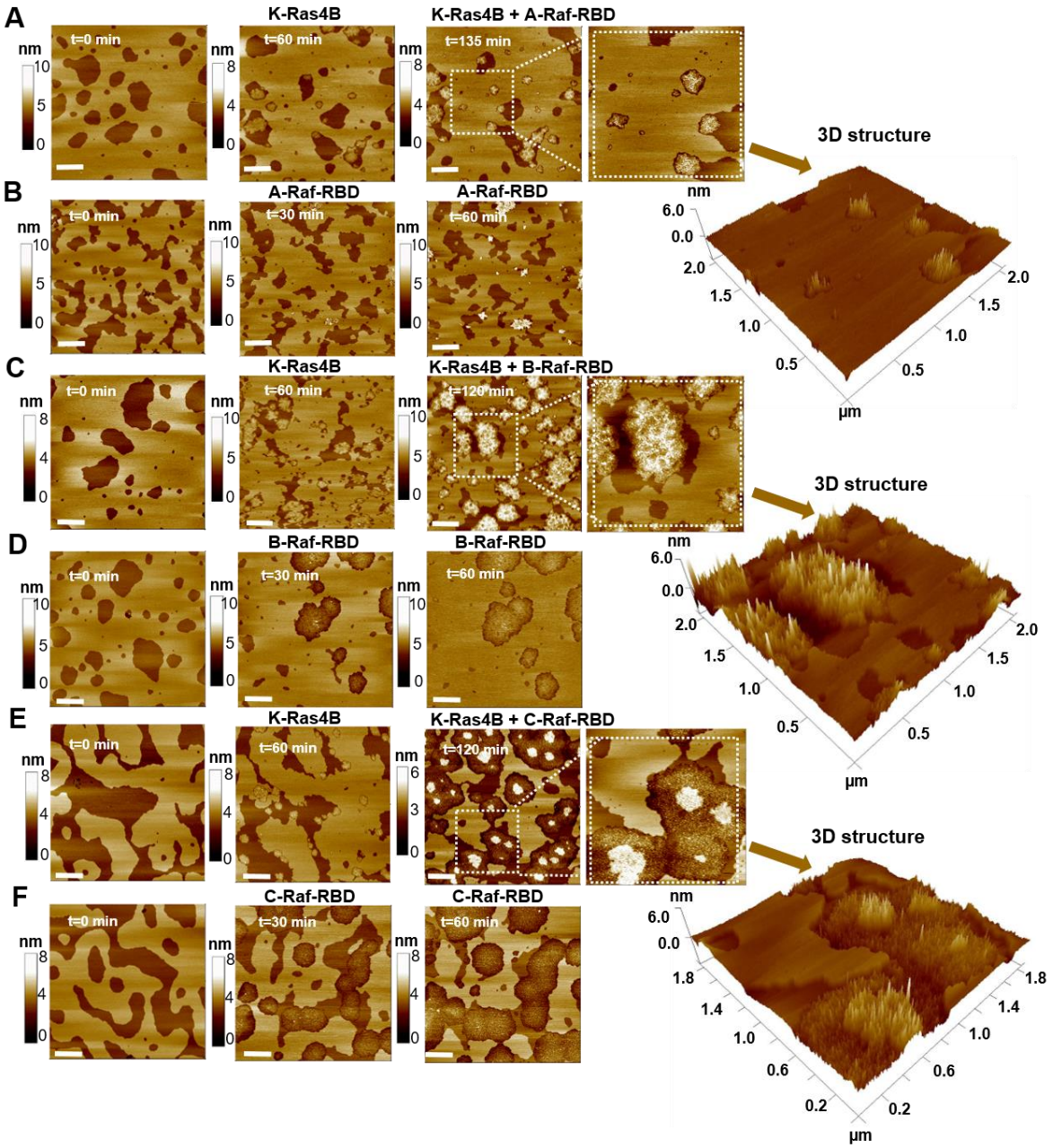

Figure 4-4-3 A, B and C-Raf-RBD interaction with the lipid membrane (lipid composition: DOPC:DPPC:cholesterol=1:2:1) and the K-Ras4B protein in the lipid membrane. (A) A-Raf-RBD binds to K-Ras4B in the lipid membrane. (B) A-Raf-RBD interaction with the lipid membrane. (C) B-Raf-RBD

binds to K-Ras4B in the lipid membrane. (D) B-Raf-RBD interaction with the lipid membrane. (E) C-Raf-RBD binds to K-Ras4B in the lipid membrane. (F) C-Raf-RBD interaction with the lipid membrane. 3D AFM images of K-Ras4B with A-, B- and C-Raf-RBD, generated using the NanoScope version 6 software. The concentration of Raf-RBD and K-Ras4B in the AFM measurements are all 2 µM. Scale bar = 1 µm. K-Ras4B proteins were all GTP-loaded (active state).

To investigate the interaction of A-, B- and C-Raf-RBD with the lipid membrane, we carried out kinetic time-lapse AFM measurements of the A-, B- and C-Raf-RBD with the lipid membrane. Interestingly, we found that B- and C-Raf-RBD bind to the lipid membrane and localize essentially with monomeric state into the disordered phase (Figure 4-4-3 B, D and F). In contrast to B and C-Raf-RBD, A-Raf-RBD forms nanoclusters in the lipid membrane. Since the Raf-RBDs are supposed to function as a Ras binding domain, it was unexpected that Raf-RBD can interact with the lipid membrane directly. Recent NMR studies show that the surface accessible lysine (K28, K66 and K69) and arginine (R30 and R68) of the A-Raf-RBD interact with anionic membranes [205]. Sequence alignments show that C-Raf-RBD shares completely the same amino acid residues at the relevant position of A-Raf-RBD and B-Raf-RBD share the same amino acid residues at the relevant position of K28, R30 and K69 of A-Raf-RBD. The electrostatic interaction of positively charged arginine or lysine contributes to the interaction of A-, B-, and C-Raf-RBD with the lipid membrane. These findings suggest that the Raf-RBD might operate together with the Raf-CRD, which is thought to bind to the lipid membrane, allowing the Raf proteins to make contact with the lipid interface. Owing to the very short linker (6 amino acid residues) between RBD and CRD of A, B and C-Raf [194], the RBDs of A-, B- and C-Raf would be difficult to contact with the lipid membrane after binding to K-Ras4B. Combining our results obtained with previous simulation studies, we may propose that the RBDs of the three Raf isoforms support interaction with the lipid membrane and thus may help transiently to sustain partitioning of the Raf proteins at the lipid interface.

4.4.6 SOS1 (564-1049) can bind to K-Ras4B in the lipid membrane

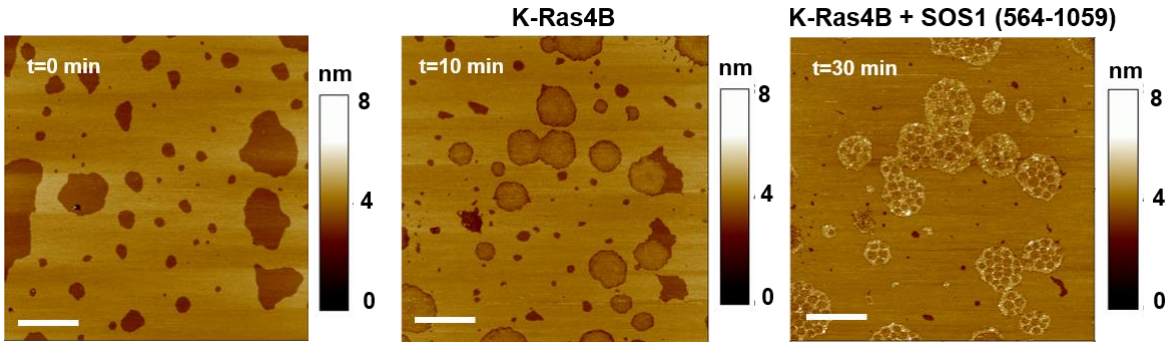

Figure 4-4-4 SOS1 (564-1059) interaction with GDP-K-Ras4B in the lipid membrane. The concentration of SOS1 (564-1059) and GDP-K-Ras4B are 2 µM. Scale bar = 1 µm.

SOS1 functions as a Ras-GEF, which catalyze the transformation of GDP-bound Ras to GTP-bound Ras. The structure of the Ras-SOS1 complex reveals that SOS1 interacts tightly with Ras in a nucleotide-free state with a displacing mechanism. The regions of Ras interacting most closely with SOS1 are the P-loop (residues 10-17), switch I (25-40) and switch II (57-75). Helix α3 (57-75) of Ras is also found to interact with SOS1 [105]. The interface between Ras and SOS1 is very hydrophilic and extensive, and opens the nucleotide binding site as a consequence of the displacement of switch I of Ras. The activation of SOS contains several processes, involving membrane recruitment, the suspension of autoinhibition and allosteric modulation by Ras proteins. The PxxP motif of C-terminal proline-rich (PR) domain of SOS is thought to initially associate with the lipid membrane. SOS contains a series of N-terminal domains. They are the Db1 homology (DH), pleckstrin homology (PH) and a histone-fold (HF) domain, which inactive SOS proteins in solution. Upon association with the lipid membranes, the autoinhibition is released [109]. However, the mechanism of SOS1 association with the lipid membranes is unclear. We applied kinetic tapping-mode AFM to study SOS1 interacting with GDP- K-Ras4B in the lipid membrane. Figure 4-4-4 shows that the height of GDP-K-Ras4B increases drastically, which indicates that SOS1 (564-1059) binds to the GDP-K-Ras4B in the lipid membrane. The data further indicates that the catalytic domain of SOS1 (752-1044) binds to GDP-K-Ras4B in the upside position.

4.4.4 Conclusion and discussion

In summary, we found that A-, B- and C-Raf-RBD are all able to recognize the K-Ras4B located in the lipid membrane. Interestingly, B- and C-Raf-RBD are able to bind to the lipid membrane however, which was unexpected through the understanding of the function of Ras binding domain. A-Raf-RBD displays a different effect when added to the lipid membrane. It is shown that the height of A-Raf-RBD in the lipid membrane is far beyond the size of the monomeric A-Raf-RBD protein, which indicates that A-Raf-RBD preferentially forms nanoclusters in the lipid membrane. Importantly, RBDs of A-, B- and C-Raf seem to control the population of Raf/K-Ras4B complexes in the lipid membrane. Considering that the formation of Raf/K-Ras4B is crucial for Ras-Raf activation, the RBD of Raf may plays a role in regulating Raf activation. We also found that SOS1 (564-1059) binds to GDP-K-Ras4B in the lipid membrane in an upside position. Complementary measurements, using X-ray scattering, FITR and FCCS as well as ITC are planned in the future to understand the interaction between Raf-RBDs, SOS1 and K-Ras4B in the lipid membranes in more detail.

5. Materials and Methods

Part of the work (chapter 5.6 and 5.7) herein has been published in the following peer-reviewed research articles and subsequently reprinted in parts with the permission of the journals. The contributions of co-authors are either distinctly marked or not shown as they are a result of this thesis.

1. L. Li, N. Erwin, S. Möbitz, F. Niemeyer, and T. Schrader, R. Winter. "Dissociation of the Signaling Protein K-Ras4B from Lipid Membranes Induced by a Molecular Tweezer." *Chem. Eur. J.*, 25 (**2019**), 9827 – 9833.

Copyright: was published online on 29 September, 2019 and DOI is 10.1002/chem.201901861. In this publication is partially reproduced in section 5.6 and 5.7 with the permission by John Wiley & Sons, Inc. Copyright ©2015Wiley-VCH Verlag GmbH & Co. KGaA, Weinheim.The used text paragraphs and figures were reformatted to the format of thesis (e.g. text font, reference and figure numbering).

Author contribution: R. W. and T. S. designed the research, L. L., N. E., S. M., and F. N. performed the research, L. L. and F. N. analyzed data, L. L., T. S. and R. W. interpreted the data and wrote the paper with refinement by all co-authors.

2. L. Li, M. Dwivedi, S. Patra, N. Erwin, S. Möbitz, and R. Winter. "Probing Colocalization of N-Ras and K-Ras4B Lipoproteins in Model Biomembranes." *ChemBioChem*, 20 (**2019**), 1190-1195.

Copyright: was published online on 02 January, 2019 and DOI is 10.1002/cbic.201800776. In this publication is partially reproduced in section 5.6 and 5.7 with the permission by John Wiley & Sons, Inc. Copyright ©2015Wiley-VCH Verlag GmbH & Co. KGaA, Weinheim.The used text paragraphs and figures were reformatted to the format of the thesis (e.g. text font, reference and figure numbering).

Author contribution: R. W and L. L designed the research, L. L., M. D., S. P., N. E., S. M., performed research, L. L. analyzed data, L. L. and R. W. interpreted the data and wrote the paper with refinement by all co-authors.

3. L. Li, M. Dwivedi, N. Erwin, S. Möbitz, P. Nussbaumer, and R. Winter. "Interaction of K-Ras4B Protein with C6-ceramide Containing Lipid Model Membranes", *Biochim. Biophys. Acta, Biomembr.,* 1860 (**2018**) 1008-1014.

Author contribution: R. W. and L. L. designed the research, L. L., N. E., S. M., performed the research, L. L. analyzed data, L. L. and R. W. interpreted the data and wrote the paper with refinement by all co-authors.

5. Materials and Methods

5.1 Materials

5.1.1 Chemicals

Chemicals	Supplier
Acetic acid	Merck (Darmstadt, DE)
Acrylamid/Bisacrylamide (37.5:1, 30 % w/v)	AppliChem (Darmstadt, DE)
Agarose	Sigma-Aldrich (St. Louis, US)
Ammonium persulfate (APS)	Merck (Darmstadt, DE)
Ampicillin (Amp)	Sigma-Aldrich (St. Louis, US)
Bradford reagent	Bio-Rad (München, DE)
Bovine serum albumine (BSA)	Sigma-Aldrich (St. Louis, US)
Chloroform	Merck (Darmstadt, DE)
Dimethylsulfoxide (DMSO)	Merck (Darmstadt, DE)
Dithioerythitol (DTE)	Sigma-Aldrich (St. Louis, US)
Dithiothreitol (DTT)	Sigma-Aldrich (St. Louis, US)
Ethylenediaminetetraacetic acid (EDTA)	Merck (Darmstadt, DE)
Ethanethiol	Merck (Darmstadt, DE)
Ethanol	Merck (Darmstadt, DE)
Glycerol	Sigma-Aldrich (St. Louis, US)
GMP-PNP (Non-hydrolyzable analog of GTP)	Sigma-Aldrich (St. Louis, US)
Guanosine diphophate (GDP)	Sigma-Aldrich (St. Louis, US)
4-(2-Hydroxyethyl) piperazine-1-ethanesulfonic acid (HEPES)	AppliChem (Darmstadt, DE)
Hydrochloric acid	Merck (Darmstadt, DE)

Imidazol	Gerbu (Gaiberg, DE)
Isopropyl-β-D-thiogalactopyranoside (IPTG)	Carl Roth (Karlsruhe, Deutschland)
Kanamycin	ThermoFisher (US)
Magnesium chloride	Merck (Darmstadt, DE)
Phenylmethylsulfonylfluoride (PMSF)	Sigma-Aldrich (St. Louis, US)
Potassium dihydrogenphosphate	Sigma-Aldrich (St. Louis, US)
Potassium hydroxide	Sigma-Aldrich (St. Louis, US)
Sodium chloride	Merck (Darmstadt, DE)
Sodium dihydrogenphosphate	Merck (Darmstadt, DE)
Sodium dodecylsulphate (SDS)	Sigma-Aldrich (St. Louis, US)
Sodium hydroxide	Merck (Darmstadt, DE)
Sodium 2-mercaptoehanesulfonate (MESNA)	Sigma-Aldrich (St. Louis, US)
N,*N*,*N'*,*N'*-tetramethylethylendiamin (TEMED)	Roth (Karlsruhe, DE)
Trihydroxymethylaminomethane (TRIS)	Merck (Darmstadt, DE)
Triton X-100	Serva (Heidelberg, DE)
Urea	JT Baker (Deventer, NL)

5.1.2 Other chemicals from collaborators

Bodipy labelled C6-ceramide was a gifts from Dr. Peter Nussbaumer from the Lead Discovery Center GmbH (Dortmund, Germany) and tweezer CLR01, and CLR03 were obtained from Prof. Dr. Thomas Schrader (University of Duisburg-Essen).

5.1.3 Other materials

Materials	Supplier
Amicon Ultra-4, 15 (10K) Concentrator	Millipore, Merck (Darmstadt, Germany)
Chitin beads	New England Biolabs (Beverly, USA)
Dialysis membrane tubing (MWCO: 5-8 kDa)	Thermo Scientific (Massachusetts, USA)
Eppendorf tube (10 µL, 200 µL, 1 mL, 5 mL, 10 mL)	Eppendorf (Hamburg, Germany)
Falcon Tube (15 mL, 50 mL)	Eppendorf (Hamburg, Germany)
HiTrap Ni-NTA column	GE Healthcare (Chicago, USA)
MBPTrap column	New England Biolabs (Beverly, USA)
NAP-5 desalting column	GE Healthcare (Chicago, USA)
Superdex 26/600 Gel filtration	GE Healthcare (Chicago, USA)
Whatman FP 30/0.2 µm cellulose filter	GE Healthcare (Chicago, USA)
Low molecular weight marker	Sigma, now Merck (Darmstadt, Germany)
DNA marker 1kb	New England Biolabs (Beverly, USA)
Nuclepore track-Etch membrane	Whatman, GE Healthcare (Chicago, USA)

5.1.4 Instruments

Instruments	Supplier
Akta primer system	GE Healthcare (Chicago, USA)
Bio-Rad power-PAC 300	BIO-RAD laboratories (California, USA)
Centrifuge 5424R	Eppendorf (Hamburg, Germany)
Centrifuge Multifuge IS-R	Thermo Electron (Massachusetts, USA)

Centrifuge Avanti J-26 XP	Beckman Coulter (California, USA)
Gel-electrophoresis system	BIO-RAD laboratories (California, USA)
pH-Meter Knick Portamess 913	Knick (Berlin, Germany)
Shaker, cell culture	INFORS HT (Einsbach, Germany)
Ultrasonic cell disrupter, BRANSON Sonifier 450	EMERSON (St. Louis, USA)
UV/Visible Spectrometer	Eppendorf (Hamburg, Germany)
Gel imaging system, Alphalmager MINI	Biozym (Oldendorf, Germany)
AFM Multi-Mode	Bruker (Karlsruhe, Germany)
HALcyonics_i4	Accurion (Göttingen, Germany)
HALcyonics_MOD-I	Accurion (Göttingen, Germany)
Confocal microscopy, MRC1024	BIO-RAD (California, USA)
Confocal microscopy, Leica SP5	Leica (Wetzlar, Germany)
Confocal microscopy, Nikon eclipse TE 2000-U	Nikon (Tokyo, Japan)
Fluorescence lifetime microscopy , MicroTime 200	PicoQuant (Berlin, Germany)
Freezing drier, Christ Alpha 1-2 CD	Millrock Technology (New York, USA)
Cell culture incubator, Thermo Cell 150	Thermo Scientific (Massachusetts, USA)
Cell counter, Countess II	Thermo Scientific (Massachusetts, USA)
Water heater, RCS LAUDA, RC6	LAUDA (New Jersey, USA)
Water bath, Elmasonic S 30H	Elma Schmidbauer (Singen, Germany)
Balance	PCE instruments (Meschede, Germany)
Milli-q Water system, purelab flex2	Merck (Darmstadt, Germany)
Ultra low temperature freezer	Eppendorf (Hamburg, Germany)

Plasma Cleaner	diener electronic (Ebhausen, Germany)
K2 multifrequency phase Fluorometer	ISS (Champaign, USA)

5.1.5 Buffers and growth media

LB medium		**TB medium**	
5 g/L	Yeast extract	24 g/L	Yeast extract
10 g/L	Tryptone	12 g/L	Tryptone
10 g/L	NaCl	5 g/L	Glycerol
1L	H_2O	2.31 g	KH_2PO_4
		12.54 g	K_2HPO_4 in 100 ml H_2O
		900 mL	H_2O

Antibiotics

125 mg/L	Ampicillin
50 mg/L	Kanamycin

SDS-PAGE loading buffer		**SDS-PAGE running buffer (10x)**	
62.3 mM	Tris-HCl, pH=6.8	0.25 M	Tris-HCl
2 % (w/v)	SDS	2 M	Glycine
10 % (v/v)	Glycerol	1 % (w/v)	SDS
5 % (v/v)	β-Mercaptoethanol		
0.001% (w/v)	Bromophenol blue		

SDS-PAGE stacking gel buffer (4x)		**SDS-PAGE running gel buffer (4x)**	
0.5 M	Tris-HCl pH=6.8	1.5 M	Tris-HCl pH=8.8
0.4 % (w/v)	SDS	0.4 % (w/v)	SDS

Coomassie staining buffer	**Destaining buffer**

10 % (v/v)	acetic acid	10 % (v/v)	acetic acid
40 %	ethanol		
0.1 %	Coomassie Brilliant Blue R250		

Breaking buffer		**Storage buffer**	
20 mM	Tris	20 mM	Tris
500 mM	NaCl	100 mM	NaCl
2 mM	$MgCl_2$	2 mM	$MgCl_2$
2 mM	TCEP	pH=7.4	
pH=7.4			

Buffer A (His6-tagged protein)		**Buffer B (His6-tagged protein)**	
20 mM	Tris	20 mM	Tris
150 mM	NaCl	150 mM	NaCl
2 mM	TCEP	2 mM	TCEP
pH=7.4		0.5 M	Imidazole
		pH=7.4	

LUV formation buffer		**GUV formation buffer**	
20 mM	Tris	20 mM	Tris
5 mM	$MgCl_2$	5 mM	$MgCl_2$
pH=7.4		pH=7.4	

5.1.6 Peptides

K-Ras4B farnesylated peptide was synthesized by Eurogentec Deutschland GmbH (Köln, Germany).

5.1.7 Lipids

Lipids	Supplier
Cholesterol	Sigma-Aldrich (St. Louis, USA)
DOPC (1,2-Dioleoyl-*sn*-glycero-3-phosphocholin)	Avanti Polar Lipids (Alabaster, USA)
DPPC (1,2-Dipalmitoyl-*sn*-glycero-3-phosphocholin)	Avanti Polar Lipids (Alabaster, USA)

DOPG (2-dioleoyl-*sn*-glycero-3-phospho-(1'-rac-glycerol), sodium salt)	Avanti Polar Lipids (Alabaster, USA)
DPPG (1,2-Dipalmitoyl-*sn*-glycero-3-phosphoglycerol, sodium salt)	Avanti Polar Lipids (Alabaster, USA)
DOPS (1,2-Dioleoyl-*sn*-glycero-3-phospho-L-serin)	Avanti Polar Lipids (Alabaster, USA)
DPPS 1,2-Dipalmitoyl-*sn*-glycero-3-phospho-L-serin)	Avanti Polar Lipids (Alabaster, USA)
C6-Ceramide	Avanti Polar Lipids (Alabaster, USA)
C18-Ceramide	Avanti Polar Lipids (Alabaster, USA)
N-Rh-DHPE (*N*-(LissamineTM Rhodamine B sulfonyl)-1,2-dihexadecanoyl-sn-glycero-3-phosphoethanolamin)	ThermoFisher Scientific (Waltham, USA)
Bodipy-Cholesterol	ThermoFisher Scientific (Waltham, USA)

5.2 Molecular cloning methods

5.2.1 Plasmids and bacterial strains

Plasmids

Plasmids name	Inserted gene	Resistance	Application
pTWIN2_K-RAS4B_WT_1-174	K-Ras4B_1-174	Amp	Expression of K-Ras4B thioester proteins
pET28b_SOS1_564-1059	SOS1_564-1059	KanR	Expression of SOS1 (564-1059) proteins
pGEX-2T_A-Raf-RBD	A-Raf-RBD_14-91	Amp	Expression of A-Raf-RBD proteins
pGEX-2T_B-Raf-RBD	B-Raf-RBD_51-136	Amp	Expression of B-Raf-RBD proteins
pGEX-2T_C-Raf-RBD	C-Raf-RBD_53-131	Amp	Expression of C-Raf-RBD proteins
pMAL_6His_MBP_TEV_A-Raf-RBD-CRD	A-Raf-RBD-CRD_14-91	Amp	Expression of A-Raf-RBD-CRD proteins
pMAL_6His_MBP_TEV_B-Raf-RBD-CRD	B-Raf-RBD-CRD_51-136	Amp	Expression of B-Raf-RBD-CRD proteins

pMAL_6His_MBP_TEV_C-Raf-RBD-CRD	C-Raf-RBD-CRD_53-131	Amp	Expression of C-Raf-RBD-CRD proteins
pCDNA3.1_citrine_K-Ras4B	WT_K-Ras4B	Amp	Construct the stable cell lines that express citrine-K-Ras4B proteins in the MDCK cells (plasmid was given from MPI, Dortmund)
pCDNA3.1_mCherry_K-Ras4B	WT_K-Ras4B	Amp	Expression of K-Ras4B in the MCF-7 cells (plasmid was given from MPI, Dortmund)
pDest-566_C-Raf-RBD-CRD	C-Raf-RBD-CRD_53-131	Amp	Expression of C-Raf-RBD-CRD proteins (plasmid was given from Frederick National Laboratory for Cancer Research, USA)

Bacterial strains

XL1 Blue (Stratagene)

BL21 (DE3) Condon Plus RIL (Stratagene)

5.2.2 PCR and purification of PCR products by agarose gel electrophoresis

The 5'- and 3'- primers for PCR reaction were subsequently designed. The PCR reaction mixture was prepared followed by the steps shown in Table 5-1. The PCR reaction was performed using the PCR instrument.

Table 5-1. PCR protocol for general genes amplification.

Step	Material	Volume (µL)
1	buffer (10 x)	1x
2	DMSO	3
3	Sterile water	to 50 µL

4	Template DNA (20-100 ng)	1
5	Primers (final conc. 1 µM)	1
6	dNTPs (final conc. 200 µM)	1
7	Taq polymerase	1

Table 5-2. PCR program.

Temp (°C)	Time	Function
94	2 min	Initial denaturation
94	40 s/cycle	Denaturation
T_m-5°C	30 s/cycle	Primer annealing
72	1 min per kb	Extension
72	10 min	Final extension
16	-	Storage

Purification of PCR products by agarose gel electrophoresis

The optimal concentration of agarose was depended on the size of the DNA. The following steps were used to purify the DNA fragments.

1. Prepare the optimal concentration of agarose solution by dissolving the agarose into TAE buffer. (Heating helps to dissolve it in the TAE buffer)

2. Add ethidium bromide to a final concentration of 0.5 µg/mL.

3. Add the prepared agarose solution to the gel casting equipment and wait for 10 min.

4. Prepare the samples with 5x DNA loading buffer.

5. Load the samples into the prepared agarose gel wells and 1 kb DNA ladder was used as molecular weight marker.

6. Run the gels at 90-120 V in TAE buffer for 20 min until the DNA fragments were separated.

7. Collect the bands of interest in the agarose gels and put it into tubes.

8. Extract and purify the DNA from the gels using the gel extraction kit following the instruction of the kit.

5.2.3 Subcloning

Restriction enzyme digestion

The purified PCR product and plasmid vector were digested by the restriction enzymes at 37 °C for 1-2 h (dependent on the restriction enzyme). The reaction was stopped by addition of DNA loading buffer. Agarose gel electrophoresis was used to purify the digested products.

Table 5-3. Restriction enzyme digestion.

Step	Material	Volume (µL)
1	Sterile water	to 30 µL
2	Vector (1 µg)	11
3	Fast digestion buffer (10x)	3
4	PCR product (1 µg)	4
5	XbaI	1
6	XhoI	1

Ligation

The purified products of linear plasmid DNA was incubated with a 10-fold molar excess of the inserted gene. The reaction was performed in a ligation buffer of total volume 20 µL at 20 °C. Deactivation was carried out at 65 °C for 10 min.

Table 5-4. Ligation protocol.

Step	Material	Volume (µL)
1	Vector (0.05 µg)	2
2	Inserted gene (0.025 µg)	2
3	Ligation buffer (5x)	4
4	T4 DNA ligase	1
5	Sterile water	11

1. Add the ligated product (1 ng) to 50 µL chemical competent cells.
2. Put the mixture on ice for 30 min.
3. Heat the cells at 42 °C for 1 min.
4. Cool down on ice for 2 min.
5. Add 500 µL LB medium to the cells.
6. Incubate at 37 °C for 0.5-1 h in the shaker.
7. Slow centrifugation and discard 300 µL of supernatant.
8. Spread 100 µL of cells on agar plates supplemented with the corresponding antibiotics.
9. Inversely incubate overnight at 37 °C.

5.2.5 Colony PCR screen

1. A single bacterial colony growing on LB agar plate with the appropriate antibiotics was picked into the LB medium (2-4 mL with antibiotics) for overnight growth at 37 °C.
2. 10 µL of culture bacterial was mixed with diluted Triton-X 100 (0.05%, 10 µL) in a PCR tube.
3. Heat the mixture at 95° C for 10 min and centrifuge at 4°C.
4. PCR reaction was performed using 5 µL of the supernatant.
5. Run agarose gel electrophoresis to analyze the PCR products.

Table 5-5. Colony PCR screen protocol.

Step	Material	Volume (µL)
1	Sterile water	18.7
2	Buffer (10x)	3
3	DMSO	1.5
4	Mixture of cell lysate	5
5	Primers (final conc. 1 µM)	1

6	dNTPs (10 mM, final conc.200 µM)	0.5
7	DNA polymerase	0.3
	Total	30

5.2.6 Preparation of plasmid DNA

1. A single bacterial colony growing on LB agar plate with the appropriate antibiotics was picked into LB medium (2-4 mL with antibiotics) for overnight growth at 37° C.

2. Add 2 mL culture cells into tubes and centrifugation (maximum speed, 1 min). Discard the supernatant and repeat this step.

3. Gently vortex to resuspend the cell pellet. Add 250 µL buffer 1 with addition of RNase A.

4. Add 250 µL buffer II and mix immediately until the solution gets clear.

5. Add 350 µL buffer III and gently inverse the tube 4-5 times until the precipitate comes out with chromosomal DNA, lipids and proteins.

6. Centrifugation (maximum speed) for 10 min and remove the supernatant to a new tube.

7. Load the supernatant on a silica spin column. Centrifuge the column for 1 min at 10,000 rpm.

8. Wash the column with 700 µL DNA wash buffer (ethanol added) by centrifugation for 1 min at 10,000 rpm. Repeat this step.

9. Centrifuge the empty column at 10,000 rpm for 1 min.

10. Add 30-50 µL EB buffer to the column and wait 1 min.

11. Centrifuge at 10, 000 rpm for 1 min to get the plasmid DNA. Measure the concentration of plasmid DNA and store it at -20 °C.

5.2.7 DNA sequencing

Appropriate primers were designed for sequencing. The DNA samples were delivered to a DNA sequencing company (Microsynth SEQLAB, Göttingen, Germany) for sequencing.

5.3 Protein expression and purification methods

5.3.1 Expression and purification of A-, B- and C-Raf-RBD, A-, B- and C-Raf

A-, B- and C-Raf-RBD-CRD, SOS1 (564-1059), PDEσ

Expression of A-, B- and C-Raf-RBD in *E. coli*

1. Transform the plasmid to BL21 (DE3) cells and select it on LB agar plate containing 50 mg/L ampicillin antibiotics.

2. A single colony from the agar plate was picked into LB medium containing 150 mg/L ampicillin.

3. Incubate in the shaker at 37 °C at 160-180 rpm and allow the cells to grow overnight.

4. The pre-cultured cells were added into a 5 L flask containing LB medium with Amp and grown at 37 °C in the shaker until the absorbance at 600 nm reached 0.5-0.7.

5. Cool down the flask to 20 °C and IPTG (final conc. 0.1-0.5 mM) was added to induce protein expression overnight.

6. Prepare the SDS-PAGE sample of 30 µL cell suspension with 20 µL SDS-PAGE loading buffer, boil the sample at 95 °C for 10 min. Run SDS-PAGE to check the protein expression level.

7. Centrifuge at 6000 rpm, 4 °C for 15 min to harvest cells.

8. Discard the supernatant carefully and remove the cells to a 50 mL falcon. Cells can be stored in a -80 °C refrigerator.

Lysis of the A-, B- and C-Raf-RBD cells

1. Resuspend the cells carefully with lysis buffer (20 mM Tris, 500 mM NaCl, 2 $MgCl_2$, pH=8.0). PMSF (final conc. 1 mM) and β-mercaptoenthanol (final conc. 2 mM) were added freshly.

2. The prepared cell solutions were broken under the sonication for 40 min.

3. Centrifuge the cell lysate at 35, 000 rpm, 4 °C for 30 min.

4. Filter the supernatant through a 0.2 μm filter.

Purification

1. Load the filtrate lysate onto GST binding column (glutathione resin packed) with a low flow rate (1-2 mL/min). The column was equilibrated with equilibration buffer (buffer A) before loading the lysate.

2. Wash the column to remove unbound proteins using buffer A (3-5 CV) with a flow rate of 3 mL/min.

3. Eluted the protein with elution buffer (20-50 mM glutathione was added to buffer A).

4. Run SDS-PAGE to identify the fractions of interest.

5. Collect the fractions containing the protein of interest and exchange the buffer to low concentration of salt (20 mM Tris, 100 mM NaCl, 2 mM TCEP, pH=8.0) for Thrombin enzyme cleavage.

6. 1 U/10 μg of Thrombin enzyme was added for cleavage.

7. Run SDS-PAGE to monitor the cleavage.

8. Centrifuge at 4000 rpm for 2 min. Discard any pellet in the bottom of falcon.

9. Load the supernatant to the GST binding column with a flow rate (1 mL/min) to remove the GST tag and GST-tagged proteins.

10. Further purification of gel-filtration should be performed if necessary.

11. Collect the flow-through and concentrate it to 5 mg/mL. The proteins were frozen by liquid nitrogen and stored in a refrigerator at -80°C.

Other proteins including SOS1 (564-1059) and PDEσ were purified in a similar way.

5.3.2 Expression and purification of K-Ras4B thioester proteins

Expression of K-Ras4B-Intein-CBD in E. coli

1. Transform the plasmid to BL21 (DE3) cells and select it on LB agar plate containing 50 mg/L ampicillin antibiotics.

2. A single colony from the agar plate was picked into LB medium containing 150 mg/L ampicillin.

3. Incubate in the shaker at 37 °C at 160-180 rpm and allow the cells to grow overnight.

4. The pre-cultured cells were added into a 5 L flask containing LB medium with Amp and grown at 37 °C in the shaker until the absorbance at 600 nm reached 0.5-0.7.

5. Cool down the flask to 20 °C and IPTG (final conc. 0.1-0.5 mM) was added to induce protein expression overnight.

6. Prepare the SDS-PAGE sample of 30 µL cell suspension with 20 µL SDS-PAGE loading buffer, boil the sample at 95 °C for 10 min. Run SDS-PAGE to check the protein expression level.

7. Centrifuge at 6000 rpm, 4 °C for 15 min to harvest cells.

8. Discard the supernatant carefully and remove the cells to a 50 mL falcon. Cells can be stored in -80 °C refrigerator.

Lysis of K-Ras4B-Intein-CBD cells

1. Resuspend the cells carefully with lysis buffer (20 mM Tris, 500 mM NaCl, 2 $MgCl_2$, 10 µM GDP, pH=8.0). PMSF (final conc. 1 mM) and β-mercaptoenthanol (final conc. 2 mM) were added freshly.

2. The prepared cells solution was broken under the sonication for 40 min. Add fresh PMSF (final conc. 1 mM) and TritionX-100 (1% v/v).

3. Centrifuge the cell lysate at 35, 000 rpm, 4 °C for 30 min.

4. Filter the supernatant through a 0.2 µm filter.

Purification

1. Load the filtrate to the column packed with chitin beads with a low flow rate 0.5 mL/min overnight (12-16 h). The column was equilibrated with equilibration buffer (buffer A) before loading the lysate.

2. Wash the column to remove unbound proteins using buffer A (3-5 CV) with a flow rate of 3 mL/min.

3. Elute the protein with elution buffer (20-50 mM glutathione was added to buffer A).

4. Run SDS-PAGE to identify the fractions of interest.

5. Collect the fractions containing the protein of interest and exchange the buffer to low concentration of salt (20 mM Tris, 100 mM NaCl, 2 mM TCEP, pH=8.0) for Thrombin enzyme cleavage.

6. 1 U/10 μg of Thrombin enzyme was added for cleavage.

7. Run SDS-PAGE to monitor the cleavage.

8. Centrifuge at 4000 rpm for 2 min. Discard any pellet in the bottom of falcon.

9. Load the supernatant to the GST binding column with a flow rate (1 mL/min) to remove the GST tag and GST-tagged proteins.

10. Further purification of gel-filtration should be performed if necessary.

11. Collect the flow-through and concentrate it to 5 mg/mL. The proteins were frozen by liquid nitrogen and stored in a refrigerator at -80°C.

5.4 Protein synthesis

The synthesis of full-length K-Ras4B has been described in detail before. Briefly, the K-Ras4B thioester protein was obtained by intein technology, where K-Ras4B peptide containing an N-terminal cysteine was ligated to the C-terminal K-Ras4B protein thioester using native chemical ligation (NCL). This ligation yields the full-length protein with a native amide bond at the ligation site. After ligation, the protein was purified using a Hi-Trap SP-X1 column (GE healthcare). The purified protein solution was transferred to Tris buffer (20 mM Tris, 5 mM $MgCl_2$, pH = 7.4) by subsequent dialysis against at least 1 L Tris buffer at 4 ˚C for 2 days. The dialysed

protein solution was concentrated and freezed by liquid nitrogen and stored at -80 ˚C as stock solution.

5.5 Cell culture and imaging

Cell lines	Origin	Supplier
HeLa	Human cervical adenocarcinoma	ATCC
MDCK	Madin-darby canine kidney cells	ATCC

5.5.1 Cell culture

Table 5-6. Cell culture medium components.

DMEM	
FBS	10% (v/v)
L-glutamine	1% (v/v)
Nonessential amino acids (NEAA)	1% (v/v)
Sodium pyruvate	1% (v/v)
Penicillin-Streptomycin (sterile-filtered, suitable for cell culture) (10, 000 U/mL)	1 U

Cells were maintained in cell culture medium (preparation was shown in Table 5-6) and grown at 37 °C, 5% CO_2 in a 90% humidified incubator. When the cell density reaches 80-90%, the grown cells were washed two times with PBS buffer (steriled, suitable for cell culture) and were detached by the addition of 0.05% trypsin, 0.01% EDTA and phenol red in PBS buffer at 37 °C. The PBS buffer and trypsin should be pre-warmed before adding into the cell culture dishes. After incubation for 2-3 min, check the detached cells under the microscope. If less than 80% of cells are detached, longer incubation can be performed. However, the cell exposure to trypsin solution should be limited to 10 min. Once cells detach appear to complete, 2 mL of pre-warmed medium are added to inactive trypsin. Gently disperse the cell medium by pippeting over the cell attached in the surface of dish. Carefully transfer the suspension to a flask and centrifuge at low speed (1000 rpm) for 10 min. Discard the

supernatant and gently resuspend the cell pellet in 2 mL of pre-warmed medium. Determine the cell density of viable cells using an automated cell counter. Calculate the cells and seed the cells to a new cell culture flask with a density of 15-25%. The cells continue growing in the incubator. Examine the cells' condition within 1-2 days to ensure that the cells are healthy and free of contamination.

5.5.2 Stable cell line of Citrine-K-Ras4B generation

In order to get a cell line that constitutively expresses Citrine-tagged K-Ras4B proteins, we established a stable cell of Citrine-K-Ras4B following the protocol described as below.

1. Design and insert the gene of interest into a vector containing mCherry/GFP/Citrine gene. The vector should also encode kanamycin for selection in bacteria and neomycin (G418) for selection in mammalian cells.

2. Characterize expression of the fusion protein in the cells using transient transfection by Xtrame GENE HP DNA transfection reagent. MDCK cells are used and Western-blots are carried out to check whether the fusion protein is expressed in full-length or truncated.

3. Transfect the split low-passage cells with the constructed plasmid in a p100 dish. 3 µg of plasmid DNA of interest in 300 µL OptiMEM with 4.5 µL Xtreme GENE HP DNA transfection reagent were prepared following the protocol of transfection for this product. The prepared mixture is added to a dish containing 100,000-200,000 cells.

4. The following day, replace the medium with the medium containing G418 (400 µg-800 µg per mL medium). The cells without expressing the construct would be killed by the amount of G418. Examine the cell condition to repeat this step, normally it need to replace the old medium with the medium containing G418 every two or three days. After continuous growing in the G418-contained medium for 2-3 weeks, the selection by G418 will be complete. At some point, there will be a massive cell death, wash the dish using G418-contained medium and discard detached cells. Allow the stable attached cells to grow in the incubator.

5. To generate a single-cell derived stable cell line, colonies are picked up by a pipette with a sterile yellow tip under the inverted light microscope. It should be noted that the selected cells should be incubated at a much lower concentration of Trypsin (diluted

5-20 times, depending on the cell type and condition) for 2-5 min. This will make the pick-up easier since it weakens the attachment of stable cells with the dish. Repeat this step in case of requirement of more cells.

6. Rinse the confluent pick-up cells with PBS buffer and trypsin. Split the generated cells into 6-well plate and G418-contained medium is added to allow it to grow in the incubator.

7. Examine cells in each well under the fluorescence microscopy to decide which well of cells are worth keeping.

8. When the amount of stable expressed cells is sufficient, a lower amount of G418 should be used and keep tracking of passage numbers. Freeze the cells from early passages.

5.5.3 Cell imaging

For cell imaging, the appropriate amount of cells (cell density is normally 30-60%, which depends on the type of cells and dishes) was seeded in a 6-well or 8-well image dishes with the cell culture medium. The following day, gently remove the medium and wash it using fresh medium in the absence of phenol red. Cell imaging was carried out on a Leica SP5 confocal laser-scanning microscope (MPI Dortmund) mounted to a 60x/1.2 NA oil objective or a 40x/0.9 NA air objective. EGFP and Citrine were excited at 488 nm wavelength by a multiline Argon laser and mCherry was excited at 561 nm wavelength by a DPPS laser. The dichroic mirror DM405/488/561/633 or DM458/515 was used with proper filters to record the images. The cells in the imaging dishes were placed into an incubation chamber (kept at 37 °C, 5% CO_2) during the time of imaging, which is capable of maintaining the cells alive.

5.6 LUV and GUV preparation

5.6.1 LUV preparation

LUVs preparation was followed by a standard protocol, which applies 5 freeze-throw-vortex cycles to generate LUVs.

1. Make stock solutions of DOPC, DPPC, DOPG, DPPG and cholesterol of 10 mg/mL each in chloroform.

2. The calculated amount of lipids were added into a 1.5 mL tube and dried in the freezing drier at -20 °C overnight to yield the completely dry lipid film.

3. Tris buffer was added to the tube. Vortex several times for resuspension and incubate in a water bath (temperature should higher than the T_m of the lipid mixture) for 15 min.

4. Sonicate the mixture in a water bath for 10 min.

5. Fast freeze the lipid mixture by liquid N_2 for 2 min and thaw in the water bath for 15 min. Vortex it several times. Repeat this step 5 times.

6. Sonication was applied in the end of step 5 for 5 min.

7. Extrusion was applied to generate homogenous membranes through polycarbonate membrane with 100 nm size about 20 times.

8. The LUVs prepared are stored at 20 °C.

5.6.2 GUV preparation

GUVs were prepared using the electroformation method on an ITO coverslip, allowing conduction of electricity on the surface of the lipid film.

1. Make stock solutions of DOPC, DOPC, and cholesterol of 10 mg/mL and *N*-Rh-DHPE of 100 µM.

2. Add the calculated amount of these lipids into a 2 mL glass vial and gently vortex.

3. Place the ITO coverslip onto the port of a spin coater. It should be noted that the surface of the coated ITO should be in the front position.

4. Wash the surface of the ITO coverslip twice using 500 mL chloroform.

5. Inject 20-30 µL lipid solution to the surface ITO coverslip and turn on the spin coater immediately at 8000 rpm for 1 min.

6. Prepare an ITO coverslip without lipid film using the same method as described in step 5.

7. Dry the ITO coverslip using a freezing dryer overnight.

8. Mount the home-made and temperature-controlled chamber with the two ITO coverslips. Inject Tris buffer into the chamber. Careful injection should be performed to avoid producing bubbles.

9. The formation of GUVs was inducted by electricity through the lipid film followed the protocol described below.

a). 500 Hz, 250 mV, 5 min.

b). 500 Hz, 1.25 V, 20 min.

c). 500 Hz, 3.5 V, 90 min.

The temperature of the buffer inside the chamber should be higher than the T_m of the lipid mixture.

10. Cool down the chamber to room temperature and take the images using confocal microscopy.

5.7 Methods

5.7.1 Confocal microscopy

The cell experiments with confocal microscopy were all carried out on the Leica Sp5 laser-scanning microscopy of the MPI, Dortmund. The details of the experiments have been described in a section 5.4.3-live cell imaging. For the images taken on GUVs, the confocal microscopy (Bio-Red, PCI, TU Dortmund) was used. The GUVs prepared in the home-made chamber were imaged at the wavelength of the 561 nm laser. Adjust the focus to find the surface of the GUVs and change the system to an imaging mode. Multi-channel emission of samples were recoded. The analysis of the image including the contrast adjustment was performed using software ImageJ.

5.7.2 Fluorescence Correlation Spectroscopy (FCS) and Fluorescence Cross-Correlation Spectroscopy (FCCS)

The FCS and FCCS measurements were carried out on the Microtime 200 of PCI at TU Dortmund University. The Microtime 200 was equipped with an inverted microscopy (Olympus IX71), which was supplemented with a water immersion

objective (UplansApo, 60X, NA 1.2). To perform FCS measurements, the sample was excited using a pulsed diode laser of wavelength 485 or 560 nm (repetition rate: 20 MHz). The output of the pulsed diode laser was coupled to the main optical unit by a single-mode optical fiber. In the main optical unit, a dichroic mirror was used to guide the excitation light to the entrance port of the microscopy, where it is focused by the objective lens on the sample. Fluorescence was collected through the same path, where it was filtered by a 510 nm long-pass emission filter (HQ, Chroma, 510 LP), and spatially filtered by a 50 µm pinhole, and finally focused on a SPCM-AQR series single-photon avalanche diode (SPAD). Autocorrelation traces were obtained by using fluorescence lifetime correlation spectroscopy (FLCS). Data acquisition was performed with a TimeHarp 200 TCSPC module in a time-tagged, time-resolved mode. SymPhoTime software supplied by PicoQuant was used for the analysis of the autocorrelation curves. The autocorrelation curves obtained were fitted to a triple extended 2D curve fitting model as follows:

$$G_{2\mathrm{D}}(\tau) = \frac{1}{N}\sum_{i=1}^{n}\left[1 + (\frac{\tau}{\tau_i})^{\alpha_i}\right]^{-1} \quad \text{(S5-1)}$$

where τ_i is the diffusion time of the i^{th} diffusion species, α^i is the anomaly parameter of i^{th} diffusion species. and N is the number of diffusion species in the confocal volume. The 2D diffusion coefficient was calculated by

$$D_{i,2\mathrm{D}} = \frac{{r_0}^2}{4\tau_i} \quad \text{(S5-2)}$$

where r_0 is the effective radius of the confocal volume that was determined using a calibration dye.

PIE-FCCS was used to detect the interaction between K-Ras4B protein and C6-ceramide in the membrane. PIE-FCCS has the ability to detect the differently labeled co-diffusing particles, which can be used to resolve protein-lipid interactions in more detail. As Rhodamine-labeled K-Ras4B protein and BODIPY-labeled C6-ceramide were excited by two different lasers (blue laser: 485 nm, green laser: 560 nm) at different time points, PIE-FCCS can remove the crosstalk between the donor and acceptor and also the random and dynamic collisions. To validate the correlation data, a dually labelled (Atto488 and Atto565) oligonucleotide (ds-DNA) was used as a positive control. The cross correlation curve obtained for this dually labelled

oligonucleotide represents the maximum signal of cross-correlation possible with this instrument setup and shows that the confocal volumes of the two lasers are sufficiently overlapping. A negative control was obtained using equimolar concentrations of *N*-Rh-DHPE and Bodipy-cholesterol in a pure DOPC membrane as randomly diffusing species that are not susceptible to co-diffusion.

For the PIE-FCCS measurements, two pulsed lasers (485 nm and 560 nm, repetition rate: 20 MHz) were coupled and collimated through an optical fiber, and were used to excite the dually labelled samples. A green band pass emission filter (525/40, Chroma) and a red band pass emission filter (583QM30) were used before the green channel and red channel, respectively. Fluorescence fluctuations from both channels were then correlated to obtain a cross-correlation curve, which was then fitted to a triple extended 2D curve fitting model (S5-1). The relative cross-correlation was obtained by

$$R_{\text{cross-correlation}} = \frac{G_x(0)}{\min\{G_r(0), G_g(0)\}} \quad \text{(S5-3)}$$

where G_x is the cross correlation amplitude, G_r is the autocorrelation amplitude of Rhodamine (red) and G_g is the autocorrelation amplitude of BODIPY (green). The measurement time was 300 s for each curve. More than 50 such measurements were recorded and used to determine the cross correlation values.

Giant unilamellar vesicles (GUVs) for the fluorescence correlation spectroscopy (FCS) and PIE-FCCS measurements were prepared in a temperature-controlled homemade chamber using the electroformation method described above. The GUVs were doped with 0.005 mol % BODIPY-C6-ceramide. The microscope was connected to an in-built JPK TAO stage that can be controlled vertically, which can be used to position the confocal volume on the membrane using JPK software. Through the JPK software, the position, where the maximum intensity was obtained, was fixed for the FCS and PIE-FCCS measurements. This procedure was repeated for the same GUV at least 20 times.

5.7.3 Atomic force microscopy

30 µL of the indicated lipid composition of LUV solution and 40 µL Tris buffer (20 mM Tris, 5 mM $MgCl_2$, pH 7.4) were added to a freshly cleaved mica surface. After

incubation in a wet chamber at 70 ˚C for 2 h, the samples were rinsed carefully with Tris buffer to remove unspread vesicles. For the K-Ras4B-membrane studies, 200 µL of 2 µM unlabeled K-Ras4B proteins (in Tris buffer) were injected into the AFM fluid cell at room temperature. Measurements were performed on a MultiMode scanning probe microscope with a Nano-Scope IIIa controller (Digital Instruments, Santa Barbara, CA) and a J-Scanner (scan size 125 µm). Images were obtained by using the tapping mode in liquid with sharp nitride lever (SNL) probes mounted in a fluid cell (MTFML, Veeco (now Bruker), Karlsruhe, Germany). Tips with nominal force constants of 0.24 Nm^{-1} were used at driving frequencies of 8.9 kHz and drive amplitudes between 200 and 800 mV. Scan frequencies were between 1.2 and 2.0 Hz. Images were obtained with a resolution of 512 × 512 pixels. All measurements were carried out at room temperature and analysed using NanoScope version 5. The height differences were analysed using section plot in the NanoScope version 5 software.

5.7.4 Fluorescence spectroscopy

The fluorescence titration measurements were performed on a K2 multifrequency phase and modulation fluorometer (ISS, Champaign, IL, USA). In the titration experiment, 100 µL of the 50 µM tweezer CLR01 solution was placed in a quartz cuvette and the peptide was added stepwise. The fluorescent tweezer was excited at a wavelength of 285 nm and the emission spectra were recorded in the range of 300 to 600 nm. All measurements were performed at 25 °C using a circulating water bath.

5.7.5 Förster resonance energy transfer (FRET) measurements of N-Ras and K-Ras4B in the model membranes

The FRET measurements of N-Ras and K-Ras4B in the lipid membrane were carried out in the LUVs composed of DOPC/DPPC/cholesterol (molar ratio 1:2:1). Bodipy-labeled N-Ras (FRET-donor) and rhodamine-labeled K-Ras4B (FRET-acceptor) concentrations were both 0.6 µM. The sample was excited at 488 nm and emission spectra were collected between 502 and 700 nm. The fluorescence spectroscopic measurements were carried out using a K2 multifrequency phase and modulation

fluorometer (ISS, Urbana Champaign, IL, USA). The measuring temperature was maintained at 25 ± 0.1 °C using a circulating water bath.

5.7.6 CD spectroscopy measurements

CD spectra were recorded on a Jasco J-815 CD spectrometer from 250 to 190 nm in a 0.1 cm path length cell at room temperature. To avoid absorbance of the buffer in the spectral region of interest, K-Ras4B protein in Tris buffer was transferred to phosphate buffer (10 mM Na_2HPO_4, 2 mM KH_2PO_4, pH = 7.4) by dialysis. The tweezer CLR01 was dissolved in the phosphate buffer. The protein concentration was kept at 20 µM in each sample. The CD spectra of buffer with the respective amounts of CLR01 were subtracted from the corresponding samples data. The results shown are in an average of 25 recorded scans and are plotted as molar ellipticity.

6. Appendices

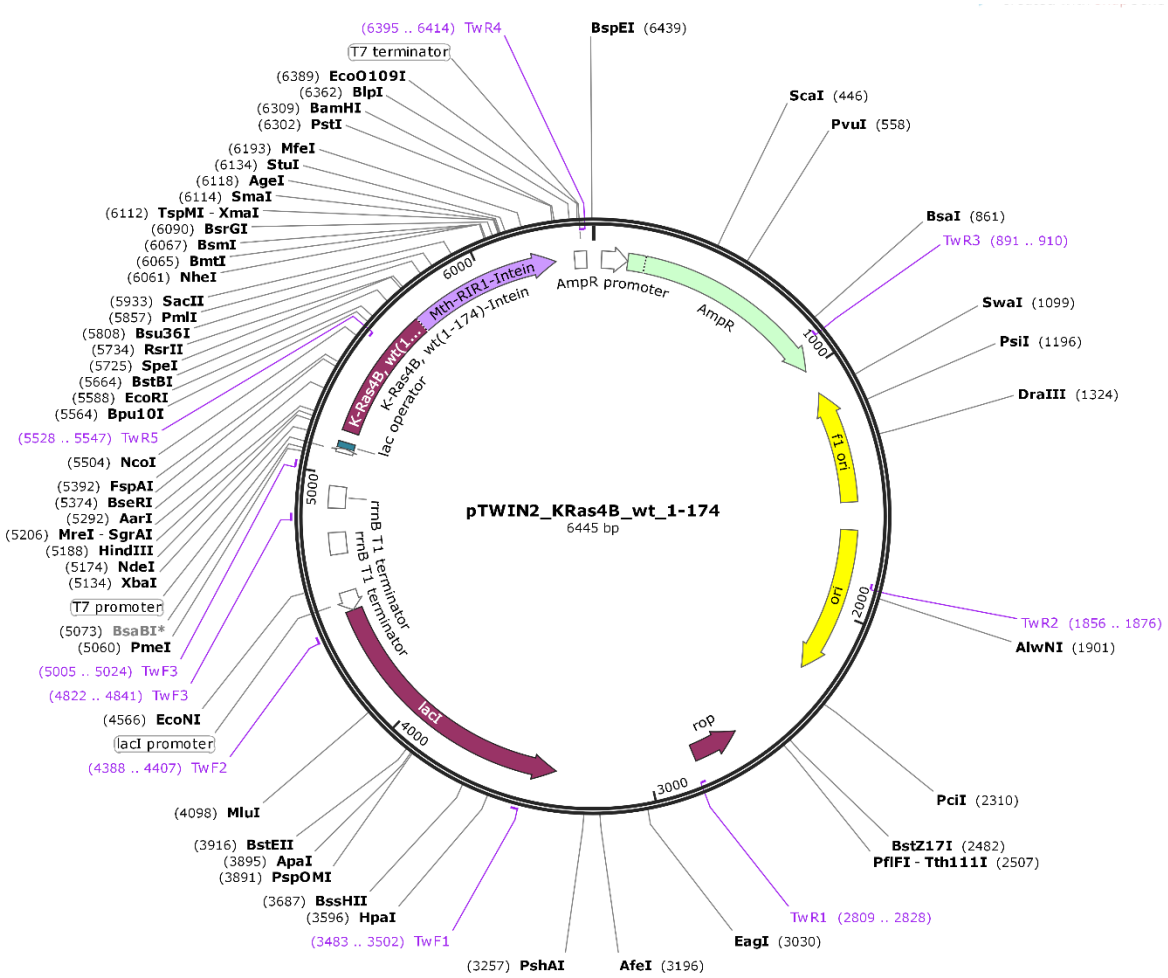

6.1.1 Plasmid map of pTWIN2_K-Ras4B-wt_1-174, which was used to express K-Ras4B (1-174) thioester proteins. Adapted using software SnapGene Viewer.

Protein sequence:

MTEYKLVVVGAGGVGKSALTIQLIQNHFVDEYDPTIEDSYRKQVVIDGETCLLD
ILDTAGQEEYSAMRDQYMRTGEGFLCVFAINNTKSFEDIHHYREQIKRVKDSED
VPMVLVGNKCDLPSRTVDTKQAQDLARSYGIPFIETSAKTRQGVDDAFYTLVRE
IRKHKEKMSKDG

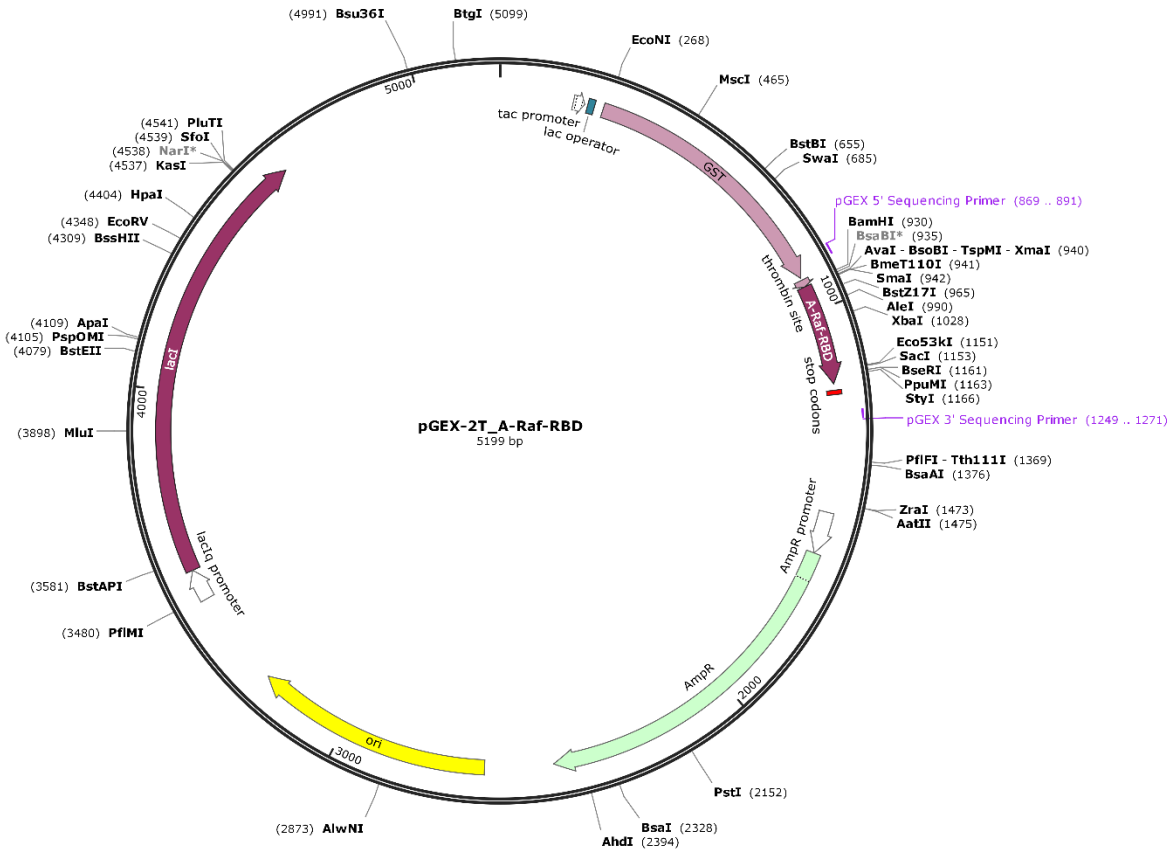

6.1.2 Plasmid map of pGEX-2T_A-Raf-RBD, which was used to A-Raf-RBD proteins. Adapted using software SnapGene Viewer.

Protein sequence:

GSPSRAVGTVKVYLPNKQRTVVTVRDGMSVYDSLDKALKVRGLNQDCCVVYRLIK
GRKTVTAWDTAIAPLDGEELIVEVLGIHRD

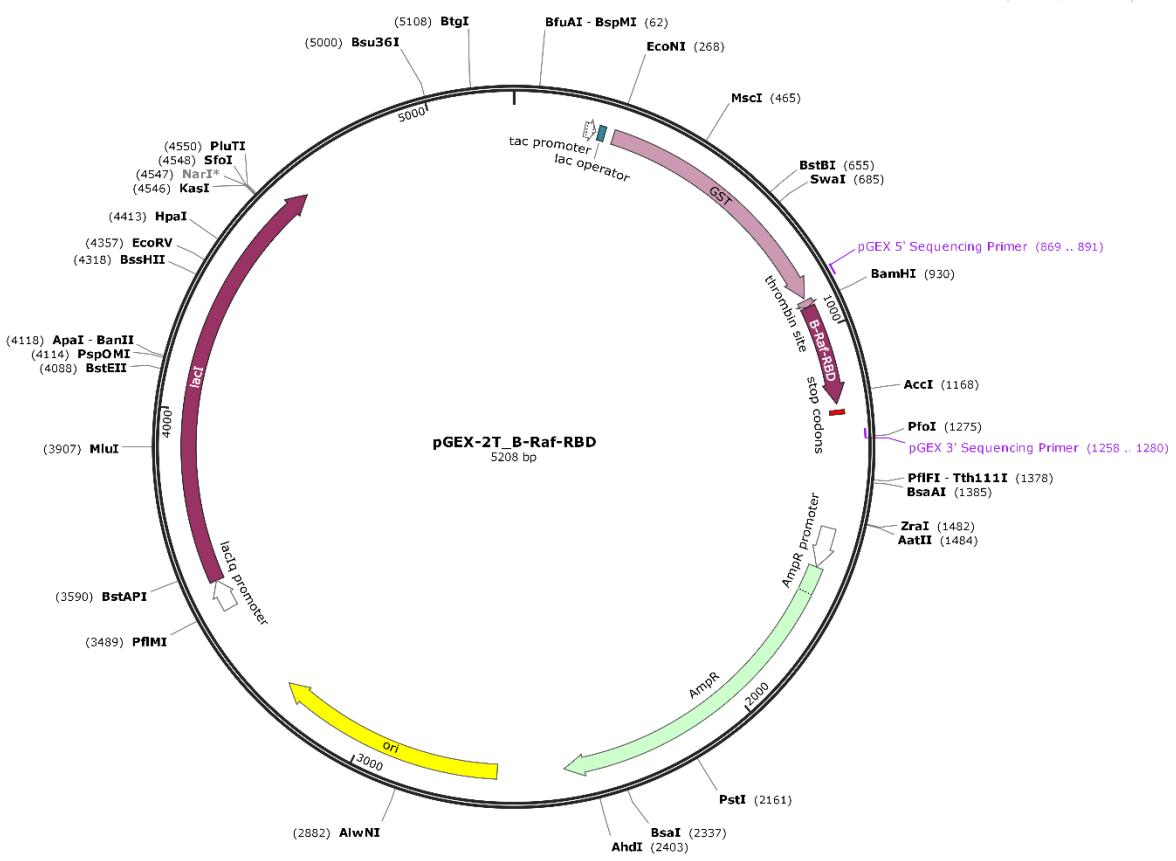

6.1.3 Plasmid map of pGEX-2T_B-Raf-RBD, which was used to B-Raf-RBD proteins. Adapted using software SnapGene Viewer.

Protein sequence:

GSKSPQKPIVRVFLPNKQRTVVPARCGVTVRDSLKKALMMRGLIPECCAVYRIQDGEKKPIGWDTDISW LTGEELHVEVLGIHRD

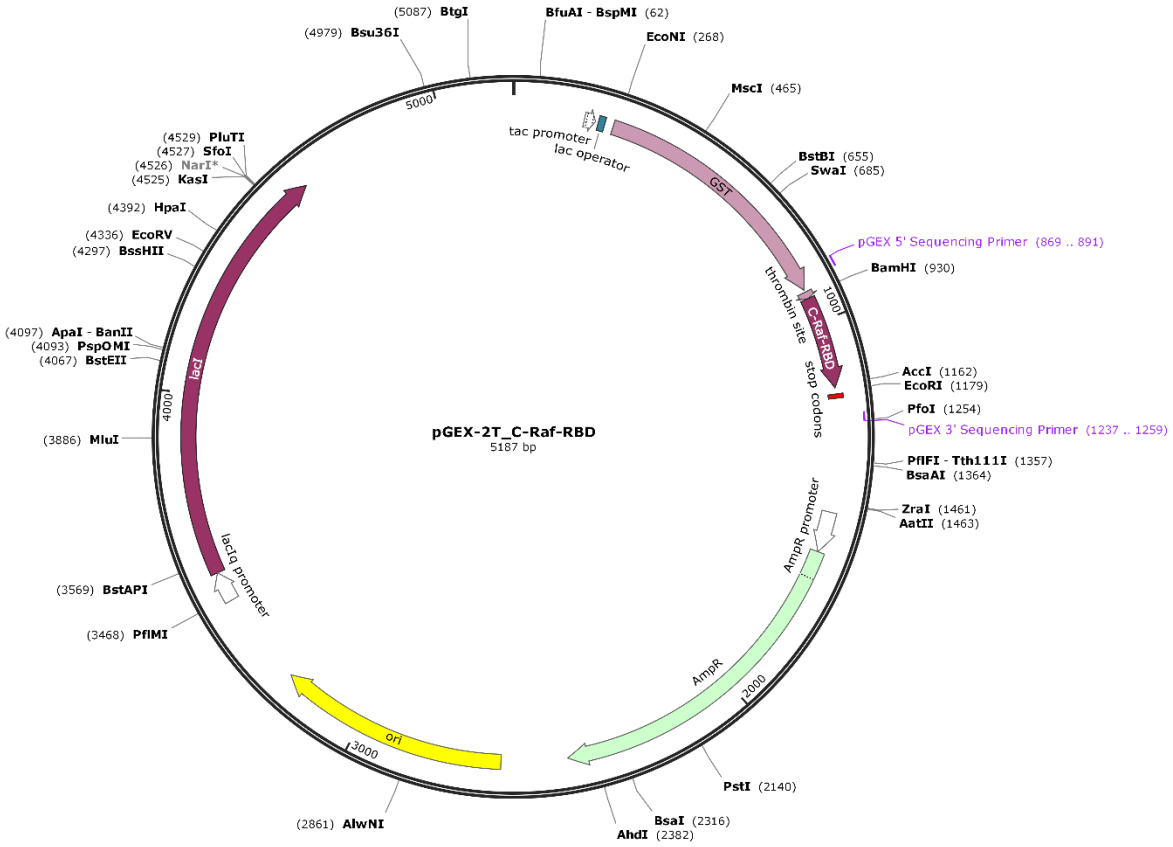

6.1.4 Plasmid map of pGEX-2T_C-Raf-RBD, which was used to B-Raf-RBD proteins. Adapted using software SnapGene Viewer.

Protein sequence:

GSKTSNTIRVFLPNKQRTVVNVRNGMSLHDCLMKALKVRGLQPECCAVFRLLHEHKGKKARLDWNTDA ASLIGEELQVDFL

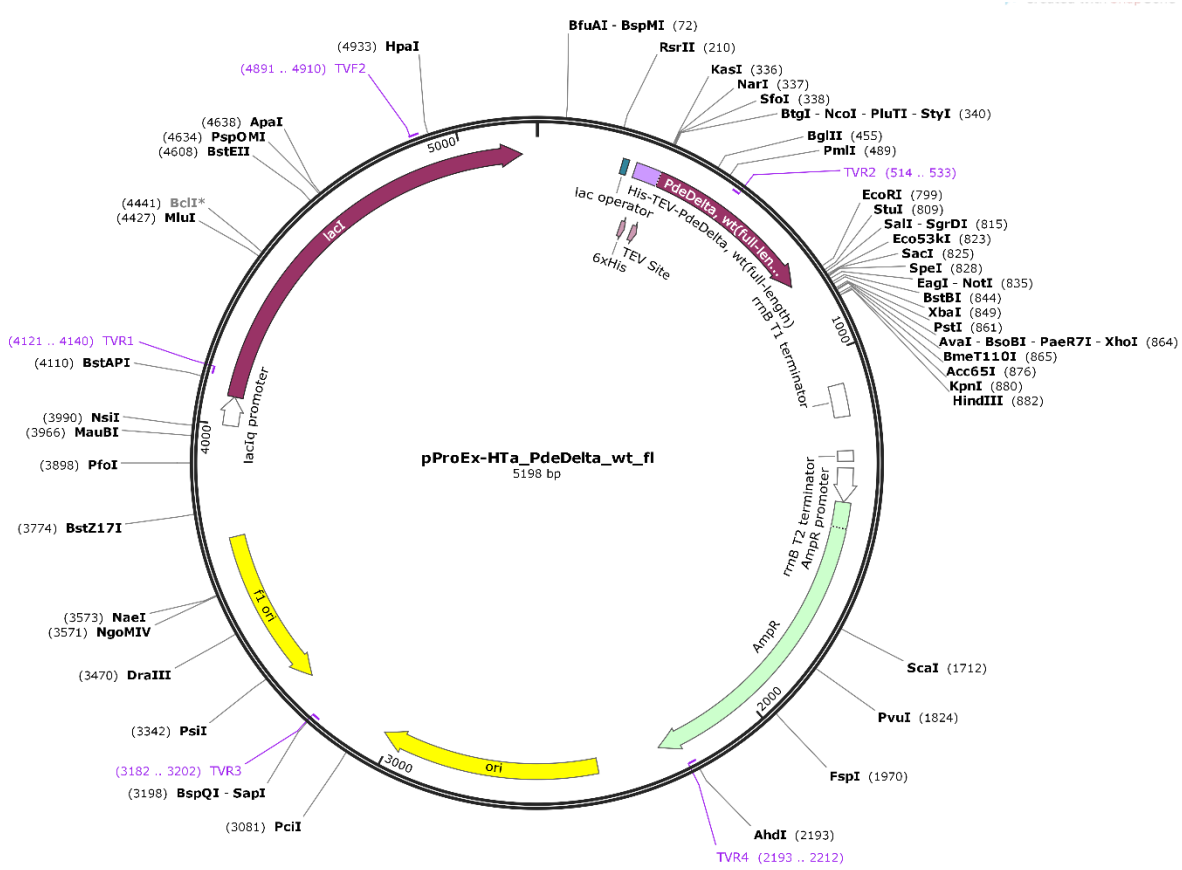

6.1.5 Plasmid map of pProEx-HTa_PdeDelta_WT_fl, which was used to express PDEσ proteins. Adapted using software SnapGene Viewer.

Protein sequence:

MSYYHHHHHHDYDIPTTENLYFQGAMAMSAKDERAREILRGFKLNWMNLRDAETGKILWQGTEDLSV
PGVEHEARVPKKILKCKAVSRELNFSSTEQMEKFRLEQKVYFKGQCLEEWFFEFGFVIPNSTNTWQSLIEA
APESQMMPASVLTGNVIIETKFFDDDLLVSTSRVRLFYV

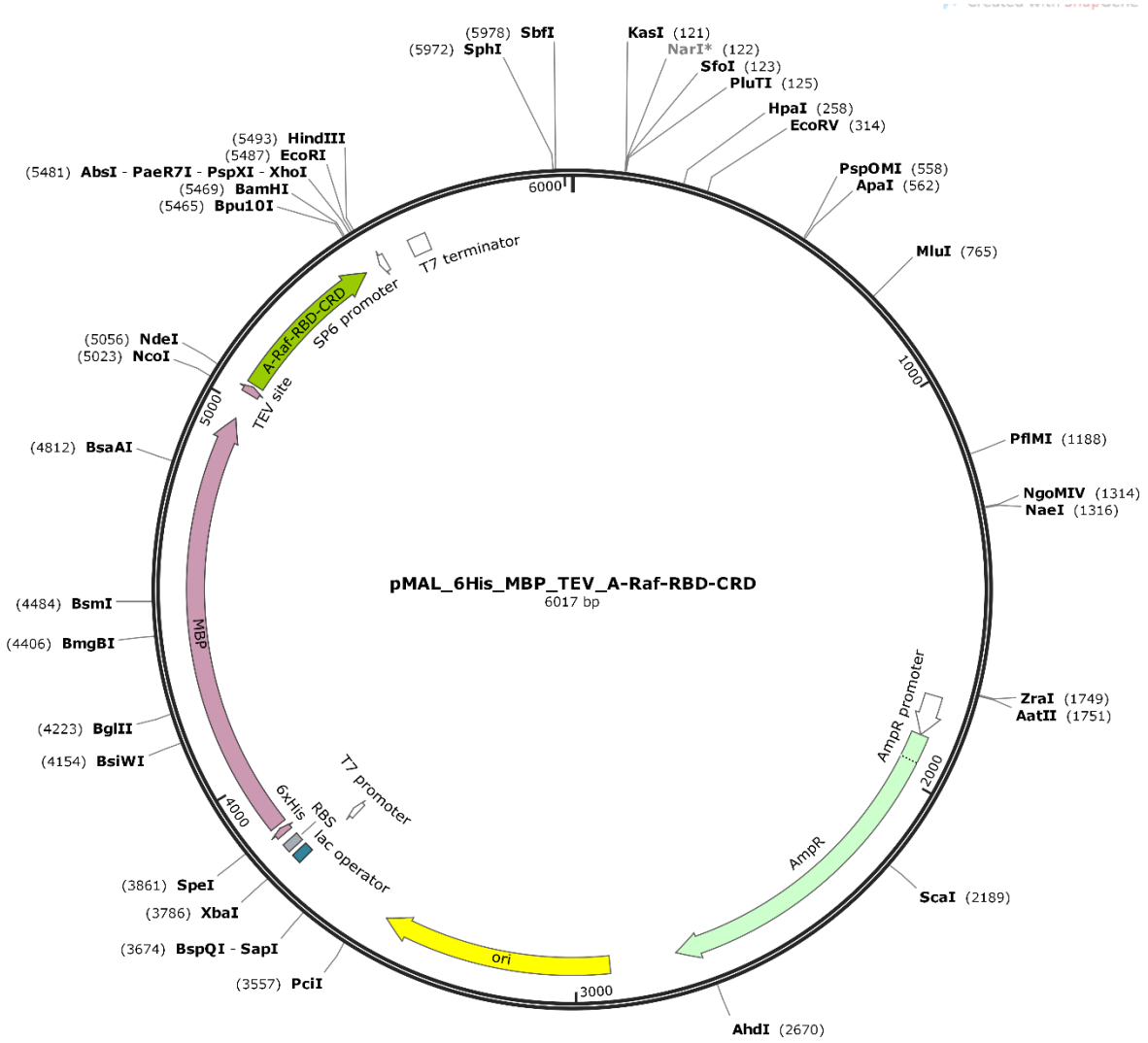

6.1.6 Plasmid map of pMAL_6His_MBP_TEV_A-Raf-RBD-CRD, which was used to express A-Raf-RBD-CRD proteins. Adapted using software SnapGene Viewer.

Protein sequence:

GHMPSRAVGTVKVYLPNKQRTVVTVRDGMSVYDSLDKALKVRGLNQDCCVVYRLIKGRKTVTAWDTAI
APLDGEELIVEVLEDVPLTMHNFVRKTFFSLAFCDFCLKFLFHGFRCQTCGYKFHQHCSSKVPTVCVDMS

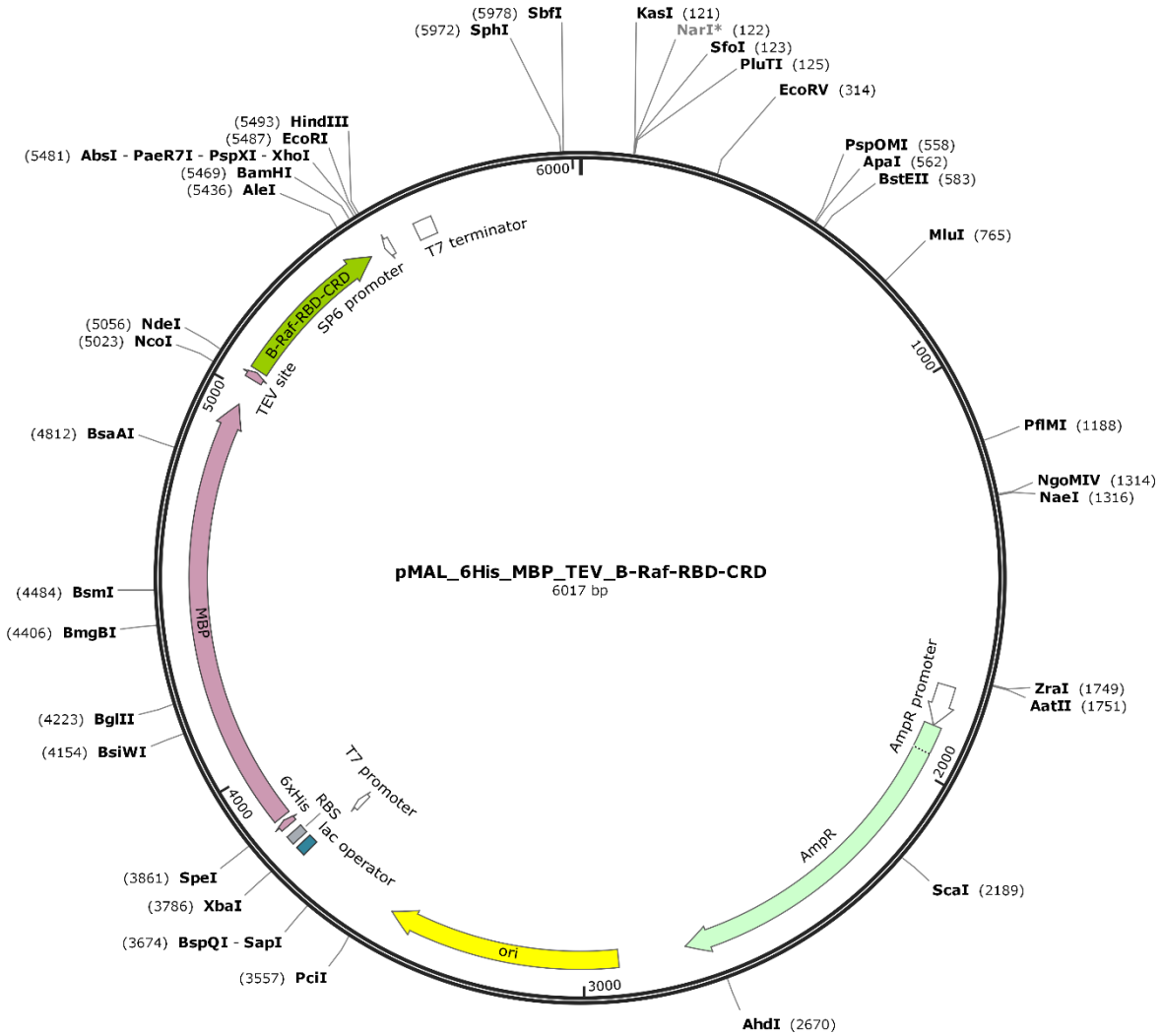

6.1.7 Plasmid map of pMAL_6His_MBP_TEV_B-Raf-RBD-CRD, which was used to express B-Raf-RBD-CRD proteins. Adapted using software SnapGene Viewer.

Protein sequence:

GHMKSPQKPIVRVFLPNKQRTVVPARCGVTVRDSLKKALMMRGLIPECCAVYRIQDGEKKPIGWDTDIS
WLTGEELHVEVLENVPLTTHNFVRKTFFTLAFCDFCRKLLFQGFRCQTCGYKFHQRCSTEVPLMCVNYD

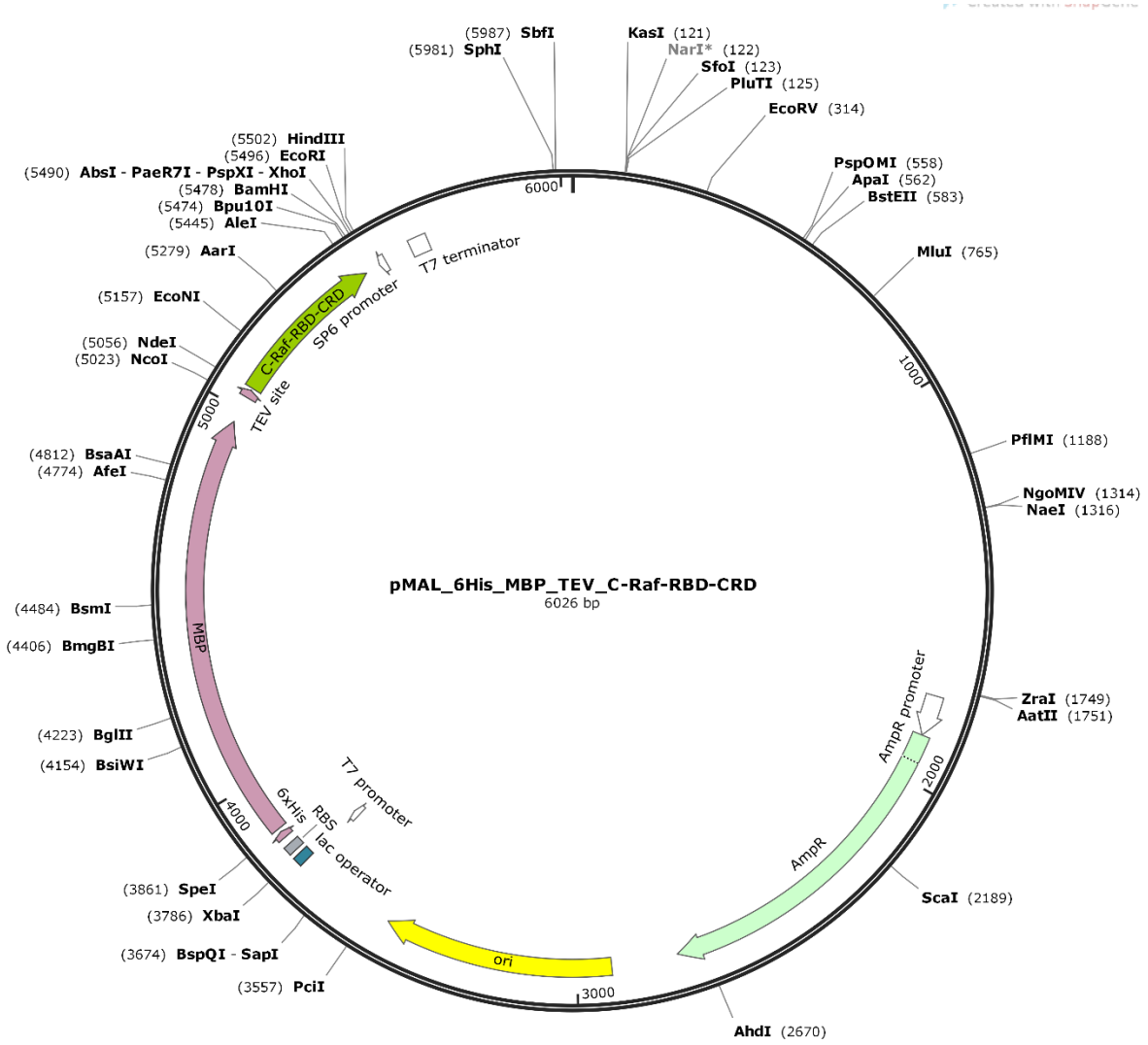

6.1.7 Plasmid map of pMAL_6His_MBP_TEV_C-Raf-RBD-CRD, which was used to express C-Raf-RBD-CRD proteins. Adapted using software SnapGene Viewer.

Protein sequence:

PSKTSNTIRVFLPNKQRTVVNVRNGMSLHDCLMKALKVRGLQPECCAVFRLLHEHKGKKARLDWNTDA
ASLIGEELQVDFLDHVPLTTHNFARKTFLKLAFCDICQKFLLNGFRCQTCGYKFHEHCSTKVPTMCVDWS

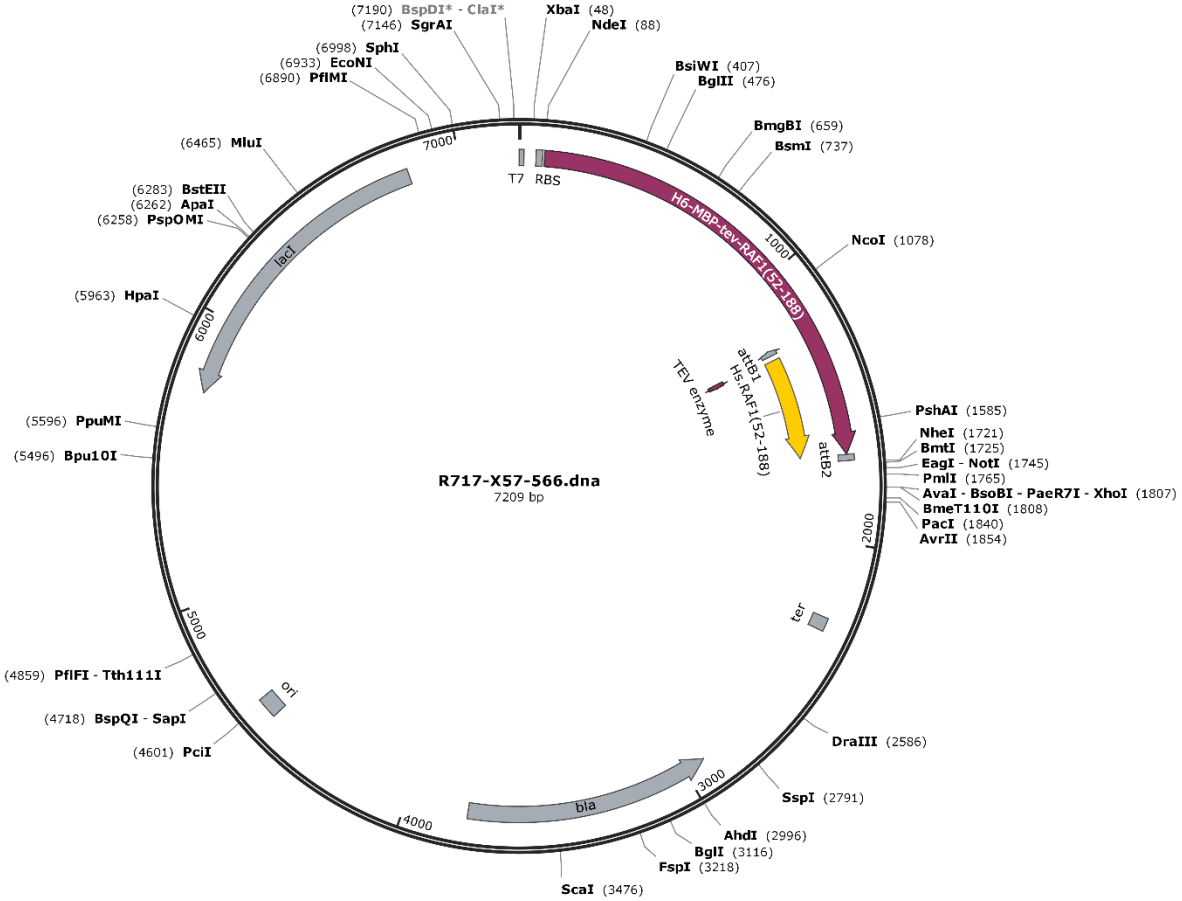

6.1.8 Plasmid map of pDest-566_6His_MBP_TEV_C-Raf-RBD-CRD, which was used to express C-Raf-RBD-CRD proteins. Adapted using software SnapGene Viewer.

Protein sequence:

SKTSNTIRVFLPNKQRTVVNVRNGMSLHDCLMKALKVRGLQPECCAVFRLLHEHKGKKARLDWNTDAA
SLIGEELQVDFLDHVPLTTHNFARKTFLKLAFCDICQKFLLNGFRCQTCGYKFHEHCSTKVPTMCVDWS

7. References

[1] D. Lingwood, and K. Simons. "Lipid rafts as a membrane-organizing principle." *Science* 327.5961 (**2010**): 46-50.

[2] G. Van Meer, D. R. Voelker, and G. W. Feigenson. "Membrane lipids: where they are and how they behave." *Nat. Rev. Mol. Cell Biol.* 9.2 (**2008**): 112.

[3] S. H. Donaldson Jr and H. B. de Aguiar. "Molecular imaging of cholesterol and lipid distributions in model membranes." *J. Phys. Chem. Lett* 9.7 (**2018**): 1528-1533.

[4] J. F. Hancock "Lipid rafts: contentious only from simplistic standpoints." *Nat. Rev. Mol. Cell Biol*. 7.6 (**2006**): 456.

[5] K. Jacobson, O. G. Mouritsen, and R. G. Anderson. "Lipid rafts: at a crossroad between cell biology and physics." *Nat. Cell Biol*. 9.1 (**2007**): 7.

[6] J. Lombard. "Once upon a time the cell membranes: 175 years of cell boundary research." *Biol. Direct* 9.1 (**2014**): 32.

[7] S. Chien, K. L. Sung, R. Skalak, S. Usami, and A. Tözeren. "Theoretical and experimental studies on viscoelastic properties of erythrocyte membrane." *Biophys. J*., 24(2), (**1978**): 463-487.

[8] P. Mazzarello. "A unifying concept: the history of cell theory." *Nat. Cell Biol*., 1(1), (**1999**): E13.

[9] L. Yetukuri, K. Ekroos, A. Vidal-Puig, M. Orešič. "Informatics and computational strategies for the study of lipids." *Mol. BioSyst*., 4(2), (**2008**): 121-127.

[10] R. P. Richter, R. Bérat, and A. R. Brisson. "Formation of solid-supported lipid bilayers: an integrated view." *Langmuir,* 22.8 (**2006**): 3497-3505.

[11] G. Van Meer, D. R. Voelker, and G. W. Feigenson. "Membrane lipids: where they are and how they behave." *Nat. Rev. Mol. Cell Biol*. 9.2 (**2008**): 112.

[12] E. Sezgin, I. Levental, S. Mayor, C. Eggeling. "The mystery of membrane organization: composition, regulation and roles of lipid rafts." *Nat. Rev. Mol. Cell Biol*., 18(6), (**2017**): 361.

[13] K. Simons, E. Ikonen. "Functional rafts in cell membranes." *Nature*, 387(6633), (**1997**): 569.

[14] S. L. Veatch, and S. L. Keller. "Organization in lipid membranes containing cholesterol." *Phys. Rev. Lett*., 89.26 (**2002**): 268101.

[15] K. Simons, and D. Toomre. "Lipid rafts and signal transduction." *Nat. Rev. Mol. Cell Biol*., 1.1 (**2000**): 31.

[16] K. Weise, G. Triola, L. Brunsveld, H. Waldmann, R. Winter. "Influence of the lipidation motif on the partitioning and association of N-Ras in model membrane subdomains." *J. Am. Chem. Soc*., (**2009**), 131, 1557-1564.

[17] K. Weise, S. Kapoor, C. Denter, J. Nikolaus, N. Opitz, S. Koch, G. Triola, A. Herrmann, H. Waldmann, R. Winter. "Membrane-mediated induction and sorting of K-Ras microdomain signaling platforms." *J. Am. Chem. Soc*., (**2011**), 133, 880-887.

[18] L. Li, M. Dwivedi, N. Erwin, S. Möbitz, P. Nussbaumer, and R. Winter. "Interaction of K-Ras4B protein with C6-ceramide containing lipid model membranes." *Biochim. Biophys. Acta, Biomembr.,* 1860(5), (**2018**): pp.1008-1014.

[19] M. P. Mingeot-Leclercq, M. Deleu, R. Brasseur, Y. F. Dufrêne. "Atomic force microscopy of supported lipid bilayers." *Nat. Protoc*., 3(10), (**2008**): 1654.

[20] N. F. Morales-Penningston, J. Wu, E. R. Farkas, S. L. Goh, T. M. Konyakhina, J. Y. Zheng, W.W. Webb, G. W. Feigenson. "GUV preparation and imaging: minimizing artifacts." *Biochim. Biophys. Acta, Biomembr.,* 1798(7), (**2010**): 1324-1332.

[21] K. Simons, and M. J. Gerl. "Revitalizing membrane rafts: new tools and insights." *Nat. Rev. Mol. Cell Biol*. 11.10 (**2010**): 688.

[22] J. L. Bos. "Ras oncogenes in human cancer: a review." *Cancer Res*., 49.17 (**1989**): 4682-4689.

[23] S. M. Sebti, and J. D. Channing. "Searching for the elusive targets of farnesyltransferase inhibitors." *Nat. Rev. Cancer,* 3.12 (**2003**): 945.

[24] I. R. Vetter and A. Wittinghofer. "The guanine nucleotide-binding switch in three dimensions." *Science,* 294.5545 (**2001**): 1299-1304.

[25] D. K. Simanshu, V. N. Dwight, F. McCormick. "RAS proteins and their regulators in human disease." *Cell,* 170.1 (**2017**): 17-33.

[26] S. B. Long, J. C. Patrick, S. B. Lorena. "Reaction path of protein farnesyltransferase at atomic resolution." *Nature,* 419.6907 (**2002**): 645.

[27] K. Scheffzek, M. R. Ahmadian, W. Kabsch, L. Wiesmüller, A. Lautwein, F. Schmitz, A. Wittinghofer. "The Ras-RasGAP complex: structural basis for GTPase activation and its loss in oncogenic Ras mutants." *Science*, 277(5324), (**1997**): 333-339.

[28] E. F. Pai, U. Krengel, G. A. Petsko, R. S. Goody, W. Kabsch, A. Wittinghofer. "Refined crystal structure of the triphosphate conformation of H-ras p21 at 1.35 A resolution: implications for the mechanism of GTP hydrolysis." *EMBO J*., 9(8), (**1990**): 2351-2359.

[29] F. McCormick. "KRAS as a therapeutic target." (**2015**): 1797-1801.

[30] J. L. Bos, H. Rehmann, A. Wittinghofer. "GEFs and GAPs: critical elements in the control of small G proteins." *Cell* 129.5 (**2007**): 865-877.

[31] J. F. Hancock, A. I. Magee, J. E. Childs, C. J. Marshall, "All ras proteins are polyisoprenylated but only some are palmitoylated." *Cell*, 57(7), (**1989**): 1167-1177.

[32] J. F. Hancock, H. Paterson, C. J. Marshall. "A polybasic domain or palmitoylation is required in addition to the CAAX motif to localize p21ras to the plasma membrane." *Cell,* 63.1 (**1990**): 133-139.

[33] J. F. Hancock. "Ras proteins: different signals from different locations." *Nat. Rev. Mol. Cell Biol.,* 4.5 (**2003**): 373.

[34] D. L. Pompliano, E. Rands, M. D. Schaber, S. D. Mosser, N. J. Anthony, J. B. Gibbs. "Steady-state kinetic mechanism of Ras farnesyl: protein transferase." *Biochem.*, 31(15), (**1992**): 3800-3807.

[35] G. L. James, J. L. Goldstein, M. S. Brown. "Polylysine and CVIM sequences of K-RasB dictate specificity of prenylation and confer resistance to benzodiazepine peptidomimetic in vitro." *J. Biol. Chem*., 270.11 (**1995**): 6221-6226.

[36] E. C. Lerner, Y. Qian, A. D. Hamilton, S. M. Sebti. "Disruption of oncogenic K-Ras4B processing and signaling by a potent geranylgeranyltransferase I inhibitor." *J. Biol. Chem.*, 270(45), (**1995**): 26770-26773.

[37] C. A. Rowell, J. J. Kowalczyk, M. D. Lewis, A. M. Garcia. "Direct demonstration of geranylgeranylation and farnesylation of Ki-Ras in vivo." *J. Biol. Chem*., 272(22), (**1997**): 14093-14097.

[38] F. L. Zhang, P. Kirschmeier, D. Carr, L. James, R. W. Bond, L. Wang, R. Patton, W. T. Windsor, R. Syto, R. Zhang, W. R. Bishop. "Characterization of Ha-ras, N-ras, Ki-Ras4A, and Ki-Ras4B as in vitro substrates for farnesyl protein transferase and geranylgeranyl protein transferase type I." *J. Biol. Chem*., 272(15), (**1997**): 10232-10239.

[39] M. D. Schaber, M. B. O'hara, V. M. Garsky, S. C. Mosser, J. D. Bergstrom, S. L. Moores, M.S. Marshall, P.A. Friedman, RA Dixon, J. B. Gibbs. "Polyisoprenylation of Ras in vitro by a farnesyl-protein transferase." *J. Biol. Chem*., 265(25), (**1990**): 14701-14704.

[40] J. F. Hancock, K. Cadwallader, C. J. Marshall. "Methylation and proteolysis are essential for efficient membrane binding of prenylated p21K‐ras (B)." *EMBO J*., 10.3 (**1991**): 641-646.

[41] E. Choy, V. K. Chiu, J. Silletti, M. Feoktistov, T. Morimoto, D. Michaelson, E. I. Ivan, M.R. Philips. "Endomembrane trafficking of ras: the CAAX motif targets proteins to the ER and Golgi." *Cell,* 98, no. 1 (**1999**): 69-80.

[42] O. Rocks, A. Peyker, M. Kahms, P. J. Verveer, C. Koerner, M. Lumbierres, J. Kuhlmann, H. Waldmann, A. Wittinghofer, P. I. Bastiaens. "An acylation cycle regulates localization and activity of palmitoylated Ras isoforms." *Science,* 307, no. 5716 (**2005**): 1746-1752.

[43] I. M. Ahearn, K. Haigis, D. Bar-Sagi, M. R. Philips. "Regulating the regulator: post-translational modification of RAS." *Nat. Rev. Mol. Cell Biol*., 13(1), (**2012**): 39.

[44] B. Binétruy, T. Smeal, M. Karin. "Ha-Ras augments c-Jun activity and stimulates phosphorylation of its activation domain." *Nature*, 351(6322), (**1991**): 122.

[45] R. Sears, F. Nuckolls, E. Haura, Y. Taya, K. Tamai, J. R. Nevins. "Multiple Ras-dependent phosphorylation pathways regulate Myc protein stability." Genes Dev., 14(19), (**2000**): 2501-2514.

[46] S. Y. Zhang, B. Sperlich, F. Y. Li, S. Al-Ayoubi, H. X. Chen, Y. F. Zhao, Y. M. Li, K. Weise, R. Winter, Y. X. Chen. "Phosphorylation weakens but does not inhibit membrane binding and clustering of K-Ras4B." *ACS Chem. Biol*., 12(6), (**2017**): 1703-1710.

[47] A. T. Sasaki, A. Carracedo, J. W. Locasale, D. Anastasiou, K. Takeuchi, E. R. Kahoud, Haviv S, Asara JM, P.P. Pandolfi, L. C. Cantley. "Ubiquitination of K-Ras enhances activation and facilitates binding to select downstream effectors." *Sci. Signal*., 4(163), (**2011**): ra13-ra13.

[48] N. Fehrenbacher, D. Bar-Sagi, M. Philips. "Ras/MAPK signaling from endomembranes." *Mol. Oncol*., 3(4), (**2009**): 297-307.

[49] N. Berndt, A. D. Hamilton, S. M. Sebti. "Targeting protein prenylation for cancer therapy." *Nat. Rev. Cancer*, 11(11), (**2011**): 775.

[50] M. Schmick, N. Vartak, B. Papke, M. Kovacevic, D. C. Truxius, L. Rossmannek, P. I. Bastiaens. "KRas localizes to the plasma membrane by spatial cycles of solubilization, trapping and vesicular transport." *Cell*, 157(2), (**2014**): 459-471.

[51] B. M. Slepchenko, J. C. Schaff, I. Macara, L. M. Loew. "Quantitative cell biology with the Virtual Cell." *Trends Cell Biol*., 13(11), (**2003**): 570-576.

[52] K. Scheffzek, M. R. Ahmadian, A. Wittinghofer. "GTPase-activating proteins: helping hands to complement an active site." *Trends Biochem. Sci*., 23(7), (**1998**): 257-262.

[53] M. E. Katz, F. McCormick. "Signal transduction from multiple Ras effectors." *Curr. Opin. Genet Dev*., 7(1), (**1997**): 75-79.

[54] Z. Fang, C. B. Marshall, T. Nishikawa, A. D. Gossert, J. M. Jansen, W. Jahnke, M. Ikura. "Inhibition of K-RAS4B by a unique mechanism of action: stabilizing membrane-dependent occlusion of the effector-binding site." *Cell Chem. Biol*., 25(11), (**2018**): 1327-1336.

[55] Y. Zhou, J. F. Hancock. "Ras nanoclusters: Versatile lipid-based signaling platforms." *Biochim. Biophys. Acta, Mol. Cell Res*., 1853(4), (**2015**): 841-849.

[56] S. J. Plowman, C. Muncke, R. G. Parton, J. F. Hancock. "H-ras, K-ras, and inner plasma membrane raft proteins operate in nanoclusters with differential dependence on the actin cytoskeleton." *Proc. Natl. Acad. Sci. U. S. A*., 102(43), (**2005**): 15500-15505.

[57] Y. I. Henis, J. F. Hancock, I. A. Prior. "Ras acylation, compartmentalization and signaling nanoclusters." *Mol. Membr. Biol*., 26(1-2), (**2009**): 80-92.

[58] Y. Zhou, P. Prakash, H. Liang, K. J. Cho, A. A. Gorfe, J. F. Hancock. "Lipid-sorting specificity encoded in K-Ras membrane anchor regulates signal output." *Cell*, 168(1-2), (2017): 239-251.

[59] D. Abankwa, A. A. Gorfe, J. F. Hancock. "Ras nanoclusters: molecular structure and assembly." *In seminars in cell & developmental biology* (Vol. 18, No. 5, pp. 599-607). Academic Press.

[60] T. Tian, A. Harding, K. Inder, S. Plowman, R. G. Parton, J. F. Hancock. "Plasma membrane nanoswitches generate high-fidelity Ras signal transduction." *Nat. Cell Biol*., 9(8), (**2007**): 905.

[61] L. Janosi, Z. Li, J. F. Hancock, A. A. Gorfe. "Organization, dynamics, and segregation of Ras nanoclusters in membrane domains." *Proc. Natl. Acad. Sci. U. S. A*., 109(21), (**2012**): 8097-8102.

[62] Y. X. Chen, S. Koch, K. Uhlenbrock, K. Weise, D. Das, L. Gremer, L. Brunsveld, A. Wittinghofer, R. Winter, G. Triola, H. Waldmann. "Synthesis of the Rheb and K-Ras4B GTPases." *Angew. Chem., Int. Ed*., 49(35), (**2010**): 6090-6095.

[63] Y. X. Chen, G. Triola, H. Waldmann. "Bioorthogonal chemistry for site-specific labeling and surface immobilization of proteins." *Acc. Chem. Res*., 44(9), (**2011**): 762-773.

[64] Z. Li, L. Janosi, A. A. Gorfe. "Formation and domain partitioning of H-ras peptide nanoclusters: effects of peptide concentration and lipid composition." *J. Am. Chem. Soc*., 134(41), (**2012**): 17278-17285.

[65] T. Tian, S. J. Plowman, R. G. Parton, Y. Kloog, J. F. Hancock. "Mathematical modeling of K-Ras nanocluster formation on the plasma membrane." *Biophys. J.*, 99(2), (**2010**): 534-543.

[66] M. Serrano, A. W. Lin, M. E. McCurrach, D. Beach, S. W. Lowe. "Oncogenic ras provokes premature cell senescence associated with accumulation of p53 and p16INK4a." *Cell*, 88(5), (1997): 593-602.

[67] G. D. Borasio, J. John, A. Wittinghofer, Y. A. Barde, M. Sendtner, R. Heumann. "ras p21 protein promotes survival and fiber outgrowth of cultured embryonic neurons." *Neuron*, 2(1), (**1989**): 1087-1096.

[68] D. Bar-Sagi, J. R. Feramisco. "Microinjection of the ras oncogene protein into PC12 cells induces morphological differentiation." *Cell*, 42(3), (**1985**): 841-848.

[69] I. A. Prior, J. F. Hancock. "Compartmentalization of Ras proteins." *J. Cell Sci*., 114(9), (**2001**): 1603-1608.

[70] J. Downward. "Targeting RAS signalling pathways in cancer therapy." *Nat. Rev. Cancer*, 3(1), (**2003**) 11.

[71] S. Schubbert, K. Shannon, G. Bollag. "Hyperactive Ras in developmental disorders and cancer." *Nat. Rev. Cancer*, 7(4), (**2007**): 295.

[72] J. J. Yunis, A. J. Boot, M. G. Mayer, J. L. Bos. "Mechanisms of ras mutation in myelodysplastic syndrome." *Oncogene*, 4(5), (**1989**): 609-614.

[73] P. J. Roberts, T. E. Stinchcombe. "KRAS mutation: should we test for it, and does it matter?." *J. Clin. Oncol*., 31(8), (**2013**): 1112-1121.

[74] Y. Pylayeva-Gupta, E. Grabocka, D. Bar-Sagi. "RAS oncogenes: weaving a tumorigenic web." *Nat. Rev. Cancer*, 11(11), (**2011**): 761.

[75] A. Fernández-Medarde, E. Santos. "Ras in cancer and developmental diseases." *Genes Cancer*, 2(3), (**2011**): 344-358.

[76] C. Wellbrock, M. Karasarides, R. Marais. "The RAF proteins take centre stage." *Nat. Rev. Mol. Cell Biol*., 5(11), (**2004**): 875.

[77] H. R. Mott, J. W. Carpenter, S. Zhong, S. Ghosh, R. M. Bell, S. L. Campbell. "The solution structure of the Raf-1 cysteine-rich domain: a novel ras and phospholipid binding site." *Proc. Natl. Acad. Sci. U. S. A*., 93(16), (**1996**): 8312-8317.

[78] T. Joneson, M. A. White, M. H. Wigler, D. Bar-Sagi. "Stimulation of membrane ruffling and MAP kinase activation by distinct effectors of RAS." *Science*, 271(5250), (**1996**): 810-812.

[79] M. T. Mazhab-Jafari, C. B. Marshall, M. J. Smith, G. M. Gasmi-Seabrook, P. B. Stathopulos, F. Inagaki, L.E. Kay, B.G. Neel, M. Ikura. "Oncogenic and RASopathy-associated K-RAS mutations relieve membrane-dependent occlusion of the effector-binding site." *Proc. Natl. Acad. Sci. U. S. A*., 112(21), (**2015**): 6625-6630.

[80] S. K. Fetics, H. Guterres, B. M. Kearney, G. Buhrman, B. Ma, R. Nussinov, C. Mattos. "Allosteric effects of the oncogenic RasQ61L mutant on Raf-RBD." *Structure*, 23(3), (**2015**): 505-516.

[81] Z. L. Li, P. Prakash, M. Buck. "A “tug of war” maintains a dynamic protein–membrane complex: molecular dynamics simulations of C-Raf RBD-CRD bound to K-Ras4B at an anionic membrane." *ACS Cent. Sci*., 4(2), (**2018**): 298-305.

[82] R. B. Blasco, S. Francoz, D. Santamaría, M. Cañamero, P. Dubus, J. Charron, M. Baccarini, M. Barbacid. "c-Raf, but not B-Raf, is essential for development of K-Ras oncogene-driven non-small cell lung carcinoma." *Cancer Cell*, 19(5), (**2011**): 652-663.

[83] A. S. Dhillon, S. Hagan, O. Rath, W. Kolch. "MAP kinase signalling pathways in cancer." *Oncogene*, 26(22), (**2007**): 3279.

[84] B. Lakshman, S. Messing, E. M. Schmid, J. D. Clogston, W. K. Gillette, D. Esposito, B. Kessing, D.A. Fletcher, D.V. Nissley, F. McCormick, A. G. Stephen. "Quantitative biophysical analysis defines key components modulating recruitment of the GTPase KRAS to the plasma membrane." *J. Biol. Chem*., 294(6), (**2019**): 2193-2207.

[85] S. A. Moodie, B. M. Willumsen, M. J. Weber, A. Wolfman. "Complexes of Ras. GTP with Raf-1 and mitogen-activated protein kinase kinase." *Science*, 260(5114), (**1993**):1658-1661.

[86] W. J. Fantl, A. J. Muslin, A. Kikuchi, J. A. Martin, A. M. MacNicol, R. W. Grosst, L. T. Williams. "Activation of Raf-1 by 14-3-3 proteins." *Nature*, 371(6498), (**1994**) 612.

[87] R. Marais, Y. Light, C. Mason, H. Paterson, M. F. Olson, C. J. Marshall. "Requirement of Ras-GTP-Raf complexes for activation of Raf-1 by protein kinase C." *Science*, 280(5360), (**1998**): 109-112.

[88] R. Marais, Y. Light, H. F. Paterson, C. J. Marshall. "Ras recruits Raf-1 to the plasma membrane for activation by tyrosine phosphorylation." *EMBO J*., 14(13), (**1995**): 3136-3145.

[89] A. K. Freeman, D. A. Ritt, D. K. Morrison. "Effects of Raf dimerization and its inhibition on normal and disease-associated Raf signaling." *Mol. Cell*, 49(4), (**2013**): 751-758.

[90] P. I. Poulikakos, C. Zhang, G. Bollag, K. M. Shokat, N. Rosen. "RAF inhibitors transactivate RAF dimers and ERK signalling in cells with wild-type BRAF." *Nature*, 464(7287), (**2010**): 427.

[91] B. H. Zhang, K. L. Guan. "Activation of B-Raf kinase requires phosphorylation of the conserved residues Thr598 and Ser601." *EMBO J*., 19(20), (**2000**): 5429-5439.

[92] P. T. Wan, M. J. Garnett, S. M. Roe, S. Lee, D. Niculescu-Duvaz, V. M. Good, C.G. Project, C.M. Jones, C.J. Marshall, C.J. Springer, D. Barford. "Mechanism of activation of the RAF-ERK signaling pathway by oncogenic mutations of B-RAF." *Cell*, (**2004**)116(6), 855-867.

[93] T. Rajakulendran, M. Sahmi, M. Lefrançois, F. Sicheri, M. Therrien. "A dimerization-dependent mechanism drives RAF catalytic activation." *Nature*, 461(7263), (**2009**): 542.

[94] Z. Karoulia, E. Gavathiotis, P. I. Poulikakos. "New perspectives for targeting RAF kinase in human cancer." *Nat. Rev. Cancer*, 17(11), (**2017**): 676.

[95] S. Gross, R. Rahal, N. Stransky, C. Lengauer, K. P. Hoeflich. "Targeting cancer with kinase inhibitors." *J. Clin. Invest*., 125(5), (**2015**): 1780-1789.

[96] R. A. Okimoto, L. Lin, V. Olivas, E. Chan, E. Markegard, A. Rymar, D. Neel, X. Chen, G. Hemmati, G. Bollag, T. G. Bivona. "Preclinical efficacy of a RAF inhibitor that evades paradoxical MAPK pathway activation in protein kinase BRAF-mutant lung cancer." *Proc. Natl. Acad. Sci. U. S. A*., 113(47), (**2016**): 13456-13461.

[97] E. L. Diamond, B. H. Durham, J. Haroche, Z. Yao, J. Ma, S. A. Parikh, Z. Wang, J. Choi, E. Kim, F. Cohen-Aubart, S. C. W. Lee. "Diverse and targetable kinase alterations drive histiocytic neoplasms." *Cancer Discovery*, 6(2), (**2016**): 154-165.

[98] P. Chardin, J. H. Camonis, N. W. Gale, L. Van Aelst, J. Schlessinger, M. H. Wigler, D. Bar-Sagi. "Human Sos1: a guanine nucleotide exchange factor for Ras that binds to GRB2." *Science*, 260(5112), (**1993**): 1338-1343.

[99] F. Lepri, A. D. Luca, L. Stella, C. Rossi, G. Baldassarre, F. Pantaleoni, V. Cordeddu, B.J. Williams, M.L. Dentici, V. Caputo, S. Venanzi. "SOS1 mutations in Noonan syndrome: molecular spectrum, structural insights on pathogenic effects, and genotype–phenotype correlations." *Hum. Mutat*., 32(7), (**2011**): 760-772.

[100] S. Corbalan-Garcia, S. S. Yang, K. R. Degenhardt, D. Bar-Sagi. "Identification of the mitogen-activated protein kinase phosphorylation sites on human Sos1 that regulate interaction with Grb2." *Mol. Cell. Biol*., 16(10), (**1996**): 5674-5682.

[101] M. J. Kim, J. S. Chang, S. K. Park, J. I. Hwang, S. H. Ryu, P. G. Suh. "Direct interaction of SOS1 Ras exchange protein with the SH3 domain of phospholipase C-γ1." *Biochemistry*, 39(29), (**2000**): 8674-8682.

[102] M. Innocenti, P. Tenca, E. Frittoli, M. Faretta, A. Tocchetti, P. P. Di Fiore, G. Scita. "Mechanisms through which Sos-1 coordinates the activation of Ras and Rac." *J Cell Biol*., 156(1), (**2002**): 125-136.

[103] X. Qian, L. Esteban, W. C. Vass, C. Upadhyaya, A. G. Papageorge, K. Yienger, J.M. Ward, D.R. Lowy, E. Santos. "The Sos1 and Sos2 Ras‐specific exchange factors: differences in placental expression and signaling properties." *EMBO J*., 19(4), (**2000**): 642-654.

[104] A. E. Roberts, T. Araki, K. D. Swanson, K. T. Montgomery, T. A. Schiripo, V. A. Joshi, L. Li, Y. Yassin, A.M. Tamburino, B.G. Neel, R. S. Kucherlapati. "Germline gain-of-function mutations in SOS1 cause Noonan syndrome." *Nat. Genet.*, 39(1), (**2007**): 70.

[105] P. A. Boriack-Sjodin, S. M. Margarit, D. Bar-Sagi, J. Kuriyan. "The structural basis of the activation of Ras by Sos." *Nature*, 394(6691), (1998): 337.

[106] L. A. Quilliam, S. Y. Huff, K. M. Rabun, W. Wei, W. Park, D. Broek, C. J. Der. "Membrane-targeting potentiates guanine nucleotide exchange factor CDC25 and SOS1 activation of Ras transforming activity." *Proc. Natl. Acad. Sci. U. S. A*., 91(18), (**1994**): 8512-8516.

[107] U. Vo, N. Vajpai, L. Flavell, R. Bobby, A. L. Breeze, K. J. Embrey, A. P. Golovanov. "Monitoring Ras interactions with the nucleotide exchange factor Son of Sevenless (Sos) using site-specific NMR reporter signals and intrinsic fluorescence." *J. Biol. Chem*., 291(4), (**2016**): 1703-1718.

[108] S. De, J. K. T. Dermawan, G. R. Stark. "EGF receptor uses SOS1 to drive constitutive activation of NFκB in cancer cells." *Proc. Natl. Acad. Sci. U. S. A.*, 111(32), (**2014**):11721-11726.

[109] S. M. Christensen, H. L. Tu, J. E. Jun, S. Alvarez, M. G. Triplet, J. S. Iwig, K.K. Yadav, D. Bar-Sagi, J.P. Roose, J. T. Groves. "One-way membrane trafficking of SOS in receptor-triggered Ras activation." *Nat. Struct. Mol. Biol*., 23(9), (**2016**): 838.

[110] H. H. Nelson, D. C. Christiani, E. J. Mark, J. K. Wiencke, J. C. Wain, K. T. Kelsey. "Implications and prognostic value of K-ras mutation for early-stage lung cancer in women." *J. Natl. Cancer Inst*., 91(23), (**1999**): 2032-2038.

[111] H. Ledford. "Cancer: the Ras renaissance." *Nat. News*, 520(7547), (**2015**): 278.

[112] B. Papke, C. J. Der. "Drugging RAS: Know the enemy." *Science*, 355(6330), (**2017**): 1158-1163.

[113] G. A. Hobbs, C. J. Der, K. L. Rossman. "RAS isoforms and mutations in cancer at a glance." *J Cell Sci*., 129(7), (**2016**): 1287-1292.

[114] I. A. Prior, P. D. Lewis, C. Mattos. "A comprehensive survey of Ras mutations in cancer." *Cancer Res*., 72(10), (**2012**): 2457-2467.

[115] C. V. Dang, E. P. Reddy, K. M. Shokat, L. Soucek. "Drugging the 'undruggable' cancer targets." *Nat. Rev. Cancer*, 17(8), (**2017**): 502.

[116] A. M. Waters, C. J. Der. "KRAS: the critical driver and therapeutic target for pancreatic cancer." *Cold Spring Harbor Perspect. Med*., 8(9), (**2018**): a031435.

[117] G. Zimmermann, B. Papke, S. Ismail, N. Vartak, A. Chandra, M. Hoffmann, H. Waldmann. "Small molecule inhibition of the KRAS–PDEδ interaction impairs oncogenic KRAS signalling." *Nature*, 497(7451), (**2013**): 638.

[118] M. C. Coffey, J. E. Strong, P. A. Forsyth, P. W. Lee. "Reovirus therapy of tumors with activated Ras pathway." *Science*, 282(5392), (**1998**): 1332-1334.

[119] D. A. Ritt, M. T. Abreu-Blanco, L. Bindu, D. E. Durrant, M. Zhou, S. I. Specht, A.G. Stephen, M. Holderfield, D. K. Morrison. "Inhibition of Ras/Raf/MEK/ERK pathway signaling by a stress-induced phospho-regulatory circuit." *Mol. Cell*, 64(5), (**2016**): 875-887.

[120] P. Upadhyaya, Z. Qian, N. G. Selner, S. R. Clippinger, Z. Wu, R. Briesewitz, D. Pei. "Inhibition of Ras signaling by blocking Ras–effector interactions with cyclic peptides." *Angew. Chem., Int. Ed*., 54(26), (**2015**): 7602-7606.

[121] C. E. Quevedo, A. Cruz-Migoni, N. Bery, A. Miller, T. Tanaka, D. Petch, C.J. Bataille, L.Y. Lee, P.S. Fallon, H. Tulmin, M. T. Ehebauer. "Small molecule inhibitors of RAS-effector protein interactions derived using an intracellular antibody fragment." *Nat. Commun*, 9(1), (**2018**): 3169.

[122] R. C. Hillig, B. Sautier, J. Schroeder, D. Moosmayer, A. Hilpmann, C. M. Stegmann, N.D. Werbeck, H. Briem, U. Boemer, J. Weiske, V. Badock. "Discovery of potent SOS1 inhibitors that block RAS activation via disruption of the RAS–SOS1 interaction." *Proc. Natl. Acad. Sci. U. S. A*., 116(7), (**2019**): 2551-2560.

[123] S. K. Athuluri-Divakar, R. Vasquez-Del Carpio, K. Dutta, S. J. Baker, S. C. Cosenza, I. Basu, Y.K. Gupta, M.R. Reddy, L. Ueno, J.R. Hart, P. K. Vogt. "A small molecule RAS-mimetic disrupts RAS association with effector proteins to block signaling." *Cell*, 165(3), (**2016**): 643-655.

[124] E. M. Kerr, E. Gaude, F. K. Turrell, C. Frezza, C. P. Martins. "Mutant Kras copy number defines metabolic reprogramming and therapeutic susceptibilities." *Nature*, 531(7592), (**2016**): 110.

[125] C. G. Kinsey, S. A. Camolotto, A. M. Boespflug, K. P. Guillen, M. Foth, A. Truong, S.S. Schuman, J.E. Shea, M.T. Seipp, J.T. Yap, L. D. Burrell. "Protective autophagy elicited by RAF→ MEK→ ERK inhibition suggests a treatment strategy for RAS-driven cancers." *Nat. Med*., 25(4), (**2019**): 620.

[126] E. White. "The role for autophagy in cancer." *J. Clin. Invest*., 125(1), (**2015**): 42-46.

[127] N. Ollivier, T. Toupy, R. C. Hartkoorn, R. Desmet, J. C. M. Monbaliu, O. Melnyk. "Accelerated microfluidic native chemical ligation at difficult amino acids toward cyclic peptides." *Nat. Commun*, 9(1), (**2018**): 2847.

[128] J. Wilken, S. B. Kent. "Chemical protein synthesis." *Curr. Opin. Biotechnol*., 9(4), (**1998**): 412-426.

[129] P. E. Dawson, T. W. Muir, I. Clark-Lewis, S. B. Kent. "Synthesis of proteins by native chemical ligation." *Science*, 266(5186), (**1994**): 776-779.

[130] P. E. Dawson, S. B. Kent. "Synthesis of native proteins by chemical ligation." *Annu. Rev. Biochem*., 69(1), (**2000**): 923-960.

[131] S. B. Kent. "Total chemical synthesis of proteins." *Chem. Soc. Rev*., 38(2), (**2009**): 338-351.

[132] T. W. Muir, D. Sondhi, P. A. Cole. "Expressed protein ligation: a general method for protein engineering." *Proc. Natl. Acad. Sci. U. S. A*., 95(12), (**1998**): 6705-6710.

[133] T. W. Muir. "Semi-synthesis of proteins by expressed protein ligation." *Annu. Rev. Biochem*., 72(1), (**2003**): 249-289.

[134] K. Severinov, T. W. Muir. "Expressed protein ligation, a novel method for studying protein-protein interactions in transcription." *J. Biol. Chem*., 273(26), (**1998**):16205-16209.

[135] T. G. Bivona. "Dampening oncogenic RAS signaling." *Science*, 363(6433), (2019): 1280-1281.

[136] K. Scheffzek, G. Shivalingaiah. "Ras-Specific GTPase-Activating Proteins—Structures, Mechanisms, and Interactions." *Cold Spring Harbor Perspect. Med*., 9(3), (**2019**): a031500.

[137] A. G. Menendez, D. J. Curzake, L. Luo, H. J. Wanebo. "C6-ceramide's effect on KRAS-defined colorectal cancer cells treated with oxaliplatin, 5-fluoruracil with and without cetuximab." *J. Clin. Oncol*., 34:4_suppl, (**2016**): 619-619

[138] L. Li, M. Dwivedi, S. Patra, N. Erwin, S. Möbitz, R. Winter. "Probing Colocalization of N‐Ras and K‐Ras4B Lipoproteins in Model Biomembranes." *ChemBioChem*, 20(9), (**2019**): 1190-1195.

[139] I.A. Prior, A. Harding, J. Yan, J. Sluimer, R.G. Parton, J.F. Hancock. "GTP-dependent segregation of H-ras from lipid rafts is required for biological activity." *Nat. Cell Biol.,* 3(**2001**): 368–375.

[140] A.D. Cox, S.W. Fesik, A.C. Kimmelman, J. Luo, C.J. Der. "Drugging the undruggable RAS: mission possible?" *Nat. Rev. Drug Discov*., 13(**2014**): 828–851.

[141] M.A. Daniels, E. Teixeiro, J. Gill, B. Hausmann, D. Roubaty, K. Holmberg, G. Werlen, G.A. Hollander, N.R. Gascoigne, E. Palmer. "Thymic selection threshold

defined by compartmentalization of Ras/MAPK signalling." *Nature,* 444 (**2006**): 724–729.

[142] Y. Zhou, C.O. Wong, K.J. Cho, D. van der Hoeven, H. Liang, D.P. Thakur, J. Luo, M. Babic, K.E. Zinsmaier, M.X. Zhu, H. Hu, K. Venkatachalam, J.F. Hancock. "Membrane potential modulates plasma membrane phospholipid dynamics and K-Ras signaling." *Science,* 349 (**2015**): 873–876.

[143] X. Nan, T.M. Tamguney, E.A. Collisson, L.J. Lin, C. Pitt, J. Galeas, S. Lewis, J.W. Gray, F. McCormick, S. Chu. "Ras-GTP dimers activate the mitogen-activated protein kinase (MAPK) pathway." *Proc. Natl. Acad. Sci. U. S. A*., 112 (**2015**): 7996–8001.

[144] J.M. Ostrem, K.M. Shokat. "Direct small-molecule inhibitors of KRAS: from structural insights to mechanism-based design." *Nat. Rev. Drug Discov*.,15 (**1990**): 771–785.

[145] M. Fillet, M. Bentires-Alj, V. Deregowski, R. Greimers, J. Gielen, J. Piette, V. Bours, M.P. Merville. "Mechanisms involved in exogenous C2-and C6-ceramide-induced cancer cell toxicity." *Biochem. Pharmacol*., 65 (**2003**): 1633–1642.

[146] A.G. Menendez, D.J. Curzake, L. Luo, H.J. Wanebo. "C6-ceramide's effect on KRAS-defined colorectal cancer cells treated with oxaliplatin, 5-fluoruracil with and without cetuximab." *J. Clin. Oncol*. 34 (**2016**): 619.

[147] P. Zhang, C. Fu, Y. Hu, C. Dong, Y. Song, E. Song. "C6-ceramide nanoliposome suppresses tumor metastasis by eliciting PI3K and PKCζ tumor-suppressive activities and regulating integrin affinity modulation." *Sci. Rep*., 5 (**2015**): 9275.

[148] K. Venkataraman, A.H. Futerman. "Ceramide as a second messenger: sticky solutions to sticky problems." *Trends Cell Biol*., 10 (**2000**): 408–412.

[149] P. Nussbaumer. "Medicinal chemistry aspects of drug targets in sphingolipid metabolism." *ChemMedChem,* 3 (**2008**): 543–551.

[150] C. Peters, A. Billich, M. Ghobrial, K. Högenauer, T. Ullrich, P. Nussbaumer. "Synthesis of borondipyrromethene (BODIPY)-labeled sphingosine derivatives by cross-metathesis reaction." *J. Org.Chem*., 72 (**2007**): 1842–1845.

[151] E. Wang, J. B. Klauda. "Molecular Dynamics Simulations of Ceramide and Ceramide-Phosphatidylcholine Bilayers." *J. Phys. Chem*. B, 121 (**2017**): 10091–10104.

[152] A. S. Klymchenko, R. Kreder. "Fluorescent probes for lipid rafts: from model membranes to living cells." *Chem. Biol*., 21 (**2014**): 97–113.

[153] N. Kahya, D. Scherfeld, K. Bacia, B. Poolman, P. Schwille. "Probing lipid mobility of raft-exhibiting model membranes by fluorescence correlation spectroscopy." *J. Biol. Chem*., 278 (**2003**): 28109–28115.

[154] P. Sawatzki Megha, T. Kolter, R. Bittman, E. London. "Effect of ceramide N-acyl chain and polar headgroup structure on the properties of ordered lipid domains (lipid rafts)." *Biochim. Biophys. Acta*, 1768 (**2007**): 2205–2212.

[155] A. Gidwani, H. A. Brown, D. Holowka, B. Baird. "Disruption of lipid order by short-chain ceramides correlates with inhibition of phospholipase D and downstream signaling by FcεRI." *J. Cell Sci*., 116 (**2003**): 3177–3187.

[156] M. R. Philips, C. J. Der. "Seeing is believing: Ras dimers observed in live cells." *Proc. Natl. Acad. Sci. U. S. A*., 112 (**2015**): 9793–9794.

[157] M. Shen, P. Pan, Y. Li, D. Li, H. Yu, T. Hou. "Farnesyltransferase and geranylgeranyltransferase I: structures, mechanism, inhibitors and molecular modelling." *Drug Discovery Today*, 20, (**2015**): 267-276;

[158] S. Dharmaiah, L. Bindu, T. H. Tran, W. K. Gillette, P. H. Frank, R. Ghirlando, D. V. Nissley, D. Esposito, F. McCormick, A. G. Stephen, D. K. Simanshu. "Structural basis of recognition of farnesylated and methylated K-Ras4B by PDEδ." *Proc. Natl. Acad. Sci. U. S. A*. (**2016**): Nov 1; 113(44):E6766-75.

[159] R. Spencer-Smith, A. Koide, Y. Zhou, R. R. Eguchi, F. Sha, P. Gajwani, D. Santana, A. Gupta, M. Jacobs, E. Herrero-Garcia, J. Cobbert, H. Lavoie, M. Smith, T. Rajakulendran, E. Dowdell, M. N. Okur, I. Dementieva, F. Sicheri, M. Therrien, J. F. Hancock, M. Ikura, S. Koide, J. P. O'Bryan. "Inhibition of RAS function through targeting an allosteric regulatory site." *Nat. Chem. Biol*. (**2017**): 13, 62-68.

[160] N. M. Baker, C. J. Der. "Cancer: Drug for an 'undruggable' protein." *Nature*, (**2013**): 497, 577-578;

[161] E. Manchado, S. Weissmueller, J. P. 4th. Morris, C. C. Chen, R. Wullenkord, A. Lujambio, E. de Stanchina, J. T. Poirier, J. F. Gainor, R. B. Corcoran, J. A. Engelman, C. M. Rudin, N. Rosen, S. W. Lowe. "A combinatorial strategy for treating KRAS-mutant lung cancer." *Nature*, (**2016**): 534, 647-651;

[162] C. Ambrogio, J. Köhler, Z. W. Zhou, H. Wang, R. Paranal, J. Li, M. Capelletti, C. Caffarra, S. Li, Q. Lv, S. Gondi, J. C. Hunter, J. Lu, R. Chiarle, D. Santamaria, K. D. Westover, P. A. Janne. "KRAS dimerization impacts MEK inhibitor sensitivity and oncogenic activity of mutant KRAS." *Cell,* (**2018**): 172, 857-868.e15.

[163] J. Guldenhaupt, T. Rudack, P. Bachler, D. Mann, G. Triola, H. Waldmann, C. Kotting, K. Gerwert. "N-Ras forms dimers at POPC membranes." *Biophys. J.,* (**2012**): 103, 1585-1593

[164] H. Zhang, X. H. Liu, K. Zhang, C. K. Chen, J. M. Frederick, G. D. Prestwich, W. Baehr. "Photoreceptor cGMP phosphodiesterase δ subunit (PDEδ) functions as a prenyl-binding protein." *J. Biol. Chem*., (**2004**): 279, 407-413.

[165] K. Weise, S. Kapoor, A. Werkmueller, S. Moebitz, G. Zimmermann, G. Triola, H. Waldmann, R. Winter. "Dissociation of the K-Ras4B/PDEδ complex upon contact with lipid membranes: membrane delivery instead of extraction." *J. Am. Chem. Soc*., (**2012**): 134, 11503-11510.

[167] H. Jang, S. J. Abraham, T. S. Chavan, B. Hitchinson, L. Khavrutskii, N. I. Tarasova, R. Nussinov, V. Gaponenko. "Mechanisms of membrane binding of small GTPase K-Ras4B farnesylated hypervariable region." *J. Biol. Chem*., (**2015**): 290, 9465–9477.

[168] A. M. Waters, C. J. Der. "KRAS: the critical driver and therapeutic target for pancreatic cancer." *Cold Spring Harbor Perspect. Med*., (**2018**): Sep 1;8(9):a031435.

[169] M. E. Welsch, A. Kaplan, J. M. Chambers, M. E. Stokes, P. H. Bos, A. Zask, Y. Zhang, M. Sanchez-Martin, M. A. Badgley, C. S. Huang, T. H. Tran, H. Akkiraju, L. M. Brown, R. Nandakumar, S. Cremers, W. S. Yang, L. Tong, K. P. Olive, A. Ferrando, B. R. Stockwell. "Multivalent small-molecule pan-RAS inhibitors." *Cell,* (**2017**): 168, 878–889.

[170] T. Schrader, G. Bitan, F. G. Klärner. "Molecular tweezers for lysine and arginine–powerful inhibitors of pathologic protein aggregation." *Chem. Commun*. (2016): 52, 11318–11334.

[171] E. Lump, L. M. Castellano, C. Meier, J. Seeliger, N. Erwin, B. Sperlich, C. M. Sturzel, S. Usmani, R. M. Hammond, J. von Einem, G. Gerold, F. Kreppel, K. Bravo-Rodriguez, T. Pietschmann, V. M. Holmes, D. Palesch, O. Zirafi, D. Weissman, A. Sowislok, B. Wettig, C. Heid, F. Kirchhoff, T. Weil, F. G. Klärner, T. Schrader, G. Bitan, E. Sanchez-Garcia, R. Winter, J. Shorter, J. Munch. "A molecular tweezer antagonizes seminal amyloids and HIV infection." *eLife*, (2015): 4, e05397.

[172] T. Vopel, K. Bravo-Rodriguez, S. Mittal, S. Vachharajani, D. Gnutt, A. Sharma, A. Steinhof, O. Fatoba, G. Ellrichmann, M. Nshanian, C. Heid, J. A. Loo, F. G. Klärner, T. Schrader, G. Bitan, E. E. Wanker, S. Ebbinghaus, E. Sanchez-Garcia. "Inhibition of huntingtin exon-1 aggregation by the molecular tweezer CLR01." *J. Am. Chem. Soc*., (**2017**): 139, 5640–5643.

[173] D. Bier, S. Mittal, K. Bravo-Rodriguez, A. Sowislok, X. Guillory, J. Briels, C. Heid, M. Bartel, B. Wettig, L. Brunsveld, E. Sanchez-Garcia, T. Schrader, C. Ottmann. "The Molecular Tweezer CLR01 Stabilizes a Disordered Protein–Protein Interface." *J. Am. Chem. Soc.,* (**2017**): 139, 16256–16263.

[174] M. Fivaz, T. Meyer. "Reversible intracellular translocation of KRas but not HRas in hippocampal neurons regulated by Ca2+/calmodulin." *J. Cell Biol*., (**2005**): 170, 429–441.

[175] E. M. Terrell, D. K. Morrison. "Ras-mediated activation of the Raf family kinases." *Cold Spring Harbor Perspect. Med*., (**2019**): 9, no. 1.

[176] S. Sarkar-Banerjee, A. Sayyed-Ahmad, P. Prakash, K. J. Cho, M. N. Waxham, J. F. Hancock, A. A. Gorfe. "Spatiotemporal analysis of K-Ras plasma membrane interactions reveals multiple high order homo-oligomeric complexes." *J. Am. Chem. Soc*., (**2017**): 139, 13466–13475.

[177] M. I. Angelova, S. Soleau, P. Meleard, F, Faucon, P, Bothorel. "Preparation of giant vesicles by external AC electric fields. Kinetics and applications." *Prog. Colloid Polym. Sci*., (**1992**): 89, 127–131.

[178] S. Dutt, C. Wilch, T. Gersthagen, P. Talbiersky, K. Bravo-Rodriguez, M. Hanni, E. Sanchez-Garcia, C. Ochsenfeld, F. G. Klärner, T. Schrader. "Molecular tweezers with varying anions: a comparative study." *J. Org. Chem*., (**2013**): 78, 6721–6734.

[179] P. Talbiersky, F. Bastkowski, F. G. Klärner, T. Schrader. "Molecular clip and tweezer introduce new mechanisms of enzyme inhibition." *J. Am. Chem. Soc*., (**2008**): 130, 9824–9828.

[180] K. Weise, D. Huster, S. Kapoor, G. Triola, H. Waldmann, R. Winter. "Gibbs energy determinants of lipoprotein insertion into lipid membranes: the case study of Ras proteins." *Faraday Discuss*., (2013): 161, 549–561.

[181] T. Maurer, L.S. Garrenton, A. Oh, K. Pitts, D. J. Anderson, N. J. Skelton, B. P. Fauber, B. Pan, S. Malek, D. Stokoe, J. M. Ludlam, K. K. Bowman, J. Wu, A. M. Giannetti, M. A. Starovasnik, I. Mellman, P. K. Jackson, J. Rudolph, W. Wang, G. Fang. "Small-molecule ligands bind to a distinct pocket in Ras and inhibit SOS-mediated nucleotide exchange activity." *Proc. Natl. Acad. Sci. U.S.A*., (2012): 109, 5299–5304.

[182] Q. Sun, J. P. Burke, J. Phan, M. C. Burns, E. T. Olejniczak, A. G. Waterson, T. Lee, O. W. Rossanese, S. W. Fesik. "Discovery of small molecules that bind to K‐Ras and inhibit Sos‐mediated activation." *Angew. Chem. Int. Ed*., (**2012**): 51, 6140–6143.

[183] J. M. Ostrem, U. Peters, M. L. Sos, J. A. Wells, K. M. Shokat. "K-Ras (G12C) inhibitors allosterically control GTP affinity and effector interactions." *Nature,* (**2013**): 503, 548–551.

[184] S. M. Sebti, C. J. Der. "Searching for the elusive targets of farnesyltransferase inhibitors." *Nat. Rev. Cancer,* (**2003**): 3, 945–951.

[185] A. A. Samatar, P. I. Poulikakos. "Targeting RAS–ERK signalling in cancer: promises and challenges." *Nat. Rev. Drug Discovery,* (**2014**): 13, 928–942.

[186] H. Lavoie, M. Therrien. "Regulation of RAF protein kinases in ERK signalling." *Nat. Rev. Mol. Cell Biol*., (**2015**): 16, 281–298.

[187] C. Heid, A. Sowislok, T. Schaller, F. Niemeyer, F.-G. Klärner, T. Schrader. "Molecular Tweezers with Additional Recognition Sites." *Chem. Eur. J*., (**2018**): 44, 11332-11343.

[188] I. M. Ahearn, K. Haigis, D. Bar-Sagi, M. R. Philips. "Regulating the regulator: Posttranslational modification of RAS." *Nat. Rev. Mol. Cell Biol*., 13(1), (**2012**): 39–51.

[189] E. K. Rowinsky, J. J. Windle, D. D. Von Hoff. "Ras protein farnesyltransferase: a strategic target for anticancer therapeutic development*." J. Clin. Oncol*., 17(11), (**1999**): 3631-3652.

[190] E. M. Terrell, E. D. David, A. R. Daniel, E. S. Nancy, E. Sheffels, R. S. Smith, D. Esposito, Y. Zhou, J. F. Hancock, R. L. Kortum, D. K. Morrison. "Distinct Binding Preferences between Ras and Raf Family Members and the Impact on Oncogenic Ras Signaling." *Mol. cell* (**2019**).

[191] X. Y. Zhang, H. Guo, Y. Huang, P. Q. Hao, Y. Yang, Y. Liu, X.X. Guo, Q. Hao, S. An, T. R. Xu. "Comparative interactome analysis reveals distinct and overlapping properties of Raf family kinases." *Biochem. Biophys. Res. Commun*., 514(4), (**2019**): 1217-1223.

[192] S. K. Fetics, H. Guterres, B. M. Kearney, G. Buhrman, B. Ma, R. Nussinov, C. Mattos. "Allosteric effects of the oncogenic RasQ61L mutant on Raf-RBD.*" Structure*, 23(3), (**2015**): 505-516.

[193] J. M. Aramini, S. M. Vorobiev, L. M. Tuberty, H. Janjua, E. T. Campbell, J. Seetharaman, M. Su, Y. J. Huang, T.B. Acton, R. Xiao, L. Tong. "The RAS-binding domain of human BRAF protein serine/threonine kinase exhibits allosteric conformational changes upon binding HRAS.*" Structure*, 23(8), (**2015**):1382-1393.

[194] S. Li, H. Jang, J. Zhang, R. Nussinov. "Raf-1 cysteine-Rich domain increases the affinity of K-Ras/Raf at the membrane, promoting MAPK signaling.*" Structure*, 26(3), (**2018**): 513-525.

[195] T. Travers, C. A. López, Q. N. Van, C. Neale, M. Tonelli, A. G. Stephen, S. Gnanakaran. "Molecular recognition of RAS/RAF complex at the membrane: Role of RAF cysteine-rich domain.*" Sci. Rep*., 8(1), (**2018**): 8461.

[196] C. J. Tsai, R. Nussinov. "Allosteric activation of RAF in the MAPK signaling pathway.*" Curr. Opin. Struct. Biol*., 53, (**2018**): 100-106.

[197] R. A. Okimoto, L. Lin, V. Olivas, E. Chan, E. Markegard, A. Rymar, D. Neel, X. Chen, G. Hemmati, G. Bollag, T. G. Bivona. "Preclinical efficacy of a RAF inhibitor that evades paradoxical MAPK pathway activation in protein kinase BRAF-mutant lung cancer.*" Proc. Natl. Acad. Sci. U. S. A*., 113(47), (**2016**): 13456-13461.

[198] J. R. Abbott, P. A. Patel, J. E. Howes, D. T. Akan, J. P. Kennedy, M. C. Burns, C.F. Browning, Q. Sun, O.W. Rossanese, A. G. Waterson. "Discovery of quinazolines that activate SOS1-mediated nucleotide exchange on RAS.*" ACS Med. Chem. Lett*., 9(9), (**2018**): 941-946.

[199] H. Jang, R. Nussinov. "Raf-1 Cysteine-Rich Domain (CRD) Promotes Active Orientation and Dimerization of K-Ras4B at the Membrane.*" Biophys. J*., 116(3), (**2019**): 205a.

[200] H. Nakhaeizadeh, E. Amin, S. Nakhaei-Rad, R. Dvorsky, M. R. Ahmadian. "The RAS-effector interface: isoform-specific differences in the effector binding regions.*" Plos One*, 11(12), (**2016**): e0167145.

[201] J. R. Roskoski. "RAF protein-serine/threonine kinases: structure and regulation.*" Biochem. Biophys. Res. Commun*., 399(3), (**2010**): 313-317.

[202] R. Marais, Y. Light, H. F. Paterson, C. S. Mason, C. J. Marshall. "Differential regulation of Raf-1, A-Raf, and B-Raf by oncogenic ras and tyrosine kinases.*" J. Biol. Chem*., 272(7), (**1997**): 4378-4383.

[203] D. Matallanas, M. Birtwistle, D. Romano, A. Zebisch, J. Rauch, A. von Kriegsheim, W. Kolch. "Raf family kinases: old dogs have learned new tricks.*" Genes Cancer*, 2(3), (**2011**): 232-260.

[204] A. Fischer, M. Hekman, J. Kuhlmann, I. Rubio, S. Wiese, U. R. Rapp. "B-and C-RAF display essential differences in their binding to Ras the isotype-specific N-

terminus of B-RAF facilitates Ras binding.” *J. Biol. Chem*., 282(36), (**2007**): 26503-26516.

[205] F. Shima, Y. Ijiri, S. Muraoka, J. Liao, M. Ye, M. Araki, K. Matsumoto, N. Yamamoto, T. Sugimoto, Y. Yoshikawa, T. Kumasaka. Structural basis for conformational dynamics of GTP-bound Ras protein. *J. Biol. Chem*., 285(29), (**2010**): 22696-22705.

Acknowledgments

I would like to extend thanks to many people, of many different groups and countries, who so generously contributed to the work presented in this thesis.

Special mention goes to my outstanding supervisor, Prof. Dr. Roland Winter who gave me the opportunity to do this interdisciplinary work in a fascinating group. Through his everlasting willingness to discuss and stimulating suggestions, this thesis evolved out successfully. His enthusiasm for research and curiosity of every scientific tiny issue inspired me to achieve this doctoral thesis. I would like to thank him for giving me so many wonderful opportunities for attending national and international conferences. I especially value his efforts in dealing with drafts of papers, conference posters and talks despite his busy schedule. In addition, my special thanks go to his effort and patience in enhancing my skills of English and presentation. His encouraging and positive attitude have undoubtedly enhanced my scientific and non-scientific abilities and will always be with me, and motivate me to go further.

I am thankful to Prof. Dr. Claus Czeslik for his invaluable suggestions and kindly help through the experimental and technical difficulties.

I want to thank Prof. Roland Winter and Prof. Dr. Claus Czeslik for examining my thesis work and for investing their precious time.

I own my sincere thanks to my additional supervisors Prof. Dr. Roger S. Goody and Prof. Dr. Yaowen Wu for their precious time for examining my doctoral work and helpful suggestions.

I highly acknowledged the generous funding and resources from TU Dortmund University, Max Planck Institute of Molecular Physiology, and International Max Planck Research School in Chemical and Molecular Biology that enabled me to pursue this work. I really appreciate the support provided by Christa Hornemann and Dr. Lucia Sironi, both professionally and personally, during my stay in Germany.

A special thanks are due to Andrea Kreusel, who helped me a lot with registration and Visa documents staff. I would like to thank Simone Möbitz for her beautiful technical

support. I enjoyed the time working with her in the S1 laboratory. Many thanks go to Bertina Schuppan for her help in the lab and office facilities.

Dr. Fu Li and Dr. Xi Chen are gratefully acknowledged for their valuable discussions and kind help for cell culture and confocal microscopy measurements. Dr. Sven A. H. Müller (MPI Dortmund, Germany) is gratefully acknowledged for his guidance of confocal microscopy.

I gratefully acknowledge Dr. Yong Zhu (University of Texas Health Science Center at Houston, USA) for the stimulating discussion with him during the Biophysical Society meeting in San Francisco, USA and the Biochemical Society meeting in Cambridge, UK. The discussion with him fruited a project in the end.

I would like to thank Dr. Frantz Jean-Francois, Dr. Simon Messing, Dr. Dominic Esposito and Carissa Grose from the Frederick National Laboratory for Cancer Research, USA for their open and unreserved discussion regarding the C-Raf-RBD-CRD protein expression, purification and sharing the plasmid of this protein with me. Dr. Felix Niemeyer (University of Duisburg-Essen, Germany) is acknowledged for the in-silico studies of the K-Ras4B-tweezer.

I have been fortunate in getting a chance to meet and work with my group members. I would like to thank all of them. Special thanks go to Dr. Mridula Dwivedi, Dr. Nelli Erwin, Dr. Mimi Gao, Dr. Satyajit Patra and Loana Arns for their kind help, scientific and non-scientific conversations as well as motivation and constructive words during my difficult time. I really appreciate the kind help from Dr. Mimi Gao through the registration and very tiny staff that I encountered in living in Germany. Loana Arns is acknowledged for proof-reading and correcting the ‘Zusammenfassung’ part of my thesis.

Last but not the least, I would like to thank my family and friends for their unrestricted support. I especially thank my parents, sisters and all my relatives for their encouragement, understanding, support and love. Without it, I will not have accomplished this thesis.

Publication

1. **L. Li**, N. Erwin, S. Möbitz, F. Niemeyer, and T. Schrader, R. Winter. "Dissociation of the Signaling Protein K-Ras4B from Lipid Membranes Induced by a Molecular Tweezer." ***Chem. Eur. J.***, 25 (**2019**), 9827 – 9833.

2. L. Laraia, A. Friese, D. P. Corkery, G. Konstantinidis, N. Erwin, W. Hofer, H. Karatas, L. Klewer, A. Brockmeyer, M. Metz, B. Schölermann, M. Dwivedi, **L. Li**, P. Rios-Munoz, M. Köhn, R. Winter, I. Vetter, S. Ziegler, P. Janning, Y.-W. Wu, and H. Waldmann. "The Cholesterol Transfer Protein GRAMD1A Regulates Autophagosome Biogenesis." ***Nat. Chem. Biol.***, 15 (**2019**), 710-720.

3. **L. Li**, M. Dwivedi, S. Patra, N. Erwin, S. Möbitz, and R. Winter. "Probing Colocalization of N-Ras and K-Ras4B Lipoproteins in Model Biomembranes." ***ChemBioChem,*** 20 (**2019**), 1190-1195.

4. M. Herzog, **L. Li**, H. J. Galla, and R. Winter. "Effect of Hyaluronic Acid on Phospholipid Model Membranes." ***Colloids Surf. B***, 173 (**2019**) 327-334.

5. **L. Li**, M. Dwivedi, N. Erwin, S. Möbitz, P. Nussbaumer, and R. Winter. "Interaction of K-Ras4B Protein with C6-ceramide Containing Lipid Model Membranes", ***Biochim. Biophys. Acta,*** 1860 (**2018**) 1008-1014.

6. **L. Li**, S. Y. Zhang, Y. M. Li, Y. X. Chen. “Dual-Labeling of Ubiquitin Protein by Chemoselective Reactions for Sensing UCH-L3.", ***Mol. BioSyst.***, 12 (**2016**), 1764-1767.

Two further publication are in preparation.

Eidesstattliche Versicherung (Affidavit)

Li, Lei
Name, Vorname
(Surname, first name)

198307
Matrikel-Nr.
(Enrollment bunmer)

Belehrung:

Wer vorsätzlich gegen eine die Täuschung über Prüfungsleistungen betreffende Regelung einer Hochschulprüfungsordnung verstößt, handelt ordnungswidrig. Die Ordnungswidrigkeit kann mit einer Geldbuße von bis zu 50.000,00 € geahndet werden. Zuständige Verwaltungsbehörde für die Verfolgung und Ahndung von Ordnungswidrigkeiten ist der Kanzler/die Kanzlerin der Technischen Universität Dortmund. Im Falle eines mehrfachen oder sonstigen schwerwiegenden Täuschungsversuches kann der Prüfling zudem exmatrikuliert werden, §63 Abs. 5 Hochschulgesetz NRW.

Die Abgabe einer falschen Versicherung an Eides statt ist strafbar.

Wer vorsätzlich eine falsche Versicherung an Eides statt abgibt, kann mit einer Freiheitsstrafe bis zu drei Jahren oder mit Geldstrafe bestraft werden, § 156 StGB. Die fahrlässige Abgabe einer falschen Versicherung an Eides statt kann mit einer Freiheitsstrafe bis zu einem Jahr oder Geldstrafe bestraft werden, § 161 StGB.

Official notification:

Any person who intentionally breaches any regulation of university examination regulations relating to deception in examination performance is acting improperly. This offence can be punished with a fine of up to EUR 50,000.00. The competent administrative authority for the pursuit and prosecution of offences of this type is the chancellor of the TU Dortmund University. In the case of multiple or other serious attempts at deception, the candidate can also be unenrolled, Section 63, paragraph 5 of the Universities Act of North Rhine-Westphalia.

The submission of a false affidavit is punishable.

Any person who intentionally submits a false affidavit can be punished with a prison sentence of up to three years or a fine, Section 156 of the Criminal Code. The negligent submission of a false affidavit can be punished with a prison sentence of up to one year or a fine, Section 161 of the Criminal Code.

I have taken note of the above official notification.

Ort, Datum
(Place, date)

Unterschrift
(Signature)

Titel der Dissertation:
(Title of the thesis):

Ich versichere hiermit an Eides statt, dass ich die vorliegende Dissertation mit dem Titel selbstständig und ohne unzulässige fremde Hilfe angefertigt habe. Ich habe keine anderen als die angegebenen Quellen und Hilfsmittel benutzt sowie wörtliche und sinngemäße Zitate kenntlich gemacht. Die Arbeit hat in gegenwärtiger oder in einer anderen Fassung weder der TU Dortmund noch einer anderen Hochschule im Zusammenhang mit einer staatlichen oder akademischen Prüfung vorgelegen.

I hereby swear that I have completed the present dissertation independently and without inadmissible external support. I have not used any sources or tools other than those indicated and have identified literal and analogous quotations. The thesis in its current version or another version has not been presented to the TU Dortmund University or another university in connection with a state or academic examination.

*Please be aware that solely the German version of the affidavit ("Eidesstattliche Versicherung") for the PhD thesis is the official and legally binding version.

Ort, Datum
(Place, date)

Unterschrift
(Signature)

Permission

JOHN WILEY AND SONS LICENSE TERMS AND CONDITIONS

Aug 17, 2019

This Agreement between Lei Li ("You") and John Wiley and Sons ("John Wiley and Sons") consists of your license details and the terms and conditions provided by John Wiley and Sons and Copyright Clearance Center.

License Number	4651420285269
License date	Aug 17, 2019
Licensed Content Publisher	John Wiley and Sons
Licensed Content Publication	Chemistry - A European Journal
Licensed Content Title	Dissociation of the Signaling Protein K-Ras4B from Lipid Membranes Induced by a Molecular Tweezer
Licensed Content Author	Lei Li, Nelli Erwin, Simone Möbitz, et al
Licensed Content Date	Jul 1, 2019
Licensed Content Volume	25
Licensed Content Issue	42
Licensed Content Pages	7
Type of Use	Dissertation/Thesis
Requestor type	Author of this Wiley article
Format	Print and electronic
Portion	Full article
Will you be translating?	No
Title of your thesis / dissertation	Mechanistic studies of Ras nanoclusters and Ras effectors interacting with the lipid membrane
Expected completion date	Dec 2019
Expected size (number of pages)	
Requestor Location	Lei Li Otto-Hahn-Str. 4a 44227 Dortmund Dortmund, NRW 44149 Germany Attn: Lei Li
Publisher Tax ID	EU826007151
Total	**0.00 EUR**
Terms and Conditions	

Permission

TERMS AND CONDITIONS

This copyrighted material is owned by or exclusively licensed to John Wiley & Sons, Inc. or one of its group companies (each a"Wiley Company") or handled on behalf of a society with which a Wiley Company has exclusive publishing rights in relation to a particular work (collectively "WILEY"). By clicking "accept" in connection with completing this licensing transaction, you agree that the following terms and conditions apply to this transaction (along with the billing and payment terms and conditions established by the Copyright Clearance Center Inc., ("CCC's Billing and Payment terms and conditions"), at the time that you opened your RightsLink account (these are available at any time at http://myaccount.copyright.com).

Terms and Conditions

- The materials you have requested permission to reproduce or reuse (the "Wiley Materials") are protected by copyright.

- You are hereby granted a personal, non-exclusive, non-sub licensable (on a stand-alone basis), non-transferable, worldwide, limited license to reproduce the Wiley Materials for the purpose specified in the licensing process. This license, **and any CONTENT (PDF or image file) purchased as part of your order,** is for a one-time use only and limited to any maximum distribution number specified in the license. The first instance of republication or reuse granted by this license must be completed within two years of the date of the grant of this license (although copies prepared before the end date may be distributed thereafter). The Wiley Materials shall not be used in any other manner or for any other purpose, beyond what is granted in the license. Permission is granted subject to an appropriate acknowledgement given to the author, title of the material/book/journal and the publisher. You shall also duplicate the copyright notice that appears in the Wiley publication in your use of the Wiley Material. Permission is also granted on the understanding that nowhere in the text is a previously published source acknowledged for all or part of this Wiley Material. Any third party content is expressly excluded from this permission.

- With respect to the Wiley Materials, all rights are reserved. Except as expressly granted by the terms of the license, no part of the Wiley Materials may be copied, modified, adapted (except for minor reformatting required by the new Publication), translated, reproduced, transferred or distributed, in any form or by any means, and no derivative works may be made based on the Wiley Materials without the prior permission of the respective copyright owner.**For STM Signatory Publishers clearing permission under the terms of the STM Permissions Guidelines only, the terms of the license are extended to include subsequent editions and for editions in other languages, provided such editions are for the work as a whole in situ and does not involve the separate exploitation of the permitted figures or extracts,** You may not alter, remove or suppress in any manner any copyright, trademark or other notices displayed by the Wiley Materials. You may not license, rent, sell, loan, lease, pledge, offer as security, transfer or assign the Wiley Materials on a stand-alone basis, or any of the rights granted to you hereunder to any other person.

- The Wiley Materials and all of the intellectual property rights therein shall at all times remain the exclusive property of John Wiley & Sons Inc, the Wiley Companies, or their respective licensors, and your interest therein is only that of having possession of and the right to reproduce the Wiley Materials pursuant to Section 2 herein during the continuance of this Agreement. You agree that you own no right, title or interest in or to the Wiley Materials or any of the intellectual property rights therein. You shall have no rights hereunder other than the license as provided for above in Section 2. No right, license or interest to any trademark, trade name, service mark or other branding ("Marks") of WILEY or its licensors is granted hereunder, and you agree that you shall not assert any such right, license or interest with respect thereto

- NEITHER WILEY NOR ITS LICENSORS MAKES ANY WARRANTY OR REPRESENTATION OF ANY KIND TO YOU OR ANY THIRD PARTY, EXPRESS, IMPLIED OR STATUTORY, WITH RESPECT TO THE MATERIALS OR THE ACCURACY OF ANY INFORMATION CONTAINED IN THE MATERIALS, INCLUDING, WITHOUT LIMITATION, ANY IMPLIED WARRANTY OF MERCHANTABILITY, ACCURACY, SATISFACTORY QUALITY, FITNESS FOR A PARTICULAR PURPOSE, USABILITY, INTEGRATION OR NON-INFRINGEMENT AND ALL SUCH WARRANTIES ARE HEREBY EXCLUDED BY WILEY AND ITS LICENSORS AND WAIVED BY YOU.

- WILEY shall have the right to terminate this Agreement immediately upon breach of this Agreement by you.

- You shall indemnify, defend and hold harmless WILEY, its Licensors and their respective directors, officers, agents and employees, from and against any actual or threatened claims, demands, causes of action or proceedings arising from any breach of this Agreement by you.

- IN NO EVENT SHALL WILEY OR ITS LICENSORS BE LIABLE TO YOU OR ANY OTHER PARTY OR ANY OTHER PERSON OR ENTITY FOR ANY SPECIAL, CONSEQUENTIAL, INCIDENTAL, INDIRECT, EXEMPLARY OR PUNITIVE DAMAGES, HOWEVER CAUSED, ARISING OUT OF OR IN CONNECTION WITH THE DOWNLOADING, PROVISIONING, VIEWING OR USE OF THE MATERIALS REGARDLESS OF THE FORM OF ACTION, WHETHER FOR BREACH OF CONTRACT, BREACH OF WARRANTY, TORT, NEGLIGENCE, INFRINGEMENT OR OTHERWISE (INCLUDING, WITHOUT LIMITATION, DAMAGES BASED ON LOSS OF PROFITS, DATA, FILES, USE, BUSINESS OPPORTUNITY OR CLAIMS OF THIRD PARTIES), AND WHETHER OR NOT THE PARTY HAS BEEN ADVISED OF THE POSSIBILITY OF SUCH DAMAGES. THIS LIMITATION SHALL APPLY NOTWITHSTANDING ANY FAILURE OF ESSENTIAL PURPOSE OF ANY LIMITED REMEDY PROVIDED HEREIN.

- Should any provision of this Agreement be held by a court of competent jurisdiction to be illegal, invalid, or unenforceable, that provision shall be deemed amended to achieve as nearly as possible the same economic effect as the original provision, and the legality, validity and enforceability of the remaining provisions of this Agreement shall not be affected or impaired thereby.

- The failure of either party to enforce any term or condition of this Agreement shall not constitute a waiver of either party's right to enforce each and every term and condition of this Agreement. No breach under this agreement shall be deemed waived or excused by either party unless such waiver or consent is in writing signed by the party granting such waiver or consent. The waiver by or consent of a party to a breach of any provision of this Agreement shall not operate or be construed as a waiver of or consent to any other or subsequent breach by such other party.

- This Agreement may not be assigned (including by operation of law or otherwise) by you without WILEY's prior written consent.

- Any fee required for this permission shall be non-refundable after thirty (30) days from receipt by the CCC.

- These terms and conditions together with CCC's Billing and Payment terms and conditions (which are incorporated herein) form the entire agreement between you and WILEY concerning this licensing transaction and (in the absence of fraud) supersedes all prior agreements and representations of the parties, oral or written. This Agreement may not be amended except in writing signed by both parties. This Agreement shall be binding upon and inure to the benefit of the parties' successors, legal representatives, and authorized assigns.

- In the event of any conflict between your obligations established by these terms and conditions and those established by CCC's Billing and Payment terms and conditions, these terms and conditions shall prevail.

- WILEY expressly reserves all rights not specifically granted in the combination of (i) the license details provided by you and accepted in the course of this licensing transaction, (ii) these terms and conditions and (iii) CCC's Billing and Payment terms and conditions.

- This Agreement will be void if the Type of Use, Format, Circulation, or Requestor Type was misrepresented during the licensing process.

- This Agreement shall be governed by and construed in accordance with the laws of the State of New York, USA, without regards to such state's conflict of law rules. Any legal action, suit or proceeding arising out of or relating to these Terms and Conditions or the breach thereof shall be instituted in a court of competent jurisdiction in New York County in the State of New York in the United States of America and each party hereby consents and submits to the personal jurisdiction of such court, waives any objection to venue in such court and consents to service of process by registered or certified mail, return receipt requested, at the last known address of such party.

JOHN WILEY AND SONS LICENSE TERMS AND CONDITIONS

Aug 17, 2019

This Agreement between Lei Li ("You") and John Wiley and Sons ("John Wiley and Sons") consists of your license details and the terms and conditions provided by John Wiley and Sons and Copyright Clearance Center.

License Number	4651420368063
License date	Aug 17, 2019
Licensed Content Publisher	John Wiley and Sons
Licensed Content Publication	ChemBioChem
Licensed Content Title	Probing Colocalization of N-Ras and K-Ras4B Lipoproteins in Model Biomembranes
Licensed Content Author	Lei Li, Mridula Dwivedi, Satyajit Patra, et al
Licensed Content Date	Mar 21, 2019
Licensed Content Volume	20
Licensed Content Issue	9
Licensed Content Pages	6
Type of Use	Dissertation/Thesis
Requestor type	Author of this Wiley article
Format	Print and electronic
Portion	Full article
Will you be translating?	No
Title of your thesis / dissertation	Mechanistic studies of Ras nanoclusters and Ras effectors interacting with the lipid membrane
Expected completion date	Dec 2019
Expected size (number of pages)	
Requestor Location	Lei Li Otto-Hahn-Str. 4a 44227 Dortmund Dortmund, NRW 44149 Germany Attn: Lei Li
Publisher Tax ID	EU826007151
Total	**0.00 EUR**
Terms and Conditions	

TERMS AND CONDITIONS

This copyrighted material is owned by or exclusively licensed to John Wiley & Sons, Inc. or one of its group companies (each a"Wiley Company") or handled on behalf of a society with which a Wiley Company has exclusive publishing rights in relation to a particular work (collectively "WILEY"). By clicking "accept" in connection with completing this licensing transaction, you agree that the following terms and conditions apply

to this transaction (along with the billing and payment terms and conditions established by the Copyright Clearance Center Inc., ("CCC's Billing and Payment terms and conditions"), at the time that you opened your RightsLink account (these are available at any time at http://myaccount.copyright.com).

Terms and Conditions

- The materials you have requested permission to reproduce or reuse (the "Wiley Materials") are protected by copyright.

- You are hereby granted a personal, non-exclusive, non-sub licensable (on a stand-alone basis), non-transferable, worldwide, limited license to reproduce the Wiley Materials for the purpose specified in the licensing process. This license, **and any CONTENT (PDF or image file) purchased as part of your order,** is for a one-time use only and limited to any maximum distribution number specified in the license. The first instance of republication or reuse granted by this license must be completed within two years of the date of the grant of this license (although copies prepared before the end date may be distributed thereafter). The Wiley Materials shall not be used in any other manner or for any other purpose, beyond what is granted in the license. Permission is granted subject to an appropriate acknowledgement given to the author, title of the material/book/journal and the publisher. You shall also duplicate the copyright notice that appears in the Wiley publication in your use of the Wiley Material. Permission is also granted on the understanding that nowhere in the text is a previously published source acknowledged for all or part of this Wiley Material. Any third party content is expressly excluded from this permission.

- With respect to the Wiley Materials, all rights are reserved. Except as expressly granted by the terms of the license, no part of the Wiley Materials may be copied, modified, adapted (except for minor reformatting required by the new Publication), translated, reproduced, transferred or distributed, in any form or by any means, and no derivative works may be made based on the Wiley Materials without the prior permission of the respective copyright owner.**For STM Signatory Publishers clearing permission under the terms of the STM Permissions Guidelines only, the terms of the license are extended to include subsequent editions and for editions in other languages, provided such editions are for the work as a whole in situ and does not involve the separate exploitation of the permitted figures or extracts,** You may not alter, remove or suppress in any manner any copyright, trademark or other notices displayed by the Wiley Materials. You may not license, rent, sell, loan, lease, pledge, offer as security, transfer or assign the Wiley Materials on a stand-alone basis, or any of the rights granted to you hereunder to any other person.

- The Wiley Materials and all of the intellectual property rights therein shall at all times remain the exclusive property of John Wiley & Sons Inc, the Wiley Companies, or their respective licensors, and your interest therein is only that of having possession of and the right to reproduce the Wiley Materials pursuant to Section 2 herein during the continuance of this Agreement. You agree that you own no right, title or interest in or to the Wiley Materials or any of the intellectual property rights therein. You shall have no rights hereunder other than the license as provided for above in Section 2. No right, license or interest to any trademark, trade name, service mark or other branding ("Marks") of WILEY or its licensors is granted hereunder, and you agree that you shall not assert any such right, license or interest with respect thereto

- NEITHER WILEY NOR ITS LICENSORS MAKES ANY WARRANTY OR REPRESENTATION OF ANY KIND TO YOU OR ANY THIRD PARTY, EXPRESS, IMPLIED OR STATUTORY, WITH RESPECT TO THE MATERIALS OR THE ACCURACY OF ANY INFORMATION CONTAINED IN THE MATERIALS, INCLUDING, WITHOUT LIMITATION, ANY IMPLIED WARRANTY OF MERCHANTABILITY, ACCURACY, SATISFACTORY QUALITY, FITNESS FOR A PARTICULAR PURPOSE, USABILITY, INTEGRATION OR NON-INFRINGEMENT AND ALL SUCH WARRANTIES ARE HEREBY EXCLUDED BY WILEY AND ITS LICENSORS AND WAIVED BY YOU.

- WILEY shall have the right to terminate this Agreement immediately upon breach of this Agreement by you.

- You shall indemnify, defend and hold harmless WILEY, its Licensors and their respective directors, officers, agents and employees, from and against any actual or threatened claims, demands, causes of action or proceedings arising from any breach of this Agreement by you.

- IN NO EVENT SHALL WILEY OR ITS LICENSORS BE LIABLE TO YOU OR ANY OTHER PARTY OR ANY OTHER PERSON OR ENTITY FOR ANY SPECIAL, CONSEQUENTIAL, INCIDENTAL, INDIRECT, EXEMPLARY OR PUNITIVE DAMAGES, HOWEVER CAUSED, ARISING OUT OF OR IN CONNECTION WITH THE DOWNLOADING, PROVISIONING, VIEWING OR USE OF THE MATERIALS REGARDLESS OF THE FORM OF ACTION, WHETHER FOR BREACH OF CONTRACT, BREACH OF WARRANTY, TORT, NEGLIGENCE, INFRINGEMENT OR OTHERWISE (INCLUDING, WITHOUT LIMITATION, DAMAGES BASED ON LOSS OF PROFITS, DATA, FILES, USE, BUSINESS OPPORTUNITY OR CLAIMS OF THIRD PARTIES), AND WHETHER OR NOT THE PARTY HAS BEEN ADVISED OF THE POSSIBILITY OF SUCH DAMAGES. THIS LIMITATION SHALL APPLY NOTWITHSTANDING ANY FAILURE OF ESSENTIAL PURPOSE OF ANY LIMITED REMEDY PROVIDED HEREIN.

- Should any provision of this Agreement be held by a court of competent jurisdiction to be illegal, invalid, or unenforceable, that provision shall be deemed amended to achieve as nearly as possible the same economic effect as the original provision, and the legality, validity and enforceability of the remaining provisions of this Agreement shall not be affected or impaired thereby.

- The failure of either party to enforce any term or condition of this Agreement shall not constitute a waiver of either party's right to enforce each and every term and condition of this Agreement. No breach under this agreement shall be deemed waived or excused by either party unless such waiver or consent is in writing signed by the party granting such waiver or consent. The waiver by or consent of a party to a breach of any provision of this Agreement shall not operate or be construed as a waiver of or consent to any other or subsequent breach by such other party.

- This Agreement may not be assigned (including by operation of law or otherwise) by you without WILEY's prior written consent.

- Any fee required for this permission shall be non-refundable after thirty (30) days from receipt by the CCC.

- These terms and conditions together with CCC's Billing and Payment terms and conditions (which are incorporated herein) form the entire agreement between you and WILEY concerning this licensing transaction and (in the absence of fraud) supersedes all prior agreements and representations of the parties, oral or written. This Agreement may not be amended except in writing signed by both parties. This Agreement shall be binding upon and inure to the benefit of the parties' successors, legal representatives, and authorized assigns.

- In the event of any conflict between your obligations established by these terms and conditions and those established by CCC's Billing and Payment terms and conditions, these terms and conditions shall prevail.

- WILEY expressly reserves all rights not specifically granted in the combination of (i) the license details provided by you and accepted in the course of this licensing transaction, (ii) these terms and conditions and (iii) CCC's Billing and Payment terms and conditions.

- This Agreement will be void if the Type of Use, Format, Circulation, or Requestor Type was misrepresented during the licensing process.

- This Agreement shall be governed by and construed in accordance with the laws of the State of New York, USA, without regards to such state's conflict of law rules. Any legal action, suit or proceeding arising out of or relating to these Terms and Conditions or the breach thereof shall be instituted in a court of competent jurisdiction in New York County in the State of New York in the United States of America and each party hereby consents and submits to the personal jurisdiction of such court, waives any objection to venue in such court and consents to service of process by registered or certified mail, return receipt requested, at the last known address of such party.

WILEY OPEN ACCESS TERMS AND CONDITIONS

Wiley Publishes Open Access Articles in fully Open Access Journals and in Subscription journals offering Online Open. Although most of the fully Open Access journals publish open access articles under the terms of the Creative Commons Attribution (CC BY) License only, the subscription journals and a few of the Open

Access Journals offer a choice of Creative Commons Licenses. The license type is clearly identified on the article.

The Creative Commons Attribution License

The Creative Commons Attribution License (CC-BY) allows users to copy, distribute and transmit an article, adapt the article and make commercial use of the article. The CC-BY license permits commercial and non-

Creative Commons Attribution Non-Commercial License

The Creative Commons Attribution Non-Commercial (CC-BY-NC)License permits use, distribution and reproduction in any medium, provided the original work is properly cited and is not used for commercial purposes.(see below)

Creative Commons Attribution-Non-Commercial-NoDerivs License

The Creative Commons Attribution Non-Commercial-NoDerivs License (CC-BY-NC-ND) permits use, distribution and reproduction in any medium, provided the original work is properly cited, is not used for commercial purposes and no modifications or adaptations are made. (see below)

Use by commercial "for-profit" organizations

Use of Wiley Open Access articles for commercial, promotional, or marketing purposes requires further explicit permission from Wiley and will be subject to a fee.

Further details can be found on Wiley Online Library http://olabout.wiley.com/WileyCDA/Section/id-410895.html

Other Terms and Conditions:

v1.10 Last updated September 2015

Questions? customercare@copyright.com or +1-855-239-3415 (toll free in the US) or +1-978-646-2777.